STRUCTURAL DESIGN OF RC STRUCTURES FROM SUSTAINABLE DEVELOPMENT PERSPECTIVE

A Thesis Submitted to
the Graduate School of
İzmir Institute of Technology
in Partial Fulfillment of the Requirements for Degree of

MASTER OF SCIENCE

In Civil Engineering

by

Ekin GÜLTEPE

November 2023
İZMİR

We approve the thesis of **Ekin GÜLTEPE**

Examining Committee Members:

Prof. Dr. Cemalettin DÖNMEZ
Department of Civil Engineering, İzmir Institute of Technology

Assoc. Prof. Dr. Çağlayan HIZAL
Department of Civil Engineering, Ege University

Assist. Prof. Dr. Korhan Deniz DALGIÇ
Department of Civil Engineering, İzmir Institute of Technology

24 November 2023

Prof. Dr. Cemalettin DÖNMEZ
Supervisor
Department of Civil Engineering
İzmir Institute of Technology

Prof. Dr. Cemalettin DÖNMEZ
Head of the Department of Civil Engineering

Prof. Dr. Mehtap EANES
Dean of the Graduate School

ACKNOWLEDGMENT

I would like to express my deepest gratitude to my supervisor Prof. Dr. Cemalettin Dönmez. His guidance, support, and motivation became a light in my way to continue and complete this study. I learned how to be a researcher and acquired the essential skills and mindset of a researcher under his mentorship.

I also would like to express my special thanks to Assist. Prof. Dr. Egemen Sönmez, Prof. Dr. Mustafa Emre İlal, and Dr. Mümine Gerçek Gün for their support and guidance during this study. Their insights were important in shaping the outcome of this study.

I also thank the members of my defense jury, Assoc. Prof. Dr. Çağlayan Hızal and Assist. Prof. Dr. Korhan Deniz Dalgıç, for generously contributing their time and valuable comments.

I am deeply grateful to my parents for their endless support and belief in me during my whole life.

Special thanks go to my friends and colleagues, Derya Çakmak, Bengisu Yılmaz, Hilal Çelik, Kürşat Çağrı Yakıcı with whom we shared both joyful and challenging moments during this study.

Finally, I want to express my appreciation to all those who have played a role in this academic journey, contributing to its successful culmination.

To my parents,

ABSTRACT

STRUCTURAL DESIGN OF RC STRUCTURES FROM SUSTAINABLE DEVELOPMENT PERSPECTIVE

The growth of the population and changing demands have become a significant problem due to the limited resources of the earth. Climate change has increased the occurrence of natural events and probable disasters due to insufficient infrastructure. The economic, environmental, and social aspects of the problem necessitate sustainable practices. On the other hand, probable disaster dictates design decisions to keep the physical environment intact and resilient. Hence, the expectations from the construction industry are high. The industry also needs to tackle the task of lowering the existing high consumption levels of natural resources and energy. Being resilient under seismic events is paramount for the areas that have high seismicity. The general trend of using less material for sustainability purposes conflicts with the resilient seismic design decisions which typically cause an increase in the initial consumptions. The studies on resilience and sustainability hint that there might be design opportunities that serve both purposes together. In this study, such an opportunity for RC residential buildings is focused. The resilience and energy cost of a conventional moment-resisting frame and the same frame with increased robustness through the addition of shear walls are studied. It is presumed in addition to the increased robustness, the thermal impact of the additional concrete mass will create an advantage for energy consumption in the life cycle of the building. The design decision for shear walls is based on the proposal by Hassan and Sozen (1997). Nonlinear time history analysis is performed for both frames according to Turkish Earthquake Regulation. Results show that the robust frame has the needed resilience. The energy analysis shows that the frame with shear walls has significantly higher consumption initially. However, when the thermal impact of the concrete is included in the full life cycle, the energy consumption difference reduces from 18% to 4%. As a result, it could be stated that providing sufficient robustness to the structure by shear walls at targeted locations provides an opportunity to have a resilient and sustainable structure with a minor increase in total energy cost throughout the life cycle of the structure.

ÖZET

SÜRDÜRÜLEBİLİR KALKINMA PERSPEKTİFİNDEN BETONARME YAPILARDA YAPISAL TASARIM

Nüfus artışı ve değişen ihtiyaçlar karşısında dünyanın kaynaklarının sınırlı olması insanlık medeniyetinin kendini devam ettirebilmesi açısından ciddi bir sorun haline gelmiştir. İklim değişikliği aşırı doğa olaylarının görülme sıklığını arttırmış ve altyapı yetersizliği nedeniyle olası felaketlere yol açmaktadır. Sorunun ekonomik, çevresel ve sosyal boyutu sürdürülebilir uygulamaları zorunlu kılmaktadır. Öte yandan olası bir felakette fiziksel çevrenin bütünlüğünü ve fonksiyonlarını devam ettirebilme ihtiyaçları dirençlilik kararlarına ihtiyaç duymaktadır. Bu nedenle inşaat sektöründen beklentiler yüksektir. Aynı zamanda sektör doğal kaynakların ve enerjinin mevcut yüksek tüketim seviyelerini düşürmek zorunluluğu altındadır. Depremselliği yüksek bölgelerde sismik olaylara karşı dirençlilik çok önemlidir. Sürdürülebilirlik amacıyla daha az malzeme kullanılması yönündeki genel eğilim, genellikle başlangıç tüketimlerinde artışa neden olan dirençli sismik tasarım kararlarıyla çelişkiler içermektedir. Dirençlilik ve sürdürülebilirlik üzerine yapılan çalışmalar, bazı tasarım yaklaşımlarının dirençlilik ve sürdürülebilirliğin aynı anda gerçekleşebilme fırsatları olabileceğine işaret etmektedir. Bu çalışmada betonarme konut binaları için böylesi bir tasarım kararına odaklanılmıştır. Geleneksel moment aktaran bir çerçeve ve aynı çerçevenin perde duvarların eklenmesiyle gürbüzlüğü artırılarak dirençliliği ve enerji maliyetlerinde oluşan değişimler incelenmiştir. İlave beton kütlesinin gürbüzlüğü arttırması yanında termal etkisiyle binanın yaşam döngüsü enerji tüketimi açısından avantaj yaratacağı öngörülmektedir. Perde duvarların tasarım kararı Hassan ve Sözen (1997)'in önerisine dayandırılmıştır. Her iki çerçeve için de Türkiye Deprem Yönetmeliği'ne göre doğrusal olmayan zaman tanım alanı analizi yapılmıştır. Sonuçlar, gürbüz çerçevenin gerekli dirençliliğe sahip olduğunu göstermektedir. Enerji analizi, perde duvarlı çerçevenin başlangıçta daha yüksek tüketime sahip olduğunu göstermekle beraber tüm yaşam döngüsü göz önüne alındığında enerji tüketim farkı %18'den %4'e düşmektedir. Sonuç olarak, enerji verimliliği ve gürbüzlüğü bir arada düşünülerek yerleştirilen perde duvarlar ile yapılan bir tasarım, yapının yaşam döngüsü boyunca toplam enerji maliyetinde küçük bir artışla, dirençliliği yüksek ve sürdürülebilir bir yapıya sahip olma fırsatı sağlamaktadır.

TABLE OF CONTENTS

LIST OF FIGURES

Figure **Page**

Figure **Page**

Figure **Page**

Figure **Page**

Figure **Page**

Figure **Page**

Figure **Page**

Figure **Page**

Figure **Page**

Figure **Page**

Figure **Page**

LIST OF TABLES

Table **Page**

CHAPTER 1

INTRODUCTION

1.1. Introduction

The natural resource consumption of human activity reached to levels beyond the planet Earth could provide sustainably. Even if through technological developments, the usable biocapacity of the Earth has increased about 27% in the past 50 years, still more resources are consumed than renewed naturally. Consumption beyond capacity leads to the disruption of the natural cycles of the Earth and to further degradation. The Earth has been in overshoot since the 1970's, and, nowadays, it is necessary to have 1.7 Earths worth of natural resources through natural cycles to overcome the demand (Pomè, 2021)

Sustainability is an answer for the needed action to balance the needs of the present and future without collapsing the base natural cycles. Sustainable development aims to meet the needs of the present without compromising the future generations' capability to meet their own needs (United Nations, 1987). There are three pillars of sustainability: economy, environment, and society. Considering the increasing rate of disasters and the resulting increased economic costs and social impacts, it is necessary to find a solution for immediate recovery after the catastrophic events. These solutions should have a possible minimum effect on people's lives and should not choke the flourishment of human civilization. The United Nations has established "Sustainable Development Goals" with seventeen main targets to mitigate climate change, provide equality, and end poverty, which can be observed in Figure 1.1.

According to Manfredi (2021), climate change led to the occurrence of natural events such as floods and storms, which rose by 70% between the years 2000 and 2019. Not only the frequencies but also the magnitudes of these events increase and turn into disasters. This phenomenon has economic, social, and environmental consequences.

Figure 1.1. The sustainable development goals of the United Nations (United Nations, 2023)

Sustainability transforms from the original meaning and becomes a consideration for mitigating the effects of natural events and reducing their impact. The importance of this subject is realized after facing the results of events such as rising temperatures, melting glaciers, quality deterioration in air, water, and soil, longer droughts, increased flood risks, less food security, economic losses, increased fatalities, etc. Resilience and preparedness for these events are needed to have the capability to withstand and recover as soon as possible. After natural events turn into natural disasters, additional natural resources are consumed for recovery efforts. Hence, the emissions are increasing at an accelerated pace. As a priori, it is necessary to reduce consumption levels to have a sustainable global system. It is also necessary to develop the ability to prevent the transformation of natural events into catastrophes.

The construction sector has a significant impact on the stated goals because it has major effects on the economy, environment, and social life (United Nations, 2023). Using clean production techniques in material extraction and production, avoiding pollution, and having inspection mechanisms could reduce the impact on the environment. Hence, adoption of sustainability principles in the construction industry will help to reduce the consumption of energy and natural resources, reduce waste and pollution, etc.

Earthquakes are one of the most damaging catastrophes, and the repair or reconstruction of the built environment causes a massive increase in natural resources and energy consumption. The current design level performance level of "life safety" embraces damage – structural or non-structural – in the structures, the sole performance criterion is the saving of lives. The resilient structural design was neglected with the economic concerns. The sustainability requirements and the heightened service expectations from the public demand a higher performance goal. It has become more appropriate to design structures according to immediate occupancy for the purposes of minimizing the disruption to human activity and, at the same time, saving lives. Such an approach is also in accordance with the sustainability requirements by avoiding waste and further depletion of natural resources.

Resilience is the ability to prepare for and adapt to changing conditions and to withstand and recover rapidly from disruptions (Asadi, 2020), as visualized in Figure 1.2. Resilience refers to the capacity of physical systems to resist hazards, minimize loss of functionality, and reduce recovery times and costs, and such a response is starting to be demanded after disasters. Sustainable systems consider environmental impact and conservation of resources. It is necessary to manage disaster risk adequately to provide sustainable development. A holistic view is needed to satisfy both sustainability and resilience requirements. Therefore, the adequate strength, stiffness, and serviceability of the structural systems' performance goals should be adapted to provide sustainable and resilient design.

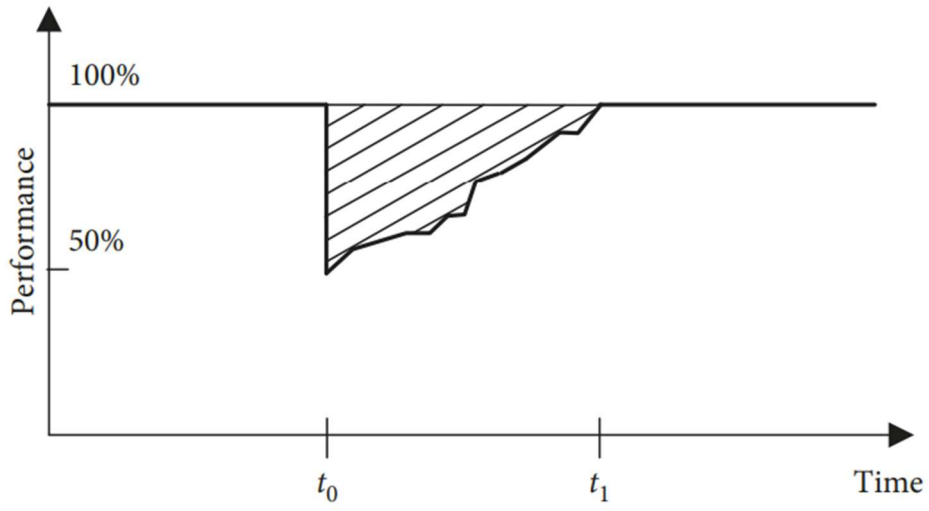

Figure 1.2.The definition of resilience (Stochino, 2019)

Resilience and sustainability have been studied separately so far but it appears that their complementary roles are needed for efficiency. Studies have been started to minimize direct and indirect losses from extreme events through resilience and robustness, as well as more effective recovery strategies. It is established that the retrofit costs and environmental impacts of a building that is built with a resilient design will be less (Asadi, 2020). Hence total life cycle costs could be reduced by increasing the initial robustness. The target resilience of the buildings after the earthquake with minimal damage will make the structures be serviceable after the event.

Structural framing of the buildings is responsible for providing the needed structural resistance to demands developed by the elements of nature. The framing is determined in the design stage and plays a major role in structural, economic, and environmental performance. The layout and the member proportions, sufficient vertical and horizontal structural elements and undisrupted force flows have a direct relationship with the robustness of the structure. The thermal properties of structural framing and the materials have an impact on energy consumption during the operational stage of the structures. Thus, the decisions during the design phase must be carefully gaged.

Typically, related studies focus on embodied or operational energy needs of a structure separately. Embodied includes the activities from extraction of raw resources to disposal of the building elements. Material processing, transportation, construction, maintenance, and repair are considered for this stage. The operational stage includes the use phase that involves ventilation, heating and cooling, lightning etc. On the other side, all the effects from production to demolition can be observed with life cycle assessment (LCA). LCA includes the examination of the potential environmental impacts of buildings, products, or services throughout their whole life cycle (Skanska, 2019).

Sustainability is often associated with less material, less cost, and extended lifetime. This often directs designers to the reduction of material to be sustainable. If only sustainability is considered, leaning of the system for material reduction creates the risk of ignoring the needed resilience in the structure. Hence, sustainability related design decisions should not impair the resilience of the structure. Smart design decisions that promote the dual use of the material for sustainability and resilience should be sought. Properties like durability and thermal mass are some advantages of reinforced concrete buildings that should be harnessed (Caverzan, 2018; Asadi, 2020). Asadi (2020) reported

that about 30% of all the energy consumed in a structure during its lifespan is in the form of embodied energy. An optimization considering both the embodied and operational energy consumptions is needed.

In this study an attempt to use shear walls as dual elements to serve for improving the earthquake resistance and the energy efficiency a building will be performed. Further details are provided below.

1.2. Objective & Scope

The main objective of this study is to perform a case study to demonstrate the dual use of structural elements for sustainability and resilience purposes. The focus will be residential buildings due to their sheer number and the excess damage observed in earthquakes. Approximately 90% of all the damaged structures and 50% of all the losses resulting from building damage in earthquakes are associated to the residential sector (Menna, 2013).

Resilience against earthquake demands could be satisfied by controlling the developed drift levels in structures during extreme events. A robust structural frame is needed. The increase in robustness is typically accompanied by an increase in the material used. This translated to the use of more concrete and steel for reinforced concrete structures. Hence, initial material or the embodied energy use of the structure increases. There is an opportunity for the possible balancing act for the increased material use by the inherent thermal mass of concrete for compensating the higher initial embodied energy of the structure. Savings in the operational phase of the building's life cycle (Asadi, 2020) could be instrumental for this purpose. Such an act necessitates smart arrangement of the location of the structural elements considered by thermal advantages. Also, the energy consumption in full life cycle and the improved resilience through better performance in earthquake resistance should be considered.

Several researchers studied the sustainability of resilient structures. It is commonly concluded that (Gencturk, 2016) the sustainability of resilient structures should be evaluated considering the costs due to repair or rebuilding. The case study building in this study is a conventionally designed low-rise RC structure that will be

improved for better robustness and resilience. The improved design is attempted to utilize the thermal mass effect of the increased concrete mass for energy efficiency in the full life cycle of the structure. The repair costs, life cycle assessment, and energy analysis during the operational phase will be included for better projection. It is considered and tested whether a holistic vision will be more instrumental for a better decision.

The prototype conventional moment-frame RC structure is compared with an improved resilient RC structure that has pre-defined amount of shear walls to control the drift. The resilient prototype structure is expected to reduce the environmental impact by balancing the life-cycle energy cost and the cost resulting from the repair of the structure. Possible benefits related to the thermal mass and the configuration of the shear walls are introduced in the early design stage decisions and are decided based on the operational energy at the preliminary modeling in Revit. Revit is an Autodesk program that allows professionals to model shapes, structures, and systems in 3D with parametric accuracy, precision, and ease (Autodesk Revit, 2021). The selected conventional and modified frames are subjected to nonlinear time history analysis to evaluate earthquake performances to service, design, and maximum credible earthquake levels according to Turkish Seismic Regulation (TER2018). In order to avoid the near-fault effects, the buildings are selected to be 15-20 km away from the neighboring faults. The analyses of the structures were made in accordance with the TER2018. The ground motion sets are selected to minimize the pulse effects. The structures' nonlinear analyses are performed with OpenSees software in three dimensions. The life cycle assessment and energy analysis are performed with eTool and Open Studio, respectively. Hence, the planned study will provide both the earthquake performance and the full life cycle energy costs for evaluating the success of the dual use shear walls.

1.3. Outline of Thesis

In Chapter 2, a literature survey is done.

In Chapter 3, building layout selection is presented, the analysis of two different systems is performed and the ground motion selection is done.

In Chapter 4, the nonlinear analysis of the two structural systems is performed.

In Chapter 5, operational analysis is done by Sketchup open studio and EnergyPlus and Cerclos LCA is done.

In Chapter 6, the discussion and result are presented.

CHAPTER 2

LITERATURE REVIEW

2.1. Introduction

Built environments, such as buildings, bridges, tunnels, power plants, dams, and water networks are built for the purpose of transporting people and goods, and providing shelter, water, and energy. It plays an important role in creating the base environment for human civilization as it is known. Thus, the construction industry has an important impact on the development and sustainability of human civilization. It contributes 13% to the world's total GDP (Mavi, 2021). Construction activity starts with extracting materials from nature and ends with the demolition of the structures and utilization of the debris. Due to volume and the extent of the reach, it has a serious impact on the environment and the economy considering the whole lifecycle. On the other hand, structures could play an important role in developing sustainable human activity attempts by just reducing their environmental impact.

It should be mentioned that the total life cycle of the structures from the production of the materials to the construction and demolition, as well as the repair of the structural damage has an impact on the outcome. Attaining the sustainability goals necessitates sufficient performance during these extreme events and surviving the event with the minimum damage. These subjects have started to be studied by researchers from different perspectives. The following literature could be summarized in relation to the objective of the study.

2.2. Literature Review

Merrill and Giamarelos (2019) pointed out that in Roman times, the structures were seen as a legacy to be passed on to future generations and represent their

achievements. The strength and durability are the key concepts in these structures. This leads to the thought that resilient structures have been aimed at as latent since long ago.

Mohammadgholibeyki (2023) pointed out that the building sector is responsible for 1/3 of greenhouse gas (GHG) emissions and 40% of total primary energy consumption. 11% of 39% of energy consumption resulted from manufacturing structural materials and products such as steel, cement, and glass, as stated in the Global Alliance for Buildings and Construction report (2019). Ferraira (2023) and Abouhamad (2021) mentioned that buildings are the largest material consumers in Europe, representing 50% of all extracted materials, 42% of the final energy consumption, 35% of GHG emissions, and 32% of the waste flow. Son (2021) pointed out that concrete and reinforced steel contribute to about 65% of building GHG, with 40% of CO_2 emissions generated by concrete. Cement alone is responsible for 4% of CO_2 emissions globally, as mentioned in Griffin (2018). The location and orientation of the building affects the global warming potential (GWP) of the building with energy consumption, sunlight, natural ventilation, and transport. Asadi (2020) mentioned that 30% of all energy consumed in a building during its lifespan is in the form of embodied energy. The structural operational stage is responsible for 30–40% of global carbon emissions, Zhong (2016). After the demolition of the buildings, recycling or reuse should be done, considering the hazardous effects and resistance quality of the material. Construction and demolition waste comprises 46% of the total waste of the EU, 40% of China, and 20% of Japan, Purchase (2022). Pongiglione and Calderini (2016) mentioned that the construction industry should move from a linear to a circular system and embrace an approach from cradle to cradle.

The concrete and steel industries have an impact on the environment during the material production phase and it constitutes 90% of the embodied energy in structures, Abouhamad (2021). Concrete and steel are commonly used materials, as reinforced concrete and steel structures are common types. Caverzan (2018) mentioned that frequent use will continue due to no alternatives.

Pongiglione and Calderini (2016) mentioned that structural systems have an effect of 10% on a structure's whole lifecycle, from material production to demolition. The structure inventory is expected to be doubled as the global population to be 11 billion by 2050, Abouhamad (2021). Thus, there is an increasing demand, and the impact of the

structural systems on sustainable development goals should be integrated from a life cycle perspective.

Bragança (2014) stated that making decisions about the structure from performance, economic, environmental, and social aspects in the early design stage resulted in better results on impacts than the decisions in the construction and service stages as can be observed in Figure 2.1.

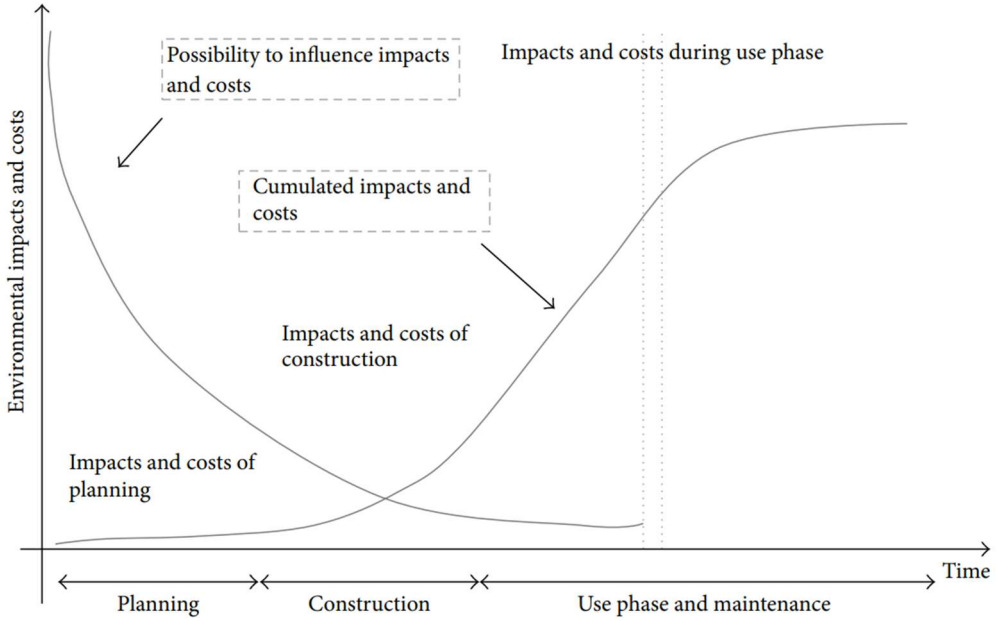

Figure 2.1. The environmental impact of construction stages (Bragança, 2014)

Sattar (2018) pointed out that the U.S. Senate demands the structures to be more resistant to all kinds of natural disasters and ensure the safety of people, and asked NIST to develop regulations in this direction. The consequences of the disasters lead to consider immediate occupancy in regular structures rather than the minimum requirements of the regulations. This practice was reasonable enough since structures will satisfy both life and structure and its contents safety. Improved regulations not only allow people to use their homes and workplaces immediately after the disaster but also minimize expensive recovery costs. The cost of the typical structural system is almost 10–20% of the total construction cost, Menna (2013). Robustness improvement causes an increment in this amount, and it is known to be quite low considering the paramount results.

Simonen (2018) mentioned that non-structural elements dominate repair costs. Hence, design decisions should be made by paying attention to the 1% non-structural elements total annihilation drift limit of the current practice, as mentioned by Algan (1982).

Wei (2015) stated that repair consumption made up 2.1% of the total GHG of Japan after the 2011 Tohoku earthquake in Japan. According to Wei, earthquake-induced restoration creates 25% of the embodied energy of the building in a 5-story building. The results show that if a structure loses its functionality and needs to be recovered or demolished, its consequences will be crucial to society, the economy, and the environment. Debris disposal and demolition are equivalent to 15% of embodied energy; it can reach 42% of the total energy consumption of rehabilitation in some cases. Salgado and Guner (2021) mentioned that collapse lowers the recycling ratio. As Wei (2015) mentioned, an additional 2% of initial energy investment (in materials that met the higher seismic criteria) yielded a 9% net decrease in total lifetime environmental impacts in terms of CO_2 emissions.

Mohammadgholibeyki (2023) stated that in the last two decades, the purpose has been to design high-performance buildings with low energy use while ensuring cost efficiency. Nouri (2021) mentioned that by increasing the strength of the structures, the initial environmental cost increases, but the expected damage costs and, in some cases, the total life-cycle costs are reduced.

Gencturk (2016) mentioned that resilient structures are more sustainable when considering the repair of buildings. Asadi (2020) performed a complete building energy simulation in the research. According to this study, increasing the shear wall ratio effectively reduces direct monetary loss and downtime as well as energy consumption. Moment frame systems' repair results have more embodied energy compared to shear wall systems.

Mergos (2019) proposed that low ductility leads to CO_2 emission increase sharper than medium and high ductility. Anwar (2019) states that non-ductile structures cannot easily gain serviceability after a design earthquake even after repair.

Although there has been noticeable progress in the field, the level of building damage during natural events highlights the fact that sustainable infrastructure is still a

far target, Keskin (2021). On the other hand, the public demands immediate recovery after extreme events.

FEMA P-2090/NIST SP-1254 report (2021) pointed out that the recovery speed has significant impact on the decision of people to stay, rebuild, or leave. The cost of damage and time required for recovery after extreme events is significantly higher than expected or people are willing to accept. One of the FEMA study states that 20 to 40% of buildings that satisfy the requirements of regulations in an affected region would not be available for occupancy following an earthquake, and 15 to 20% would be economically unrepairable. It should be reminded most of the old buildings don't satisfy the current requirements of the regulations. The recent earthquakes in 2023 Kahramanmaraş proved that these ratios are even higher in Türkiye, (Republic of Türkiye Presidency of Strategy and Budget, 2023). Even though there is strong evidence that robust design from the beginning is the key, communities are not willing to bear the up-front construction costs for resilient buildings yet, even if the long-term benefits exceed the upfront costs. Further research is necessary to prove the case. Improved design also reduces current operation and maintenance costs, hence could be utilized for sustainability purposes.

CHAPTER 3

DESIGN OF THE FRAMES

3.1. Building Layouts

It is necessary to define two frames for the purpose of the study. The first frame should be representative of the typical design practice, and the second frame should be designed to optimize the robustness and the energy efficiency. Shear walls are the preferred members to optimize the stiffness and the thermal mass properties of the frame. The optimization is based on the targeted robustness and the thermal impact of concrete. The target robustness will be decided based on a proposal which is derived from observations of structural performances in the damaging earthquakes of the last three decades. The decision about the thermal performance is based on the analysis of preliminary system selections by Revit software. This process includes the analysis of the heating and cooling loads. Revit results are used at the initial stages, EnergyPlus is used for final decision.

The selection of the plan layout is a crucial step for the robustness and sustainability of the structure frames. The layout also needed to satisfy the architectural plans, as seen in Figure 3.1. Several layouts are studied to reach a targeted optimized plan. Structural member sizes should also be in compliance with the structural needs. These requirements highlight the interdisciplinary nature of the process.

Dimensions of the structural and non-structural elements, insulation thicknesses, material types, the thermal mass coefficients, conductivity of the materials, etc. are affecting the overall thermal performance of the building. The same set of materials are used in both frames for a convenient comparison. The default thermal properties of the materials in the software are selected.

Energy consumption comparison of the alternatives considers both the embodied and the operational energy. Even though the embodied energy cost of the robust alternatives is higher, the savings in the operational energy create the potential to match

the initial investment. Hence, the layout decision should consider total energy. The preliminary member sizes prevent conclusive calculations at this stage. On the other hand, the decision is based on the relative efficiency of the operational energy which does not require exact member sizes. Regardless, there is room for educated decisions using the ratio between the increase in the concrete consumption and the operational energy decrease.

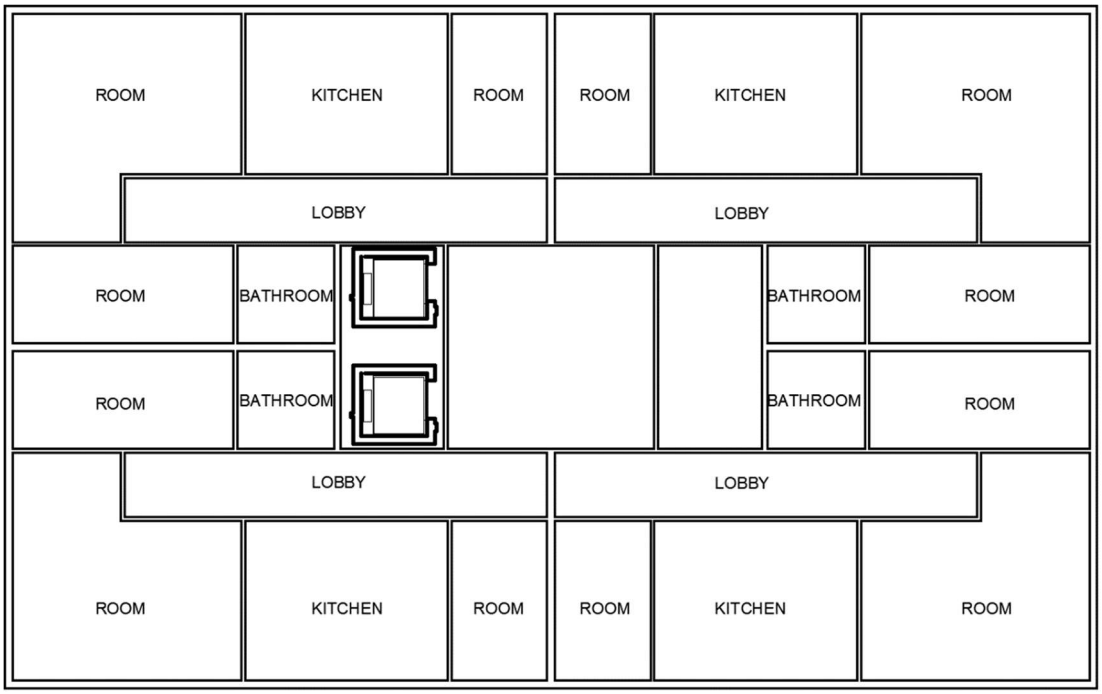

Figure 3.1. The architectural plan of the structure

The layout in Figure 3.2 is selected as the moment-resisting frame system. It is a regular frame with continuous grid lines. The structural frame preferences in Türkiye typically have discontinuous grid lines and less robust systems as a result. The selected moment frame is inherently more robust than the typical moment frame in Türkiye. Several plans were studied for the RC system with shear walls to observe how the thermal impact changes with the configuration. Among the three layouts with shear walls (Figure 3.3-3.5), the layout in Figure 3.5 is the worse option structurally. Between the other two, the layout in Figure 3.3 is selected based on the Revit analysis, due to its relative advantage in operational energy. Global results of the frames Revit analysis are presented in Table 3.1. The given results are the energy flow velocities of the individual layouts.

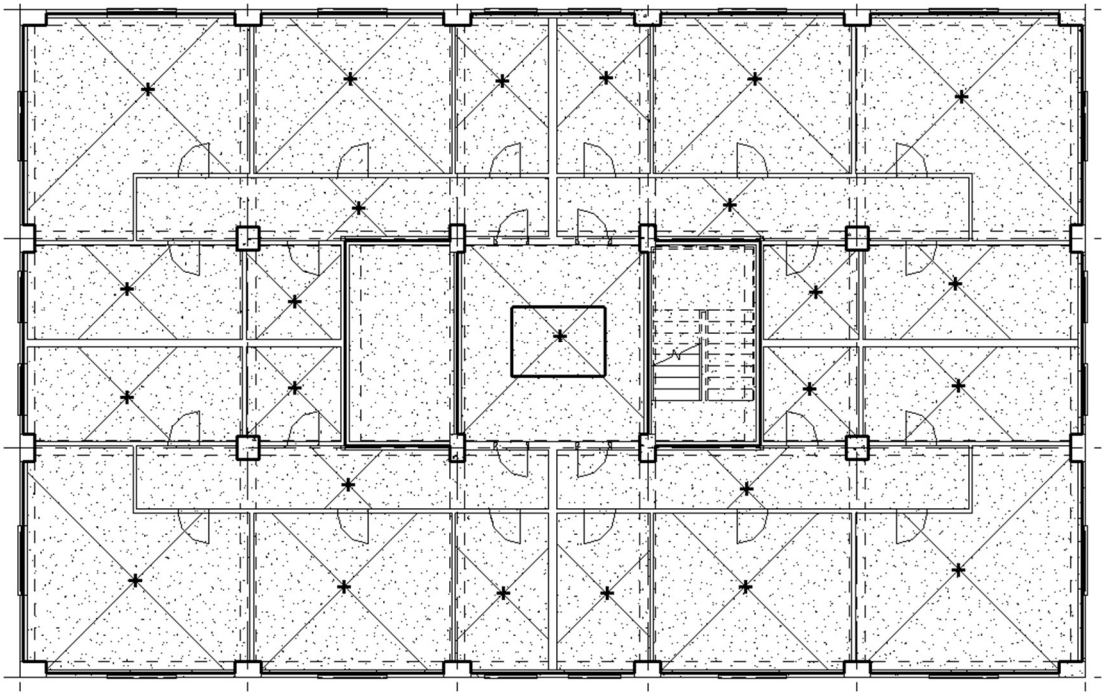

Figure 3.2. The layout of moment resisting frame

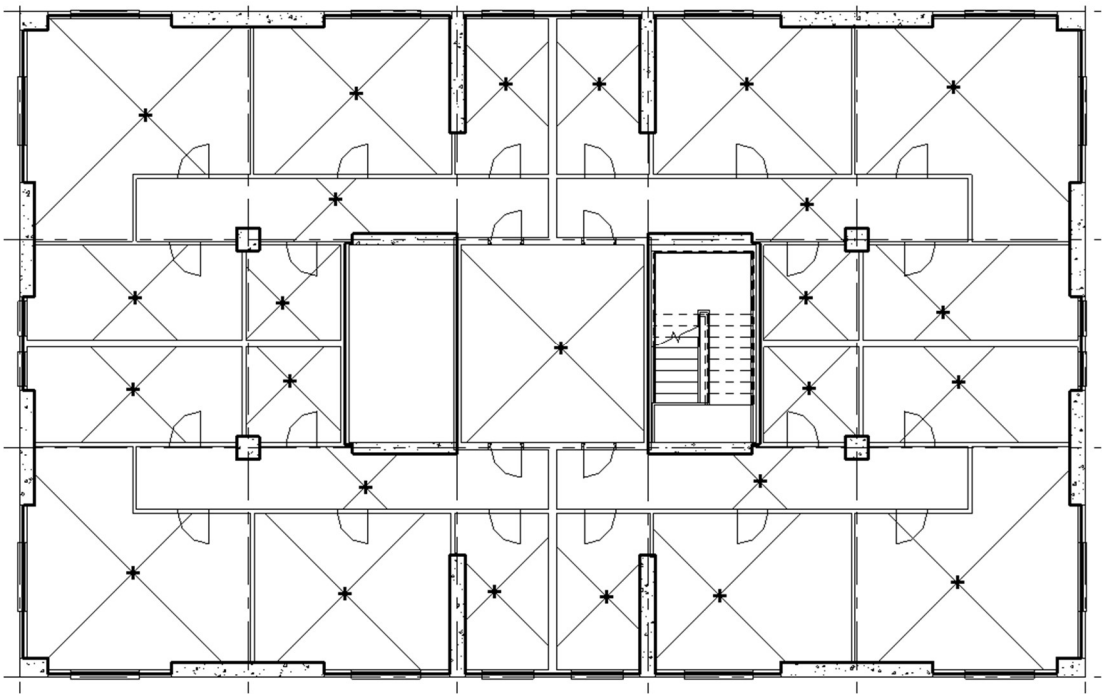

Figure 3.3. The layout of reinforced concrete system with shear wall prototype 1

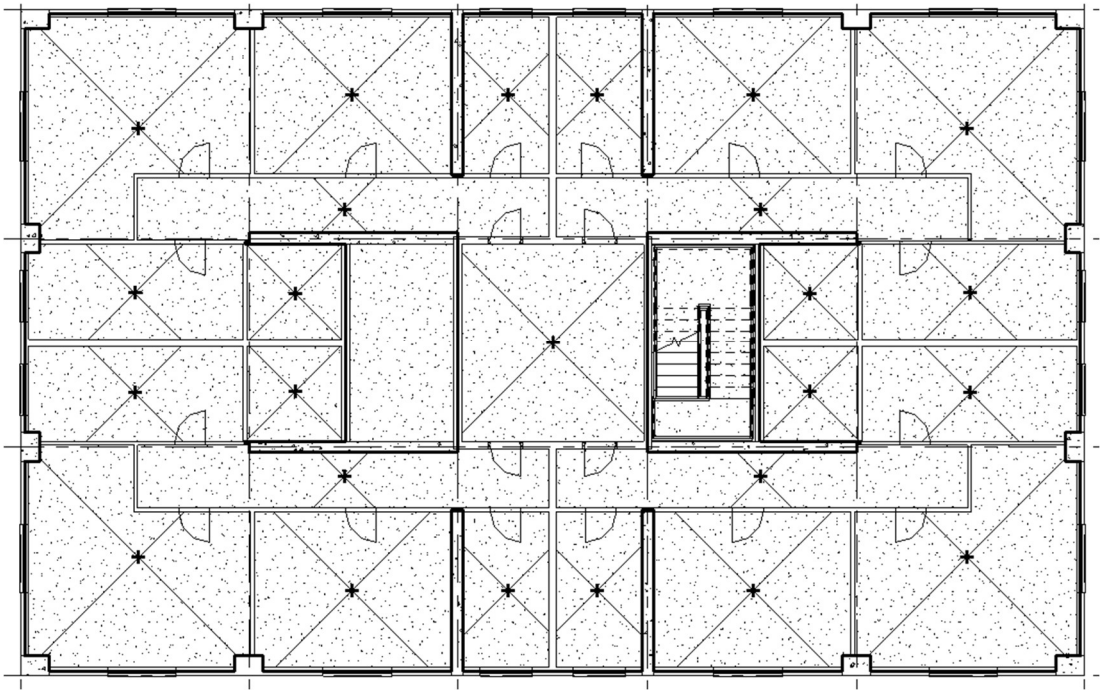

Figure 3.4. The layout of reinforced concrete system with shear wall prototype 2

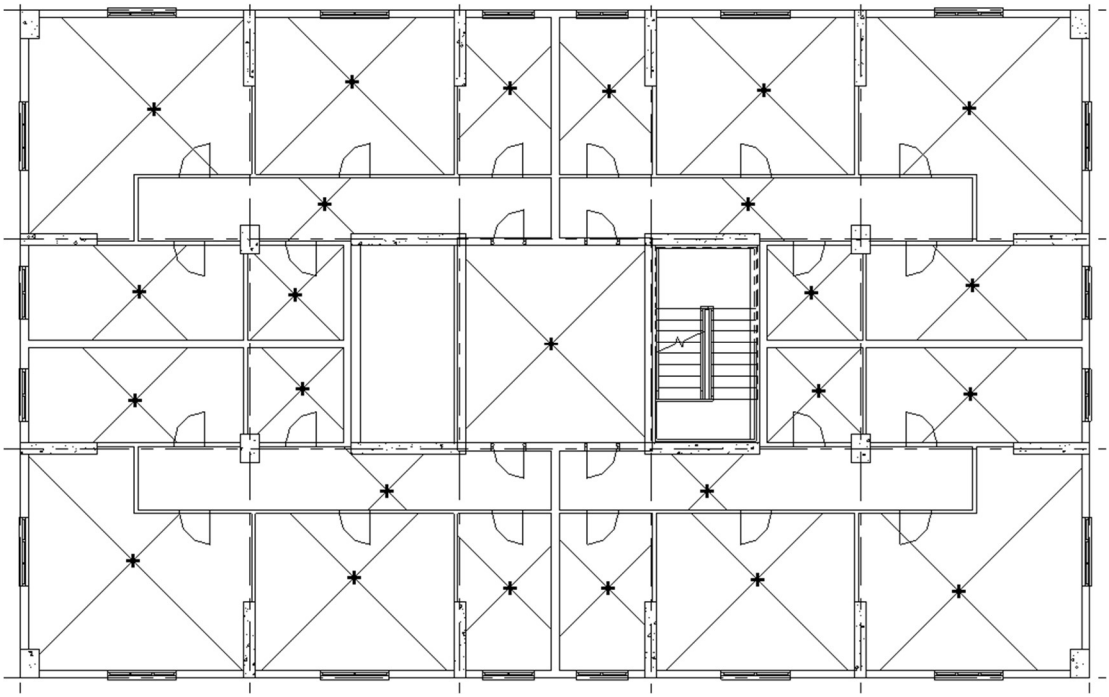

Figure 3.5. The layout of reinforced concrete system with shear wall prototype 3

Table 3.1.The load report of heating and cooling of building for the layout of moment resisting frame and reinforced concrete systems with shear walls prototypes

Calculated Results	MRF	SW-1	SW-2	SW-3
Peak Cooling Total Load (W)	141,958	134,002	149,485	127,265
Peak Heating Load (W)	88,366	95,410	94,414	86,724

3.2. Hassan Index

Hassan and Sozen (1997) proposed a simple classification method to evaluate the risk of failure of the RC structures in earthquakes. The index value is calculated based on the vertical structural element dimensions and the total floor area. Hassan and Sozen (1997) originally studied on the data from 1992 Erzincan earthquake but later the 1968 Tokachi-Oki (Shiga, 1977) and 1985 Chile earthquake (Riddell, 1987) data re-worked and studied in Hassan Index format. Some of the following severe earthquakes have also been studied by different researchers worldwide. A total of 15 earthquakes in 12 countries are studied in Hassan format (Yildirim, 2023).

Hassan and Sozen defined three index values. The wall index (WI) and the column index (CI) are the indices calculated based on the building information. The priority index (PI) as the summation of the WI and CI. The calculation is performed for the “critical” story, typically the ground floor. The total cross-sectional area of in-plane reinforced concrete walls in one horizontal direction and 1/10 of the cross-sectional area of the non-structural masonry separation walls in the same horizontal direction are summed up for WI calculations. Division of these values by the total floor area above the calculated level in the building resulted in the WI values. After performing the calculation for each direction, the smaller value WI value governs as the building WI. The CI is calculated as the division of the half of total cross-sectional area of the columns to the total floor area above at the same floor. The PI is the summation and CI and WI. The index definitions are also presented in Equations 3.1, 3.2, 3.3, 3.4, and 3.5.

A reconnaissance study is performed after the 2023 Kahramanmaraş Earthquakes (Yildirim, 2023) and data gathered is presented in Hassan Index format, Figure 3.6. CI and WI form the X-axis and the Y-axis, respectively. The PI could be represented as a

line on the figure. The PI reference to 0.25% by Hassan and Sozen (1997) is also drawn on the figure. It could be observed from the graph that the probability of risk for severe damage is increasing for lower PI value. It could be observed that the 0.25% PI value could be a good filter to separate the high-risk zone.

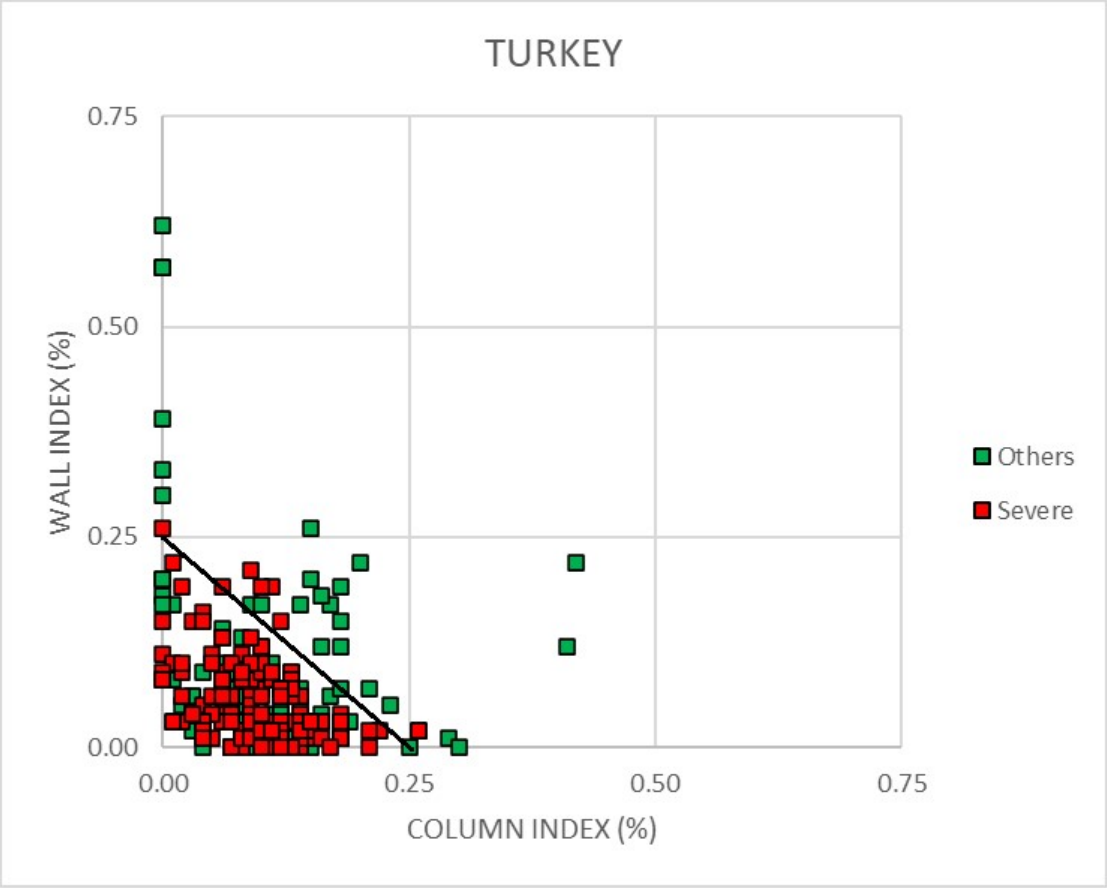

Figure 3.6. The cumulative Hassan Index data of Kahramanmaraş (Yildirim, 2023)

$$WI = \frac{A_{wt}}{A_{ft}} * 100 \tag{3.1}$$

$$A_{wt} = A_{cw} + \frac{A_{mw}}{10} \tag{3.2}$$

$$CI = \frac{A_{ce}}{A_{ft}} * 100 \tag{3.3}$$

$$A_{ce} = \frac{A_{col}}{2} \tag{3.4}$$

$$PI = WI + CI \tag{3.5}$$

A_{wt}: effective cross-sectional area of walls in a given horizonal direction

A_{ft}: total floor area above base in a building

A_{mw}: cross-section area of nonreinforced masonry filler walls in one horizontal direction at base

A_{cw}: total cross-sectional area of reinforced concrete walls in one horizontal direction at base

A_{ce}: effective cross-sectional area of columns at base

A_{col}: total cross-sectional area of columns above base

WI: Wall Index

CI: Column Index

PI: Priority Index

If the Hassan index values of the frames proposed in the study are calculated. The probable seismic damage risk of the frames could be judged based on the Hassan index. The calculated values are also presented graphically in Figure 3.7.

Calculation for the moment resisting frame:

$$CI = \frac{((0.6 * 0.6 * 4) + (0.4 * 0.7 * 20))/2}{490 * 6} * 100 = 0.12$$

$$WI = 0$$

$$PI = 0.12 + 0 = 012$$

Calculation for RC frame with shear wall:

$$CI = \frac{((0.6 * 0.6 * 4) + (0.5 * 0.75 * 4))/2}{490 * 6} * 100 = 0.05$$

$$WI_X = \frac{(0.4 * 4 * 4) + (0.3 * 2.75 * 4)}{490 * 6} * 100 = 0.33$$

$$WI_Y = \frac{(0.4 * 3 * 4) + (0.4 * 3.2 * 4)}{490 * 6} * 100 = 0.34$$

$$PI = 0.05 + 0.3299 = 0.38$$

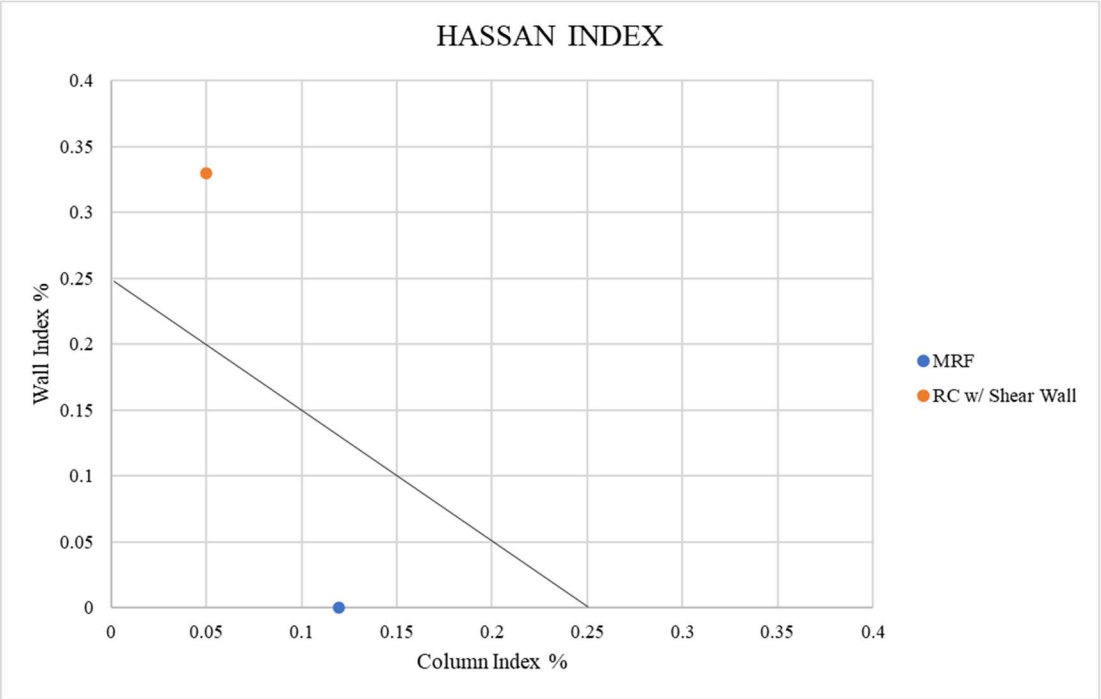

Figure 3.7. The Hassan Index graph of the structures

Hence, the provided amount of shear walls with a WI of 0.33% is expected to limit the drift demand and based on the field experience it is highly plausible that the structure will not suffer heavy damage. The nonlinear analysis results in the next chapter will provide further information in this respect.

3.3. Moment Resisting Frame

The structure has a typical story height of 3 m and consists of 6 stories. The plan dimensions are as presented in Figure 3.8.

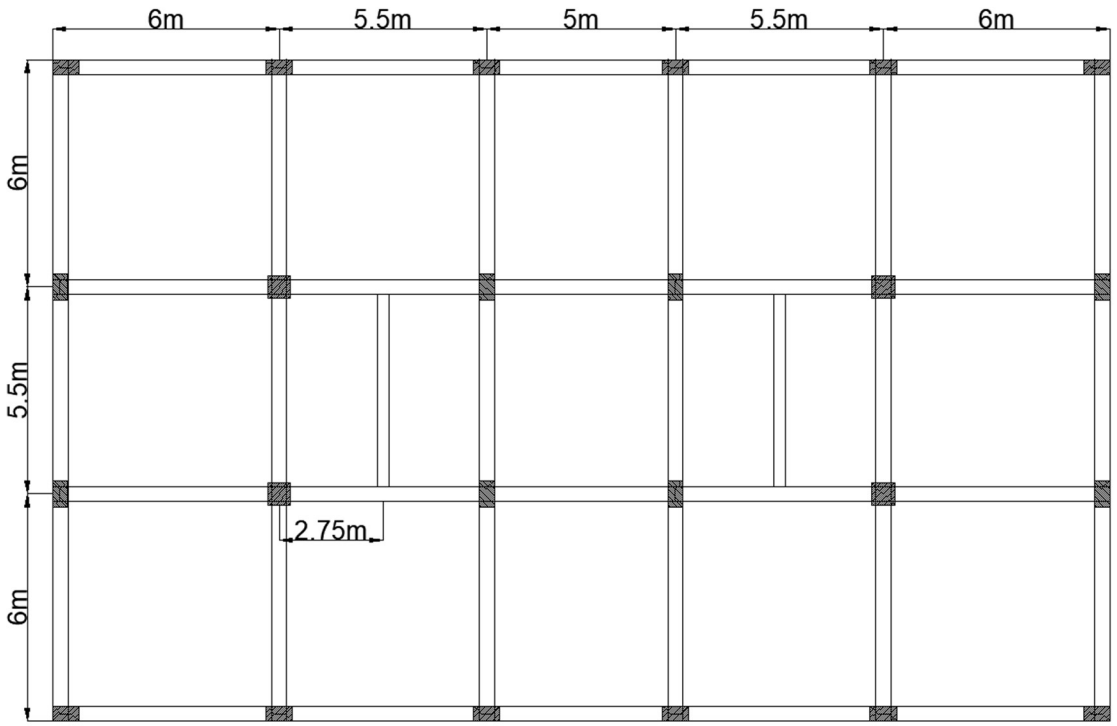

Figure 3.8. The structural plan of the moment resisting frame

The structural materials are chosen similar to current Turkish practice. C30 concrete and S420 reinforcement are used. The seismic design is conducted according to the Turkish Earthquake Regulation (TER-2018) for a design earthquake level of DD-2. It has a return period of 475-years and is typical for residential structures. The location of the structures selected as Kadıköy, Istanbul, with coordinates 40.993505N and 29.036987E. This specific location has a high seismic demand within Turkish seismic risk definitions. Seismic parameters for earthquake loads are obtained from the "https://tdth.afad.gov.tr". The soil type is selected as ZC. The design spectrum is calculated according to TER-2018 definitions, which are stated in Section 2.3.4 in the regulation and summarized in Equations 3.6, 3.7, 3.8, 3.9, and 3.10. The S_{DS} and S_{D1} values are computed as 1.15 and 0.40, respectively.

$$S_{ae}(T) = \left(0.4 + 0.6\frac{T}{T_A}\right)S_{DS}, \qquad 0 \le T \le T_A \tag{3.6}$$

$$S_{ae}(T) = S_{DS}, \qquad T_A \le T \le T_B \tag{3.7}$$

$$S_{ae}(T) = \frac{S_{D1}}{T}, \qquad T_B \le T \le T_L \tag{3.8}$$

$$S_{ae}(T) = \frac{S_{D1}T_L}{T^2}, \qquad T_B \le T \le T_L \tag{3.9}$$

$$T_A = 0.2\frac{S_{D1}}{S_{DS}}, \qquad T_B = 0.2\frac{S_{D1}}{S_{DS}}, \qquad T_L = 6s \tag{3.10}$$

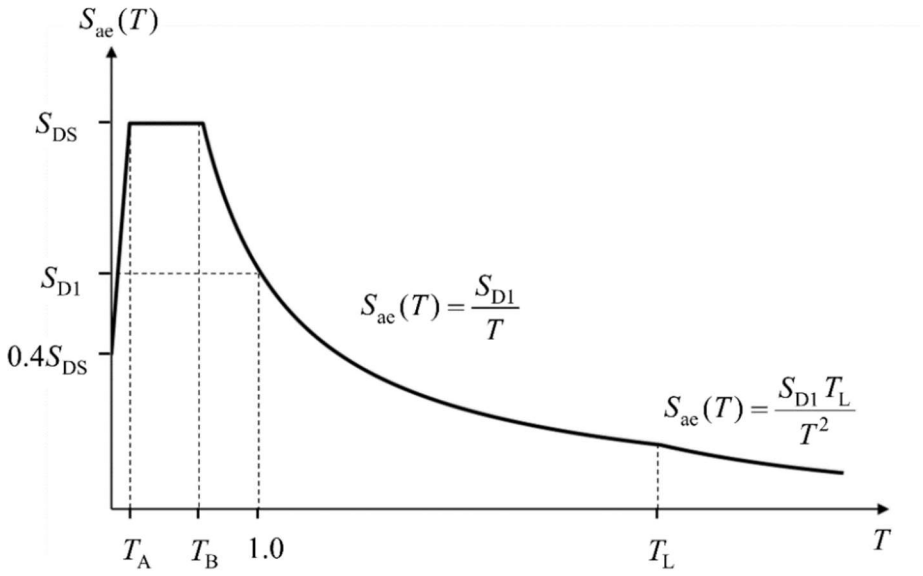

Figure 3.9. The elastic design spectrum from TER-2018

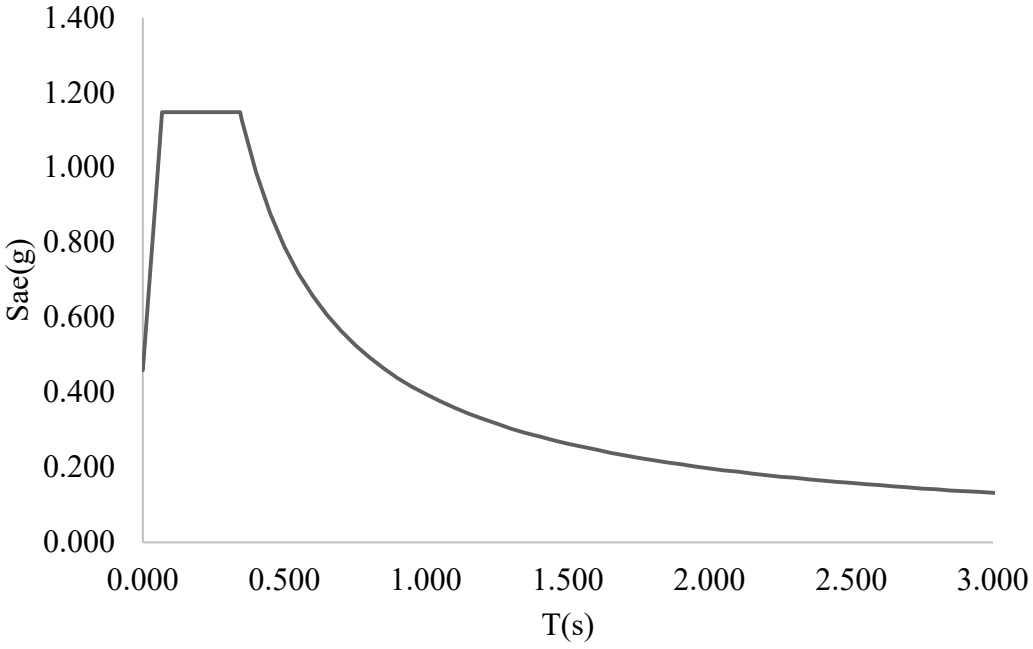

Figure 3.10. The calculated elastic design spectrum for DD-2 level

The building importance coefficient is taken as 1.0 according to Table 3.1 of the TER-2018 and represented in Table 3.2 in this study.

According to the structural system of the building from Table 4.1 of the TER-2018, the response modification (R) and overstrength factors (O) of the frame are 8 and 3, respectively. The table is given in Table 3.3. Since the building height class is 5, the requirement of being greater than 2 for allowable building height class is met.

The effective stiffness multipliers of the structural elements in the linear model of the moment resisting frame are determined according to Table 4.2 of the TER-2018 which is repeated in Table 3.4. The effective stiffness multipliers for flexure in columns and beams are taken as 0.7 and 0.35 respectively.

Slab Thickness:

The minimum slab thickness is calculated according to article 11.4.2 of TS500. The requirement is defined by the formula presented in Equation 3.11. The slab thickness is chosen as 15 cm for the whole structure to cover all the slabs and avoid varying the slab thickness in a story. The slab is modeled as a rigid diaphragm in numerical modeling.

$$h \geq \frac{l_{sn}}{15+\frac{20}{m}}\left(1-\frac{a_s}{4}\right) \tag{3.11}$$

h: slab thickness

l_{sn}: span of the slab in short direction

α_s: the ratio of the total of the slab continuous edge lengths to the total of the edge lengths

m: the ratio of the long side of the slab to the short side, (l_l/l_s)

Table 3.2. Building Importance Coefficients

Building Occupancy Category	Usage of Building	Building Importance Factor (I)
BKS=1	Buildings that need to be used after an earthquake, buildings which are densely populated for a long time, buildings which are used for protection to valuable article and buildings which contains hazardous material a) Buildings that need to be used after an earthquake (Hospitals, Fire Stations, PTT and other telecommunication facilities, Terminals, Power stations, Municipality buildings, First-aid and Disaster planning stations) b) Schools and other educational buildings, dormitories, military posts, prisons, etc. c) Museums d) Building used to store toxic and explosive things	1.5
BKS=2	Buildings which are densely populated for a short time Shopping Centers, Sport facilities, Cinema, Theatre and Concert Hall, and Sanctuary etc.	1.2
BKS=3	Other Buildings which are not given in the BKS=1 and BKS=2 explanations (Houses, workplaces, hotels, industrial structures as buildings, etc.)	1.0

Table 3.3.Structural System Behavior Coefficient, Resistance Excess Coefficient and Permissible Building Height Classes for Building Structural Systems

Load Bearing System	Response Modification Factor (R)	Overstrength Factor (O)	Building Height Class (BYS)
A. CAST IN PLACE REINFIRCED CONCRETE LOAD BEARING SYSTEMS			
A1. HIGH DUCTILITY SYSTEMS			
A11. Buildings that resist earthquake loads by concrete moment resisting frames	8	3	BYS≥3
A12. Buildings that resist earthquake loads by coupled shear walls	7	2.5	BYS≥2
A13. Buildings that resist earthquake loads by solid shear walls	6	2.5	BYS≥2

Table 3.4.Effective Section Stiffness Factors of Reinforced Concrete Structural System Elements

Reinforced Concrete Load Bearing System Member	Effective Stiffness Factor	
Shear Wall-Slab (In-plane)	***Axial***	***Shear***
Shear Wall	0.50	0.50
Basement Shear Wall	0.80	0.50
Slab	0.25	0.25
Shear Wall-Slab (Out-plane)	***Bending***	***Shear***
Shear Wall	0.25	1.00
Basement Shear Wall	0.50	1.00
Slab	0.25	1.00
Frame Member	***Bending***	***Shear***
Coupling Beam	0.15	1.00
Frame Beam	0.35	1.00
Frame Column	0.70	1.00
Shear Wall (Equivalent Frame)	0.50	0.50

Beam Dimensions:

Preliminary decisions of the beam heights are based on the TS500 definitions for the beams that do not carry brittle partition elements. The needed maximum height of the beams is calculated as 55 cm. The shear safety of beam-column joint governs the width of the beam and 40x55 cm beams have been selected. According to the results of the analysis with the earthquake loads, the final design decisions of the beams' dimensions and the reinforcement ratios are given in Table 3.5. The layout of the beam types is shown in Figure 3.11. Transverse reinforcements are selected as 2ϕ8 with 8 cm spacing in critical region. A typical example of reinforcement detailing of beams is given in Figure 3.12.

Table 3.5. The designed beam types, dimensions, and tension reinforcement ratios

Beam Type	Dimensions	ρ (Tension)	Reinforcement Placement (Top/Bottom/Middle)
TYPE 1	40x55cm	0.86%	2Φ22/5Φ22/2Φ22+2Φ22
TYPE 2	30x55cm	0.57%	2Φ20/3Φ20/2Φ20
TYPE 3	40x55cm	0.57%	2Φ20/4Φ20/2Φ20+2Φ20
TYPE 4	40x55cm	1.00%	2Φ22/6Φ22/2Φ22+2Φ22

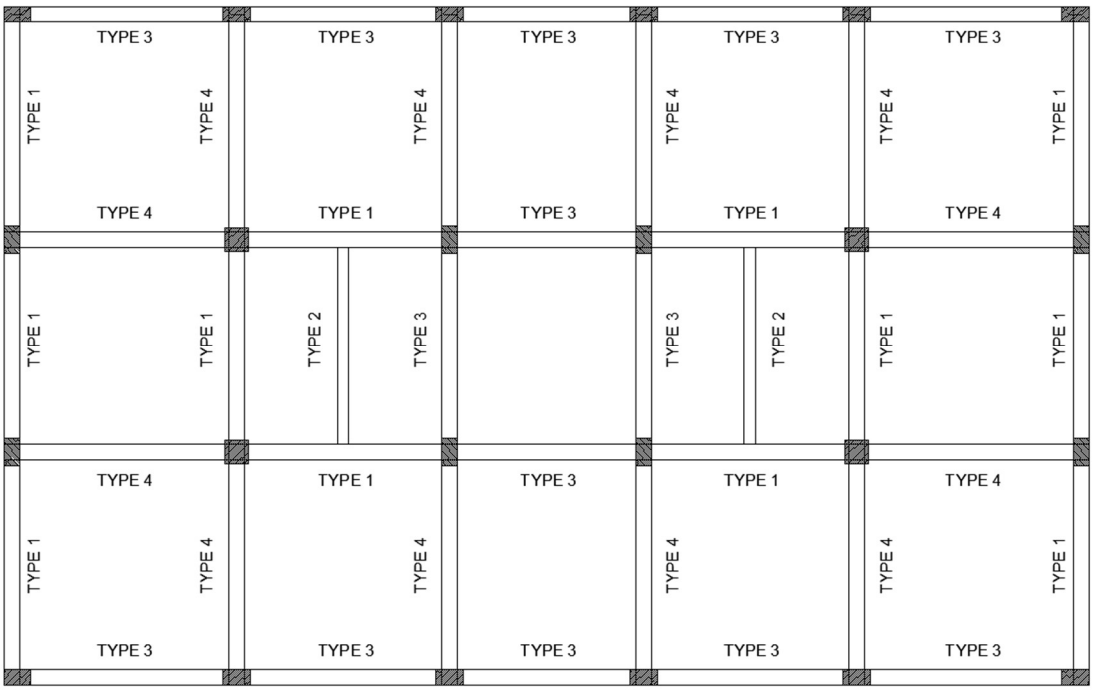

Figure 3.11. The layout of beams

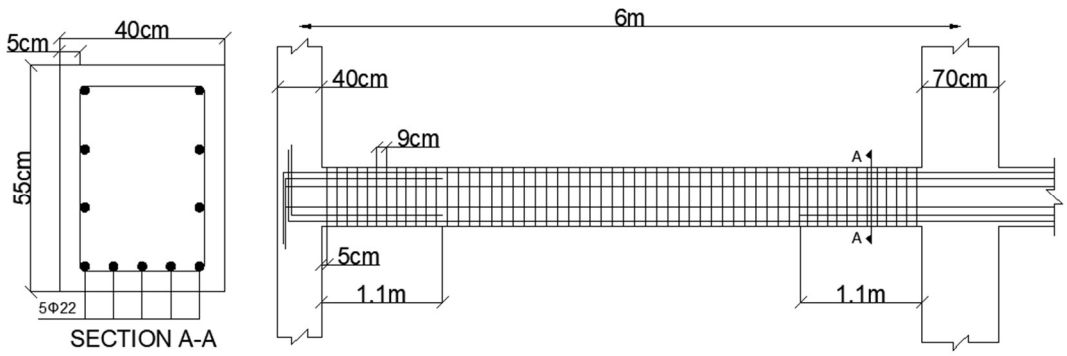

Figure 3.12.The section and reinforcement detailing of Type 1 beam in the MRF design

Column Dimensions:

The preliminary cross sections are defined considering the loads from tributary areas. The limit stated in the 7.7 section of the TS500, which $0.9f_{cd}A_c$ is used. 40x70 cm columns are selected as preliminary dimensions. After the analysis, the column dimensions and reinforcement ratios are calculated according to the TS500 and TER-2018 regulations, and the final decisions are presented in Table 3.6. The layout of the columns and the types are shown in Figure 3.13. According to the TER-2018 in the stirrup confinement area the stirrups are selected as 4ϕ12 with 8 cm spacing in both x and y directions. The requirements are provided in compliance with 7.5.2.3(a) for the 60x60 cm columns. The requirements are provided in compliance with 7.5.2.3(a) for the 40x70 cm columns. A typical example of reinforcement detailing of columns is given in Figure 3.14.

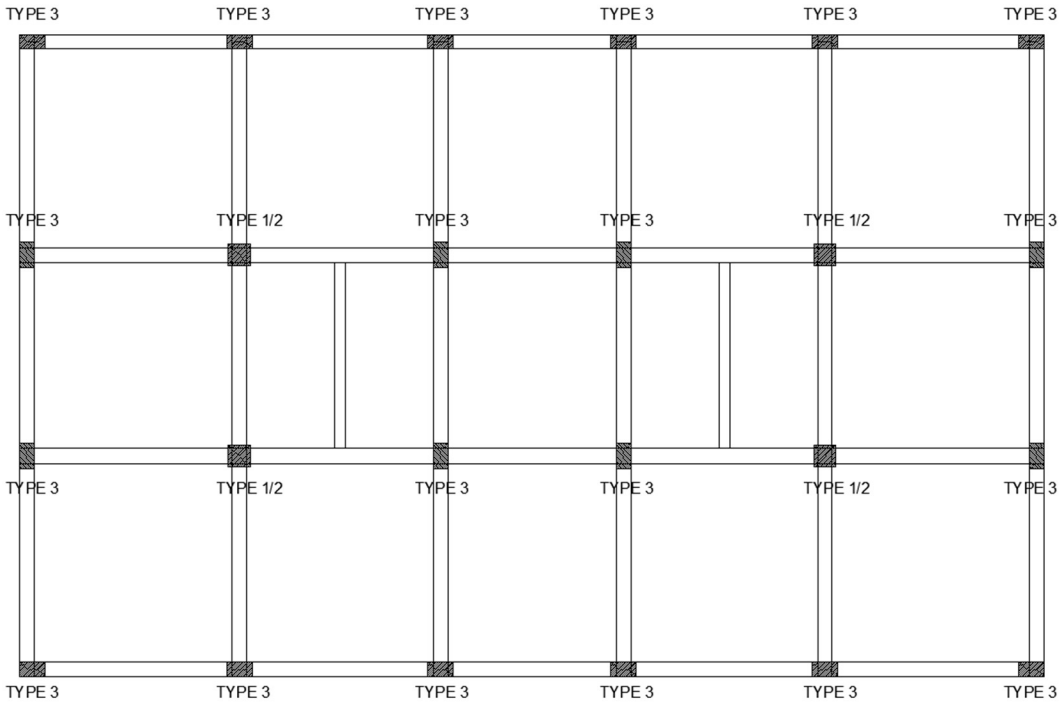

Figure 3.13. The layout plan of column types

Table 3.6.The designed column types, dimensions, and longitudinal reinforcement ratios

Column Type	**Dimensions**	**ρ**	**Reinforcement Placement (Top/Bottom/Middle)**
TYPE 1	60x60cm	1.9%	5Φ22/5Φ22/4Φ22+4Φ22
TYPE 2	60x60cm	1.6%	5Φ20/5Φ20/4Φ20+4Φ20
TYPE 3	40x70cm	1.7%	5Φ22/5Φ22/3Φ22+3Φ22

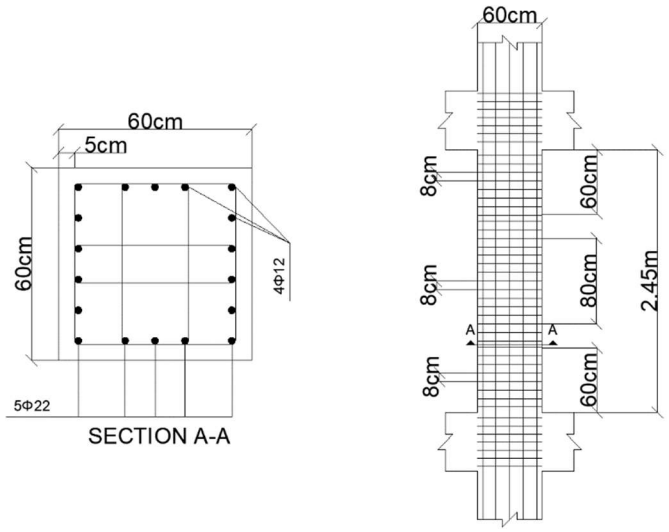

Figure 3.14. The section and reinforcement detailing of Type 1 column in the design

3.4. Frame with Shear Walls

The structure has 3 m story height and consists of six stories. The total height of the building is 18 meters. The floor plan and the dimensions of the structure are presented in Figure 3.15.

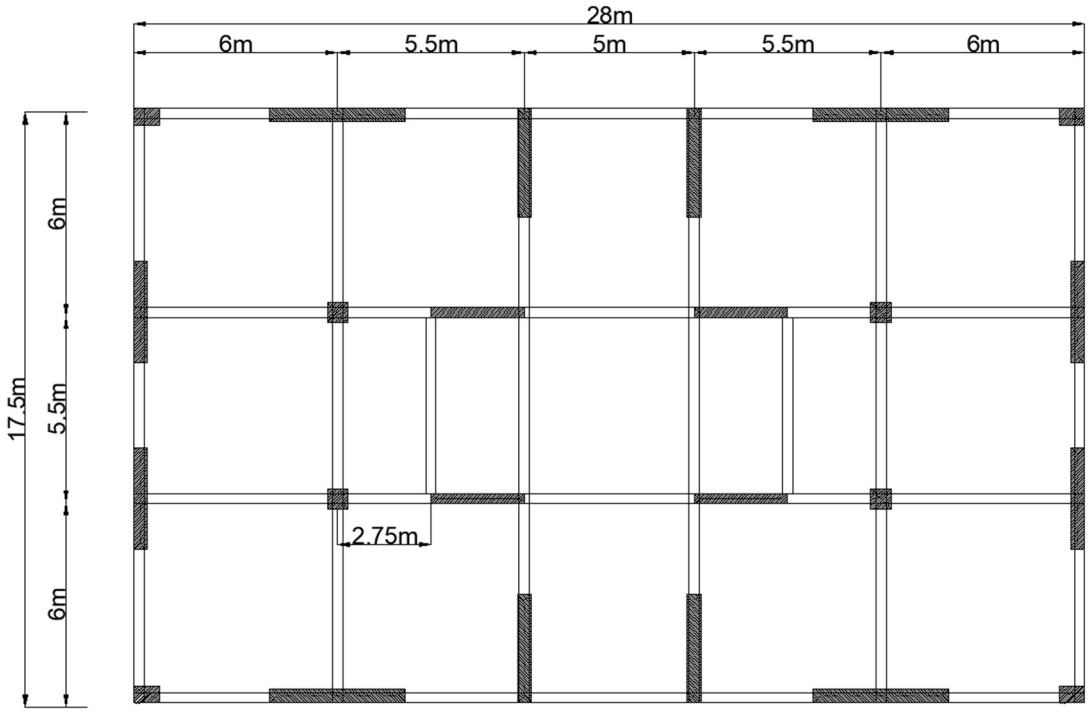

Figure 3.15. The structural plan of the reinforced concrete system with shear frame

In the design of the structure, the same concrete and reinforcement steel grades are used as used in the moment resisting frame. Also, the same procedure is followed in this building for the seismic design according to the Turkish Earthquake Regulation (TER-2018). Since the frame is assumed to be at the same location as the moment frame, the same design spectrum is valid.

The building importance coefficient is taken as 1.0 according to Table 3.1, which states TER-2018, as well as given in Table 3.2 in the previous section.

The response modification factor (R) and overstrength factor (O) are defined as 6 and 2.5, respectively, per Table 4.1 of the TER-2018 and which was repeated in Table 3.3. Same values are defined for both directions of the frame. The overturning moment control is performed, and the factors are selected in compliance with this control. Since the building height class is 5, it also meets the requirement of being greater than 2 in this analysis.

Effective stiffness multipliers of the elements are determined according to Table 4.2 in TER-2018 for use in earthquake-effective load combinations. The effective stiffness multiplier for the column and beam flexure is taken as 0.7 and 0.35, respectively. The axial and shear factors for the shear wall are taken as 0.5.

Slab Thickness:

The minimum slab thicknesses were calculated according to the TS500 requirement that is repeated in Equation 3.11. A constant value of chosen as 15 cm for the whole structure. The slab is modeled as a rigid diaphragm.

Beam Dimensions:

The height of beams is determined according to Table 13.1 in TS500. The maximum height for the beams' height is calculated as 50 cm for beams in the grids and 55 cm for beam indirect supported by beams, and 55 cm is applied only to beam indirect supported by beams. Other beams' height is selected as 50 cm due to the column-beam joint shear requirements according to the TER-18, and width of beams is selected as 30 cm. According to the results of the analysis with the earthquake loads, the final design decisions of the beams' dimensions and the reinforcement detailing are given in Table 3.7. The layout of the beam types of the building is shown in Figure 3.16. Transverse

reinforcements are selected as 2ϕ8 with 8 cm spacing in critical region. A typical example of reinforcement detailing of beams is given in Figure 3.17.

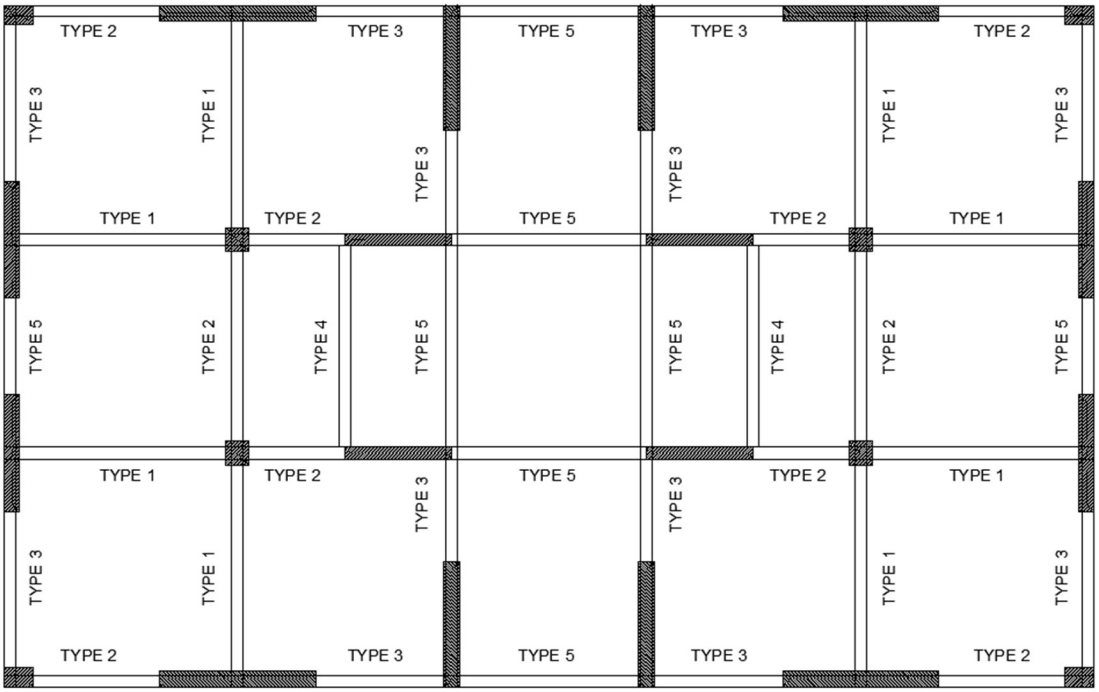

Figure 3.16. The layout plan of beam types

Table 3.7. The designed beam types, dimensions, and tension reinforcement ratios

Beam Type	**Dimensions**	**ρ (Tension)**	**Reinforcement Placement (Top/Bottom/Middle)**
TYPE 1	30x50cm	1.3%	3Φ22/5Φ22/2Φ22+2Φ22
TYPE 2	30x50cm	1.3%	2Φ22/5Φ22/1Φ22+1Φ22
TYPE 3	30x50cm	0.83%	2Φ20/4Φ20/1Φ20+1Φ20
TYPE 4	30x55cm	0.57%	2Φ20/3Φ20/1Φ20+1Φ20
TYPE 5	30x50cm	0.62%	2Φ20/3Φ20/1Φ20+1Φ20

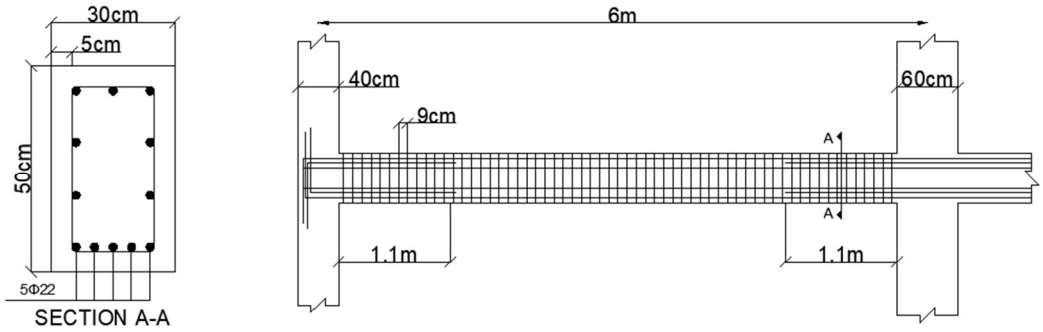

Figure 3.17. The section and reinforcement detailing of Type 1 beam in the design

Column Dimensions:

The same procedure is followed in preliminary decision of the columns dimensions as used in moment resisting frame. Columns sections are kept as 40x70 cm initially, similar to moment frame. After the analysis, the column dimensions are updated and reinforcement detailing are designed according to the TS500 and TER-2018 regulations, and the final decisions are given in Table 3.8 and the layout is presented with shear walls in Figure 3.19. The 60x60 cm columns are required due to column-beam joint shear control. According to the TER-2018 in the stirrup confinement area the stirrups are selected as 4ϕ12 with 8 cm spacing in both x and y directions. The requirements are provided in compliance with 7.5.2.3(a) for the 60x60 cm columns. According to the TER-2018 in the stirrup confinement area the stirrups are selected as 4ϕ12 with 8 cm spacing in both x and y directions. The requirements are provided in compliance with 7.5.2.3(a) for the 50x75 cm columns. A typical example of reinforcement detailing of beams is given in Figure 3.18.

Table 3.8. The designed column types, dimensions, and reinforcement ratios

Column Type	Dimensions	ρ	Reinforcement Placement (Top/Bottom/Middle)
TYPE 1	60x60cm	1.5%	4Φ20/4Φ20/3Φ20+3Φ20
TYPE 2	50x75cm	1.2%	4Φ22/4Φ22/3Φ22+3Φ22

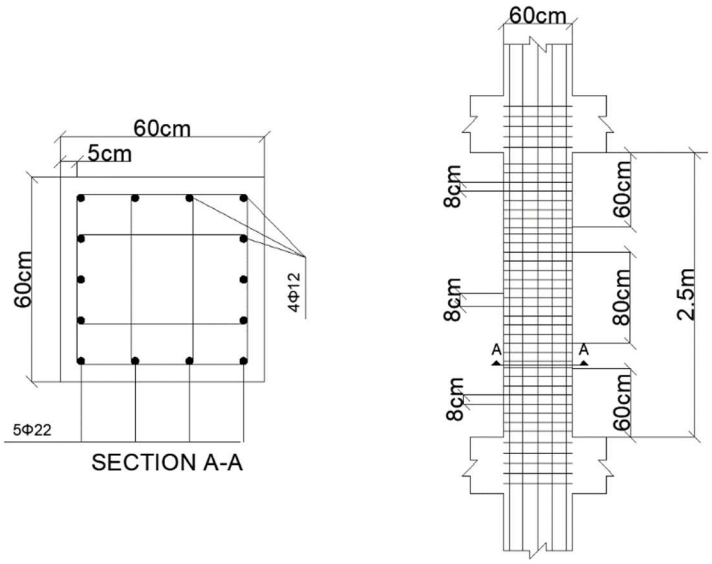

Figure 3.18. The section and reinforcement detailing of Type 1 column in the design

Shear Wall Dimensions:

The shear wall dimensions are selected considering the experience from the Hassan and Sozen (1997) index studies and the TER-2018 requirements. The final dimensions are given in Table 3.9. The column and shear wall types of the building and the layout are presented in Figure 3.19. In the first story, Type 4 is used and in the other stories Type 5 is used. In shear wall transverse reinforcement design, 4ϕ12 are selected in confined zone at the edges in shear walls with 8 cm spacing.

Table 3.9. The designed shear wall types, dimensions, and reinforcement ratios

Shear Wall Type	**Dimensions**	**ρ (Confined Zone)**	**Reinforcement Placement (Confined/Middle)**
TYPE 1	40x400cm	2.9%	(4Φ26/4Φ26/2Φ26+2Φ26+2Φ26)/46Φ26
TYPE 2	30x275cm	1.7%	(4Φ24/4Φ24/2Φ24+2Φ24)/32Φ24
TYPE 3	40x300cm	2.5%	(4Φ24/4Φ24/2Φ24+2Φ24)/22Φ24
TYPE 4	40x320cm	2.8%	(4Φ22/4Φ22/2Φ22+2Φ22+2Φ22)/38Φ22
TYPE 5	40x320cm	2.5%	(4Φ20/4Φ20/2Φ20+2Φ20+2Φ20)/46Φ20

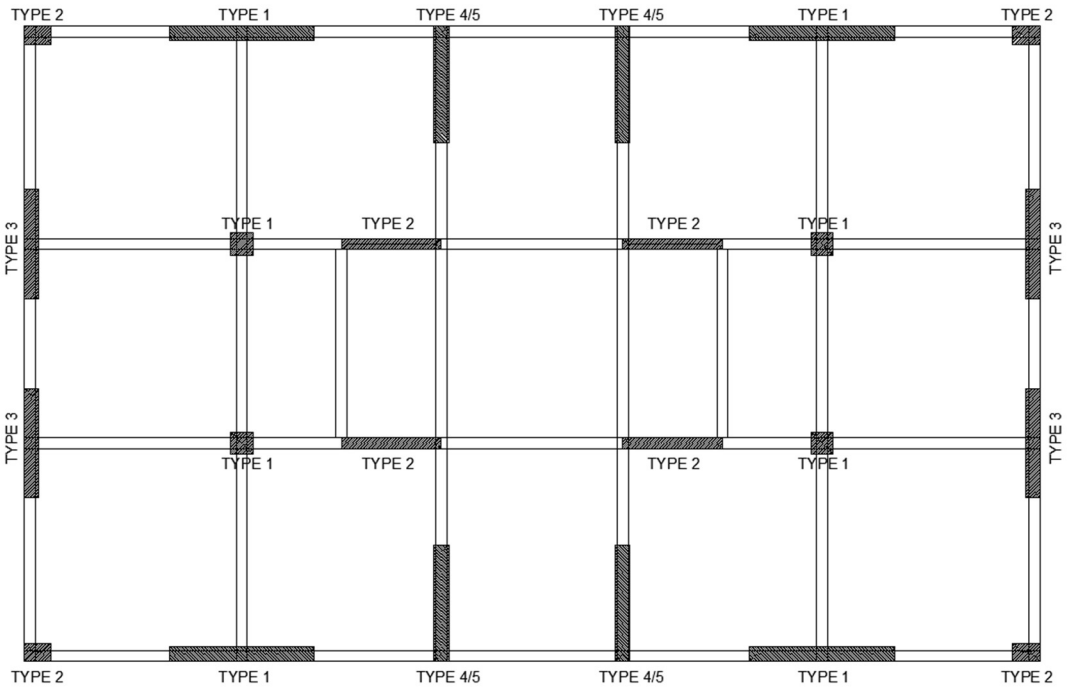

Figure 3.19. The layout plan of column and shear wall types

3.5. Selected Ground Motion Set for the Time History Analysis

The selection of the ground motions is done for the design spectra adopted from the AFAD (Disaster and Emergency Management Presidency) website for the location of Kadıköy Municipality with the coordinates of 40.993505N and 29.036987E. The selected region is not subjected to near-fault effects. According to the live fault line map provided by MTA, the selected coordinates are more than 15 km away to the nearest fault. The local soil is selected as type ZC. Target spectra for DD-1, DD-2, and DD-3 are adopted from the AFAD website. Ground motions were selected using the PEER Ground Motion Database NGA-West2. Target spectra are loaded onto the PEER NGA West2 website, which is used to get the ground motion records. A pulse-like filter is activated during the selection of the ground motion. It is reported by Kardoutsou (2017) that if the pulse indicator is greater than 0.65, records are called pulse-like, and could have a compulsive effect on the structure. Hence, pulse-like ground motions are eliminated to avoid such effects.

Ground motions are scaled automatically in the PEER database. However, in accordance with TER-18, the selected scale factors of ground motions are re-arranged. The TER-18 required ground motions to be scaled to develop an average spectrum of the selected ground motions to be greater by at least thirty percent than the target spectrum between 0.2T and 1.5T. Here, T is the period of the target structure considering the effective stiffness.

The initial periods of the designed structures are presented in Table 3.10. As mentioned, the mean of the ground motions should be greater than 1.3 times between 0.2T and 1.5T; this rule is satisfied in the scale factor determination. Although the TER-18 states that the scale factors should be larger than 0.25 and less than 4, in this study the maximum scale factor is taken as 3 with the lowest scale factor of 0.75 for DD-2 event. It is required to have at least 11 records and a maximum of three records could be from the same earthquake. The same scaling factor applies to both components of the motions.

Table 3.10. The periods in both direction of the structures

	T_1 (X-direction)	T_2 (Y-direction)
Moment Resisting Frame	1.11	1.17
Frame with Shear Walls	0.61	0.7

The selected and scaled ground motion sets are given in Table 3.11-3.13 and in Figure 20-22. The acceleration spectra in the figures are a combination of both directions.

During the ground motion selection and scaling, the PGV of the composite spectrum for DD-2 level earthquake is attempted to be kept around 50cm/s PGV. This is typical PGV value for the design level earthquake.

Table 3.11: The selected ground motion sets for DD-1 level earthquake

PEER ID	Earthquake	Year	Station	Mw	Vs30	Scale Factor
6	Imperial Valley-02	1940	El Centro Array #9	6.95	213	3.0
20	Northern Calif-03	1954	Ferndale City Hall	6.50	219	3.0
30	Parkfield	1966	Cholame - Shandon Array #5	6.19	290	2.7
68	San Fernando	1971	LA - Hollywood Stor FF	6.61	316	2.7
95	Managua_ Nicaragua-01	1972	Managua_ ESSO	6.24	289	3.0
96	Managua_ Nicaragua-02	1972	Managua_ ESSO	5.20	289	2.9
1147	Kocaeli_ Turkey	1999	Ambarli	7.51	175	1.8
1158	Kocaeli_ Turkey	1999	Duzce	7.51	282	2.5
1617	Duzce_ Turkey	1999	Lamont 375	7.14	454	2.0
8165	Duzce_ Turkey	1999	IRIGM 496	7.14	760	1.3
8166	Duzce_ Turkey	1999	IRIGM 498	7.14	425	1.9

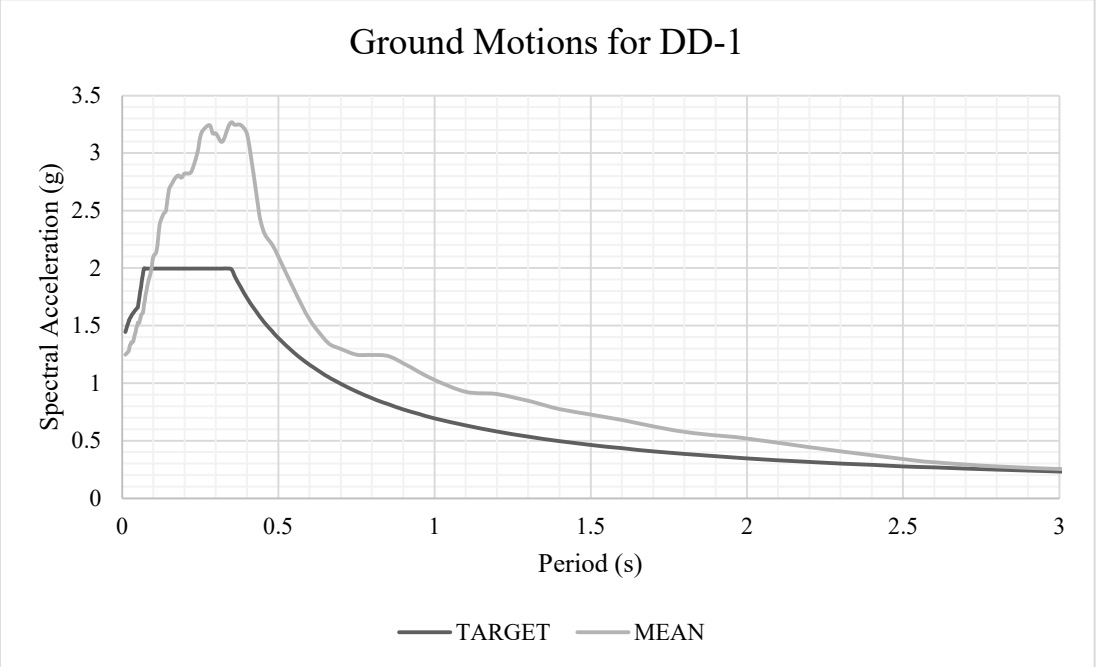

Figure 3.20. The target ground motion level and the mean of the selected ground motions for DD-1 level earthquake

Table 3.12: The selected ground motion sets for DD-2 level earthquake

PEER ID	Earthquake	Year	Station	Mw	Vs30	Scale Factor
14	Kern County	1952	Santa Barbara Courthouse	7.36	515	2.7
20	Northern Calif-03	1954	Ferndale City Hall,	6.50	219	2.0
31	Parkfield	1966	Cholame - Shandon Array #8	6.19	257	2.5
57	San Fernando	1971	Castaic - Old Ridge Route	6.61	450	2.5
70	San Fernando	1971	Lake Hughes #1	6.61	425	2.5
95	Managua_ Nicaragua-01	1972	Managua_ ESSO	6.24	289	1.1
96	Managua_ Nicaragua-02	1972	Managua_ ESSO	5.20	289	2.5
1166	Kocaeli_ Turkey	1999	Iznik	7.51	477	3.0
3744	Cape Mendocino	1992	Bunker Hill FAA	7.01	566	1.1
4458	Montenegro_ Yugoslavia	1979	Bunker Hill FAA	7.10	319	1.3
6962	Darfield_ New Zealand	2010	Bunker Hill FAA	7.00	296	0.75
8166	Duzce_ Turkey	1999	IRIGM 498	7.14	425	1.5

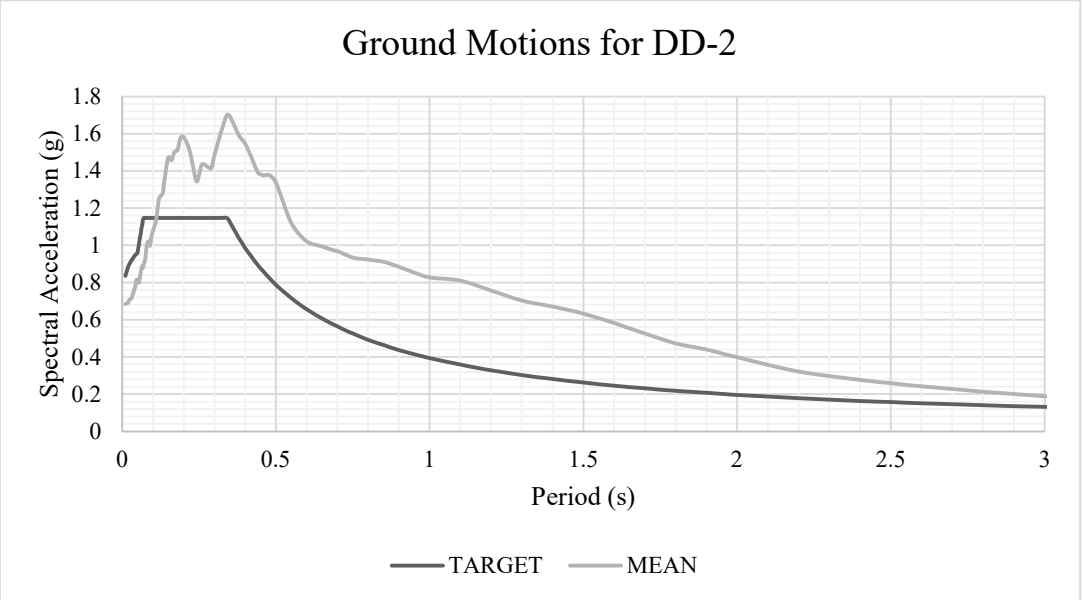

Figure 3.21. The target ground motion level and the mean of the selected ground motions for DD-2 level earthquake

Table 3.13: The selected ground motion sets for DD-3 level earthquake

PEER ID	Earthquake	Year	Station	Mw	Vs30	Scale Factor
6	Imperial Valley-02	1940	El Centro Array #9	6.95	213	0.4
8	Northern Calif-01	1941	Ferndale City Hall	6.40	219	2.1
11	Northwest Calif-03	1951	Ferndale City Hall	5.80	219	2.3
30	Parkfield	1966	Cholame - Shandon Array #5	6.19	289	0.5
50	Lytle Creek	1970	Wrightwood - 6074 Park Dr	5.33	486	2.1
70	San Fernando	1971	Lake Hughes #1	6.61	425	1.1
95	Managua_ Nicaragua-01	1972	Managua_ ESSO	6.24	289	0.4
96	Managua_ Nicaragua-02	1972	Managua_ ESSO	5.20	289	0.6
99	Hollister-03	1974	Hollister City Hall	5.14	199	1.9
102	Northern Calif-07	1975	Ferndale City Hall	5.20	219	2.7
1159	Kocaeli_ Turkey	1999	Eregli	7.51	0.06	0.8
8166	Duzce_ Turkey	1999	IRIGM 498	7.14	0.10	1.9

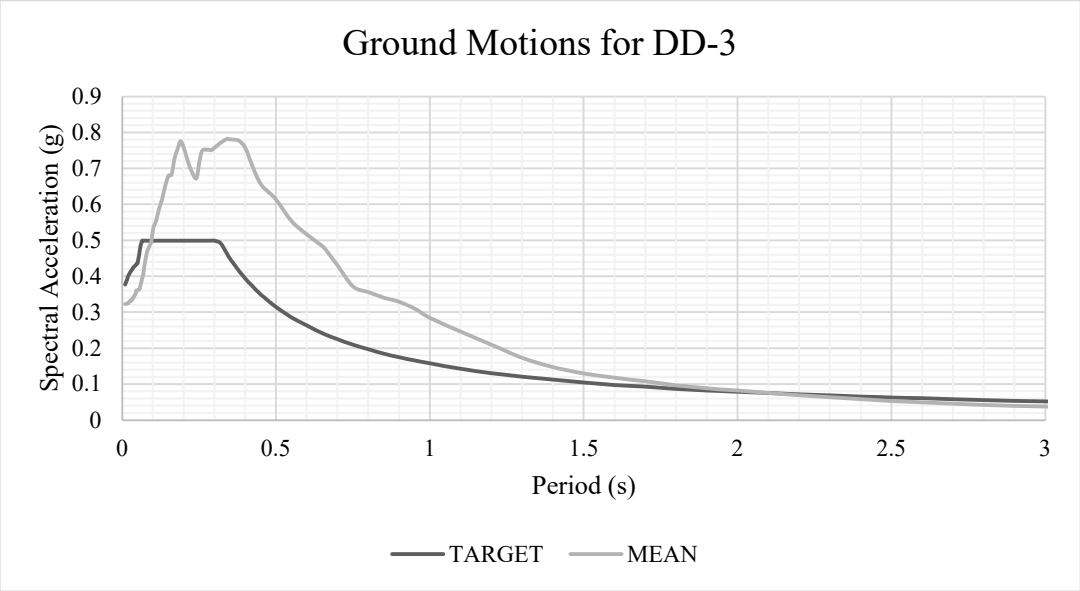

Figure 3.22. The target ground motion level and the mean of the selected ground motions for DD-3 level earthquake

CHAPTER 4

NONLINEAR ANALYSIS OF THE FRAMES

The frames defined in the previous chapter are subjected to a nonlinear analysis. The numerical model and the analysis results will be discussed in this chapter. The frames are modeled as 3D frames with OpenSees nonlinear analysis software (McKenna, 2010). OpenSees is a finite element analysis platform designed by McKenna. The beams, columns, and shear walls are modeled as wireframe elements. Slabs are not included as distinct elements to save run time in the analyses. The slab loads are directly applied to the beams by distributing the gravity loads along considering the probable yield lines. Since slabs do not exist in the models, diaphragm behavior is provided by defining corresponding constraints to joints at floor levels. Nonlinearity is simulated in a concentrated form for beams and columns and distributed form for shear walls. Hence, beams and columns are modeled with elastic frame elements along their length and concentrated nonlinear hinges at the ends. The shear walls are modeled with fiber elements with nonlinearity simulated at predefined integration points.

There are various elements and materials available in the OpenSees Platform. The selection set defined by Sönmez (2020) is adopted for the study. Sönmez proposed to use Concrete01 and Steel02 for the materials and beamWithHinges for the elements.

Among the available nonlinear modeling approaches lumped and distributed plasticity are the commonly used modeling approaches for the scale of the structures studied. Distributed and lumped plasticity model categories are decided based on the behavior that needs to be modeled. The lumped plasticity models use concentrated springs to represent sectional and material behavior and are typically suitable if the penetration of the nonlinearity can be estimated with a certain accuracy. On the other hand, distributed plasticity is preferred such an estimation is not possible. The lumped plasticity models are also preferred, if possible, to save run time.

The need for modeling the axial load flexure interaction necessitates the use of the fiber section approach for the columns. The section is divided into small parts called

fibers and material nonlinearity is assigned to these small fibers. Hence, nonlinearity is obtained directly from constitutive material models. Through the material models, the fiber-based elements could show cyclic behavior directly, hence could be used without explicit hysteresis definitions at the section or element level. It is also possible to simulate the axial load-moment interaction directly. The current models do not simulate the cyclic shear-flexure interaction. The fiber section analysis provides the moment-curvature response of the section. Nonlinear rotations are calculated with a constant curvature assumption at a predefined length. This length is called the plastic hinge length and typically defined to be half of the member depth. The probability of artificial axial loads due to the rigid diaphragms constraint at slab level on fiber section representation, concentrated moment-rotation hinges are used at the ends of the beams.

Distributed plasticity models could spread the plasticity to the entire length of the element. A fiber-based element model could be used for this purpose. In this approach, the nonlinearity in the element is followed at predefined number of stations. The sections at these stations are modeled as fiber sections to follow the moment-curvature histories. The element deformations could be obtained through integration along the member length. Distributed plasticity can be used in displacement-based and force-based formulations in OpenSees platform. Force-based elements are used in this study. The distributed plasticity approach was used for the shear walls in this study.

In OpenSees, use of fiber-based section in the plastic hinge region for beamWithHinges element permits the simulation of both lumped and distributed plasticity. If the lumped plasticity is preferred, the rest of the element is modeled as an elastic member. Such a selection enables the use of stiffness modifications in the member, which is typically defined by the codes as effective stiffness. This approach enables the introduction of the effects that could not explicitly be considered in the model. Reduction in the stiffness due flexural and shear cracking and slip of the bar at the joints are example of such effects. In this study, the lumped plasticity approach is adopted for the beams and columns due to its shorter run time and ease in application. This approach is permitted to be used by TER-2018, Article 5.3.1.

In numerical analysis, the material models are expected to represent realistic behavior. The fiber model enables us to obtain the hysteretic behavior at sectional and

element level. The confinement of concrete in the element by transverse reinforcement could also be modeled. Different concrete models are defined for unconfined and confined zones. The unconfined concrete region outside of the core area defined by transverse reinforcement is represented by plain concrete model. The confined concrete region in the core area shows increased stress and strain capacities. There are various material models to simulate confinement effects according to the arrangement and steel material properties. In this study, the Mander model was used for this purpose.

Concrete01 is used as the concrete material model. This model constructs uniaxial Kent-Scott-Park concrete material model with degraded linear unloading-reloading stiffness defined by Karsan and Jirsa and no tensile strength. The model's envelope and the hysteresis are presented in Fig 4.1 and Fig. 4.2.

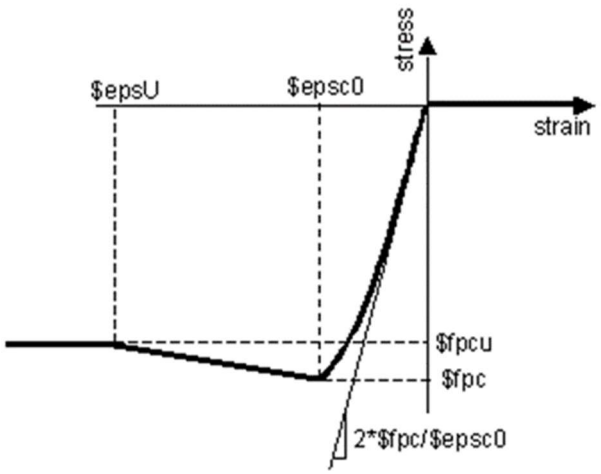

Figure 4.1. Stress-strain relationship of Concrete01 (Mazzoni et al., 2006)

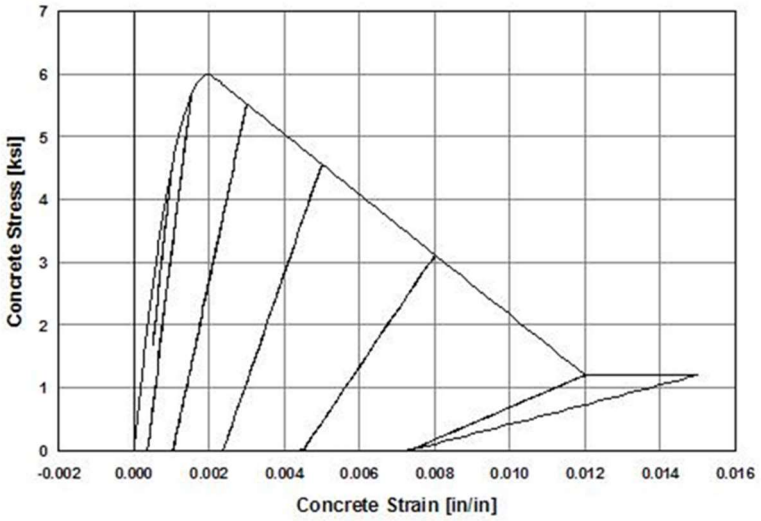

Figure 4.2. Example hysteretic behavior of Concrete01 (Mazzoni et al., 2006)

Steel02 is used as a steel reinforcement material model. The strain hardening ratio was taken as 1% in this study. Other parameters are taken as default values recommended in the OpenSees. The model's envelope and the hysteresis are presented in Fig 4.3 and Fig. 4.4.

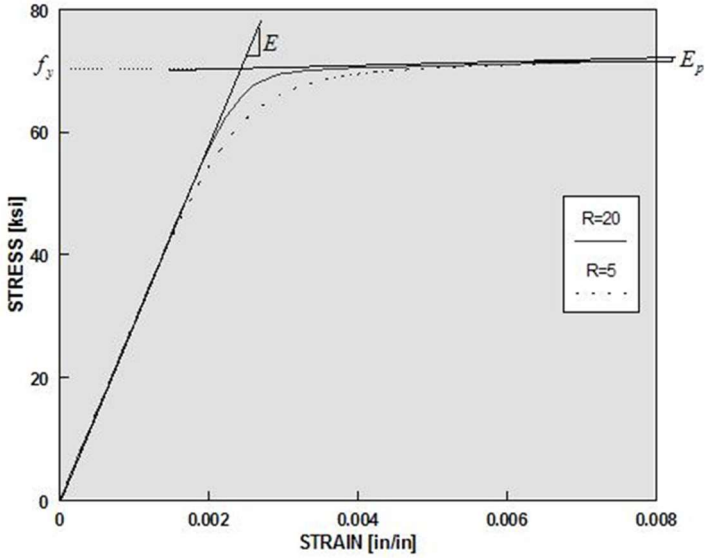

Figure 4.3. Steel02 Material – Material Parameters of Monotonic Envelope (Mazzoni et al., 2006)

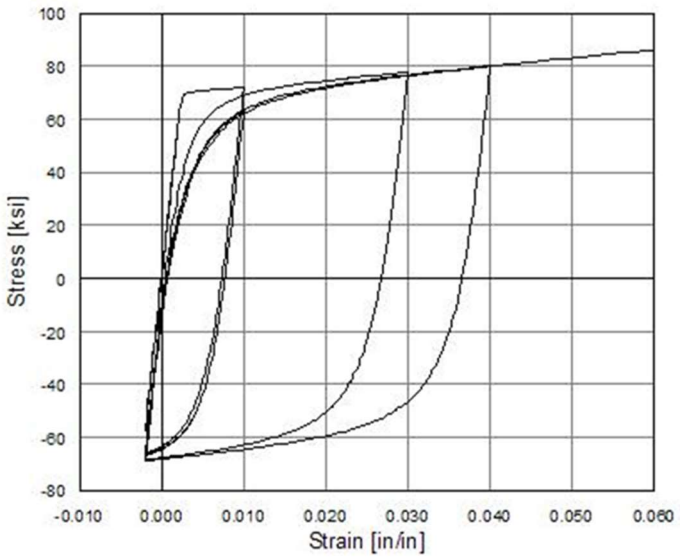

Figure 4.4. Steel02 Material – Material Parameters of Monotonic Envelope (Mazzoni et al., 2006)

The beamWithHinges (BWH) element type, Concrete01 concrete model, and Steel02 steel model were selected to be used for the nonlinear numerical modeling of the reinforced concrete frames in the OpenSees.

In the nonlinear time-history analysis 2% viscous damping was implemented and P-Δ effects are also considered during the analysis.

4.1. Moment Resisting Frame

The beams in the moment resisting frame are modeled by beamWithHinges as a lumped plasticity model in OpenSees. The plastic hinge lengths are selected as half of the height of the section as stated in article 5.4.2.3 of the Turkish Earthquake Regulation (2018). Nonlinear springs were simulated with the hysteretic material model of the software. The backbone of this model is obtained from the bilinear moment-curvature relation of the section. The bilinear curve is calculated by running a fiber section analysis of the related member and defining the needed parameters from its output.

The columns in the moment-resisting frame are modeled by beamWithHinges as a lumped plasticity model. The plastic hinge lengths are also selected by the same

procedure in the beams. Fiber-based sections are defined directly in the columns for simulating the axial load-moment interaction.

Effective stiffness was defined for the elastic length of the beam and column elements. According to Sozen (2003), half of the elastic stiffness is used for beams and columns.

4.2. Frame with Shear Walls

The beams and columns in the RC frame with shear walls are modeled similar to moment resisting frame. There are various options for modeling the shear walls in the OpenSees. SFI MVLEM, beam-column elements with fiber sections, and layered shells with plate fiber sections are examples of available models for shear walls. In this study, the forcebeamcolumn model was used since it has fiber-based approach in the entire element. Six integration points are defined along the member lengths at each story. This approach is preferred due to the fact that the plasticity in shear walls is not concentrated at the ends of the story levels. Shear walls could act like mega-members along the building height and depending on their lengths, plasticity could be distributed to full story height or further. It should also be noted that it is not possible to define effective stiffness with this approach. The shear walls are modeled as wireframes at the member centroid and rigid beams are defined from member axis to the end of the shear wall length at floor levels. The wire-frame visualization of the moment-frame is presented in Figure 4.5. The only difference of frame with shear walls is with the shear wall placements at which the center of the wall is used as the starting point of the element. It causes some shifts in the visualizations of the frame model.

According to the results of the nonlinear analysis in OpenSees, initial periods of the moment-resisting frame and frame with shear walls are 1.18-1.16s and 0.62 - 0.58s in two perpendicular directions, respectively.

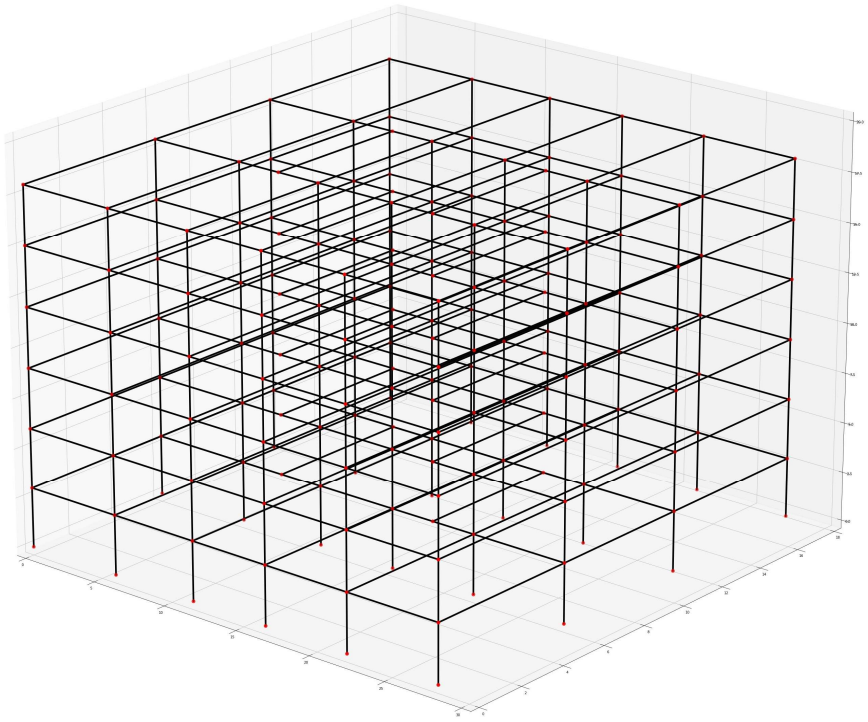

Figure 4.5. The visualization of the frame system in OpenSees

The inter-story drift ratios (IDR) for the maximum roof displacement and the envelope values at each story and the normalized displaced shape of the structures along X and Y- directions are presented in Figure 4.6 to 4.23. The results are provided for DD-1, DD-2 and DD-3 level earthquakes. The maximum displacement and drift values are also presented in Table 4.1. Results show that IDR in moment frame for DD-2 level are 1.95% for maximum roof drift and 2.03% for maximum envelope drift value. These values are in the vicinity of the 2% maximum interstory drift ratio defined in TER-2018 for DD-2 earthquake. It should be noted that this limit governs if the partition walls are insulated from the frame in engaging to resist the coming demands. Frame with shear wall maximum interstory drift ratio is 1.37% for the same event. If the DD-1 event is considered, the maximums are 2.87% and 1.88%, respectively for the moment and shear wall frame. The maximums drop to 0.6% for DD-3 earthquake level for both frames.

The deflected shape and the location of the maximum IDR are different for the frames. The moment frame deflected shape contains the characteristics of a sway frame with the maximum interstory deformations concentrated at the lower levels, specifically at the 1st and the 2nd levels, Fig. 4.6. The frame with shear walls deformed shape shows the characteristics of a cantilever and the maximum interstory deformations are taking place at the higher levels, specifically at the 5th and the 6th levels, Fig. 4.9.

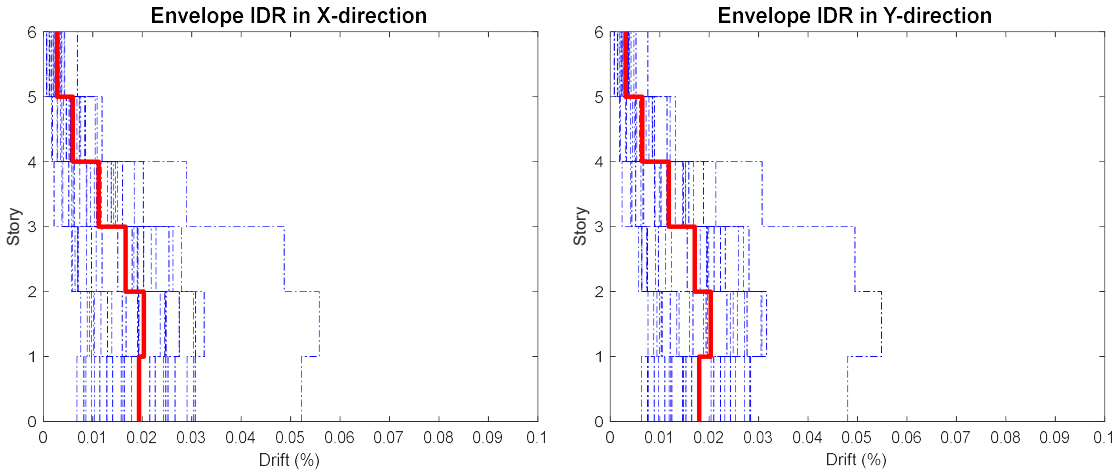

Figure 4.6. The inter story drift ratios along the X and Y directions of moment-resisting frame for the maximum envelope displacement in DD-2

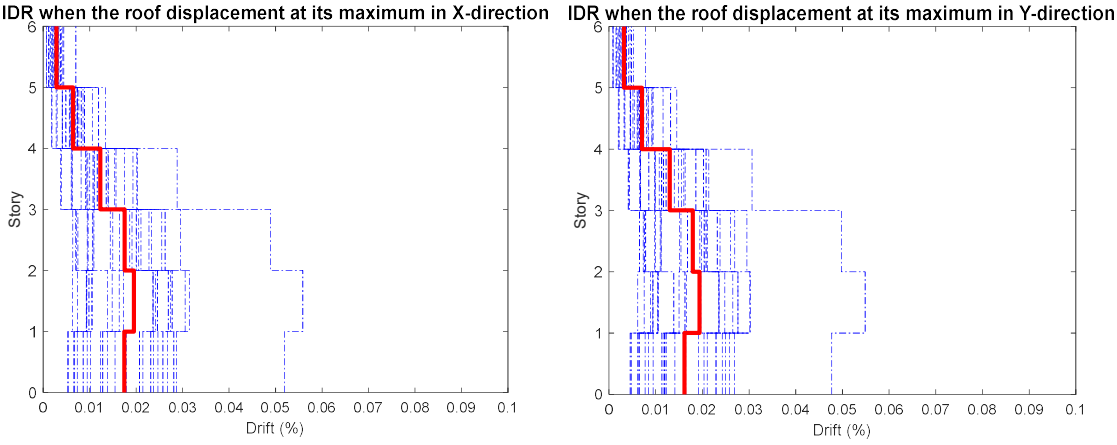

Figure 4.7. The inter story drift ratios along the X and Y directions of moment-resisting frame for when the roof displacement at its maximum in DD-2

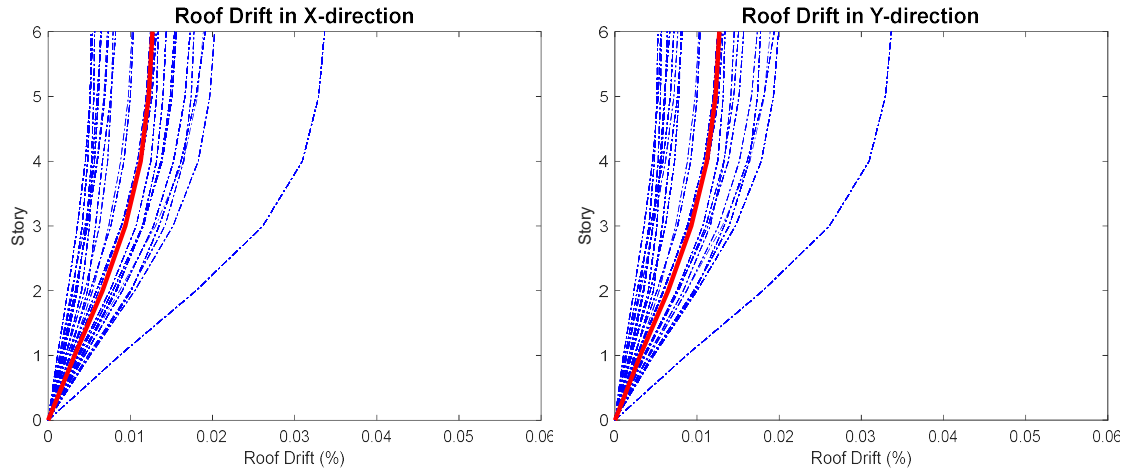

Figure 4.8. The maximum envelope roof drift shape along X and Y-directions of moment-resisting frame in DD-2

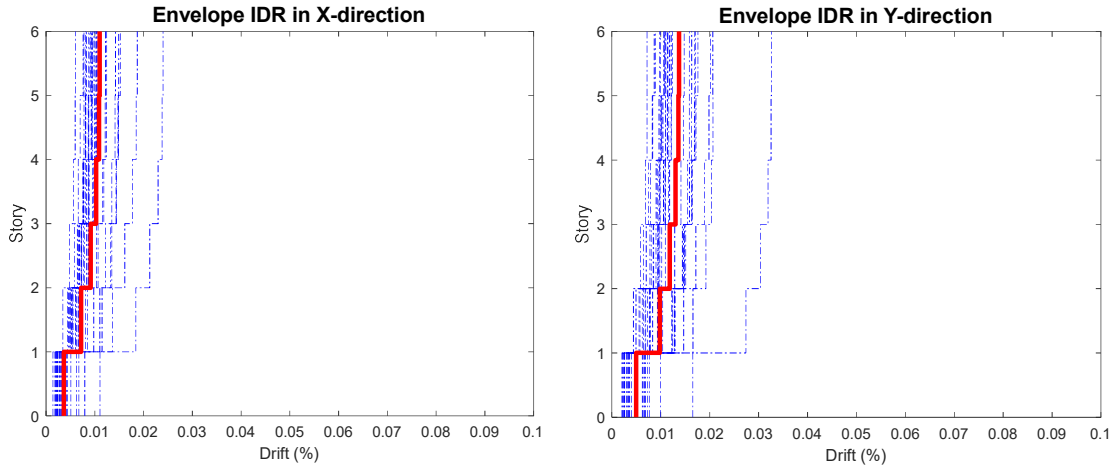

Figure 4.9. The inter story drift ratios along the X and Y directions of frame with shear walls for the maximum envelope displacement in DD-2

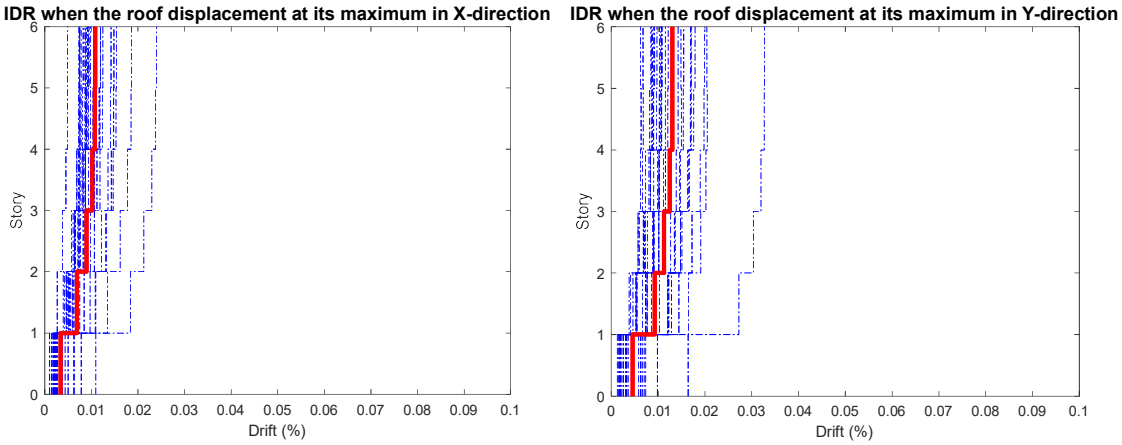

Figure 4.10. The inter story drift ratios along the X and Y directions of frame with shear walls for when the roof displacement at its maximum in DD-2

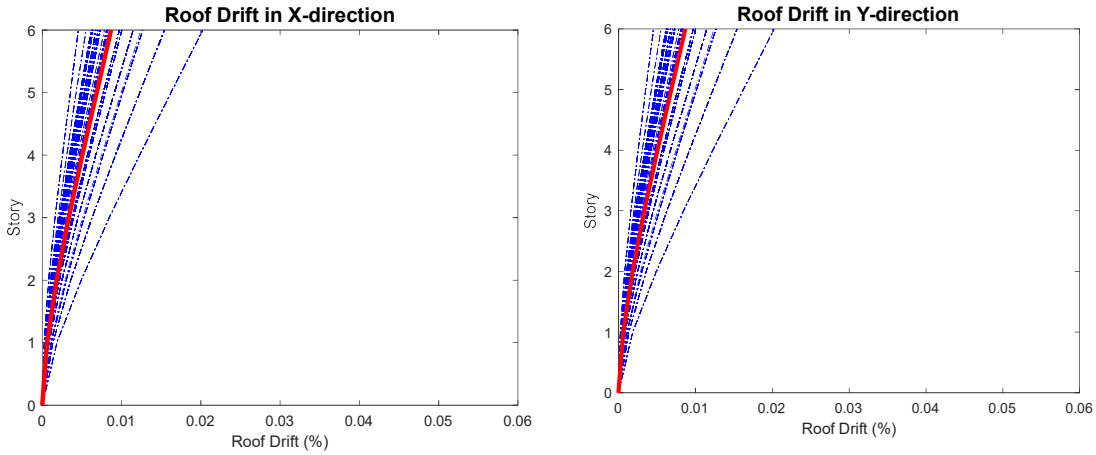

Figure 4.11. The maximum envelope displacement shape along X and Y-directions of frame with shear walls in DD-2

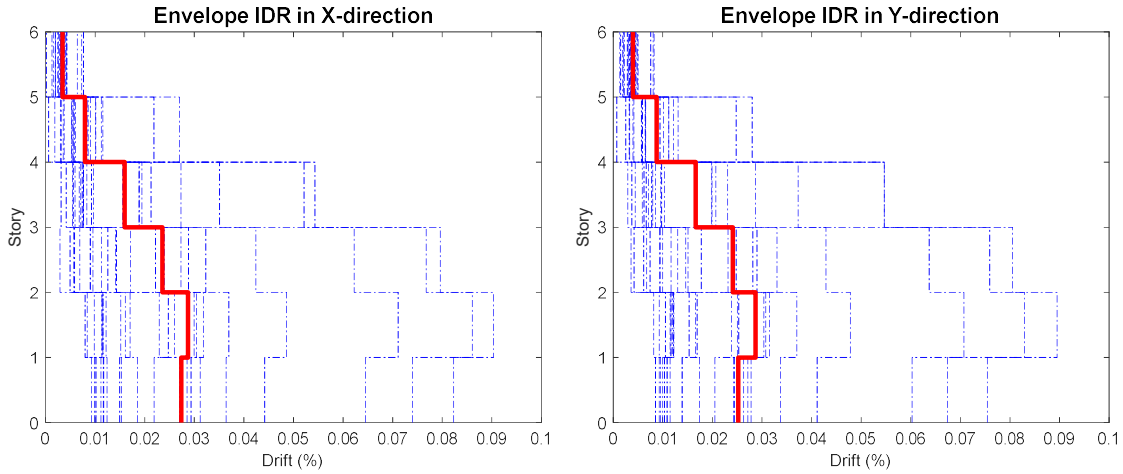

Figure 4.12. The inter story drift ratios along the X and Y directions of moment-resisting frame for the maximum envelope displacement in DD-1

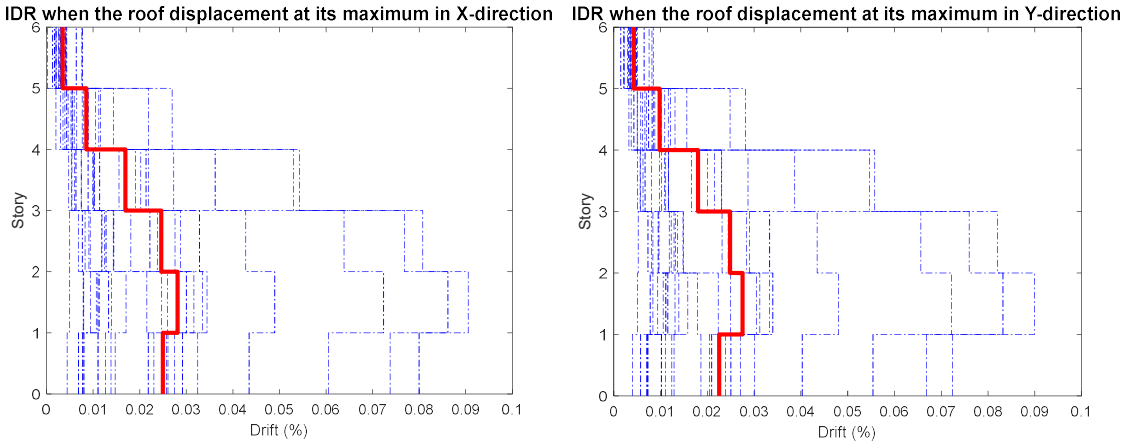

Figure 4.13. The inter story drift ratios along the X and Y directions of moment-resisting frame for when the roof displacement at its maximum in DD-1

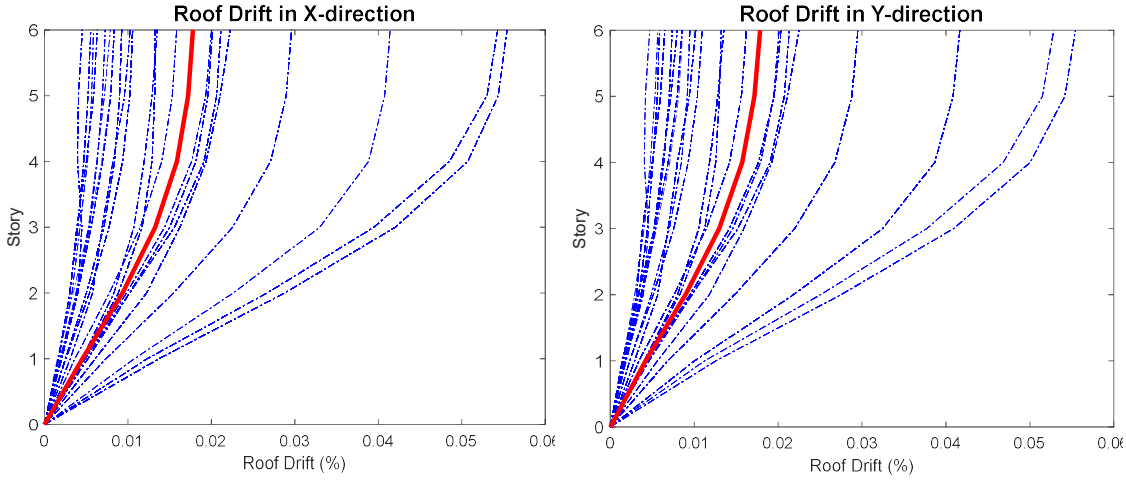

Figure 4.14. The maximum envelope displacement shape along X and Y-directions of moment-resisting frame in DD-1

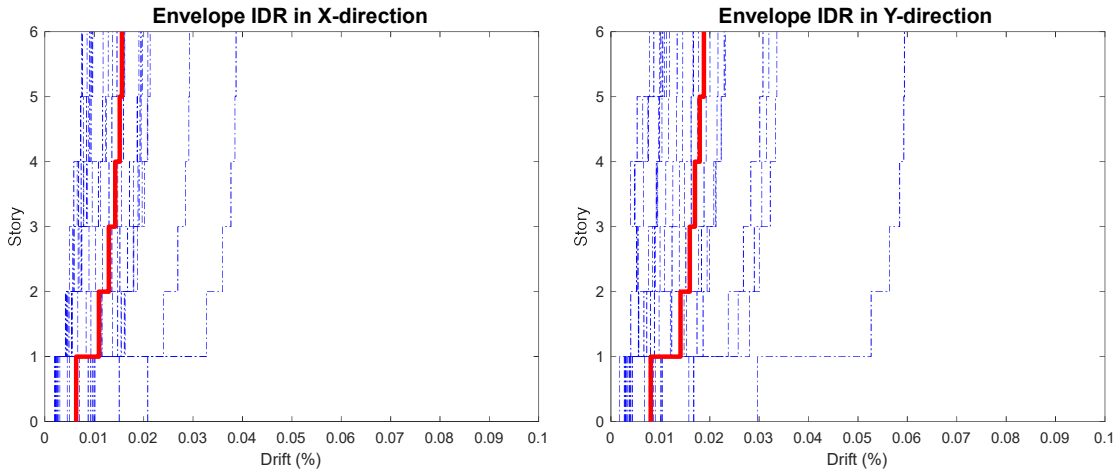

Figure 4.15. The inter story drift ratios along the X and Y directions of frame with shear walls for the maximum envelope displacement in DD-1

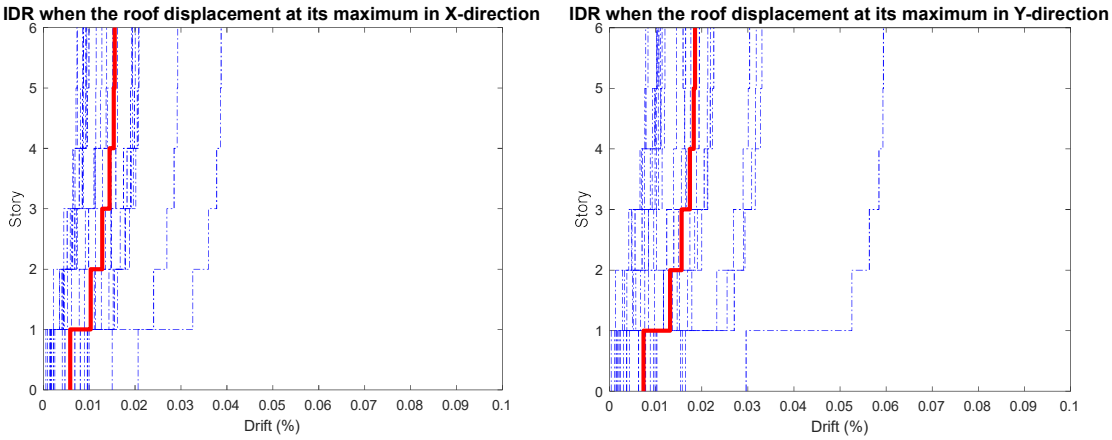

Figure 4.16. The inter story drift ratios along the X and Y directions of frame with shear walls for when the roof displacement at its maximum in DD-1

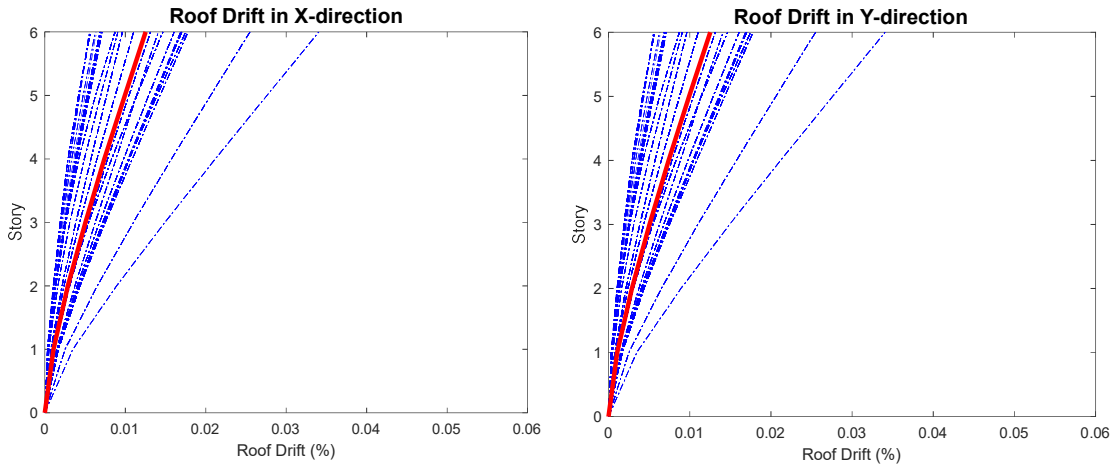

Figure 4.17. The maximum envelope displacement shape along X and Y-directions of frame with shear walls in DD-1

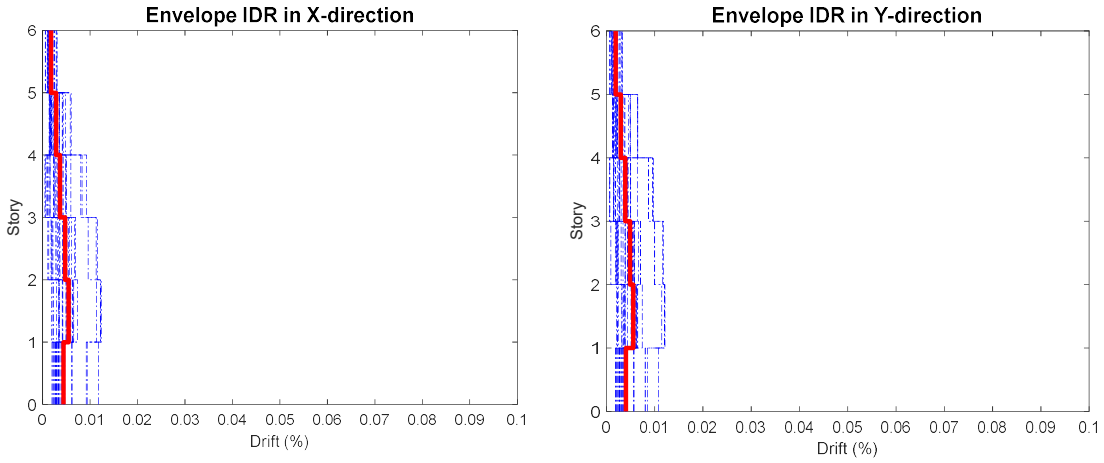

Figure 4.18. The inter story drift ratios along the X and Y directions of moment-resisting frame for the maximum envelope displacement in DD-3

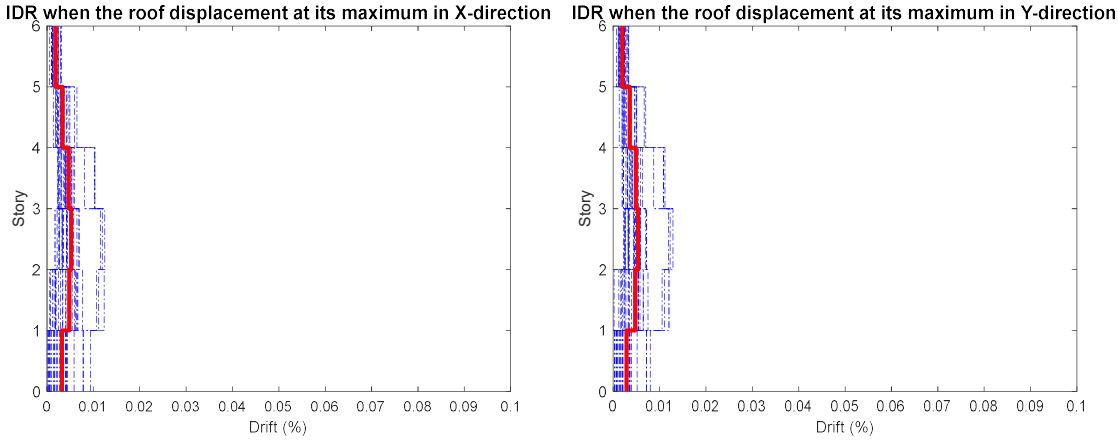

Figure 4.19. The inter story drift ratios along the X and Y directions of moment-resisting frame for when the roof displacement at its maximum in DD-3

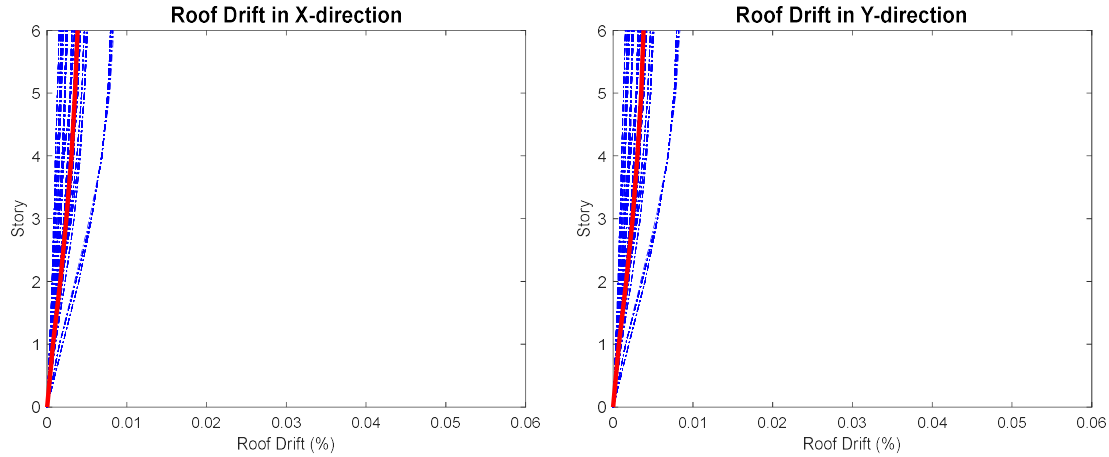

Figure 4.20. The maximum envelope displacement shape along X and Y-directions of moment-resisting frame in DD-3

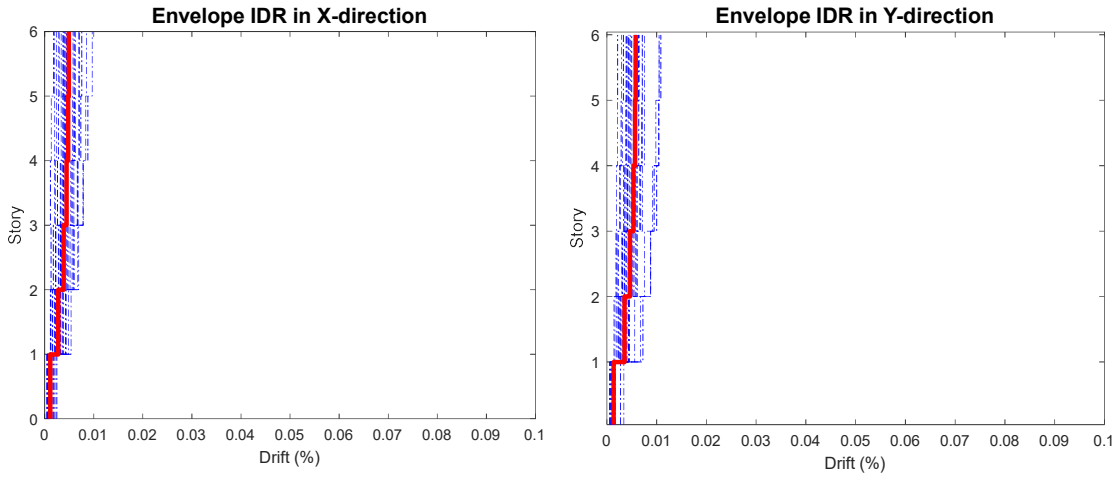

Figure 4.21. The inter story drift ratios along the X and Y directions of frame with shear walls for the maximum envelope displacement in DD-3

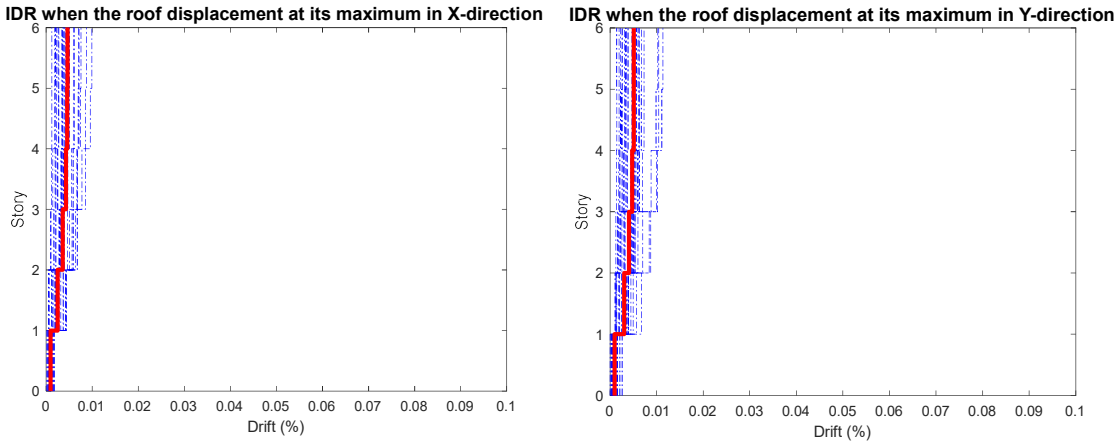

Figure 4.22. The inter story drift ratios along the X and Y directions of frame with shear walls for when the roof displacement at its maximum in DD-3

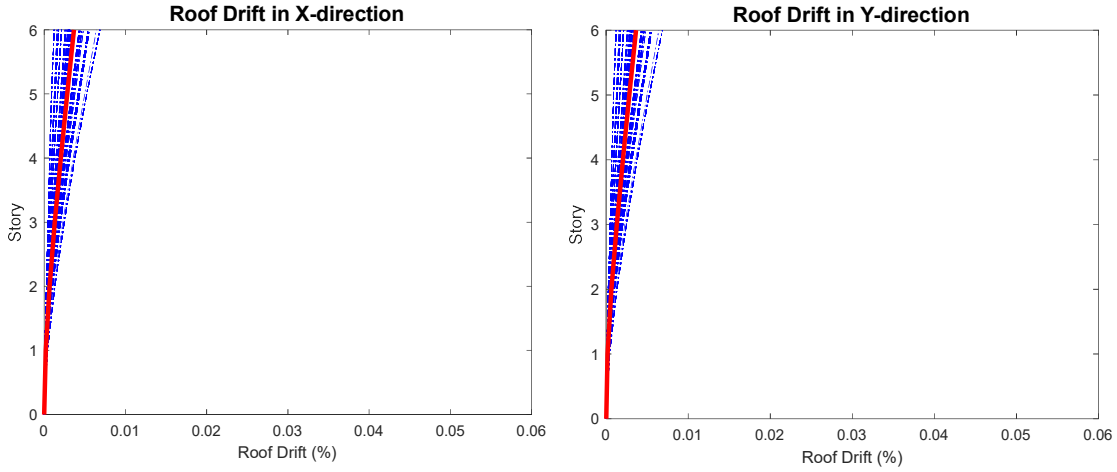

Figure 4.23. The maximum envelope displacement shape along X and Y-directions of frame with shear walls in DD-3

Table 4.1.The inter-story drift ratios at the maximum envelope drift, and when the roof displacement at its maximum, and the maximum roof drift values in both x and y direction

MRF DD-1			FRAME WITH SHEAR WALLS DD-1		
Direction	X (%)	Y (%)	Direction	X (%)	Y (%)
Roof Drift	1.78	1.78	Roof Drift	1.25	1.25
Maximum Envelope Drift	2.87	2.86	Maximum Envelope Drift	1.56	1.88
Drift when Roof Displacement at its Maximum	2.81	2.75	Drift when Roof Displacement at its Maximum	1.55	1.85
MRF DD-2			FRAME WITH SHEAR WALLS DD-2		
Direction	X (%)	Y (%)	Direction	X (%)	Y (%)
Roof Drift	1.26	1.27	Roof Drift	0.87	0.87
Maximum Envelope Drift	2.03	2.02	Maximum Envelope Drift	1.09	1.37
Drift when Roof Displacement at its Maximum	1.95	1.94	Drift when Roof Displacement at its Maximum	1.08	1.31
MRF DD-3			FRAME WITH SHEAR WALLS DD-3		
Direction	X (%)	Y (%)	Direction	X (%)	Y (%)
Roof Drift	0.38	0.38	Roof Drift	0.36	0.36
Maximum Envelope Drift	0.55	0.56	Maximum Envelope Drift	0.48	0.57
Drift when Roof Displacement at its Maximum	0.52	0.53	Drift when Roof Displacement at its Maximum	0.46	0.51

The maximum curvature developed at the elements is obtained from the fiber sections. The maximum absolute curvatures values are then multiplied with the pre-defined plastic hinge length to calculate the maximum rotations developed. These calculations are performed both for the maximum roof displacement and the envelope values for each story. Strain values of shear walls are got from the analysis results for steel and concrete separately.

The immediate occupancy, life safety, and collapse prevention plastic rotation limit values are calculated according to the TER-2018 as defined in articles from 5.8.1.2

to 5.8.1.4. The related definitions are repeated in Eq.4.1 to 4.3 for convenience. These values give the plastic limit, so the yield rotations are added to the values by calculating the plastic hinge length multiplied by the yield curvature of the section. Yield curvature values are obtained from the moment-curvature analysis of the sections in OpenSees. The ultimate curvature values are calculated by 5.8.11 from TER-2018 and stated as Eqs.4.4 to 4.8. The limitation of the shear walls is calculated with the formulas which are stated in Eqs.4.4 to 4.12.

$$\theta_P^{G\ddot{O}} = \frac{2}{3}\left[(\phi_u - \phi_y)L_P\left(1 - 0.5\frac{L_P}{L_S}\right) + 4.5\phi_u d_b\right] \quad (4.1)$$

$$\theta_P^{KH} = 0.75\theta_P^{G\ddot{O}} \quad (4.2)$$

$$\theta_P^{SH} = 0 \quad (4.3)$$

$$\varepsilon_C^{G\ddot{O}} = 0.0035 + 0.04\sqrt{\omega_{we}} \leq 0.018 \quad (4.4)$$

$$\omega_{we} = \alpha_{se}\rho_{sh,min}\frac{f_{ywe}}{f_{ce}} \quad (4.5)$$

$$\alpha_{se} = \left(1 - \frac{\Sigma a_i^2}{6b_o h_o}\right)\left(1 - \frac{s}{2b_o}\right)\left(1 - \frac{s}{2h_o}\right) \quad (4.6)$$

$$\rho_{sh,min} = \frac{A_{sh}}{b_k s} \quad (4.7)$$

$$\varepsilon_s^{G\ddot{O}} = 0.4\varepsilon_{su} \quad (4.8)$$

$$\varepsilon_C^{KH} = 0.75\varepsilon_C^{G\ddot{O}} \quad (4.9)$$

$$\varepsilon_s^{KH} = 0.75\varepsilon_s^{G\ddot{O}} \quad (4.10)$$

$$\varepsilon_C^{SH} = 0.0025 \quad (4.11)$$

$$\varepsilon_s^{SH} = 0.0075 \quad (4.12)$$

$\theta_P^{G\ddot{O}}$= Plastic rotation limit for Collapse Prevention performance level

θ_P^{KH}= Plastic rotation limit for Life Safety performance level

θ_P^{SH}= Plastic rotation limit for Immediate Occupancy performance level

$\varepsilon_C^{G\ddot{O}}$= Concrete strain limit for Collapse Prevention performance level

$\varepsilon_s^{G\ddot{O}}$= Steel strain limit for Collapse Prevention performance level

ε_C^{KH}= Concrete strain limit for Life Safety performance level

ε_s^{KH}= Steel strain limit for Life Safety performance level

ε_C^{SH}= Concrete strain limit for Immediate Occupancy performance level

ε_s^{SH}= Steel strain limit for Immediate Occupancy performance level

ε_{su}= Unit elongation of reinforcement corresponding to maximum strength

ϕ_u= Curvature before collapse [m^{-1}]

ϕ_y= Yield curvature [m^{-1}]

L_P= Plastic hinge length [m]

L_S= Shear clear length [m]

d_b= Diameter of longitudinal reinforcement (average in tension) [m]

ω_{we}= Ratio of effective confining reinforcement to mechanical reinforcement

α_{se}= Confinement reinforcement efficiency coefficient

$\rho_{sh,min}$= The smaller of the volumetric transverse reinforcement ratio in two horizontal directions

f_{ywe}= Average (expected) yield strength of transverse reinforcement [MPa]

f_{ce}= Average (expected) compressive strength of concrete [MPa]

a_i= Distance between the axes of longitudinal reinforcements supported horizontally by a stirrup arm or crossties [mm]

b_o= Section dimension between the axes of the stirrups surrounding the core concrete [mm]

h_o= Section dimension between the axes of the stirrups surrounding the core concrete [mm]

A_{sh}= Transverse reinforcement area (rectangular section) [mm^2]

b_k= Core dimension (distance between outermost transverse reinforcement axes) [mm]

s= Confinement reinforcement spacing [m]

The calculated rotations of the plastic hinges at the ends of the elements and strain values of the shear walls are presented in graphic form in Figure 4.24 to 4.167. The presentation is made by grouping the columns and shear walls and beams along X- and Y-directions in different graphs. The average maximum rotation values for all the considered earthquakes at each end of the members at every story are summarized in the graphs. The numerical values of the maximum rotations and strains are also listed in Table 4.2 with corresponding drift values. The rotation values that define the performance levels defined by the TER-2018 are also presented in the figure's vertical lines with color code.

Columns develop maximum rotations at the bottom ends of the 1st story in moment-frame. The maximum story rotations of envelope rotation are 0.018 and 0.027 radians for DD-2 and DD-1 earthquake levels, respectively. The maximum beam rotation values are 0.017 and 0.025 radians for DD-2 and DD-1 earthquake levels. Rotations are spread towards higher levels, with the largest rotations developed at lower levels. Considering that the yielding rotation is around 0.01 radians, it could be observed that yielding spreads up to 4 stories throughout the frame.

The frame with shear walls develops lower member end rotations as expected. The columns and shear walls again developed the maximum rotations at the bottom end of the 1st story. The column rotation values are 0.0025 and 0.005 radians for the DD-2 and DD-1 earthquake levels, respectively. Both values are for the envelope rotations of the average response through the time history. The shear wall strain values are 0.015 and 0.027 radians for the DD-2 and DD-1 earthquake levels, respectively. The beam rotations are 0.0125 and 0.017 radians for DD-2 and DD-1 earthquake levels, respectively. These are again the envelope values. The maximum rotations of beams develop at the upper levels and the rotation values are similar at the top three stories in a decreasing manner.

The rotation levels for both columns and beams are below 0.005 radians for DD-3 earthquake level for both frames.

Some Type-3 column bottom ends in the moment frame in the 1st story reached the life safety zone for DD-2 earthquake. In the 2nd story, some of Type-3 bottom-ends also just entered the life-safety zone. Almost all the beams of the moment-resisting frame in X-direction are within the life safety zone for the first 4 stories. Nearly all the Type-3 beams in the first story in X-direction exceeded the life safety limit and the others beyond half the way to the collapse prevention limit in the first story. Other types of beams are

also at the limit of life safety. In the 2nd story, some Type-3(6m) beams exceeded the life safety limit. Again, almost all the beams along the Y-direction of the moment-resisting frame in the first 5 stories exceeded the immediate occupancy. In the 1st story, Type-3 beams exceeded the life safety limit, and the others got closer to the life safety limit. Only the 1st story shear walls of the frame with shear walls reach to life safety level for the strain limit values of the steel. All other levels are within the immediate occupancy zone. The first story shear walls are halfway through the immediate occupancy zone. In the graphs, the material governing the performance limit is indicated with bold marks. Type-1 the columns of frame with shear walls exceed the immediate occupancy limit only in the first story in bottom ends. Some of the Type 1-2 & 5 beams in the X-direction of the frame with shear walls pass the life safety zone with increasing rotation value towards the upper stories, and others are within the immediate occupancy zone. A couple of beams in Y-direction pass to the life safety zone in all types by an increasing rate from the 1st story to the 6th story in compliance with the observed drift pattern.

Performances for DD-1 earthquake is as follows. In the 1st and 2nd stories, nearly all the beams in the X-direction exceeded the collapse prevention. In the 3rd story, nearly half of the Type-3 beams are within the life safety zone. In the first two stories, all the beams in the Y-direction exceeded collapse prevention as well. In the first two stories, all the column bottom ends exceeded the collapse prevention limit. Type-4 walls along Y-direction and Type-1 wall along X-direction pass to the collapse prevention zone in shear wall buildings. All other walls are in the life safety zone. Some of the Type-1 columns and a couple Type-2 columns exceeded the immediate occupancy limits. Type 1-2&5 beams in X-direction exceeded the immediate occupancy limit and Type-2 approached the life safety limit in all stories. Along the Y-direction some of the beams from the 3rd story and upper pass to the collapse prevention zone.

Table 4.2.The maximum rotation values of structures under DD-1 and DD-2 level earthquakes

Frame and Earthquake Level	**Rotation (rad)**	**Drift (%)**
MRF Column Max Rotation DD-1	0.027	2.87
MRF Column Max Rotation DD-2	0.018	2.03
MRF Beam Max Rotation DD-1	0.025	2.87
MRF Beam Max Rotation DD-2	0.017	2.03
Frame with Shear Walls Column Max Rotation DD-1	0.005	1.88
Frame with Shear Walls Column Max Rotation DD-2	0.0025	1.37
Frame with Shear Walls Beam Max Rotation DD-1	0.017	1.88
Frame with Shear Walls Beam Max Rotation DD-2	0.0125	1.37
Frame and Earthquake Level	**Strain**	**Drift (%)**
Frame with Shear Walls Max Strain of Shear Wall DD-1	0.027	1.88
Frame with Shear Walls Max Strain of Shear Wall DD-2	0.015	1.37

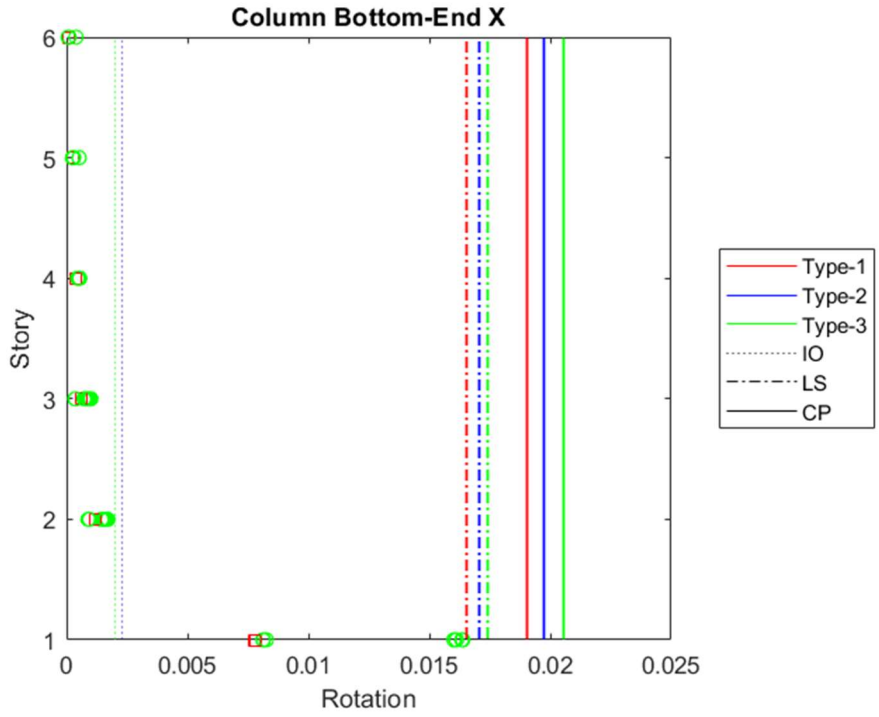

Figure 4.24. Rotations of bottom-end of column in x-direction at roof when its maximum in DD-2 level earthquake of moment-resisting frame

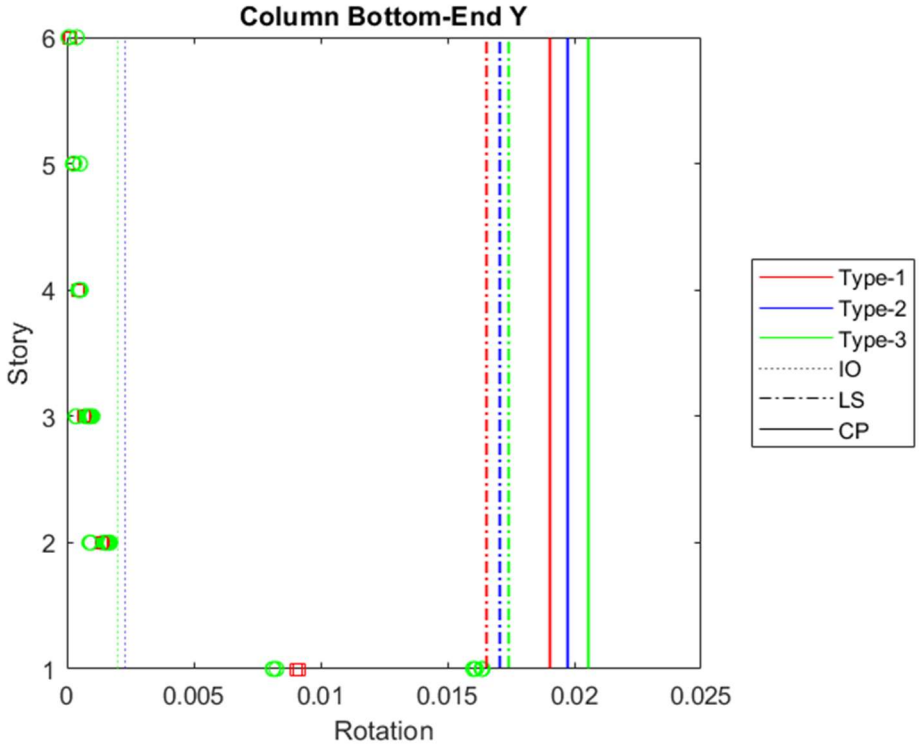

Figure 4.25. Rotations of bottom-end of column in y-direction at roof when its maximum in DD-2 level earthquake of moment-resisting frame

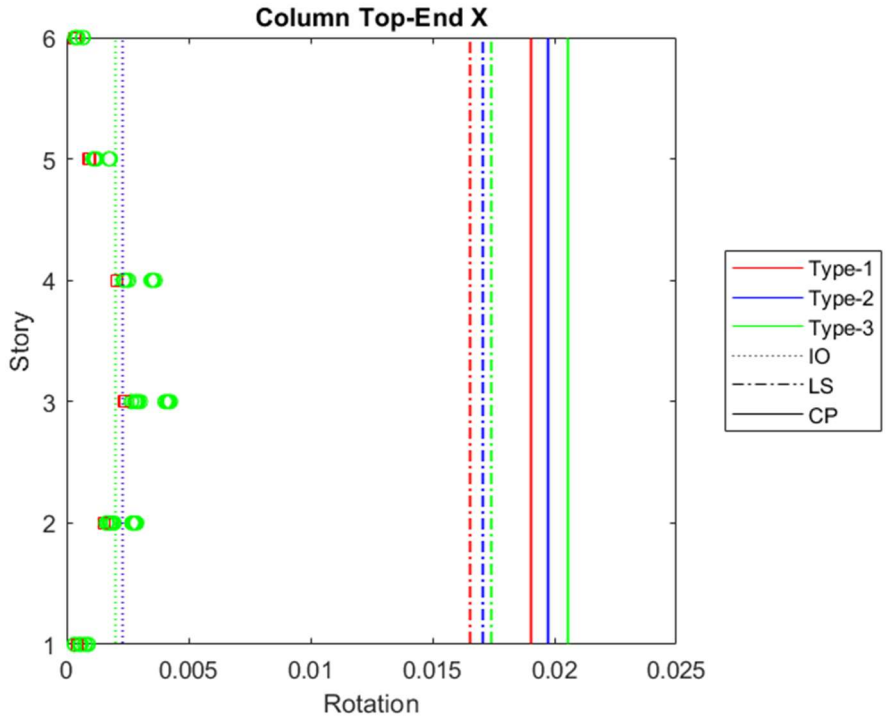

Figure 4.26. Rotations of top-end of column in x-direction at roof when its maximum in DD-2 level earthquake of moment-resisting frame

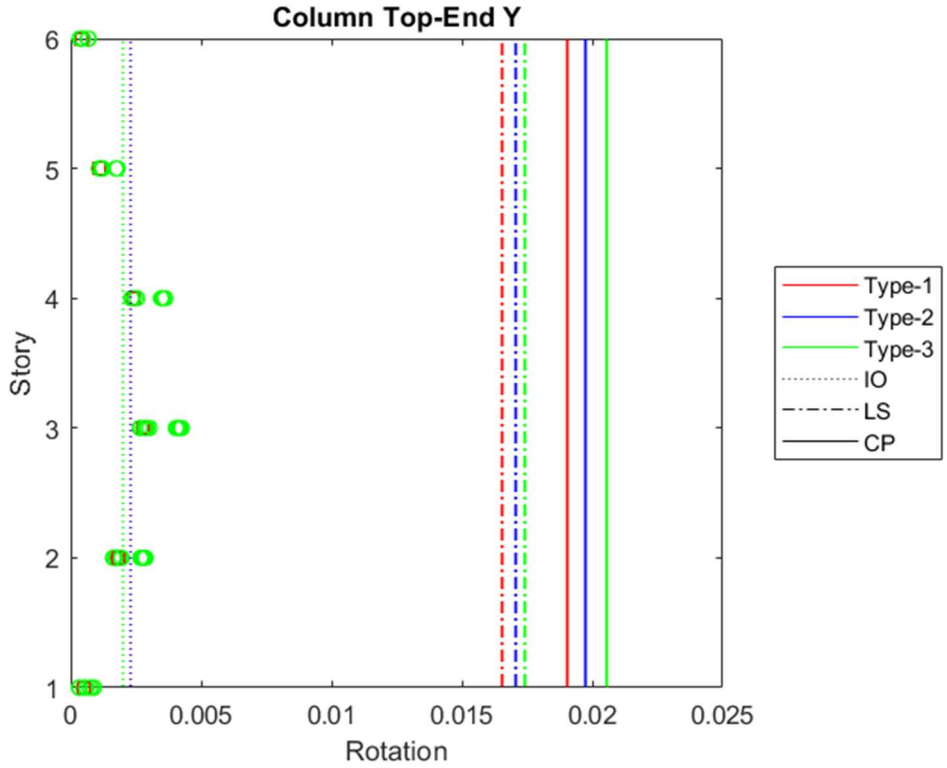

Figure 4.27. Rotations of top-end of column in y-direction at roof when its maximum in DD-2 level earthquake of moment-resisting frame

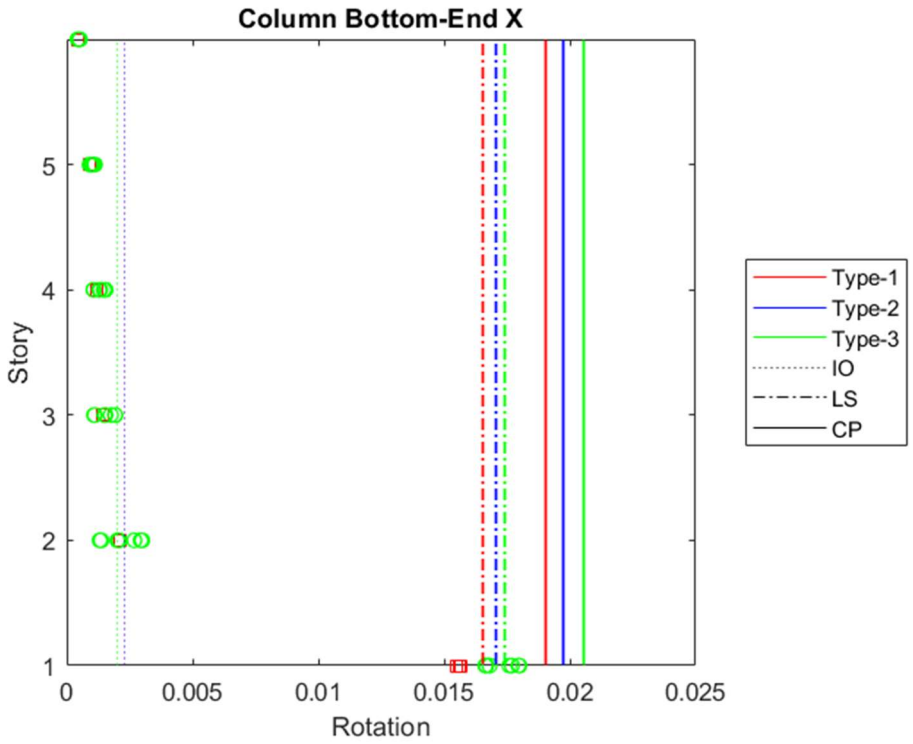

Figure 4.28. Rotations of bottom-end of column in x-direction for the maximum envelope drifts in DD-2 level earthquake of moment-resisting frame

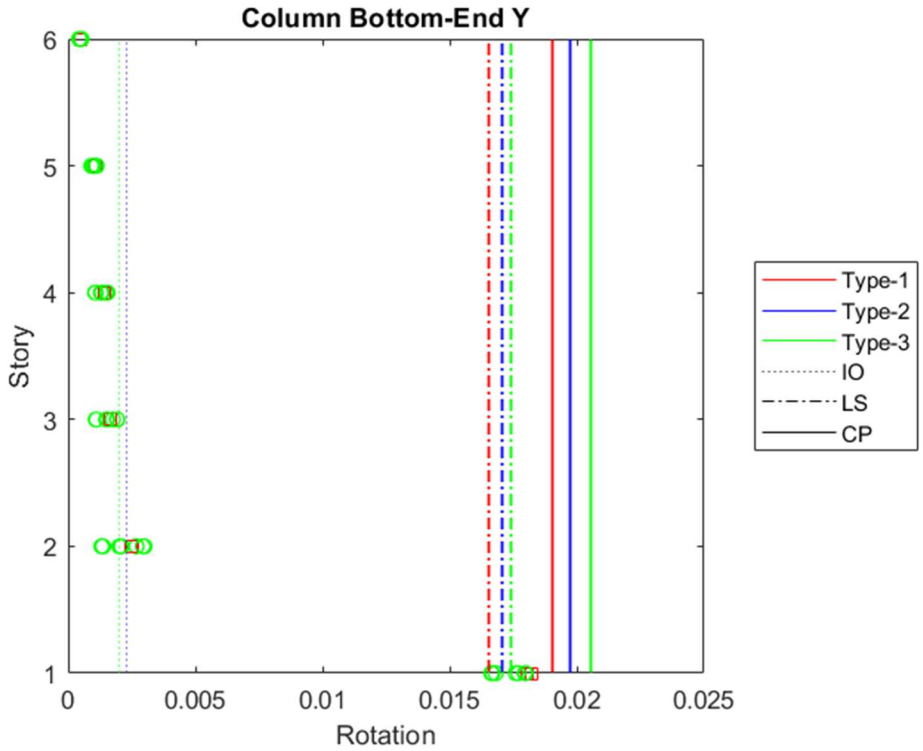

Figure 4.29. Rotations of bottom-end of column in y-direction for the maximum envelope drifts in DD-2 level earthquake of moment-resisting frame

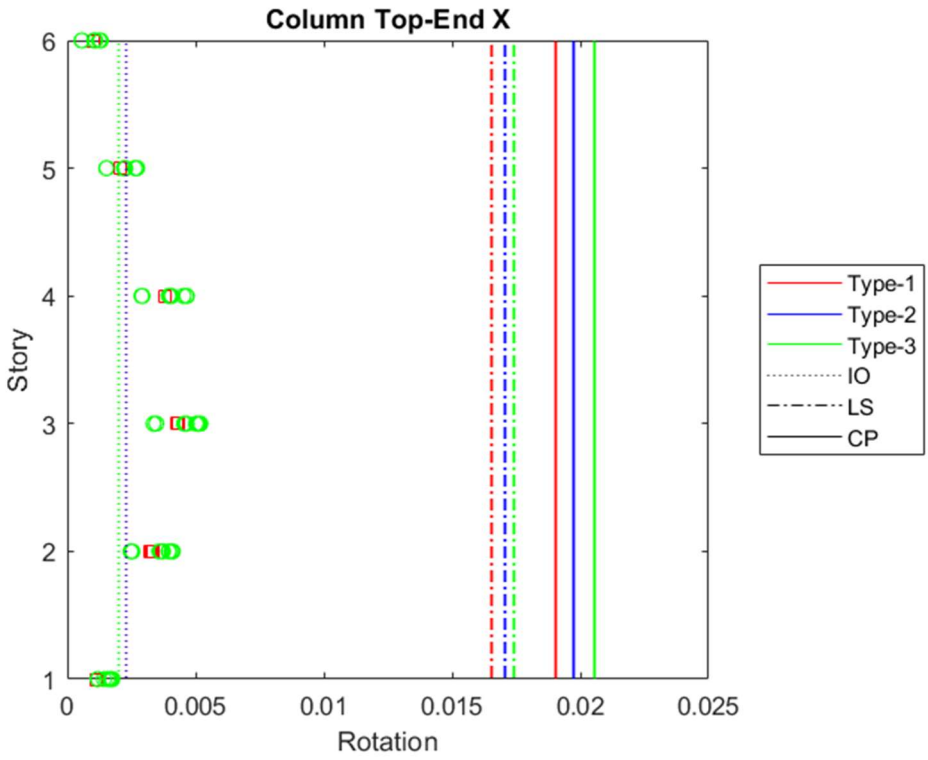

Figure 4.30. Rotations of top-end of column in x-direction for the maximum envelope drifts in DD-2 level earthquake of moment-resisting frame

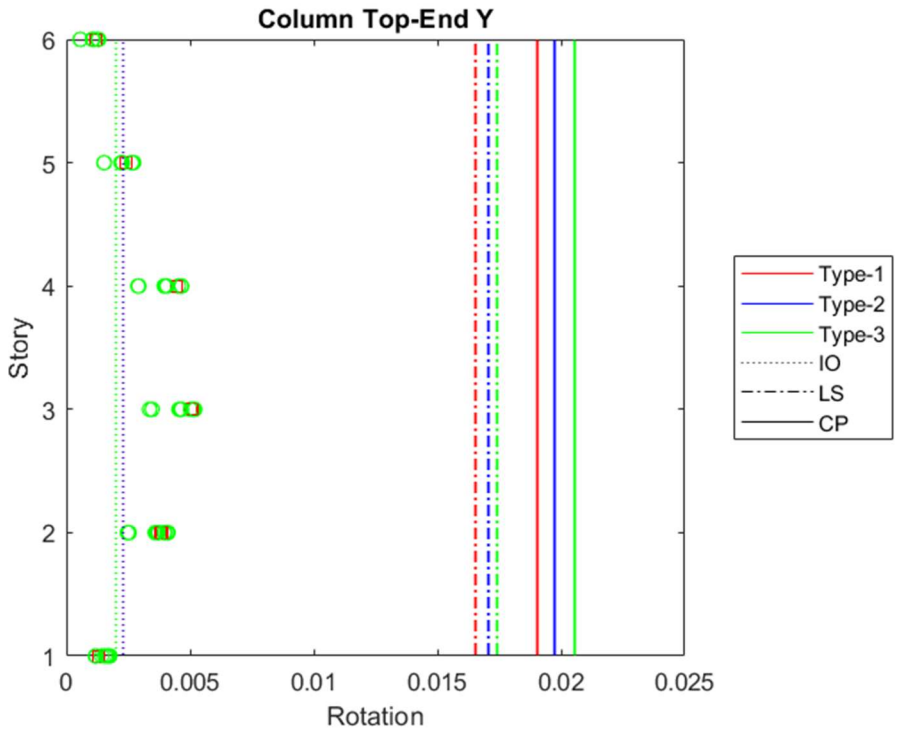

Figure 4.31. Rotations of top-end of column in y-direction for the maximum envelope drifts in DD-2 level earthquake of moment-resisting frame

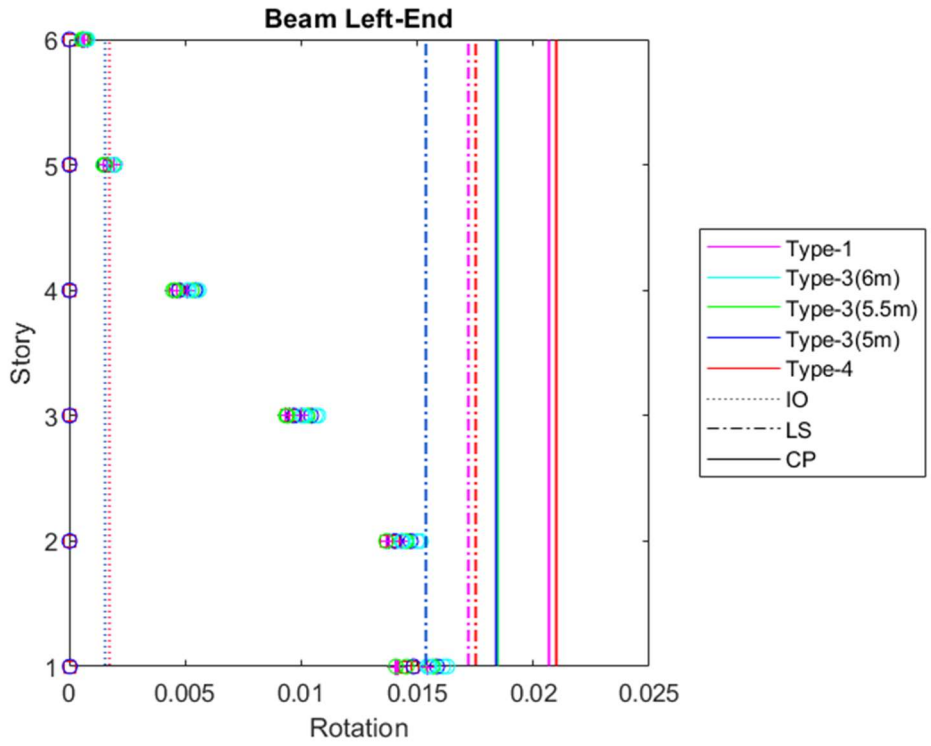

Figure 4.32. Rotations of left-end of beam in x-direction at roof when its maximum in DD-2 level earthquake of moment-resisting frame

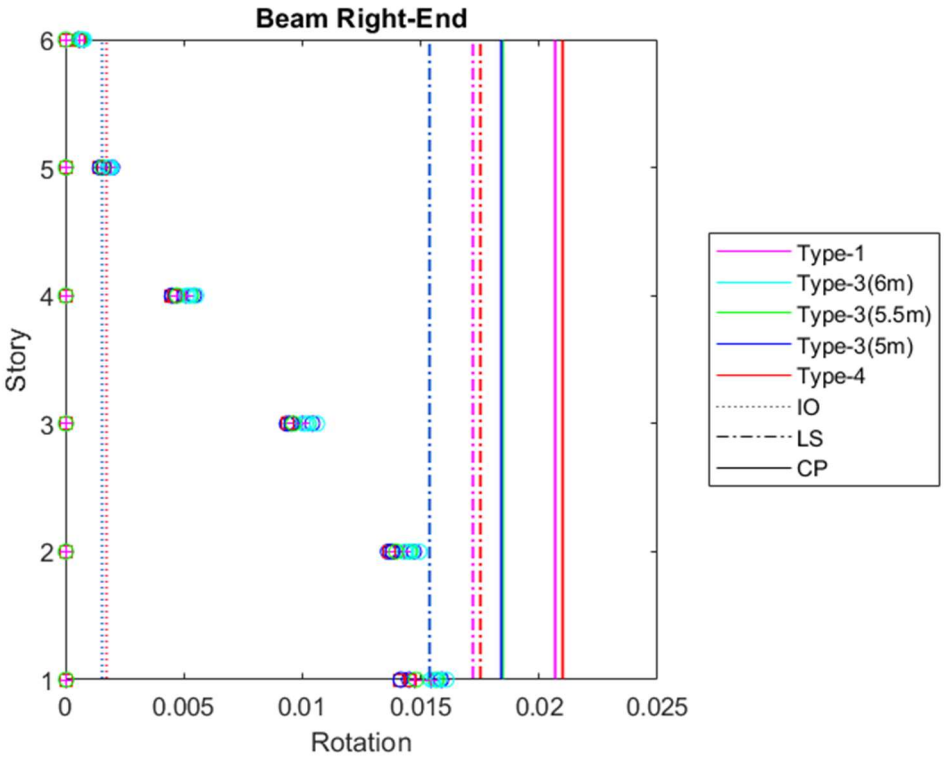

Figure 4.33. Rotations of right-end of beam in x-direction at roof when its maximum in DD-2 level earthquake of moment-resisting frame

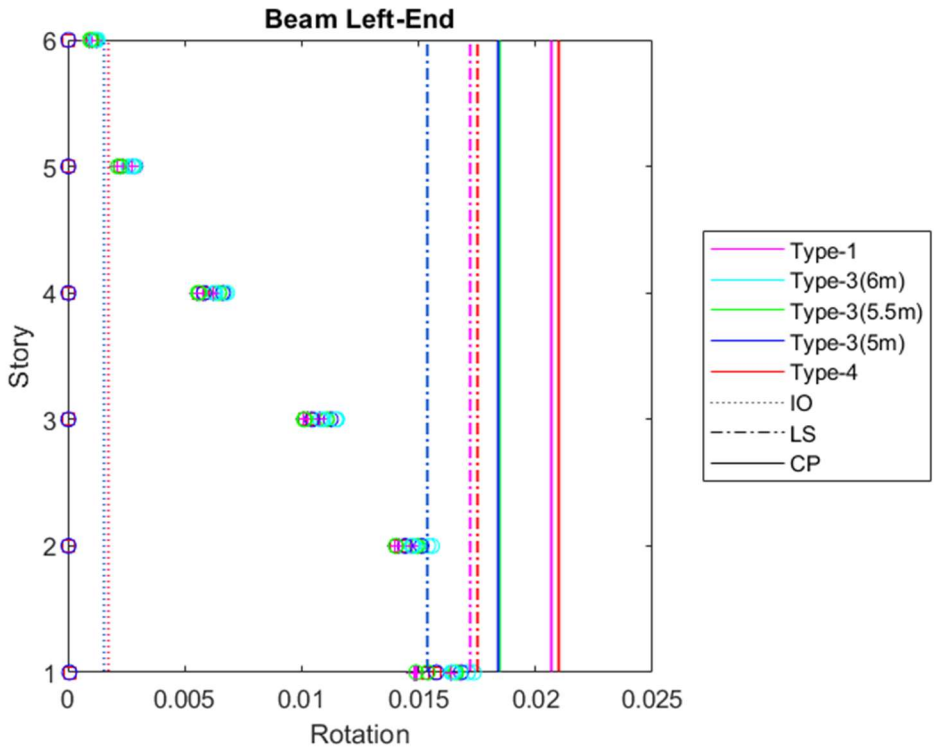

Figure 4.34. Rotations of left-end of beam in x-direction for the maximum envelope drifts in DD-2 level earthquake of moment-resisting frame

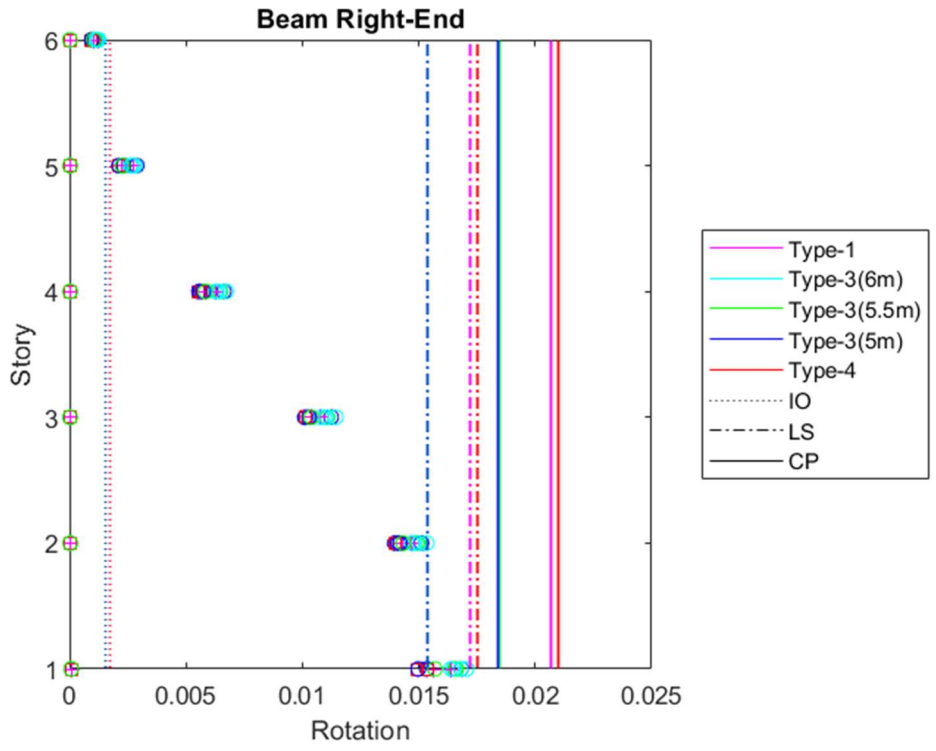

Figure 4.35. Rotations of right-end of beam in x-direction for the maximum envelope drifts in DD-2 level earthquake of moment-resisting frame

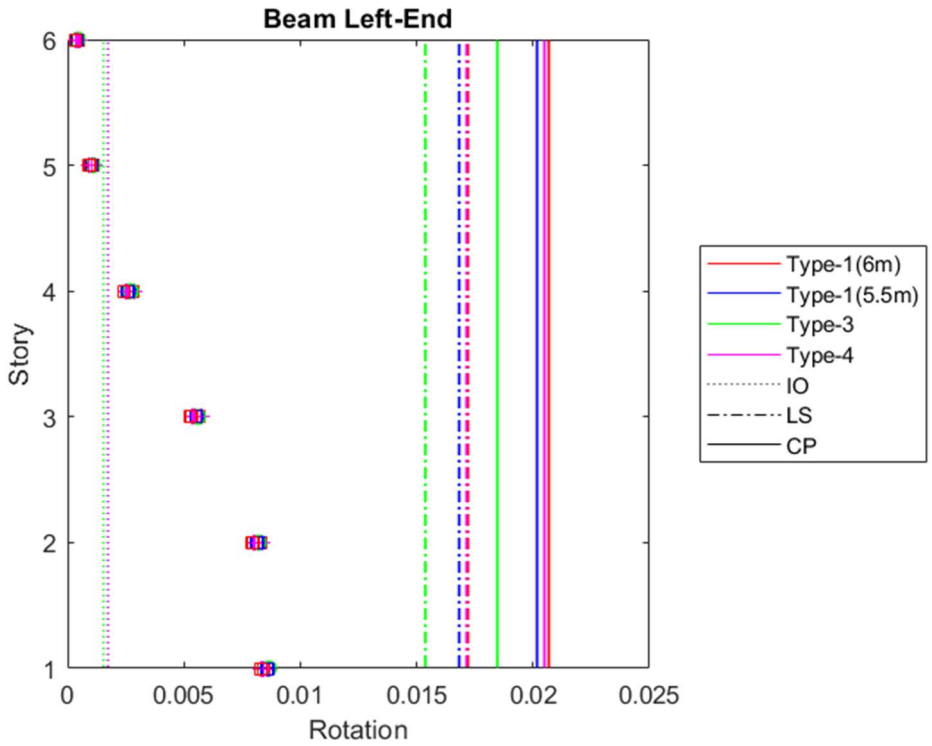

Figure 4.36. Rotations of left-end of beam in y-direction at roof when its maximum in DD-2 level earthquake of moment-resisting frame

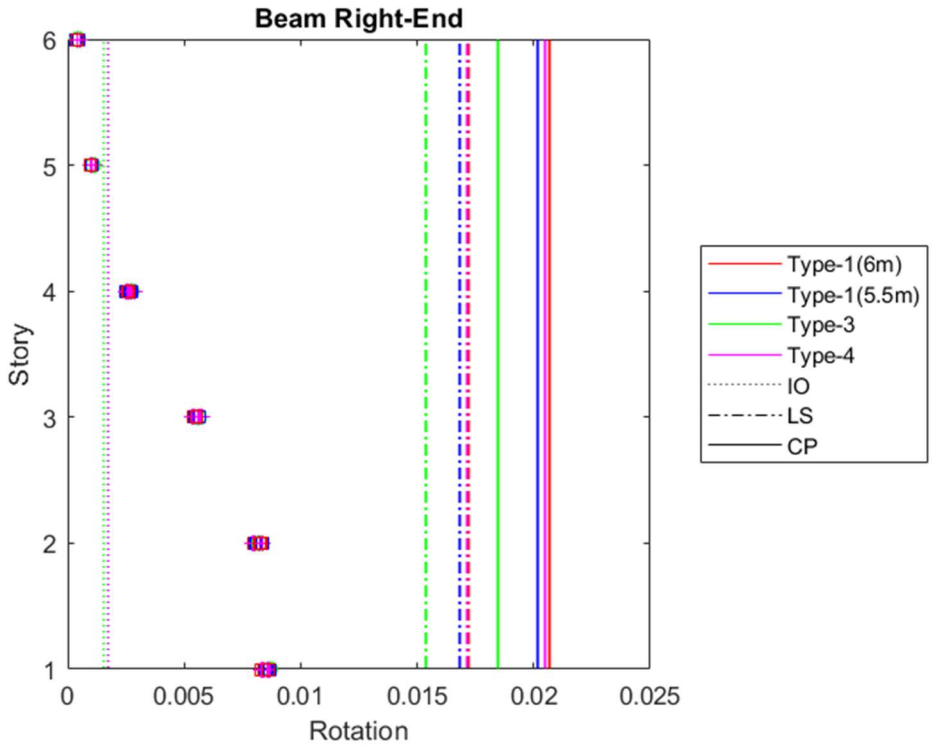

Figure 4.37. Rotations of right-end of beam in y-direction at roof when its maximum in DD-2 level earthquake of moment-resisting frame

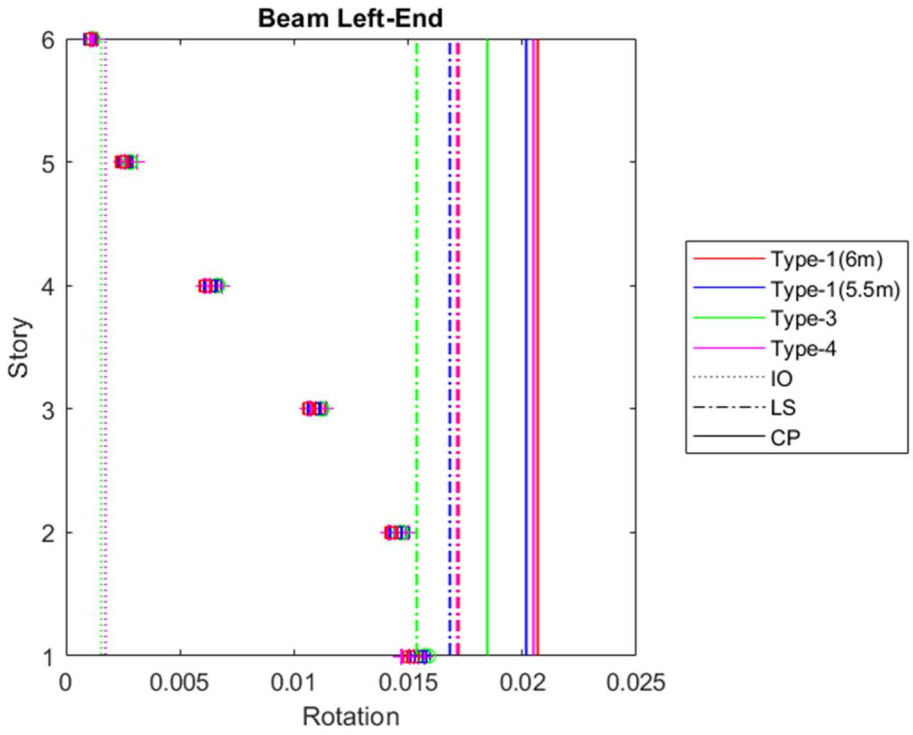

Figure 4.38. Rotations of left-end of beam in y-direction for the maximum envelope drifts in DD-2 level earthquake of moment-resisting frame

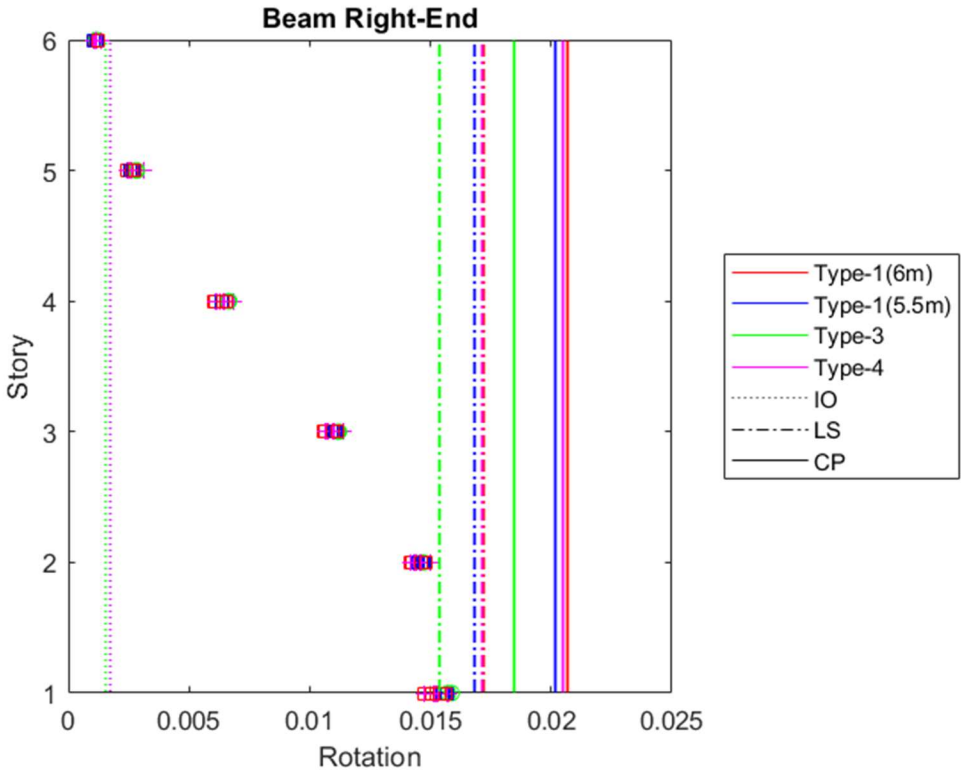

Figure 4.39. Rotations of right-end of beam in y-direction for the maximum envelope drifts in DD-2 level earthquake of moment-resisting frame

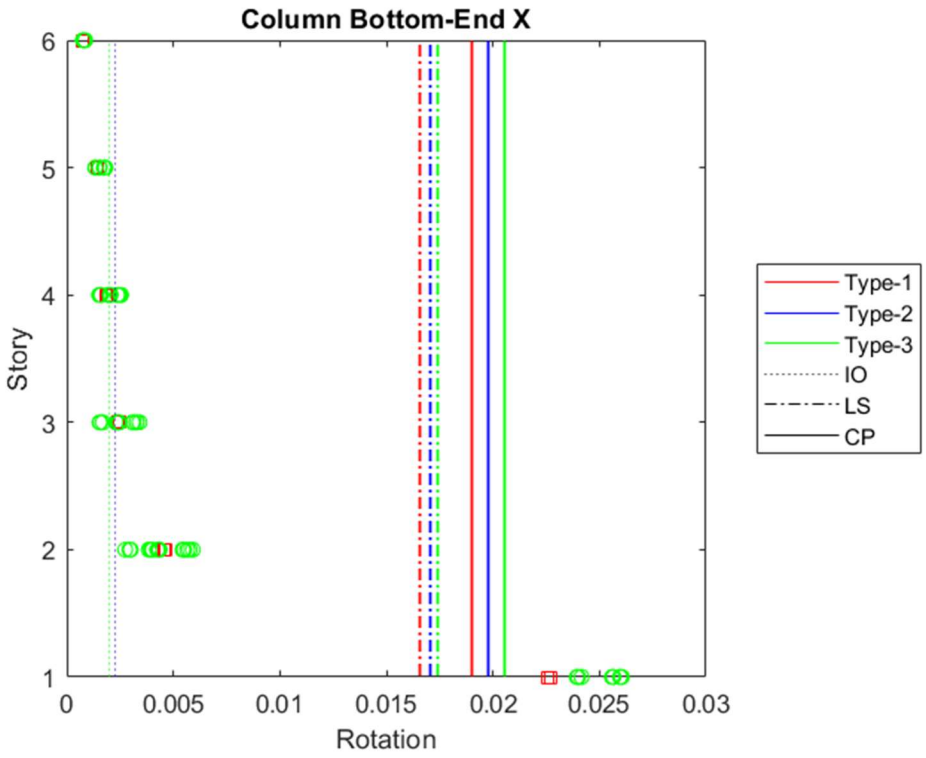

Figure 4.40. Rotations of bottom-end of column in x-direction for the maximum envelope drifts in DD-1 level earthquake of moment-resisting frame

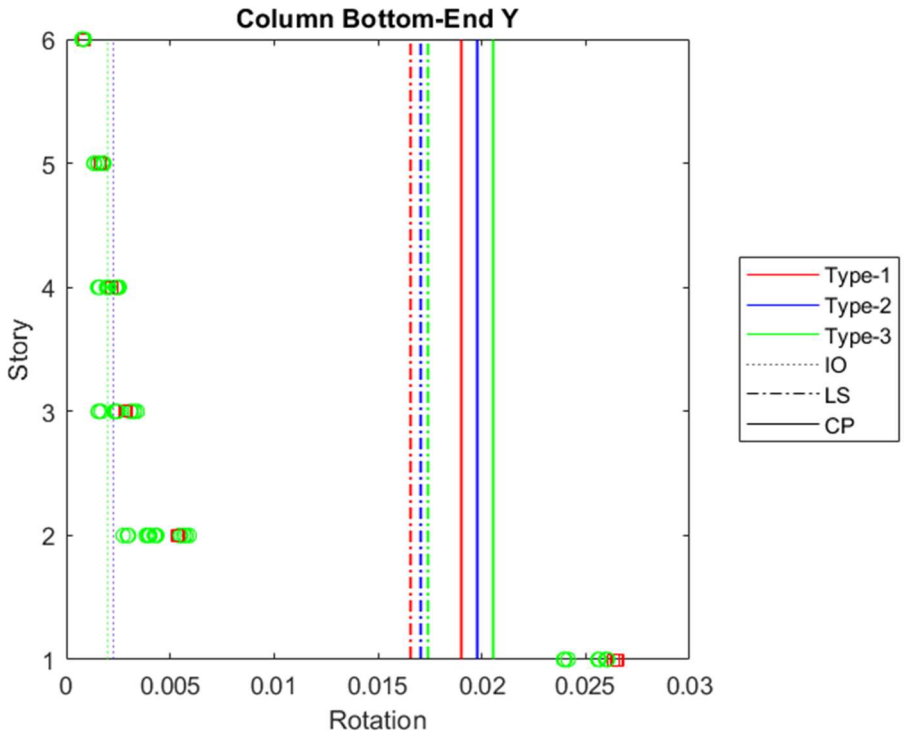

Figure 4.41. Rotations of bottom-end of column in y-direction for the maximum envelope drifts in DD-1 level earthquake of moment-resisting frame

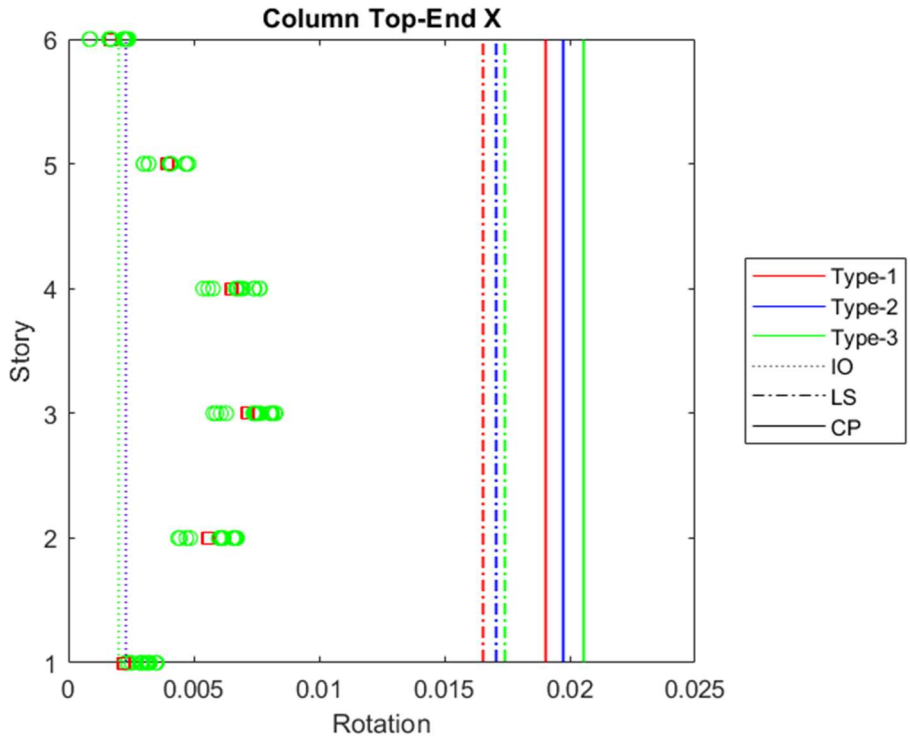

Figure 4.42. Rotations of top-end of column in x-direction for the maximum envelope drifts in DD-1 level earthquake of moment-resisting frame

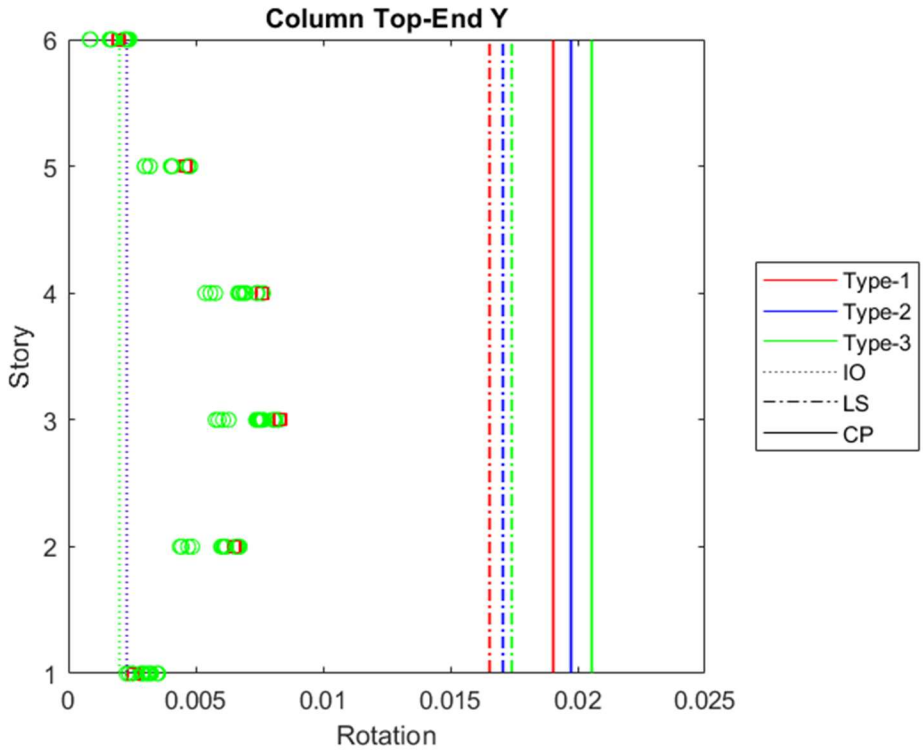

Figure 4.43. Rotations of top-end of column in y-direction for the maximum envelope drifts in DD-1 level earthquake of moment-resisting frame

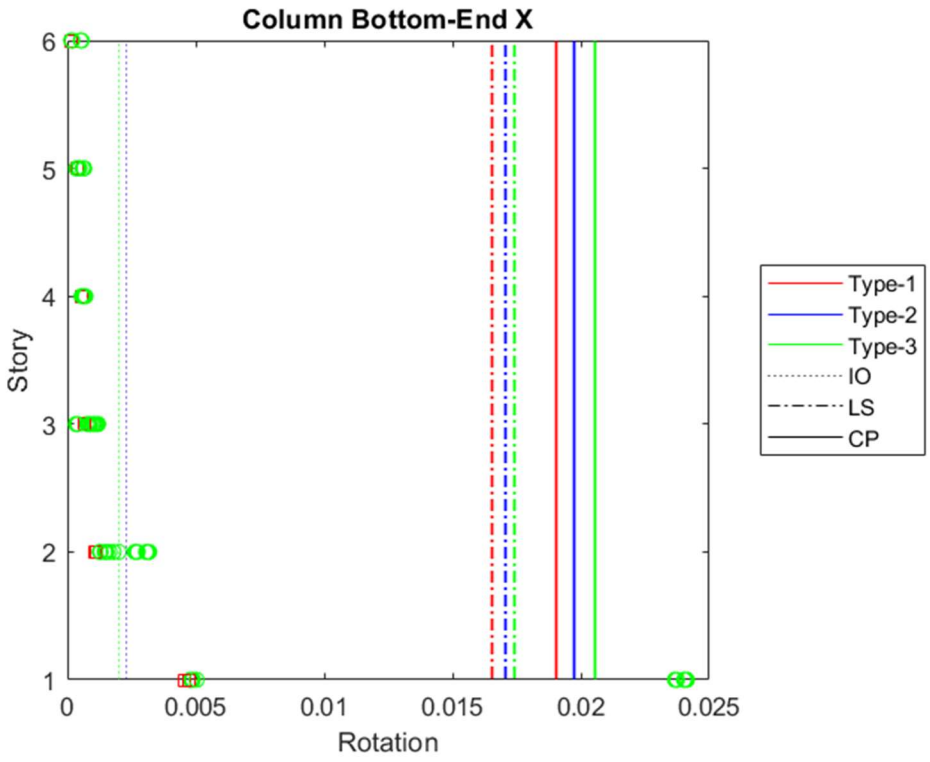

Figure 4.44. Rotations of bottom-end of column in x-direction at roof when its maximum in DD-1 level earthquake of moment-resisting frame

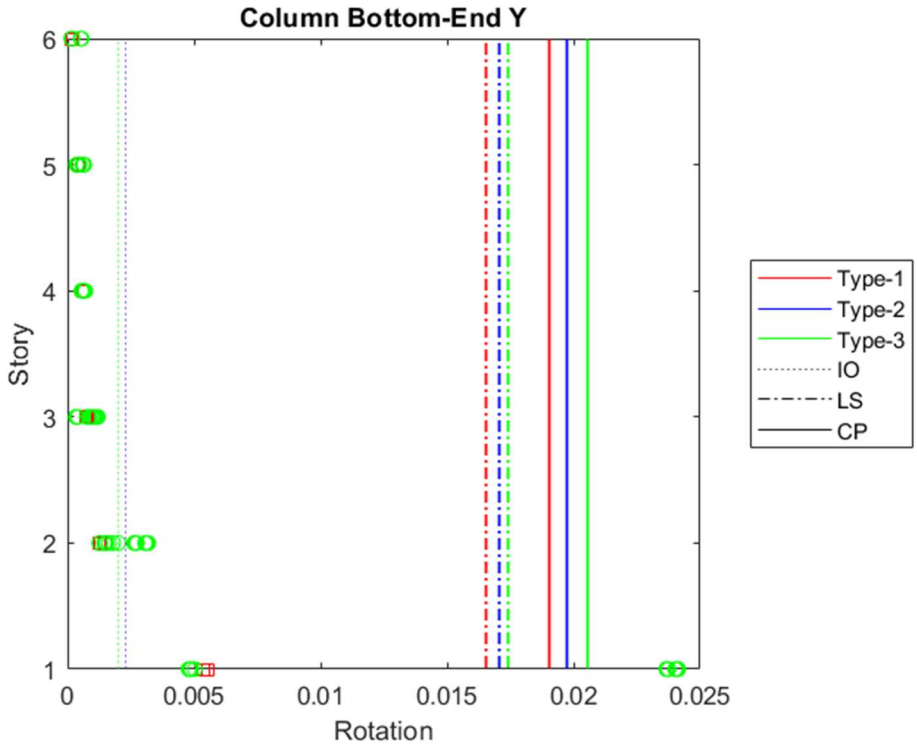

Figure 4.45. Rotations of bottom-end of column in y-direction at roof when its maximum in DD-1 level earthquake of moment-resisting frame

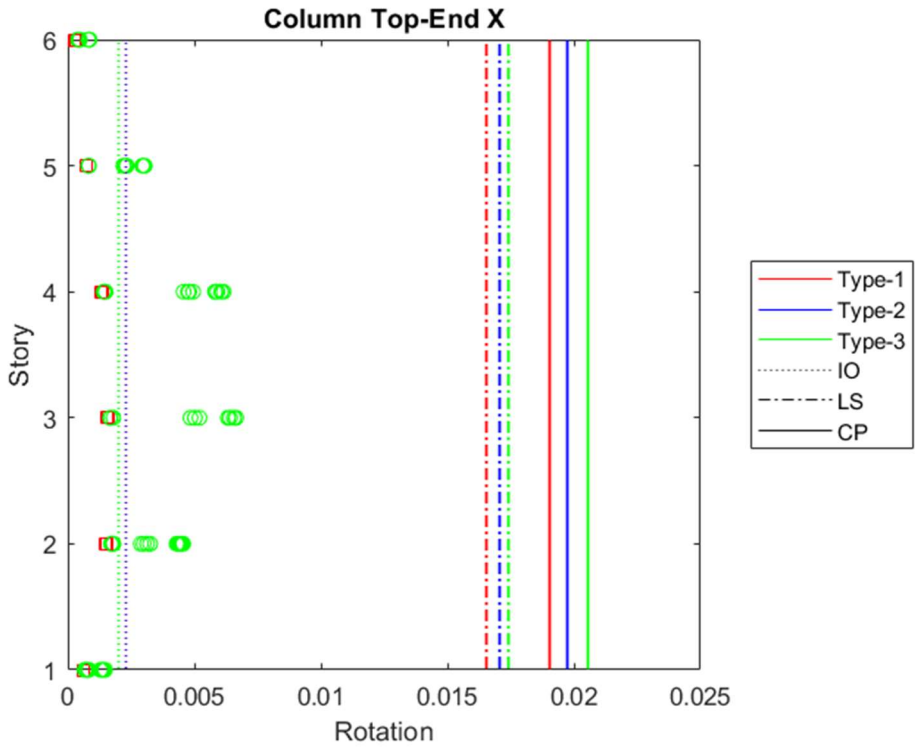

Figure 4.46. Rotations of top-end of column in x-direction at roof when its maximum in DD-1 level earthquake of moment-resisting frame

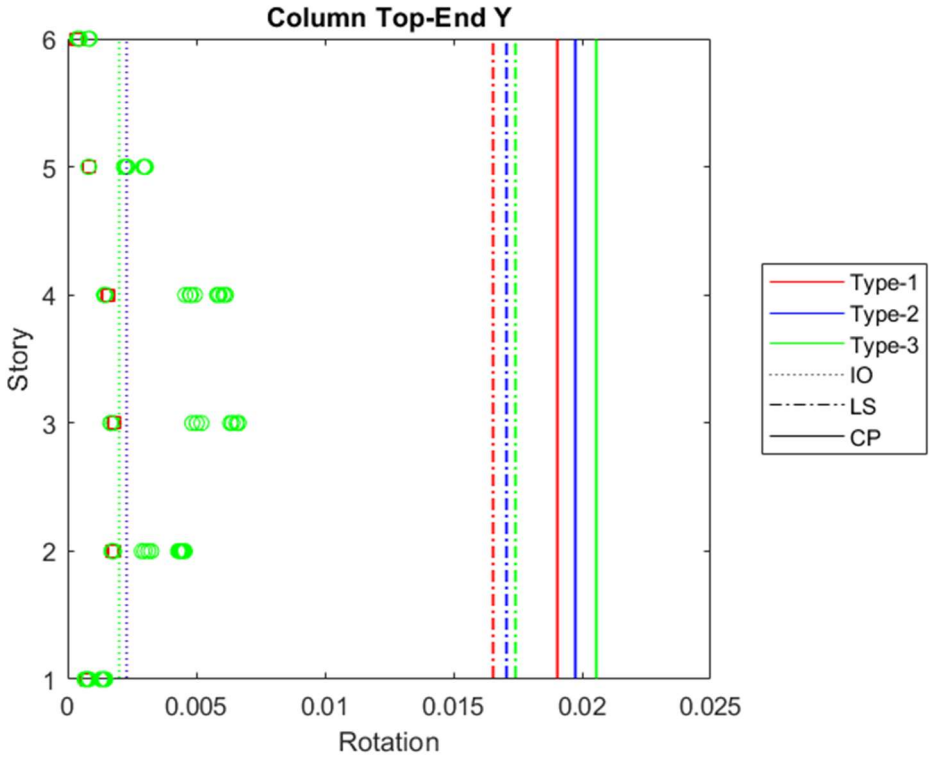

Figure 4.47. Rotations of top-end of column in y-direction at roof when its maximum in DD-1 level earthquake of moment-resisting frame

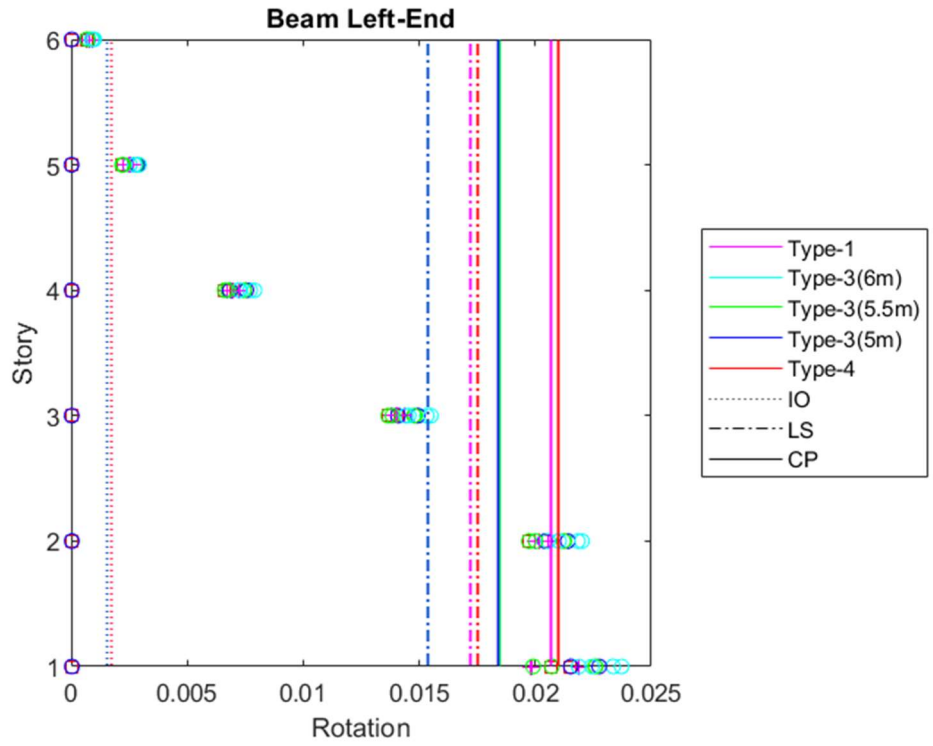

Figure 4.48. Rotations of left-end of beam in x-direction at roof when its maximum in DD-1 level earthquake of moment-resisting frame

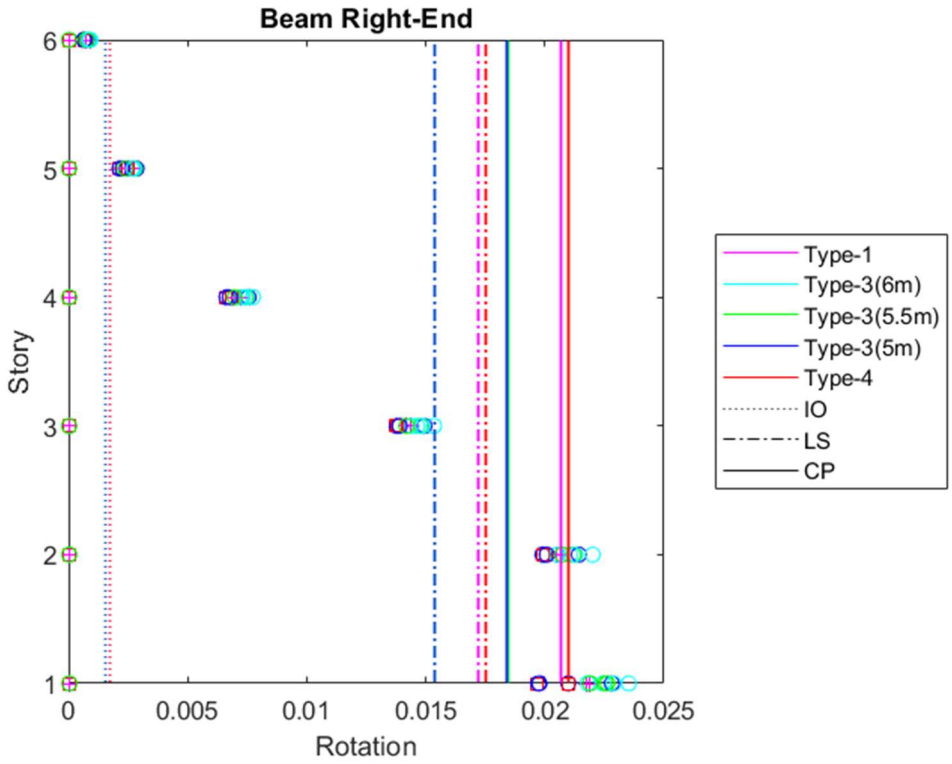

Figure 4.49. Rotations of right-end of beam in x-direction at roof when its maximum in DD-1 level earthquake of moment-resisting frame

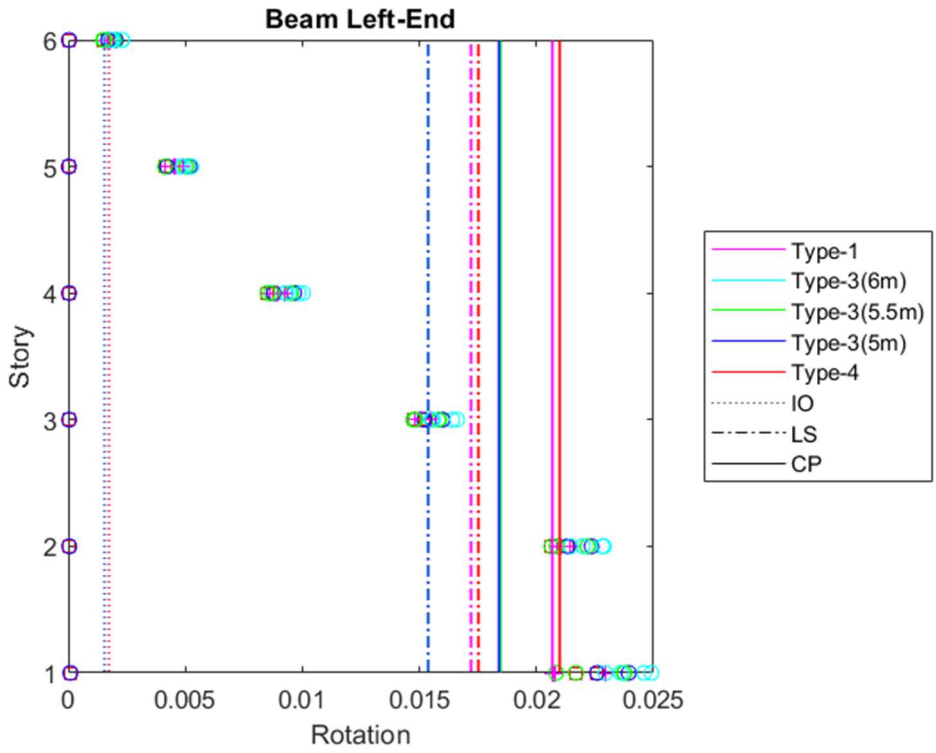

Figure 4.50. Rotations of left-end of beam in x-direction for the maximum envelope drifts in DD-1 level earthquake of moment-resisting frame

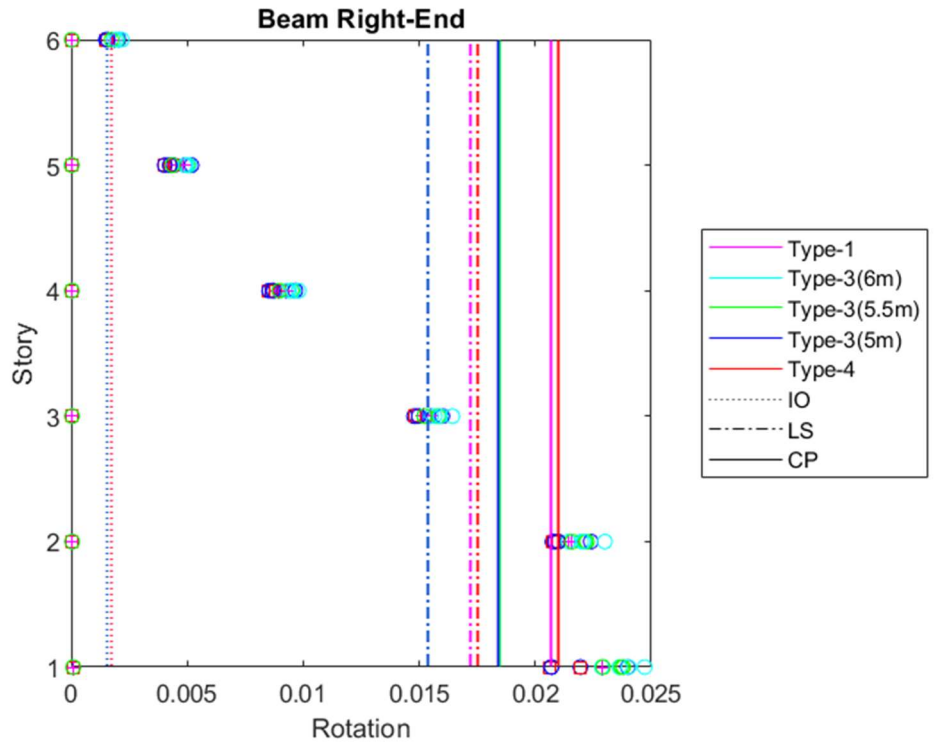

Figure 4.51. Rotations of right-end of beam in x-direction for the maximum envelope drifts in DD-1 level earthquake of moment-resisting frame

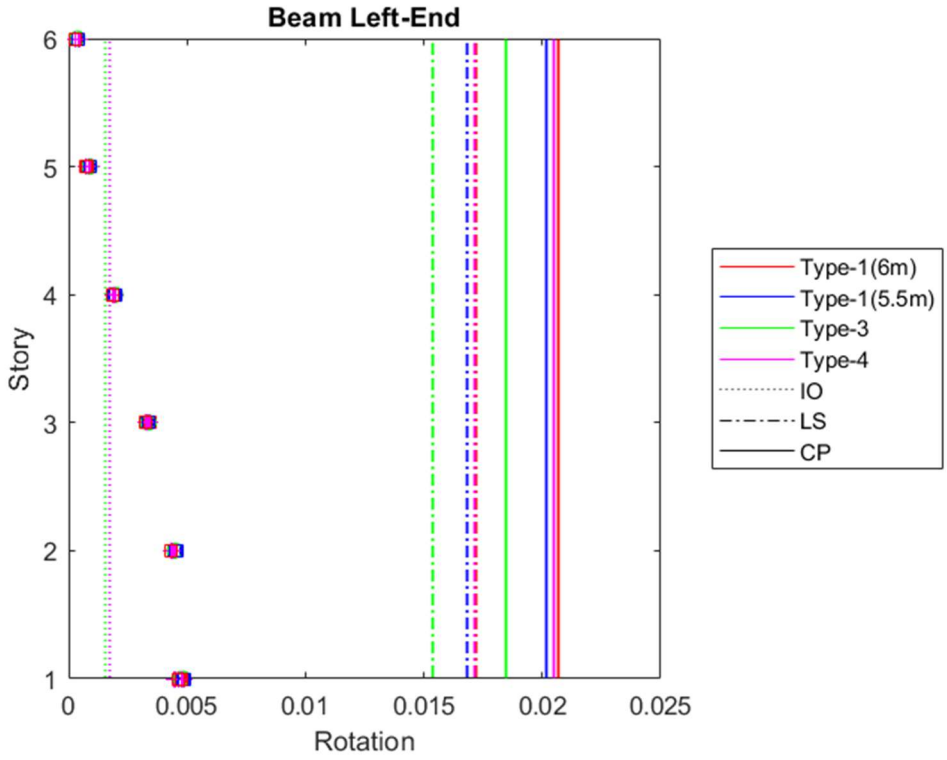

Figure 4.52. Rotations of left-end of beam in y-direction at roof when its maximum in DD-1 level earthquake of moment-resisting frame

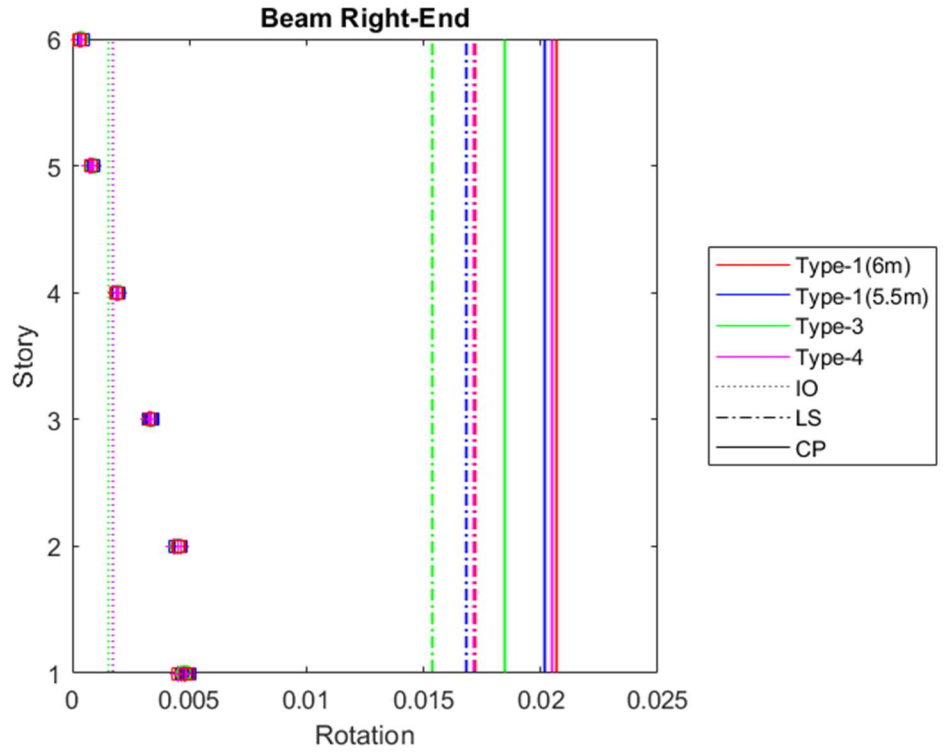

Figure 4.53. Rotations of right-end of beam in y-direction at roof when its maximum in DD-1 level earthquake of moment-resisting frame

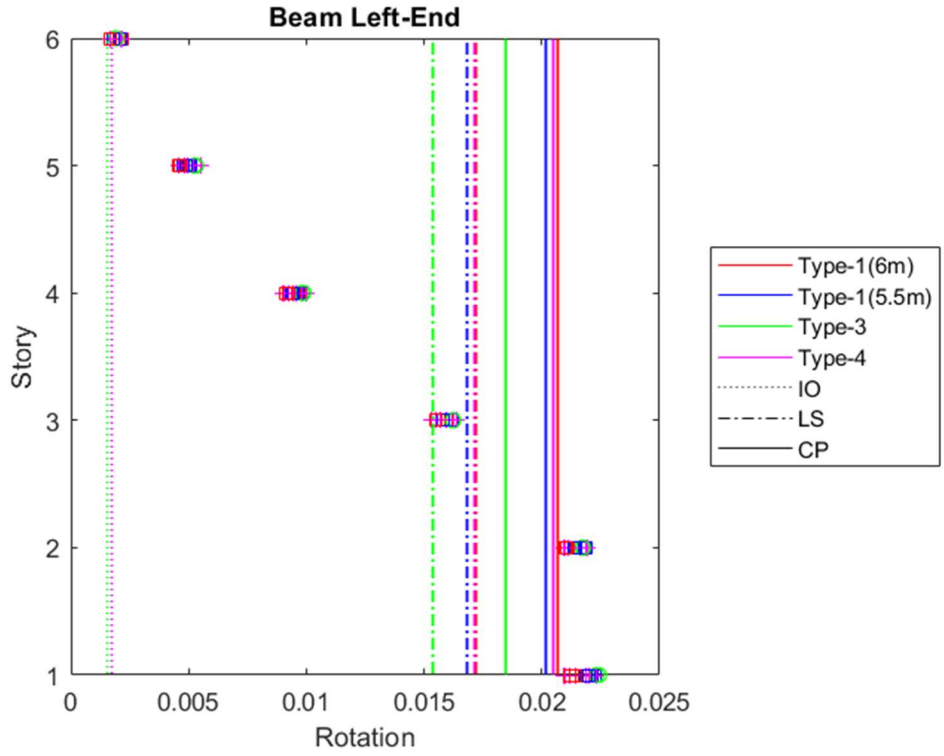

Figure 4.54. Rotations of left-end of beam in y-direction for the maximum envelope drifts in DD-1 level earthquake of moment-resisting frame

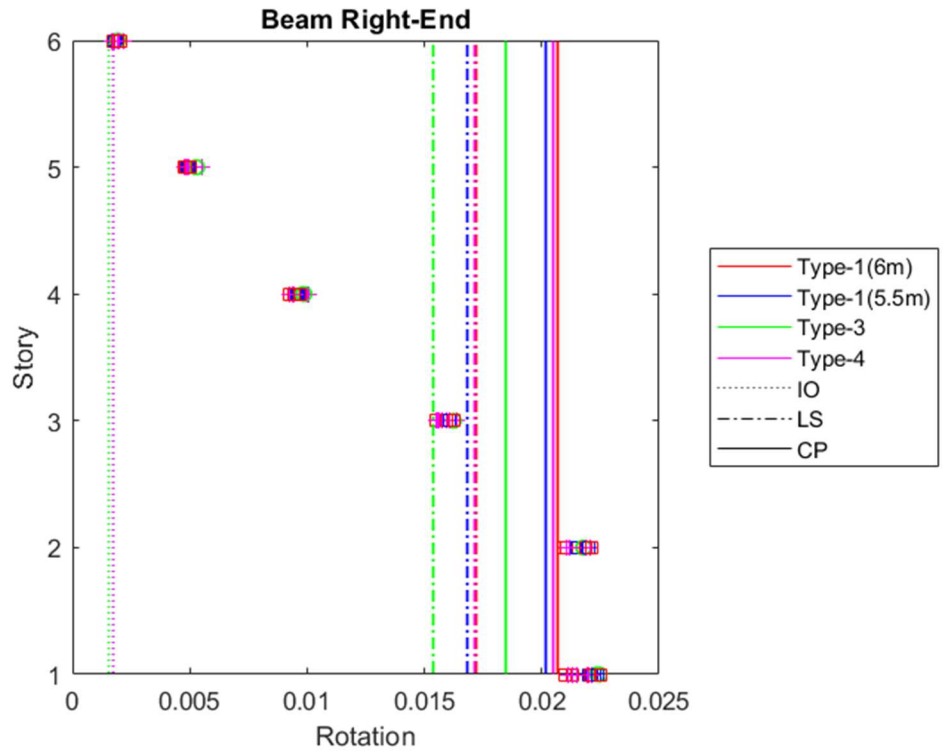

Figure 4.55. Rotations of right-end of beam in y-direction for the maximum envelope drifts in DD-1 level earthquake of moment-resisting frame

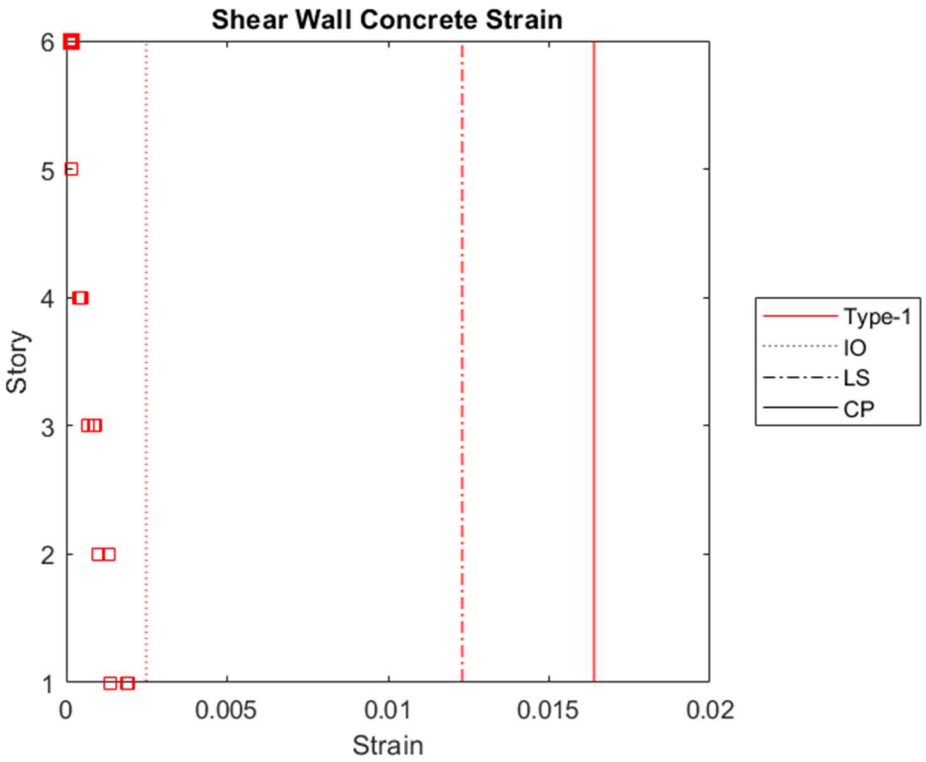

Figure 4.56. Concrete strain of bottom-end of shear wall Type-1 for the maximum envelope drifts in DD-2 level earthquake of frame with shear walls

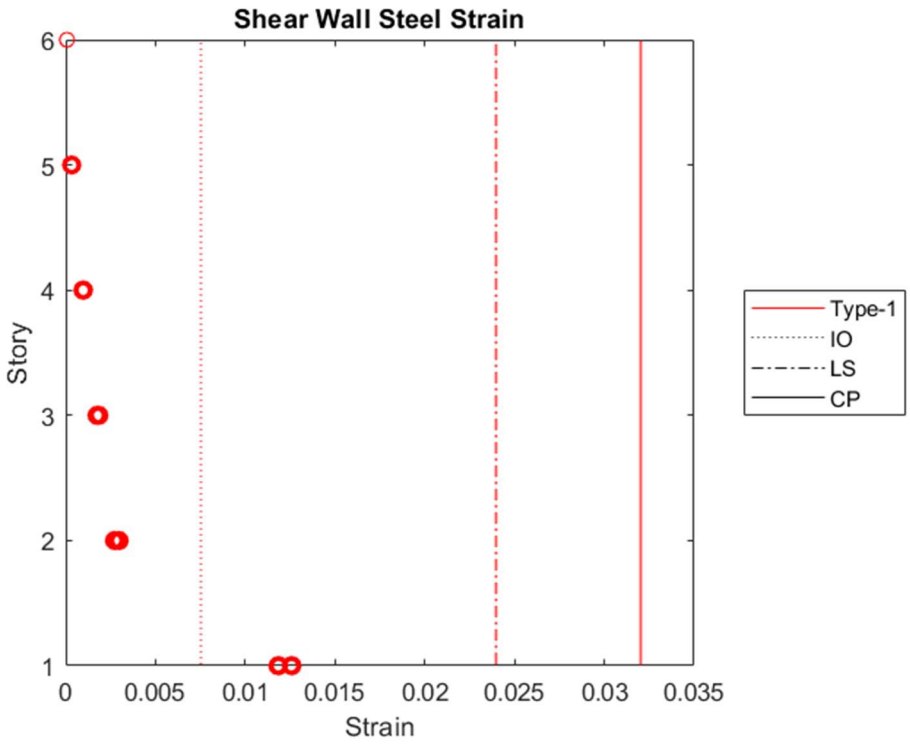

Figure 4.57. Steel strain of bottom-end of shear wall Type-1 for the maximum envelope drifts in DD-2 level earthquake of frame with shear walls

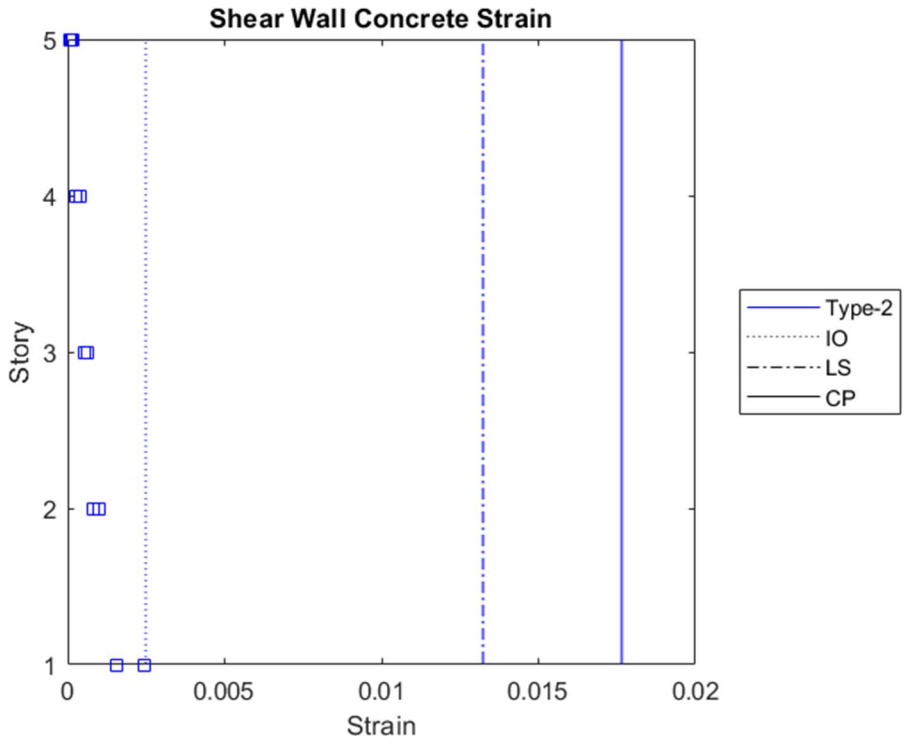

Figure 4.58. Concrete strain of bottom-end of shear wall Type-2 for the maximum envelope drifts in DD-2 level earthquake of frame with shear walls

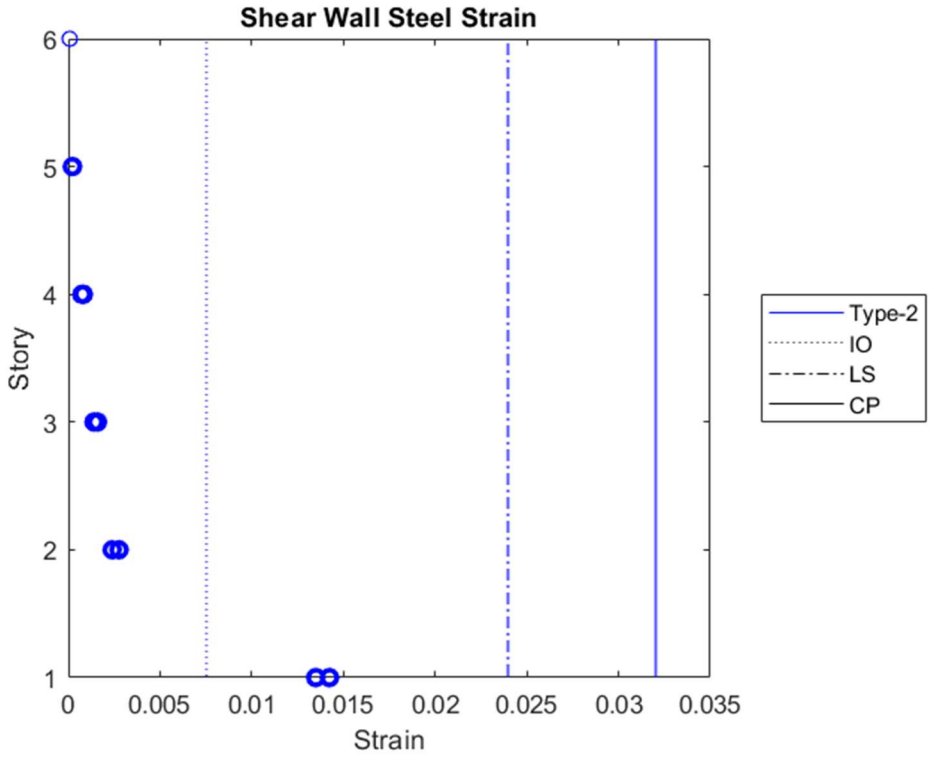

Figure 4.59. Concrete strain of bottom-end of shear wall Type-2 for the maximum envelope drifts in DD-2 level earthquake of frame with shear walls

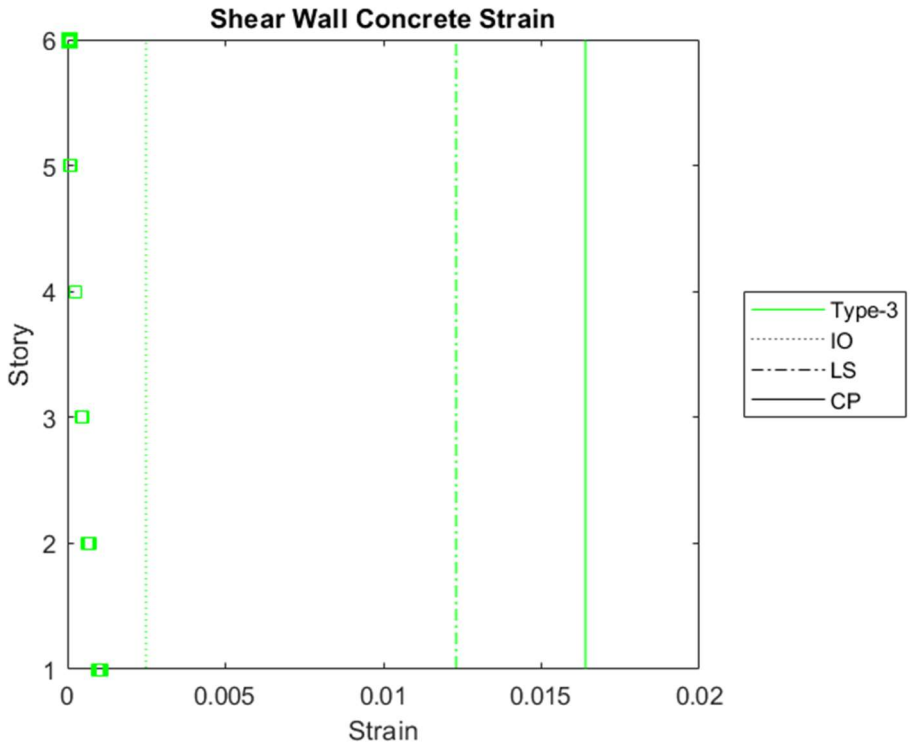

Figure 4.60. Concrete strain of bottom-end of shear wall Type-3 for the maximum envelope drifts in DD-2 level earthquake of frame with shear walls

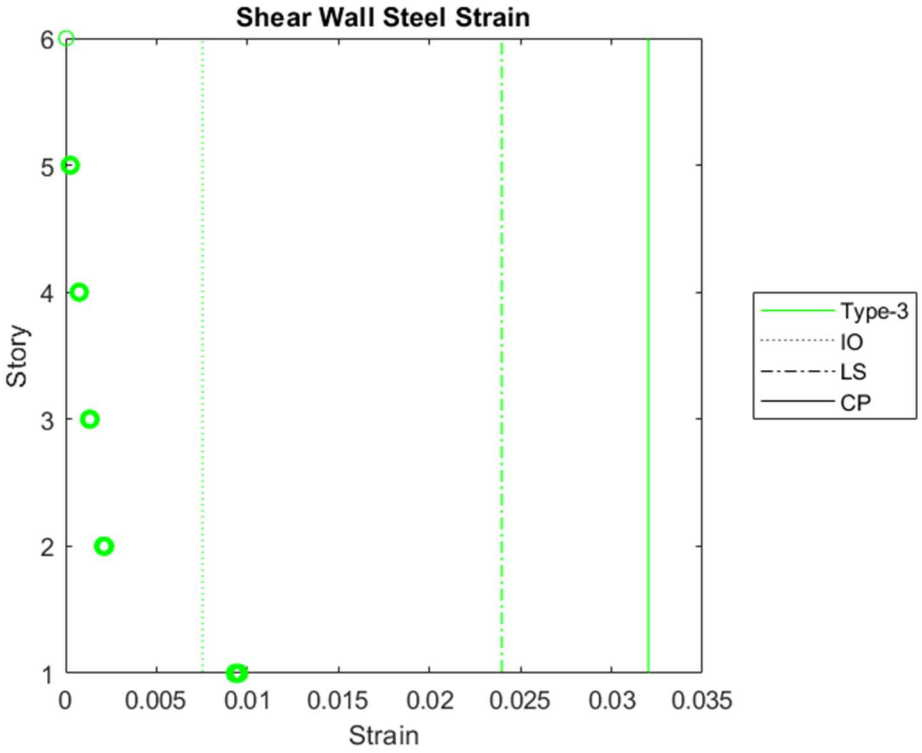

Figure 4.61. Concrete strain of bottom-end of shear wall Type-3 for the maximum envelope drifts in DD-2 level earthquake of frame with shear walls

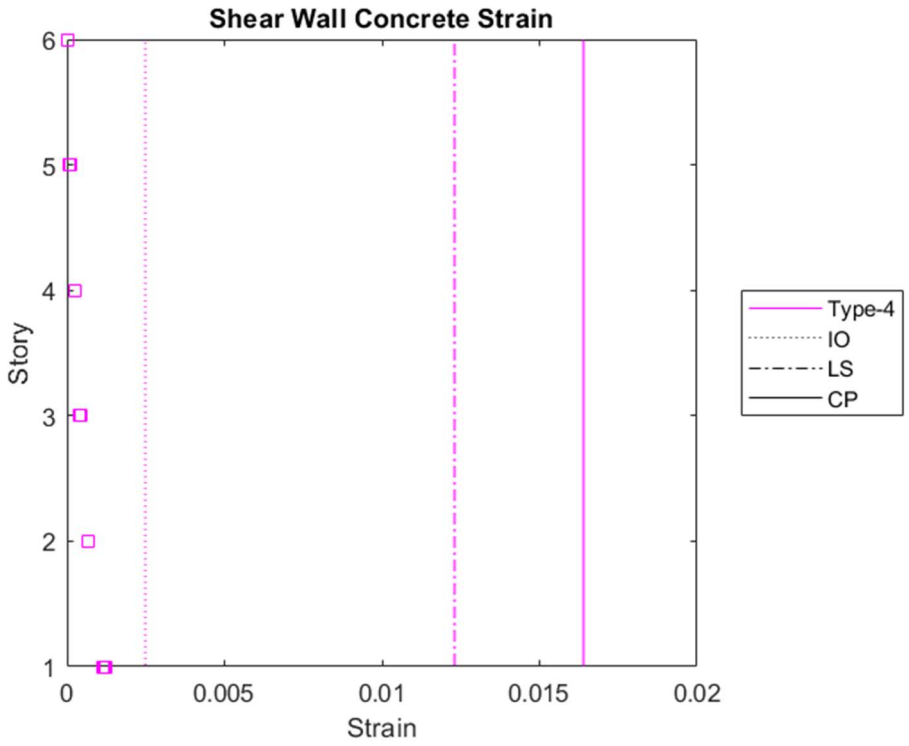

Figure 4.62. Concrete strain of bottom-end of shear wall Type-4 for the maximum envelope drifts in DD-2 level earthquake of frame with shear walls

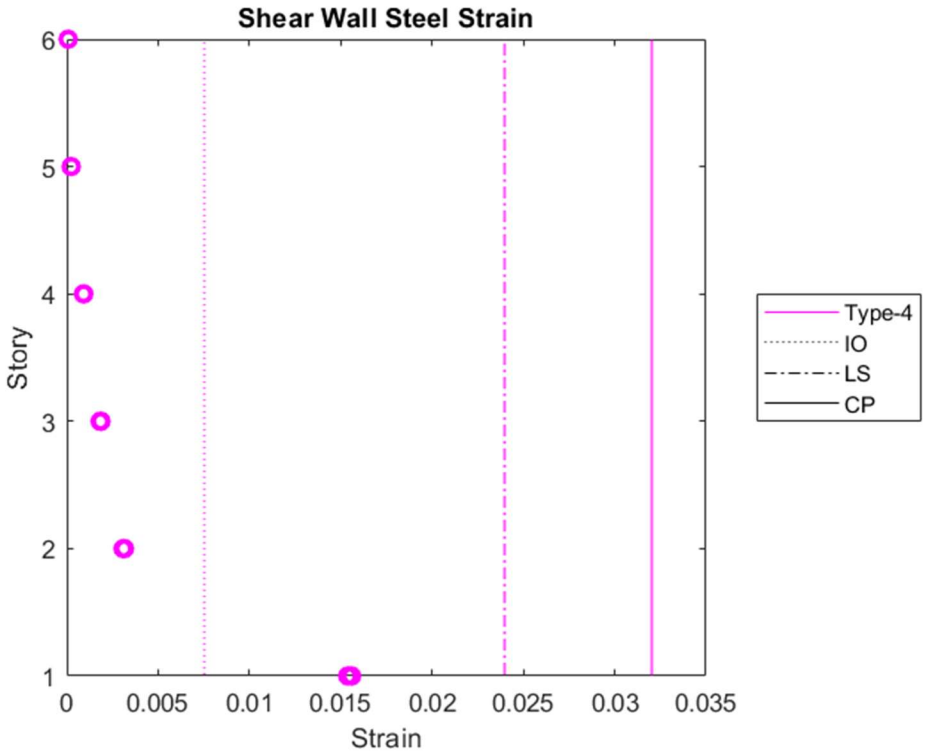

Figure 4.63. Concrete strain of bottom-end of shear wall Type-4 for the maximum envelope drifts in DD-2 level earthquake of frame with shear walls

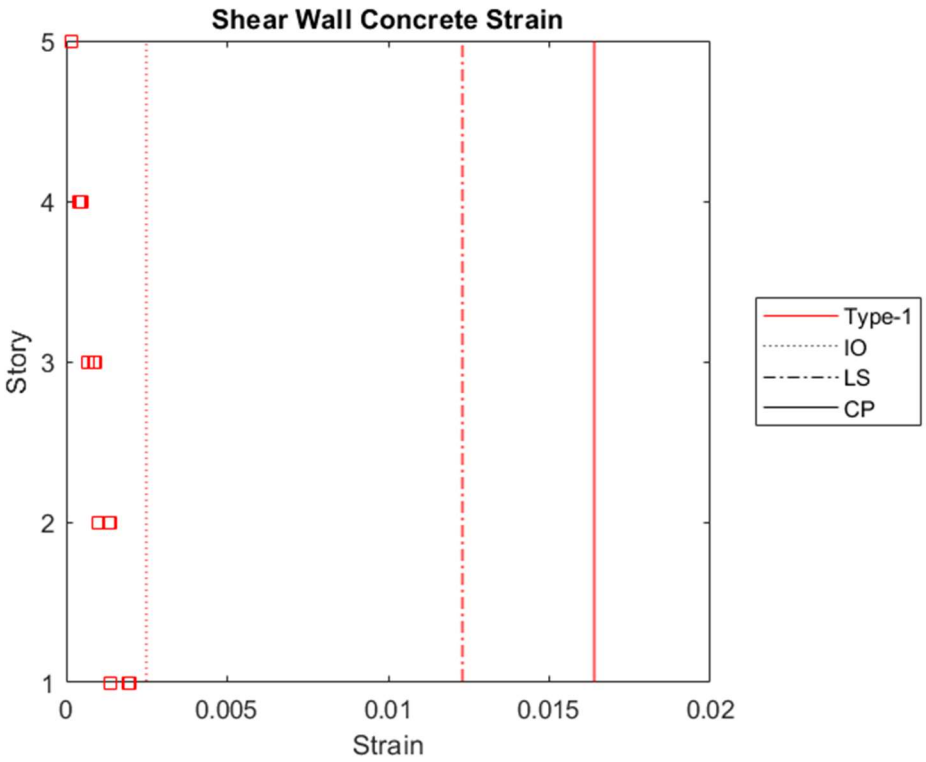

Figure 4.64. Concrete strain of bottom-end of shear wall Type-1 at roof when its maximum in DD-2 level earthquake of frame with shear walls

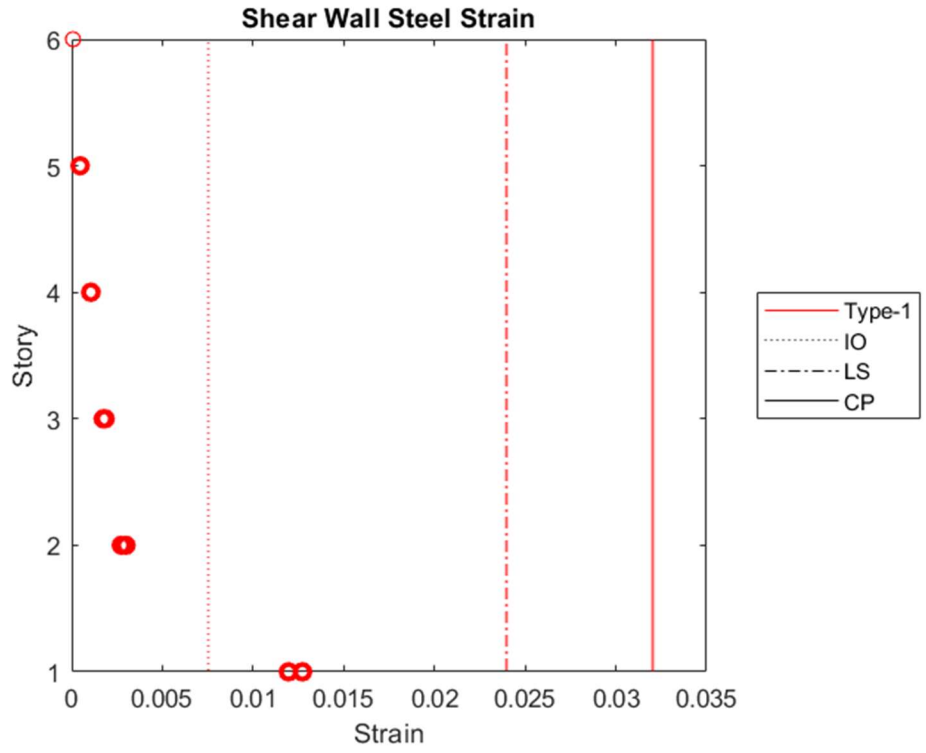

Figure 4.65. Steel strain of bottom-end of shear wall Type-1 at roof when its maximum in DD-2 level earthquake of frame with shear walls

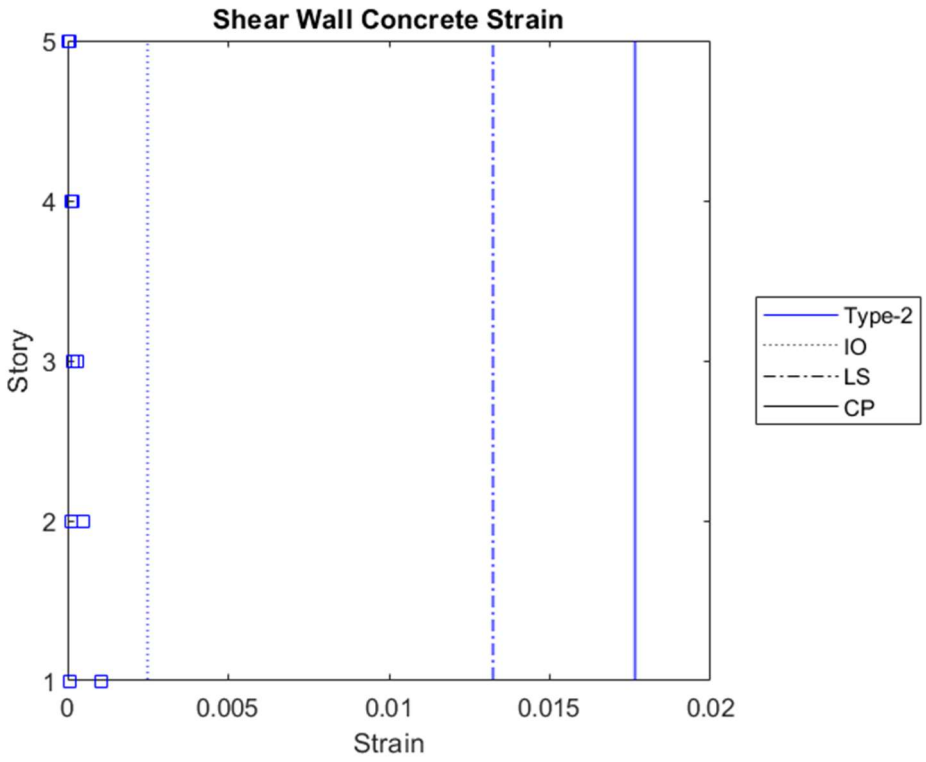

Figure 4.66. Concrete strain of bottom-end of shear wall Type-2 at roof when its maximum in DD-2 level earthquake of frame with shear walls

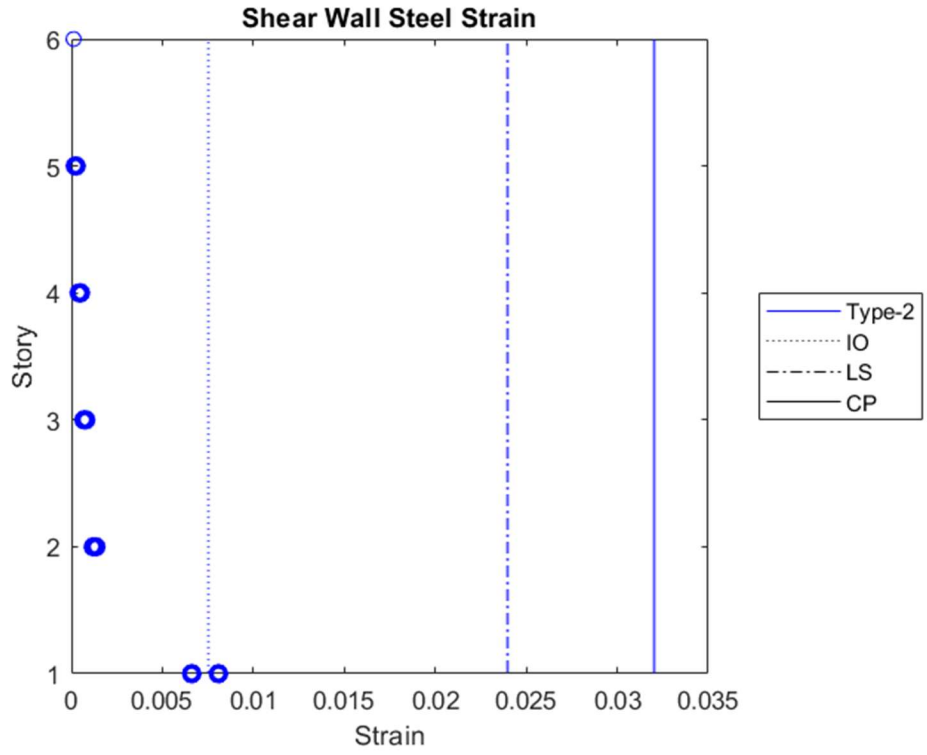

Figure 4.67. Steel strain of bottom-end of shear wall Type-2 at roof when its maximum in DD-2 level earthquake of frame with shear walls

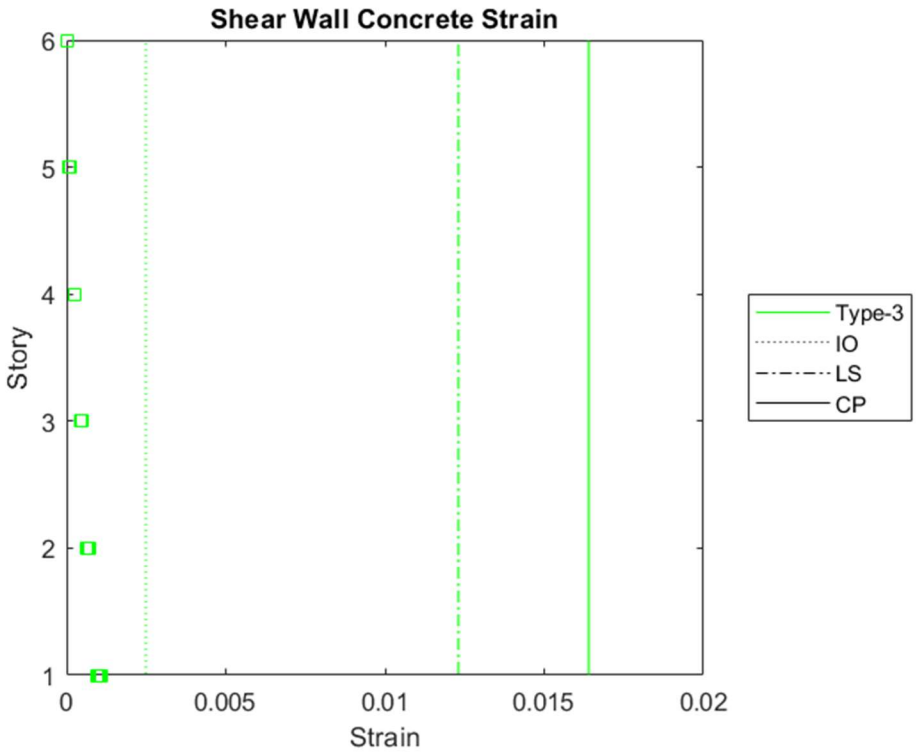

Figure 4.68. Concrete strain of bottom-end of shear wall Type-3 at roof when its maximum in DD-2 level earthquake of frame with shear walls

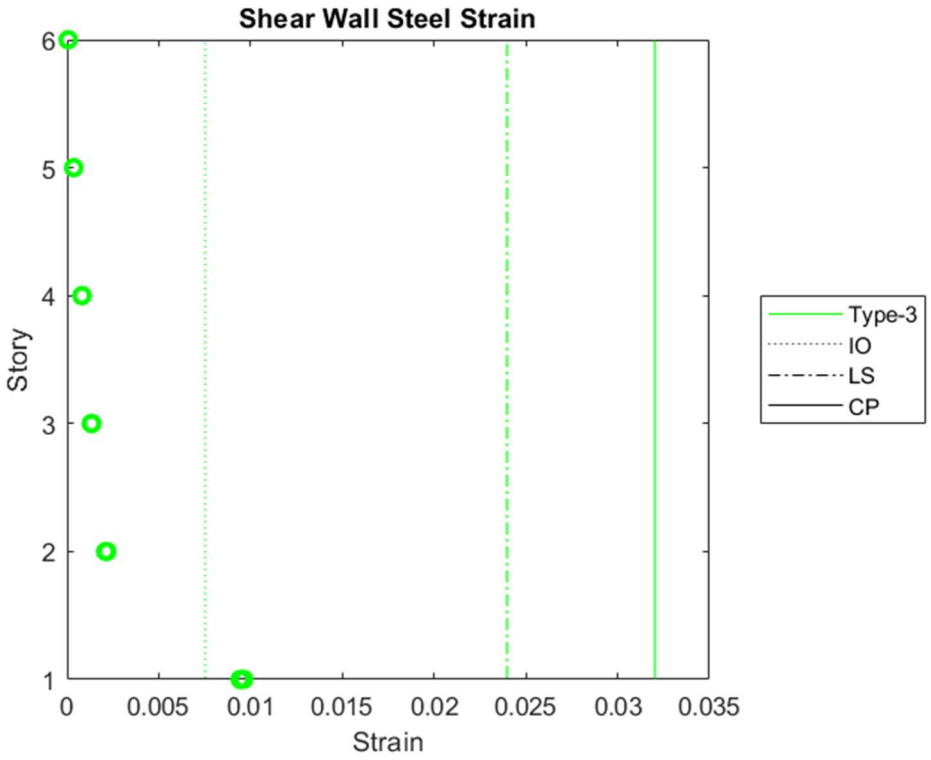

Figure 4.69. Steel strain of bottom-end of shear wall Type-3 at roof when its maximum in DD-2 level earthquake of frame with shear walls

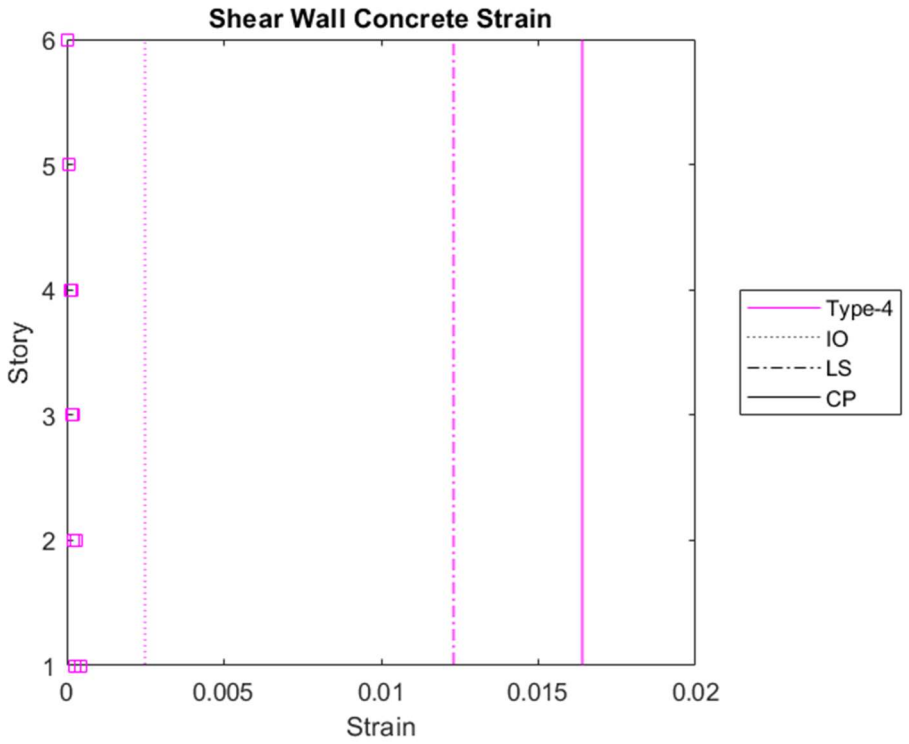

Figure 4.70. Concrete strain of bottom-end of shear wall Type-4 at roof when its maximum in DD-2 level earthquake of frame with shear walls

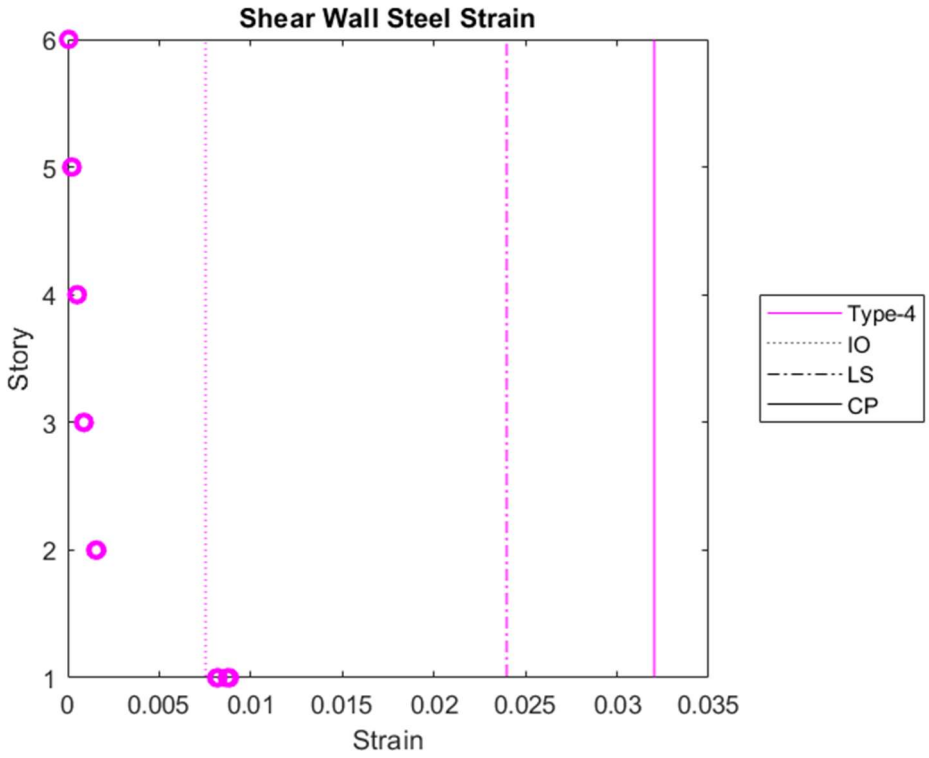

Figure 4.71. Steel strain of bottom-end of shear wall Type-4 at roof when its maximum in DD-2 level earthquake of frame with shear walls

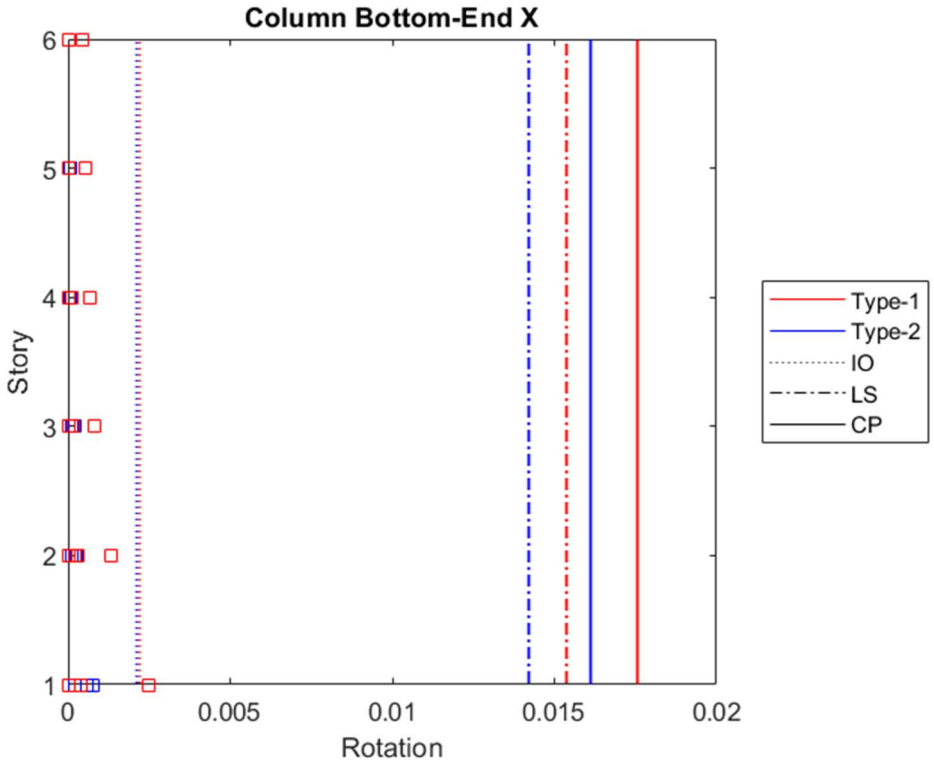

Figure 4.72. Rotations of bottom-end of column in x-direction for the maximum envelope drifts in DD-2 level earthquake of frame with shear walls

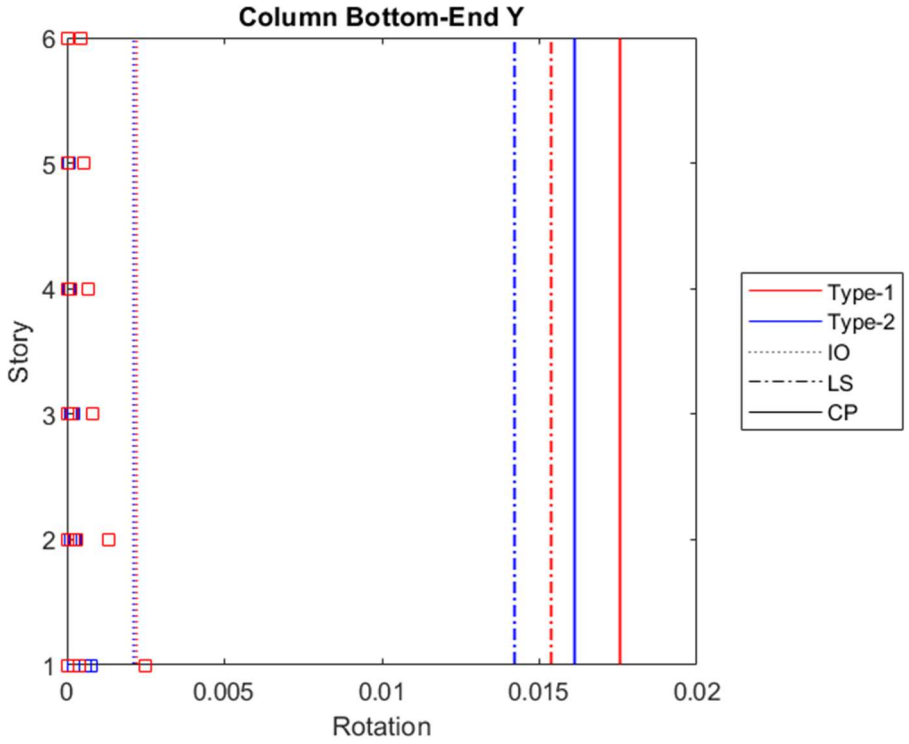

Figure 4.73. Rotations of bottom-end of column in y-direction for the maximum envelope drifts in DD-2 level earthquake of frame with shear walls

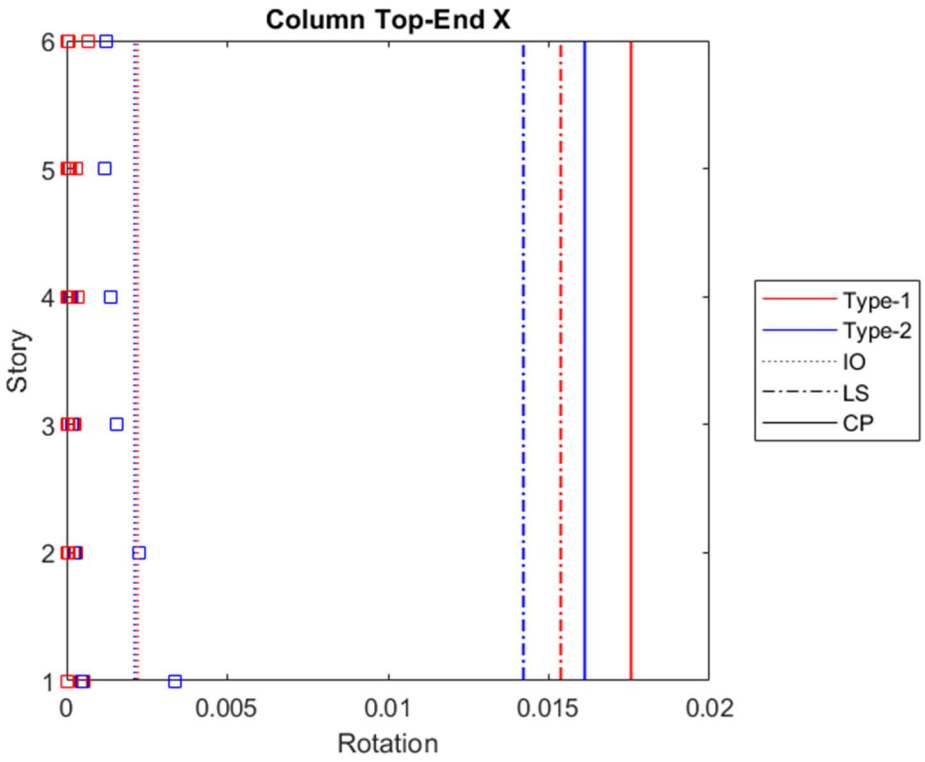

Figure 4.74. Rotations of top-end of column in x-direction for the maximum envelope drifts in DD-2 level earthquake of frame with shear walls

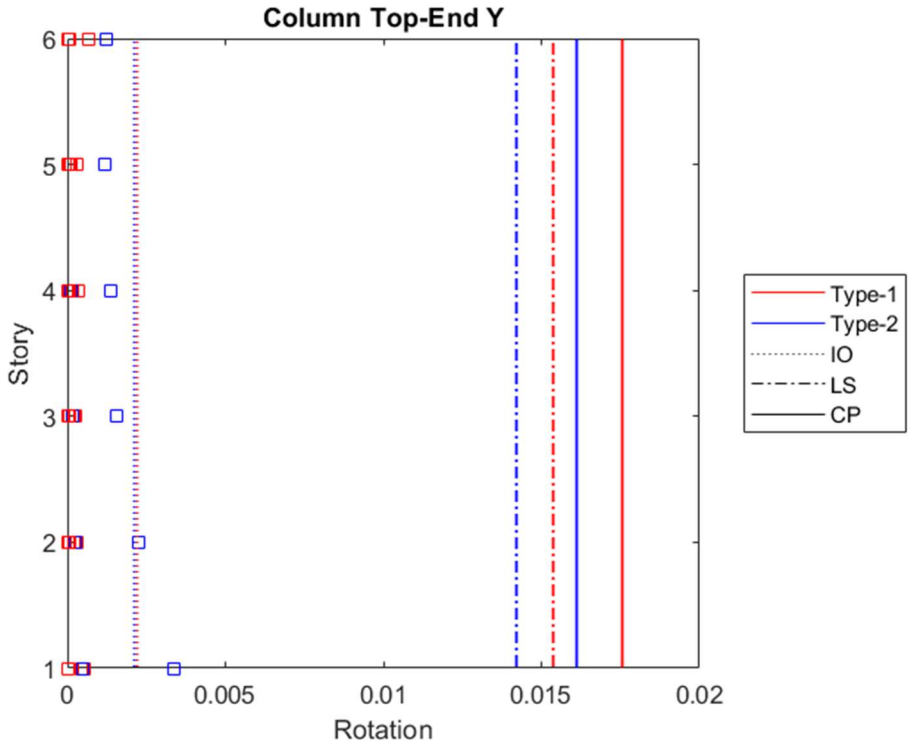

Figure 4.75. Rotations of top-end of column in y-direction for the maximum envelope drifts in DD-2 level earthquake of frame with shear walls

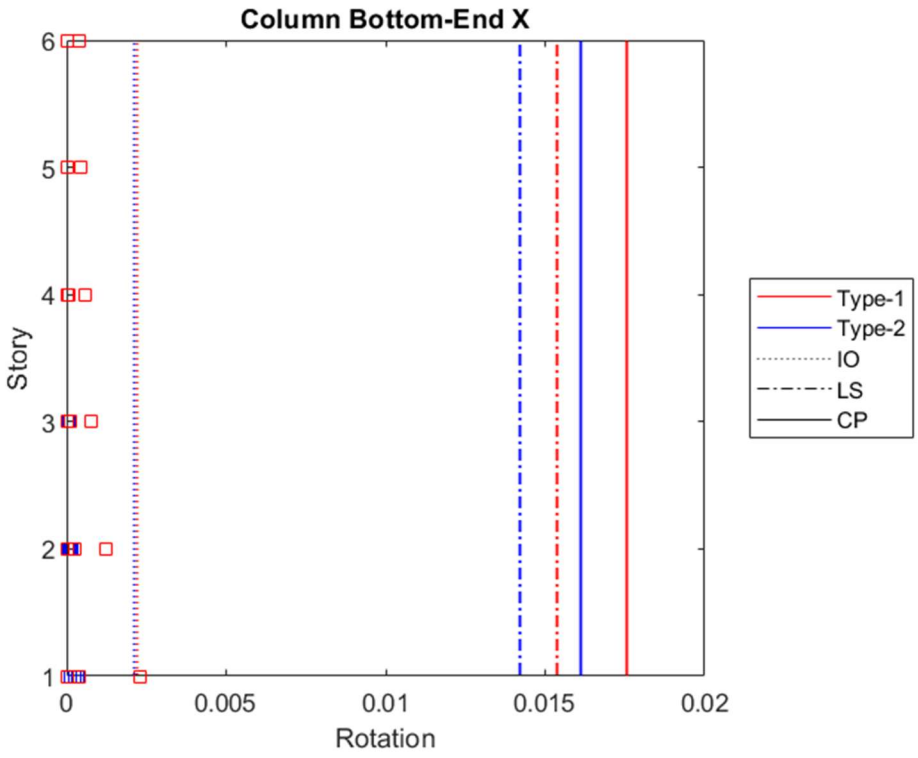

Figure 4.76. Rotations of bottom-end of column in x-direction at roof when its maximum in DD-2 level earthquake of frame with shear walls

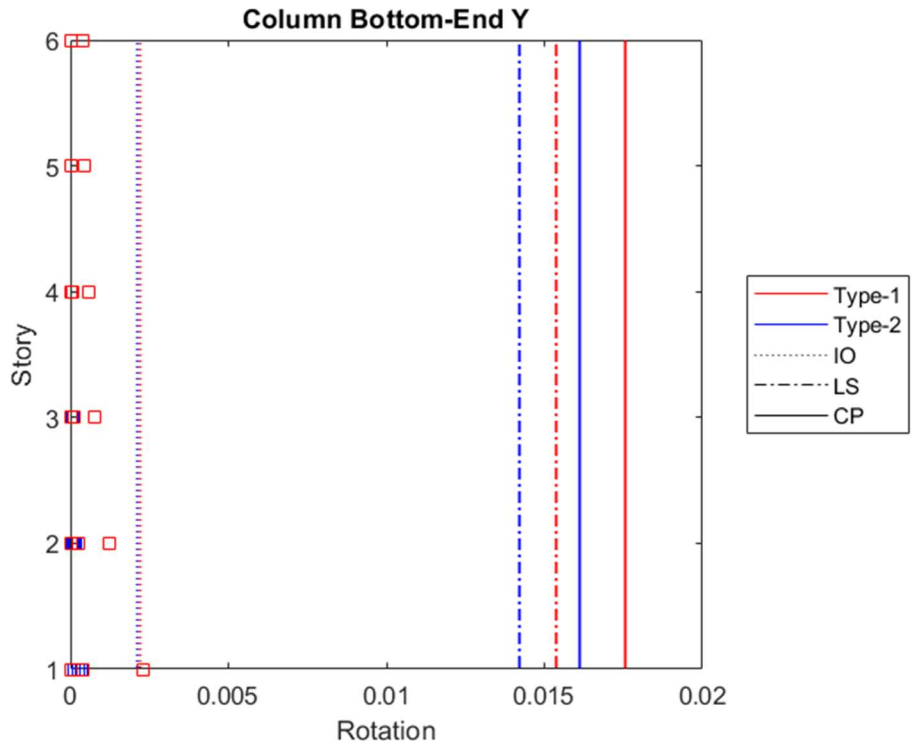

Figure 4.77. Rotations of bottom-end of column in y-direction at roof when its maximum in DD-2 level earthquake of frame with shear walls

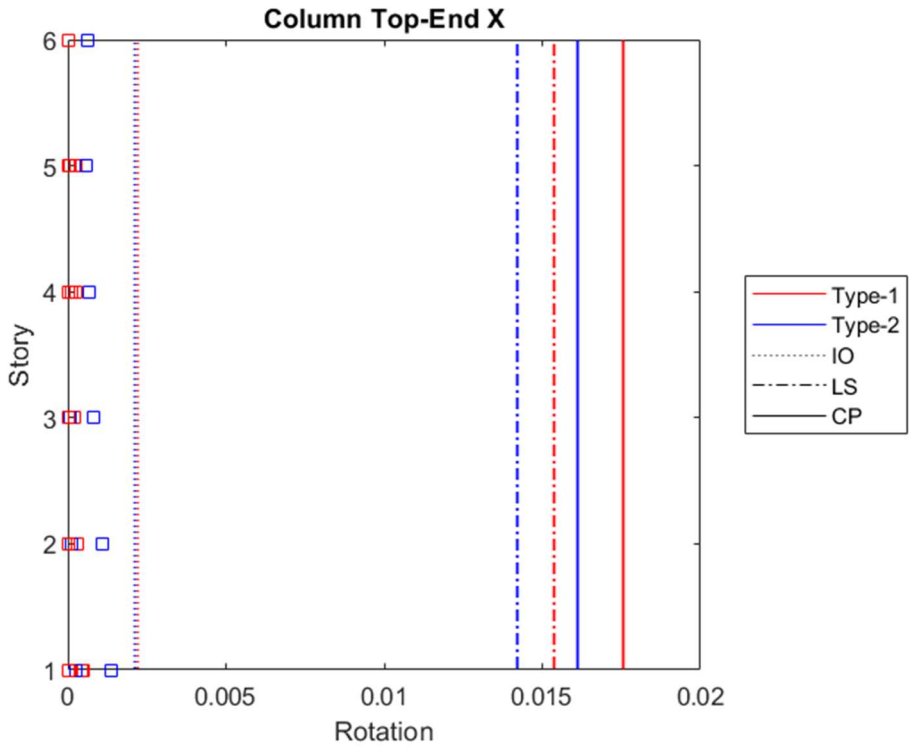

Figure 4.78. Rotations of top-end of column in x-direction at roof when its maximum in DD-2 level earthquake of frame with shear walls

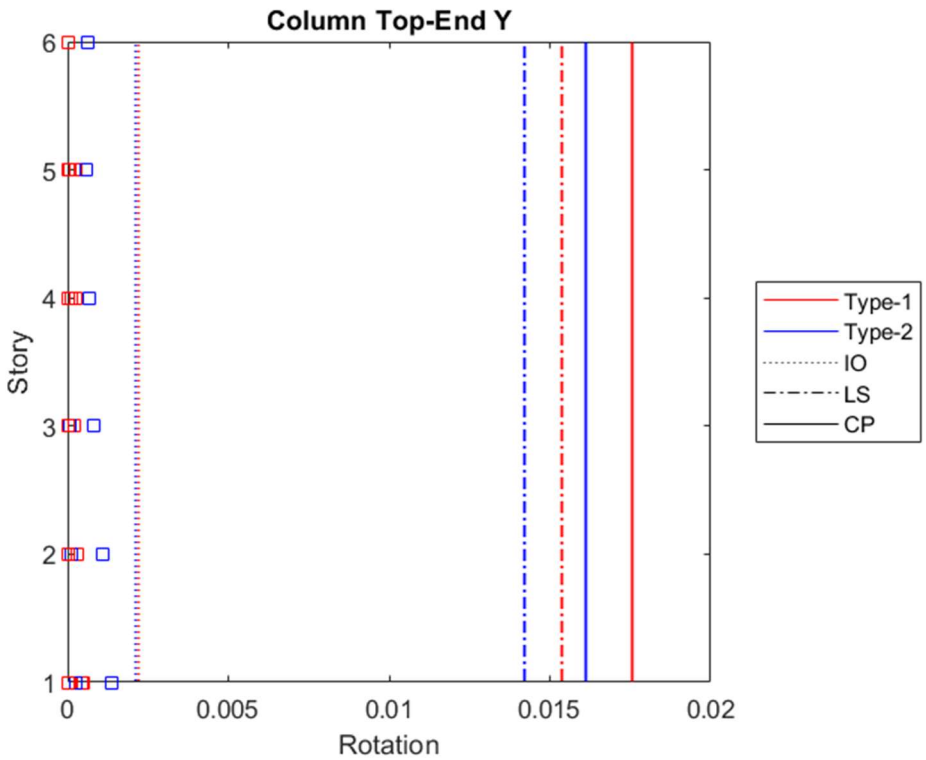

Figure 4.79. Rotations of top-end of column in y-direction at roof when its maximum in DD-2 level earthquake of frame with shear walls

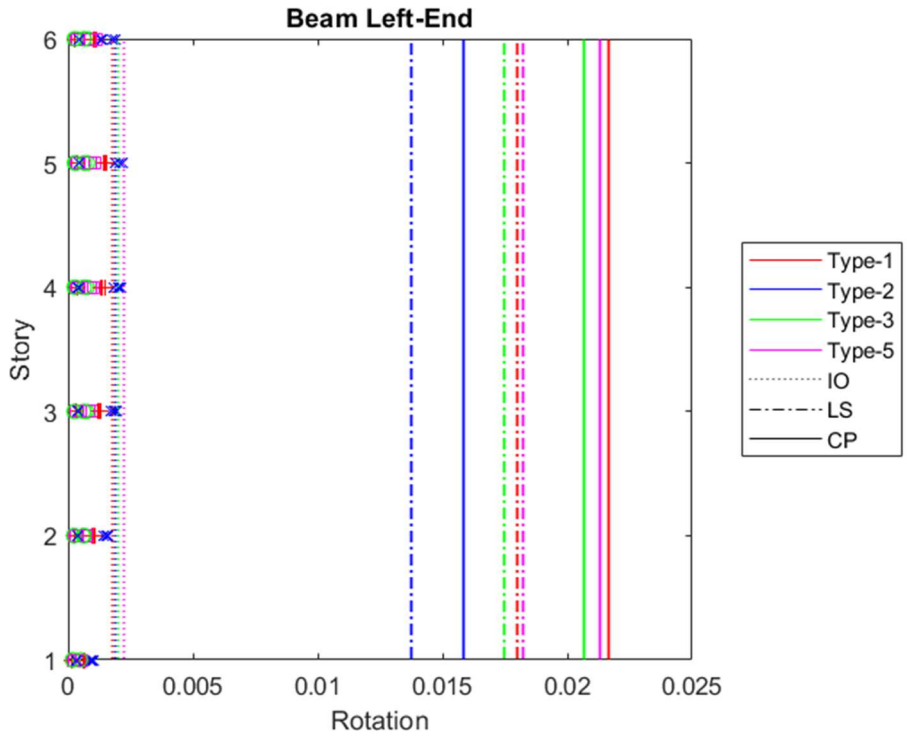

Figure 4.80. Rotations of left-end of beam in x-direction at roof when its maximum in DD-2 level earthquake of frame with shear walls

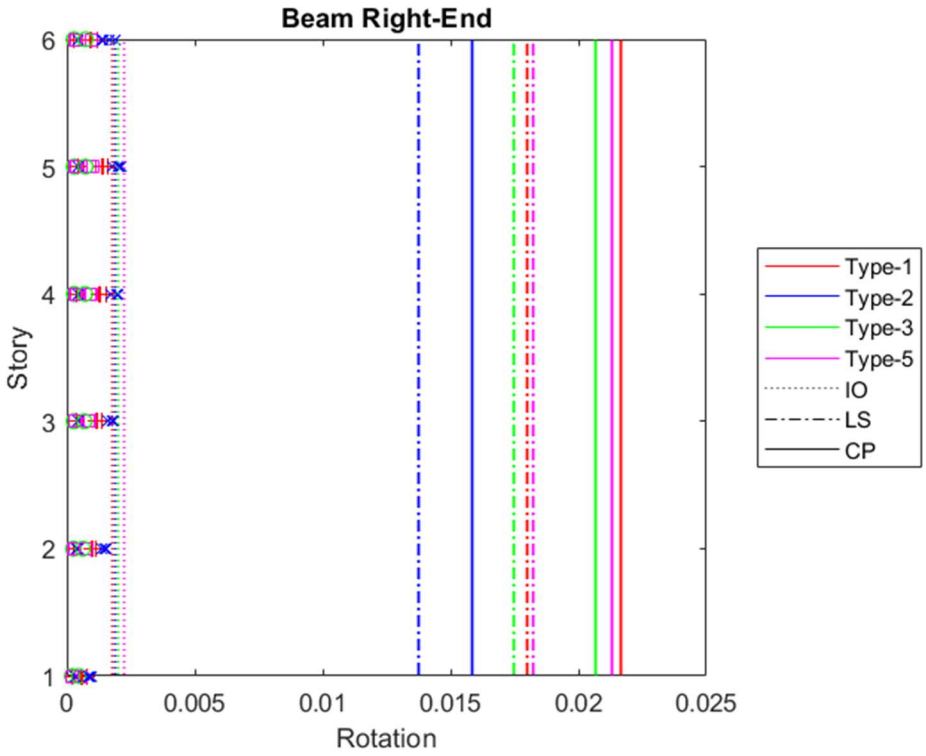

Figure 4.81. Rotations of right-end of beam in x-direction at roof when its maximum in DD-2 level earthquake of frame with shear walls

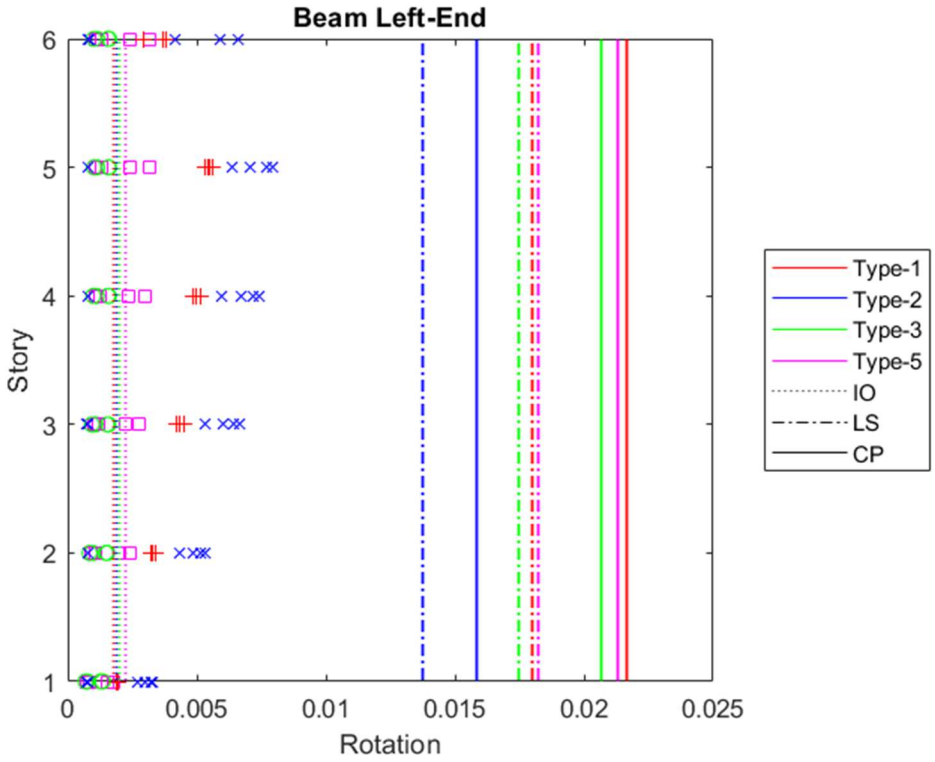

Figure 4.82. Rotations of left-end of beam in x-direction for the maximum envelope drifts in DD-2 level earthquake of frame with shear walls

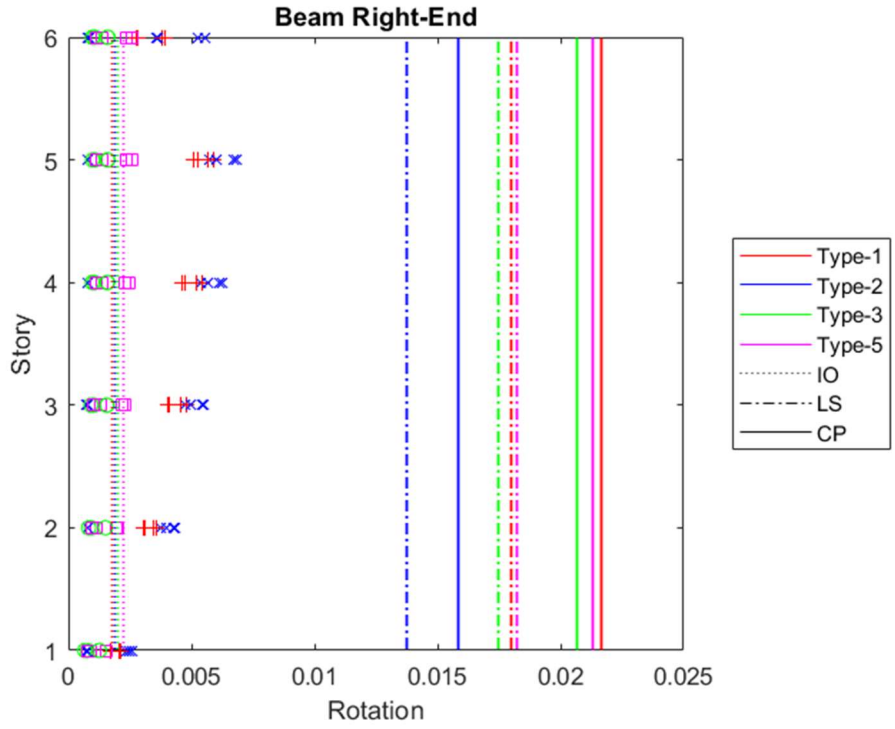

Figure 4.83. Rotations of right-end of beam in x-direction for the maximum envelope drifts in DD-2 level earthquake of frame with shear walls

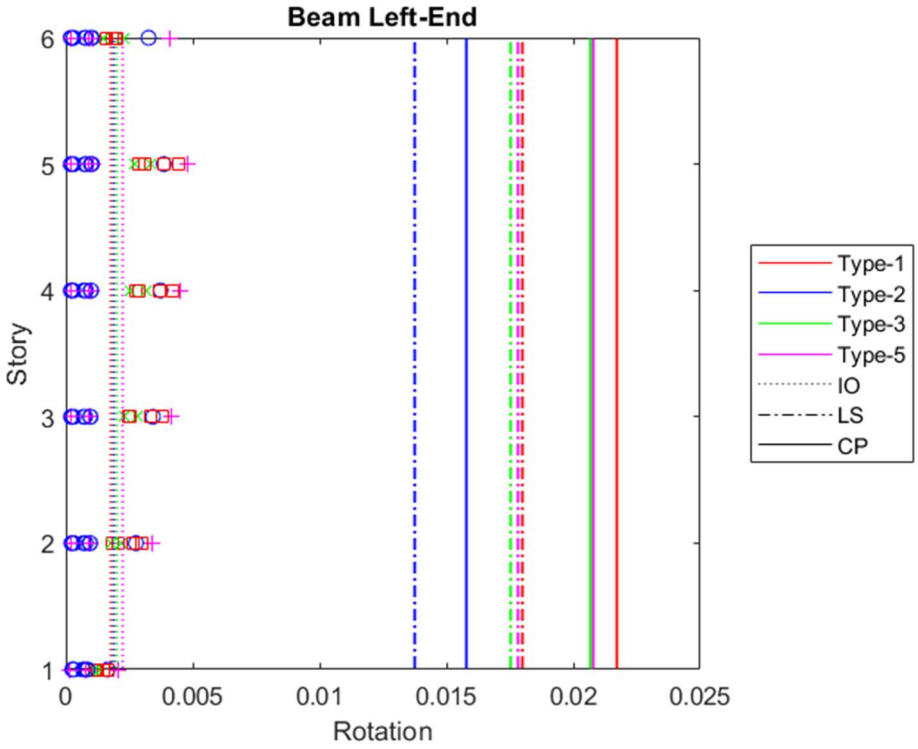

Figure 4.84. Rotations of left-end of beam in y-direction at roof when its maximum in DD-2 level earthquake of frame with shear walls

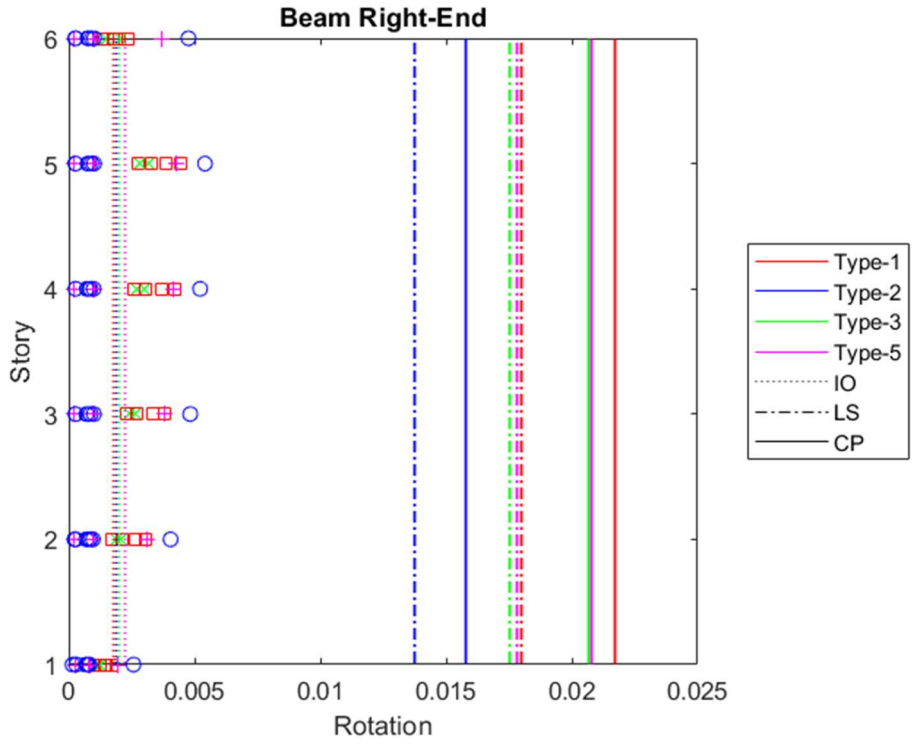

Figure 4.85. Rotations of right-end of beam in y-direction at roof when its maximum in DD-2 level earthquake of frame with shear walls

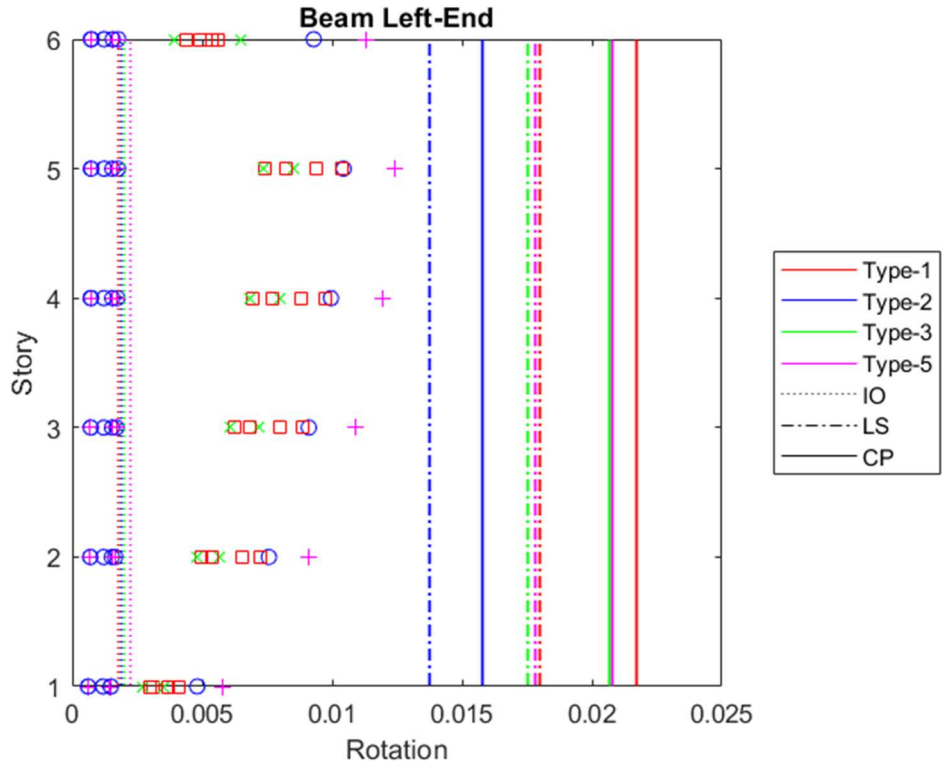

Figure 4.86. Rotations of left-end of beam in y-direction for the maximum envelope drifts in DD-2 level earthquake of frame with shear walls

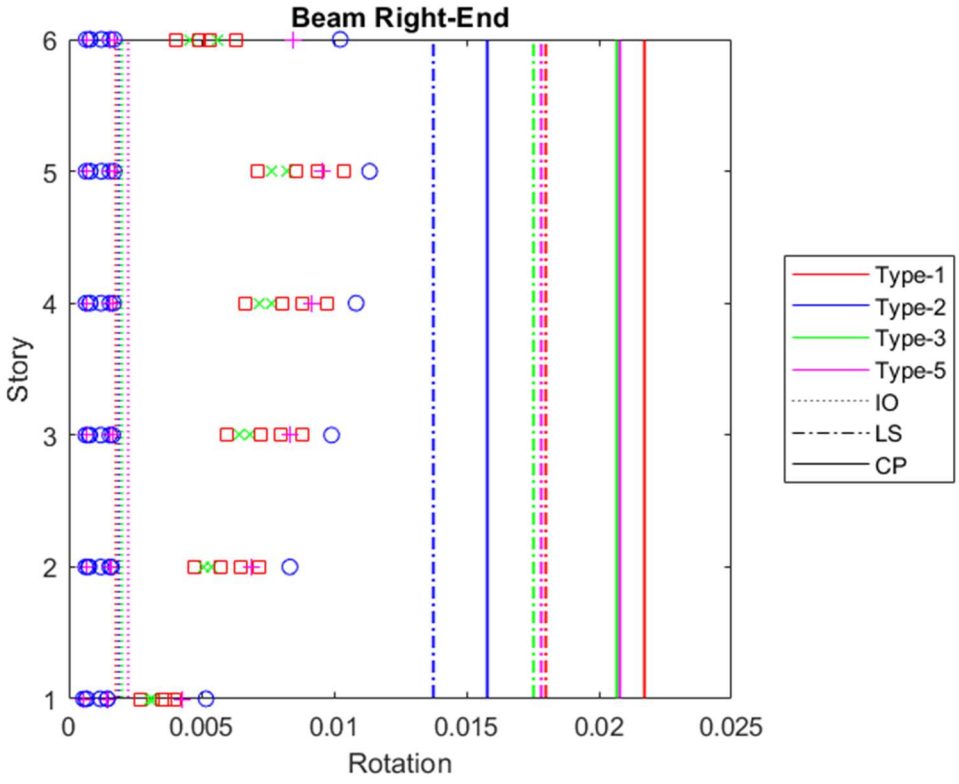

Figure 4.87. Rotations of right-end of beam in y-direction for the maximum envelope drifts in DD-2 level earthquake of frame with shear walls

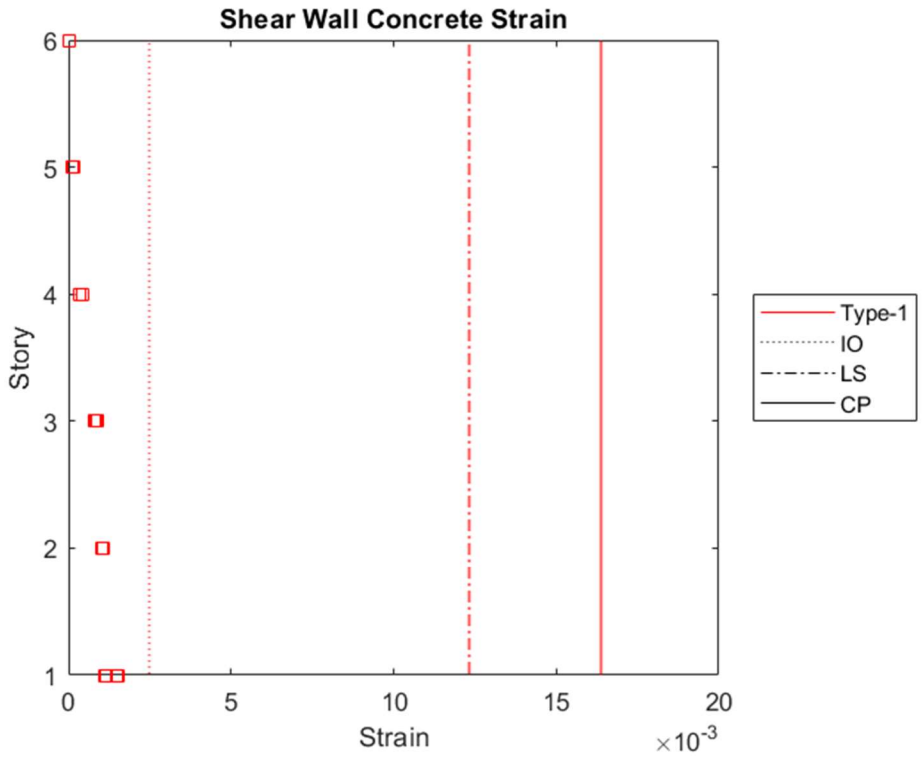

Figure 4.88. Concrete strain of bottom-end of shear wall Type-1 for the maximum envelope drifts in DD-1 level earthquake of frame with shear walls

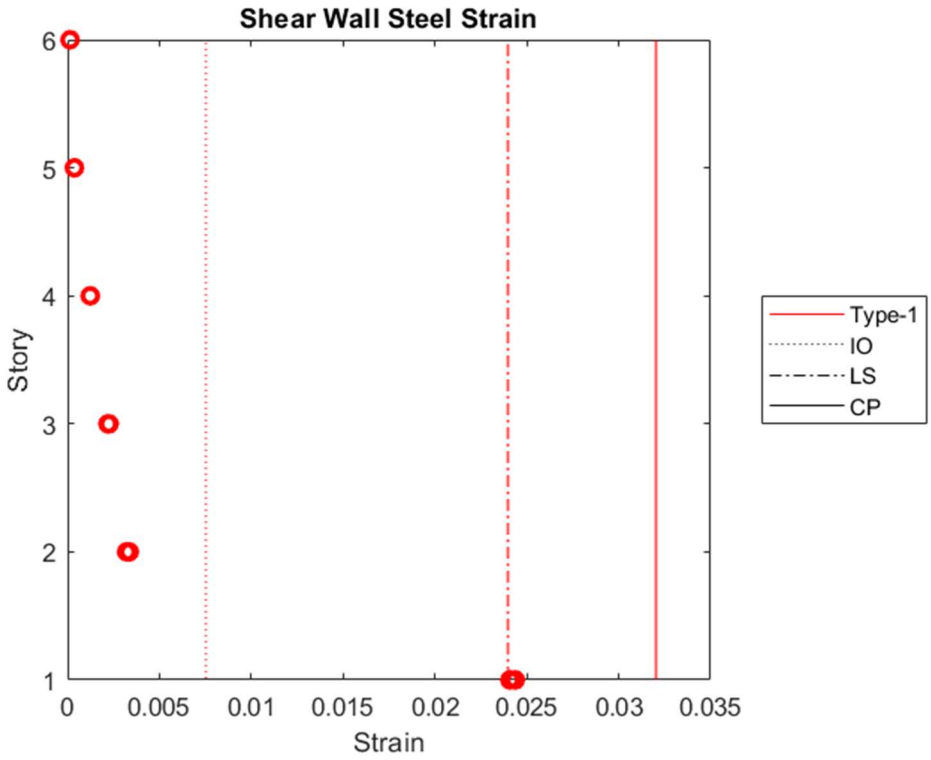

Figure 4.89. Concrete strain of bottom-end of shear wall Type-1 for the maximum envelope drifts in DD-1 level earthquake of frame with shear walls

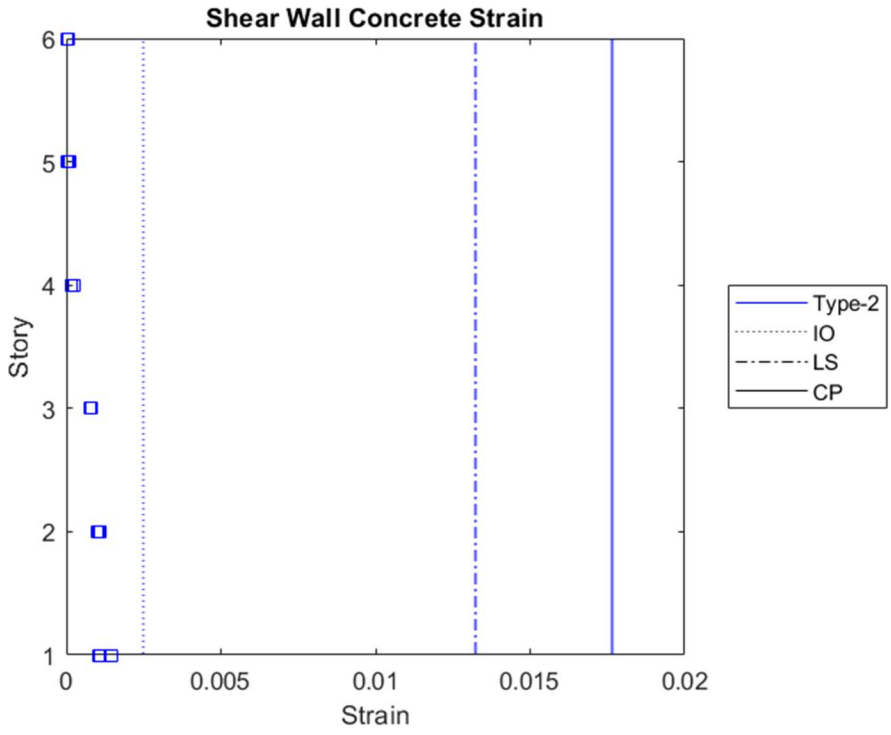

Figure 4.90. Concrete strain of bottom-end of shear wall Type-2 for the maximum envelope drifts in DD-1 level earthquake of frame with shear walls

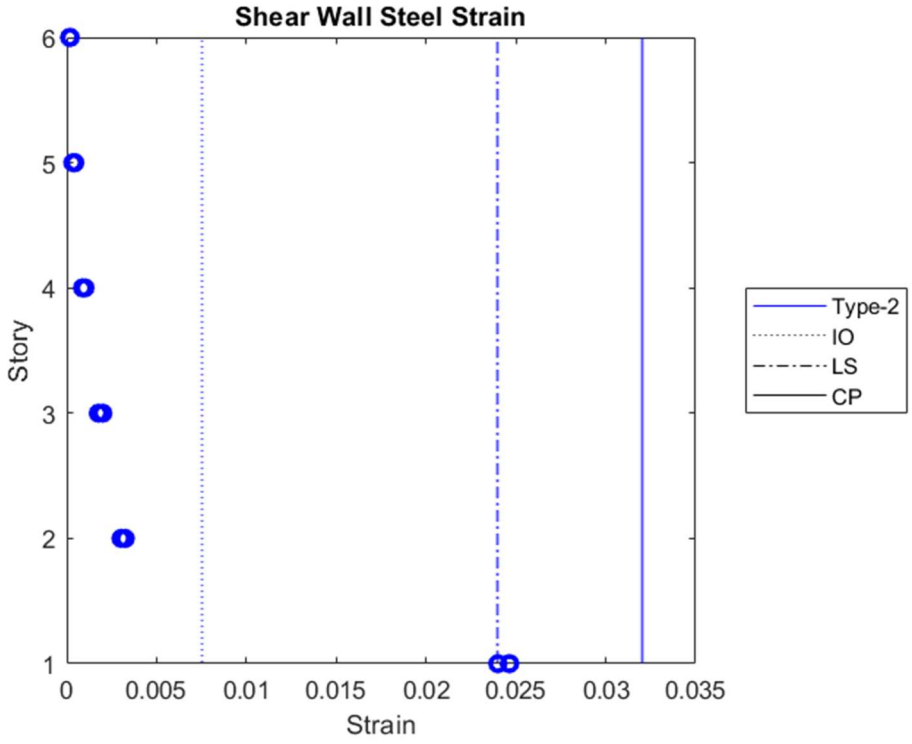

Figure 4.91. Concrete strain of bottom-end of shear wall Type-2 for the maximum envelope drifts in DD-1 level earthquake of frame with shear walls

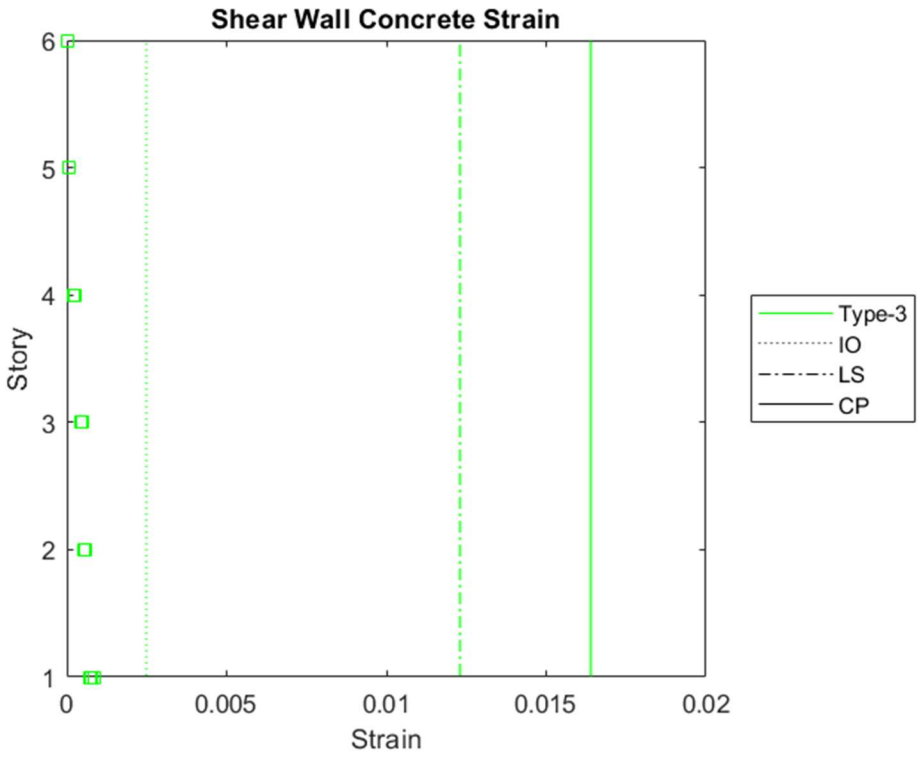

Figure 4.92. Concrete strain of bottom-end of shear wall Type-3 for the maximum envelope drifts in DD-1 level earthquake of frame with shear walls

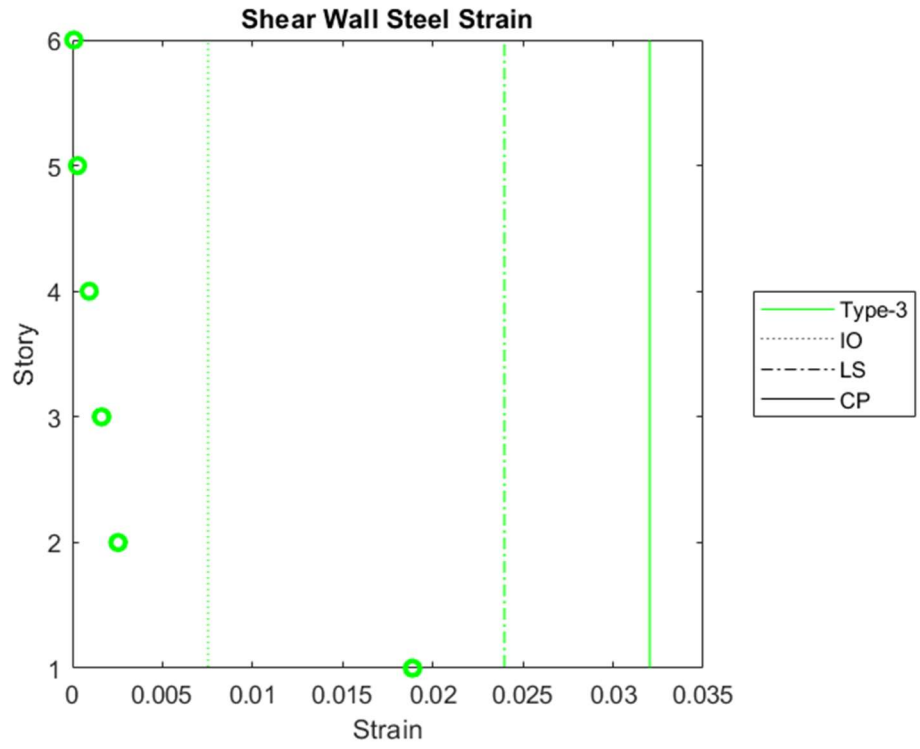

Figure 4.93. Concrete strain of bottom-end of shear wall Type-3 for the maximum envelope drifts in DD-1 level earthquake of frame with shear walls

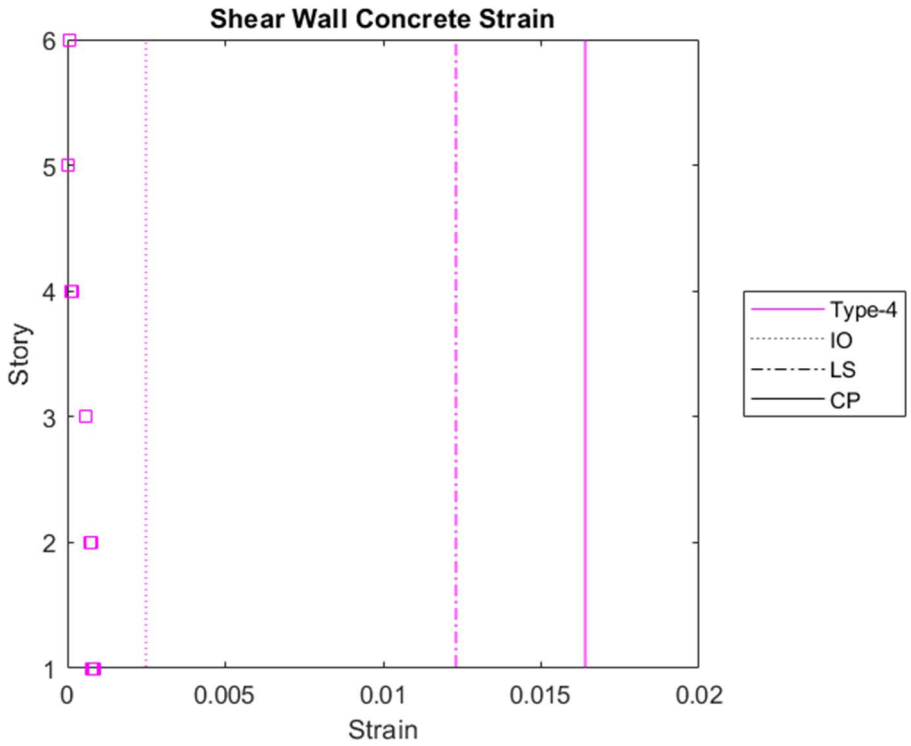

Figure 4.94. Concrete strain of bottom-end of shear wall Type-4 for the maximum envelope drifts in DD-1 level earthquake of frame with shear walls

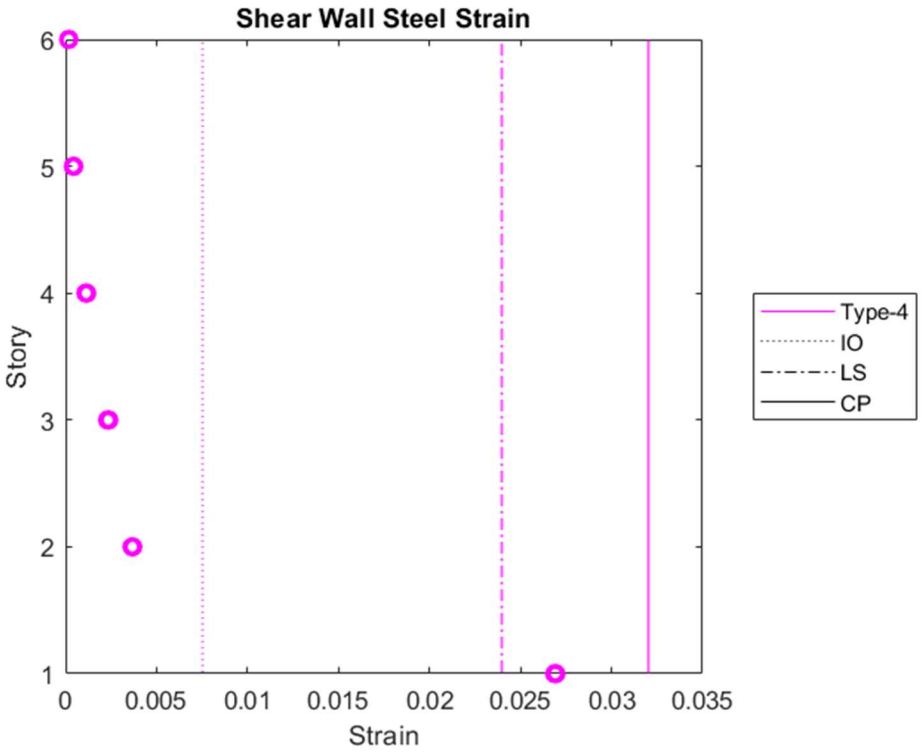

Figure 4.95. Concrete strain of bottom-end of shear wall Type-4 for the maximum envelope drifts in DD-1 level earthquake of frame with shear walls

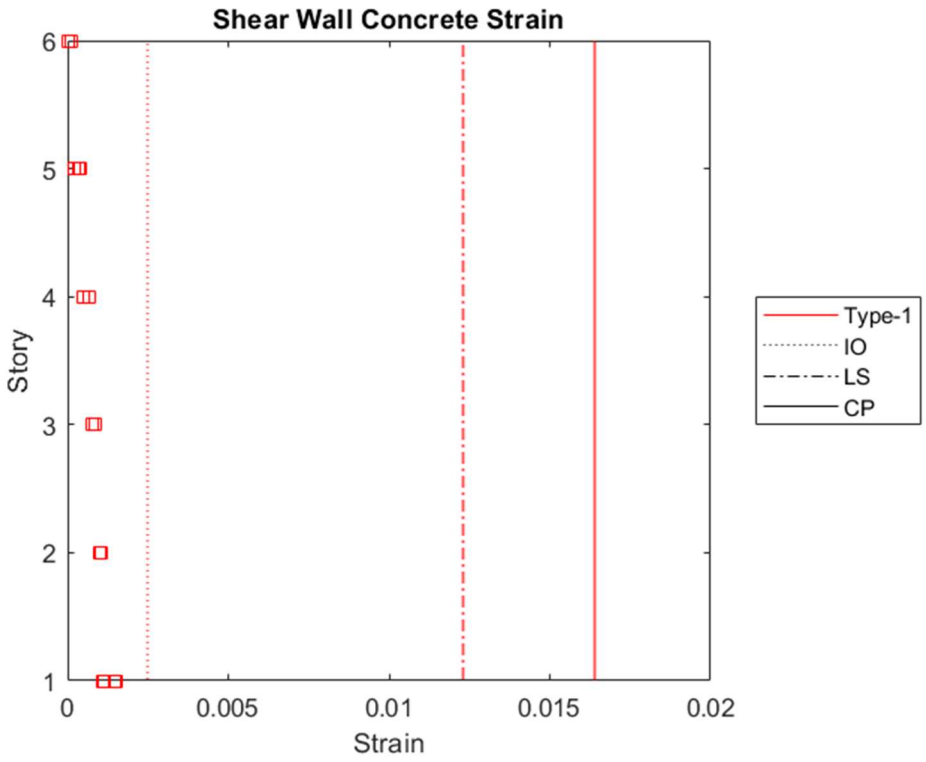

Figure 4.96. Concrete strain of bottom-end of shear wall Type-1 at roof when its maximum in DD-1 level earthquake of frame with shear walls

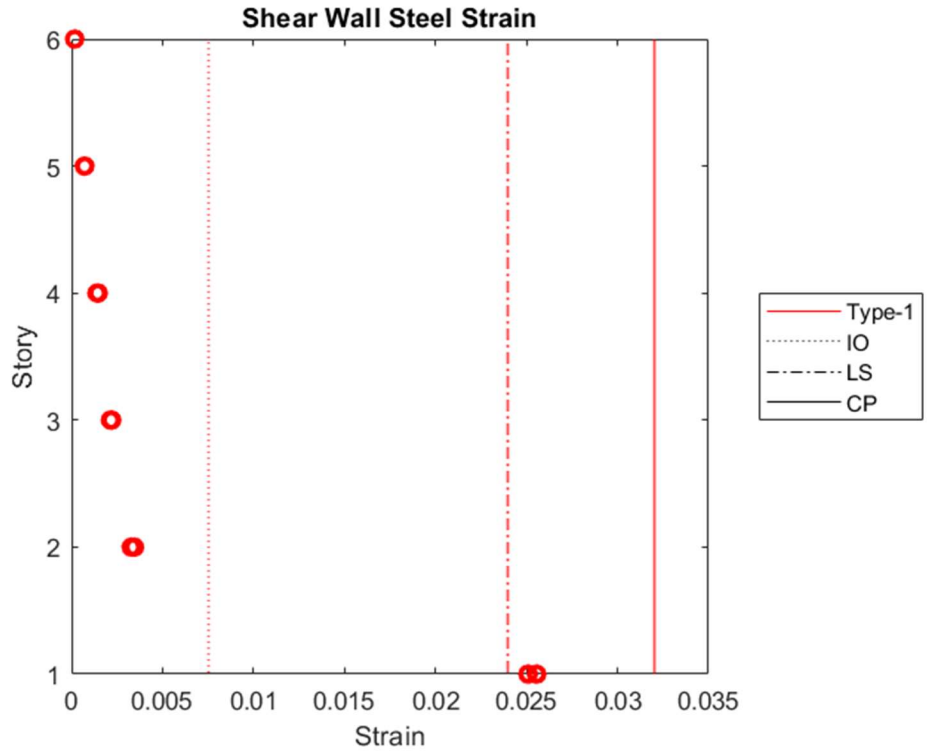

Figure 4.97. Concrete strain of bottom-end of shear wall Type-1 at roof when its maximum in DD-1 level earthquake of frame with shear walls

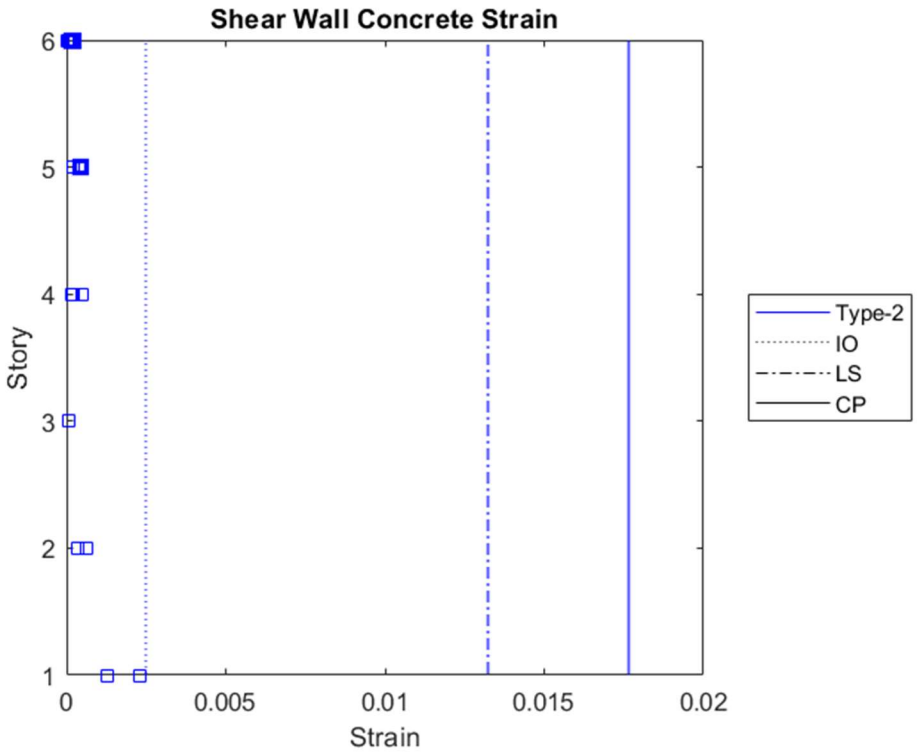

Figure 4.98. Concrete strain of bottom-end of shear wall Type-2 at roof when its maximum in DD-1 level earthquake of frame with shear walls

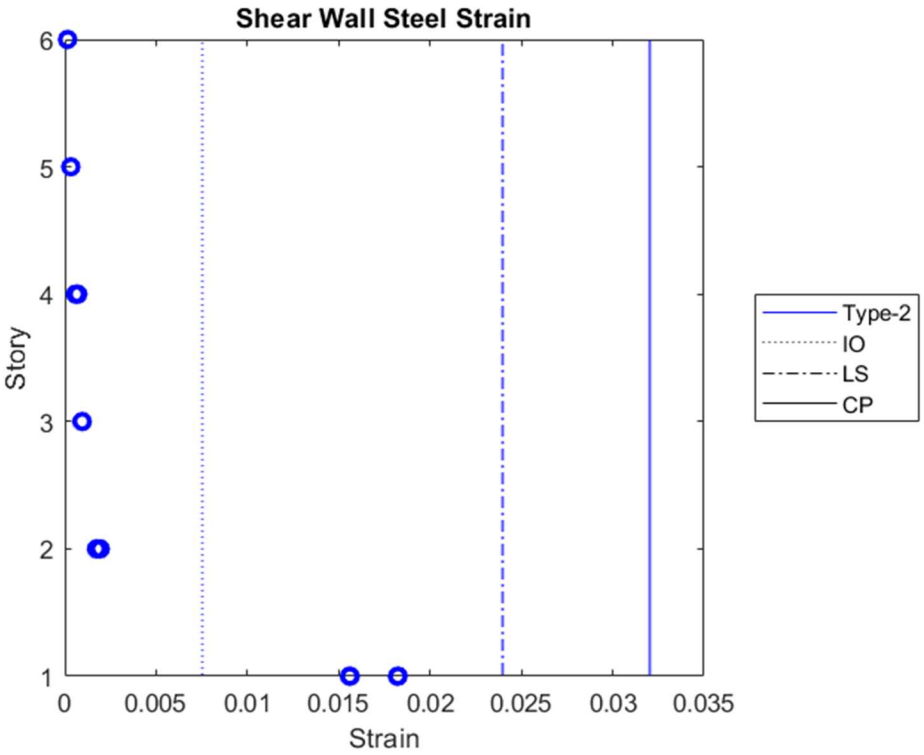

Figure 4.99. Concrete strain of bottom-end of shear wall Type-2 at roof when its maximum in DD-1 level earthquake of frame with shear walls

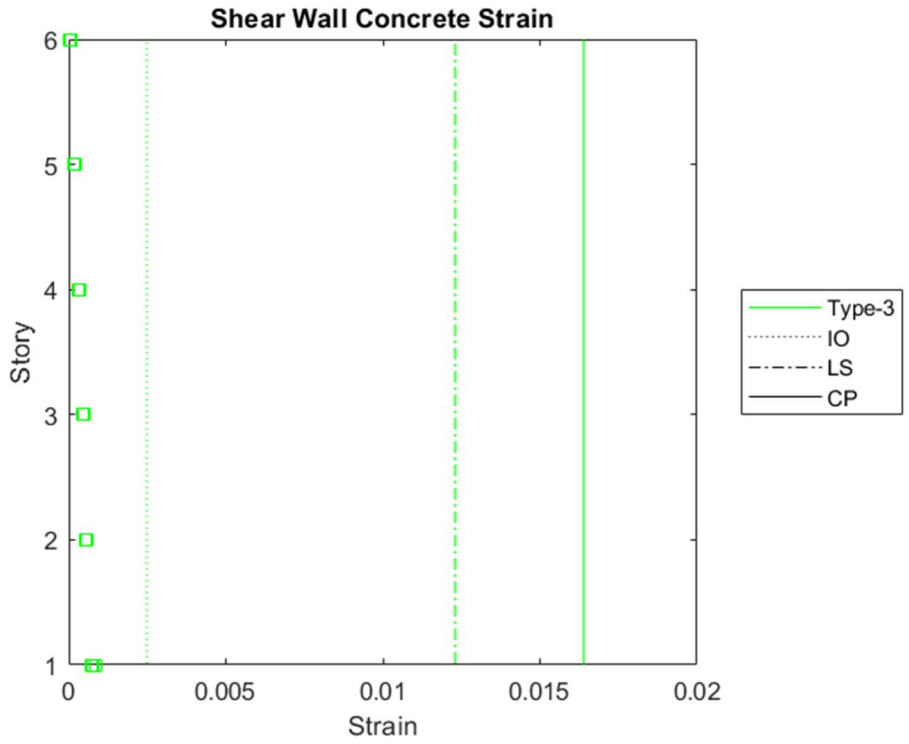

Figure 4.100. Concrete strain of bottom-end of shear wall Type-3 at roof when its maximum in DD-1 level earthquake of frame with shear walls

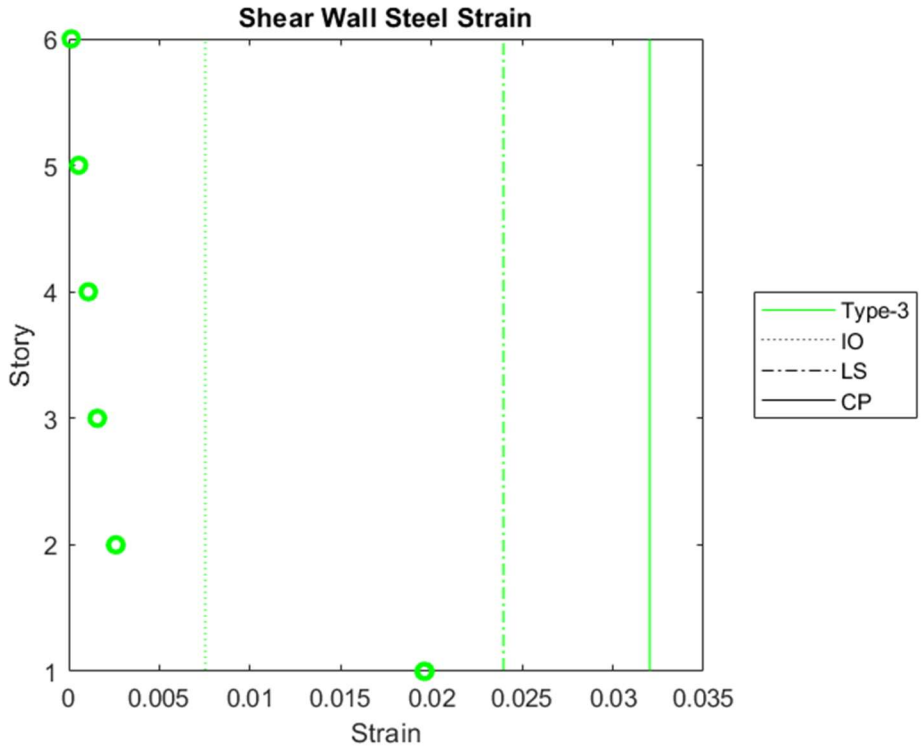

Figure 4.101. Steel strain of bottom-end of shear wall Type-3 at roof when its maximum in DD-1 level earthquake of frame with shear walls

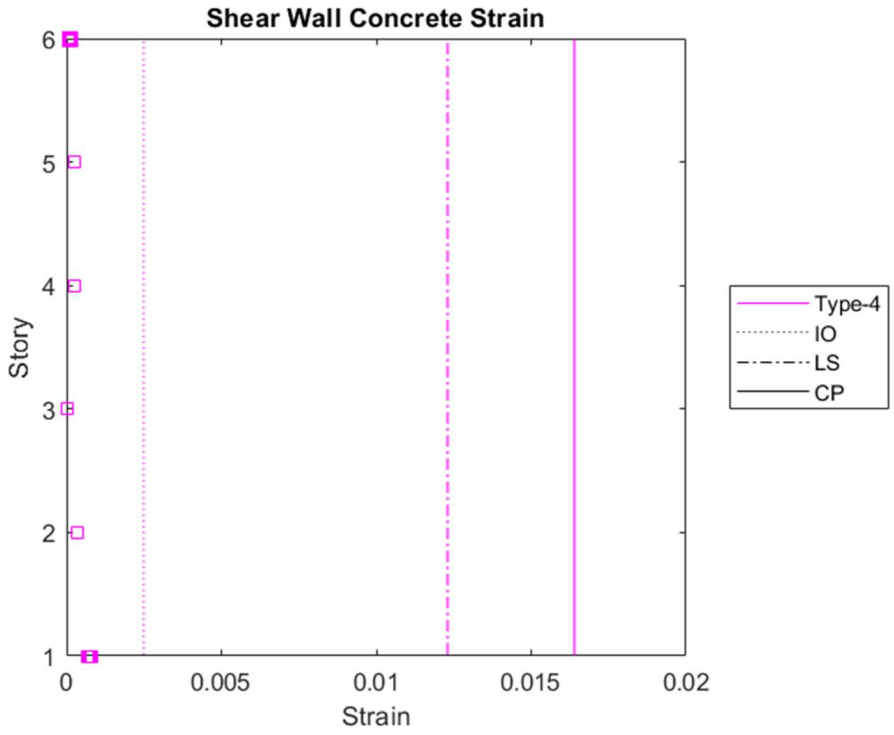

Figure 4.102. Concrete strain of bottom-end of shear wall Type-4 at roof when its maximum in DD-1 level earthquake of frame with shear walls

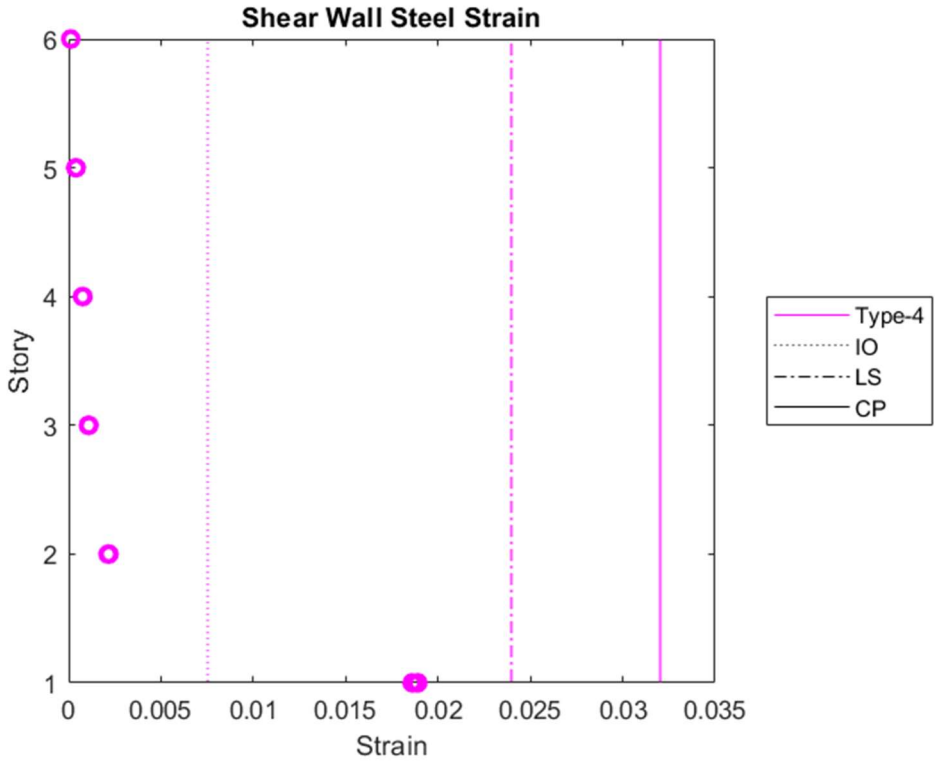

Figure 4.103. Steel strain of bottom-end of shear wall Type-4 at roof when its maximum in DD-1 level earthquake of frame with shear walls

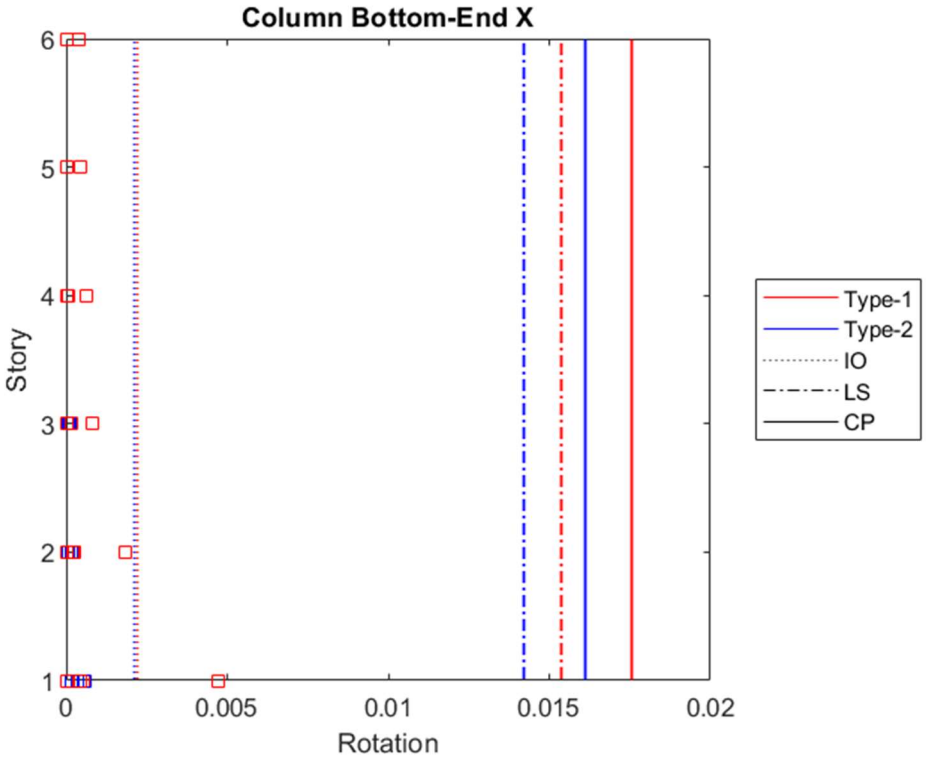

Figure 4.104. Rotations of bottom-end of column in x-direction for the maximum envelope drifts in DD-1 level earthquake of frame with shear walls

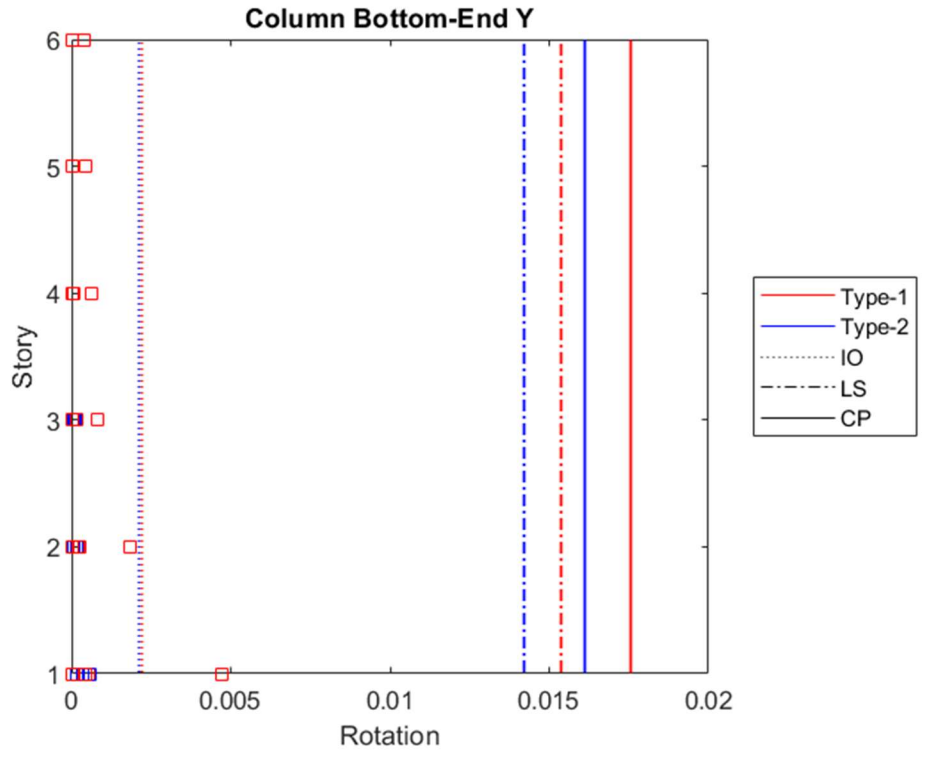

Figure 4.105. Rotations of bottom-end of column in y-direction for the maximum envelope drifts in DD-1 level earthquake of frame with shear walls

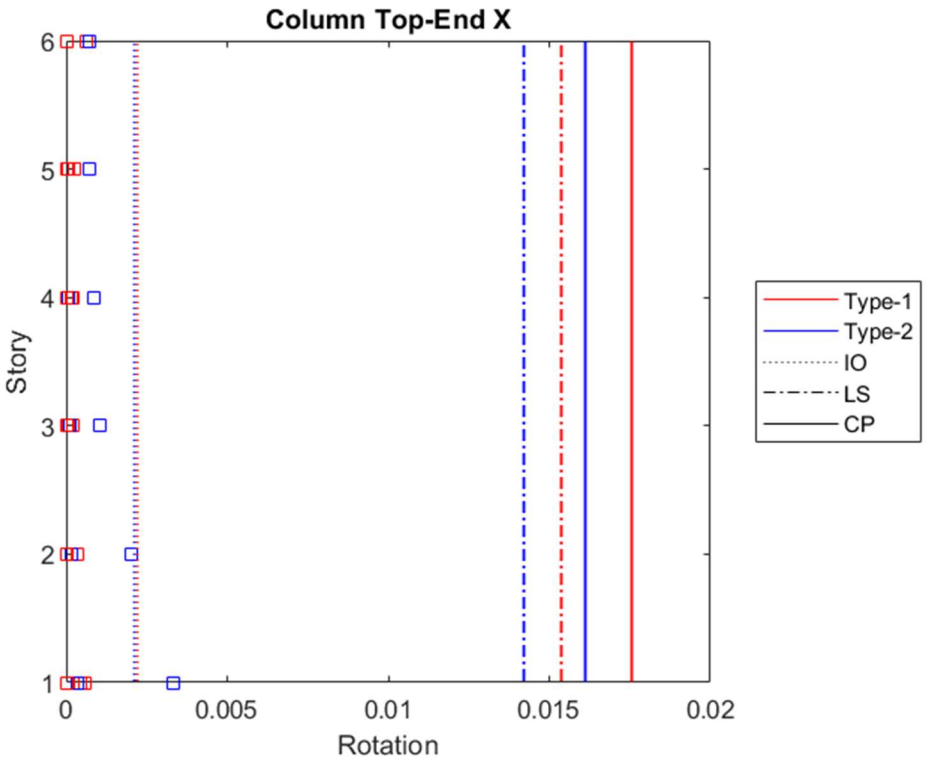

Figure 4.106. Rotations of top-end of column in x-direction for the maximum envelope drifts in DD-1 level earthquake of frame with shear walls

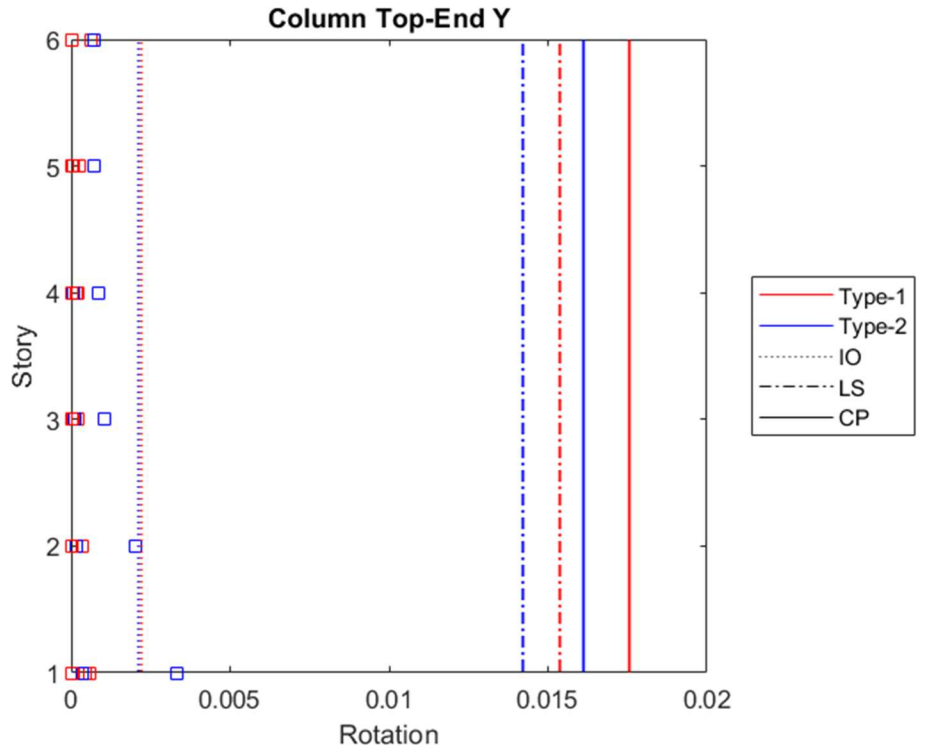

Figure 4.107. Rotations of top-end of column in y-direction for the maximum envelope drifts in DD-1 level earthquake of frame with shear walls

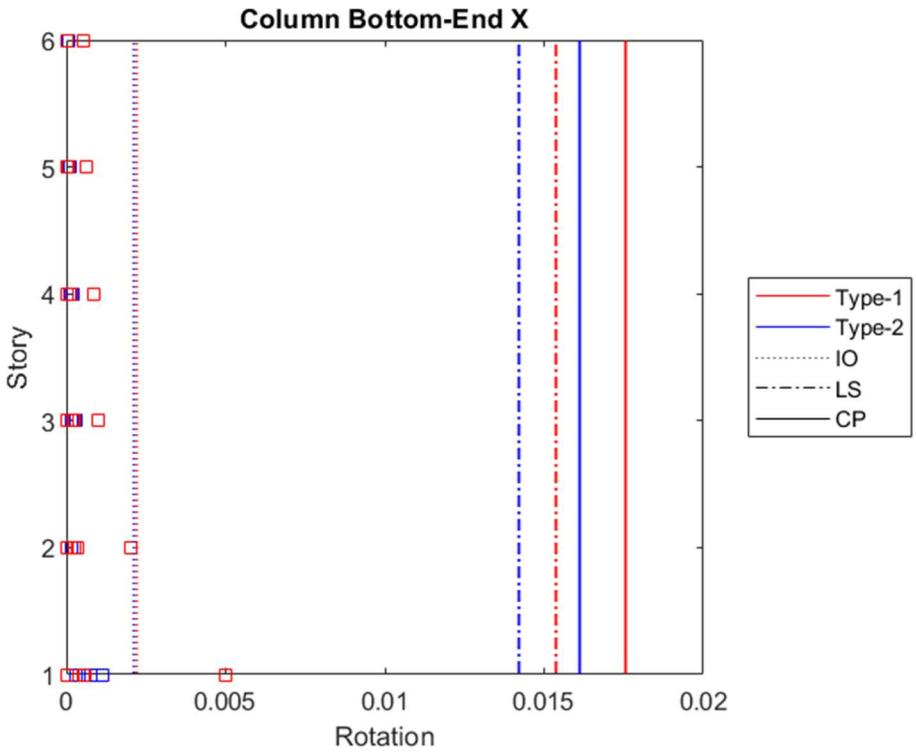

Figure 4.108. Rotations of bottom-end of column in x-direction at roof when its maximum in DD-1 level earthquake of frame with shear walls

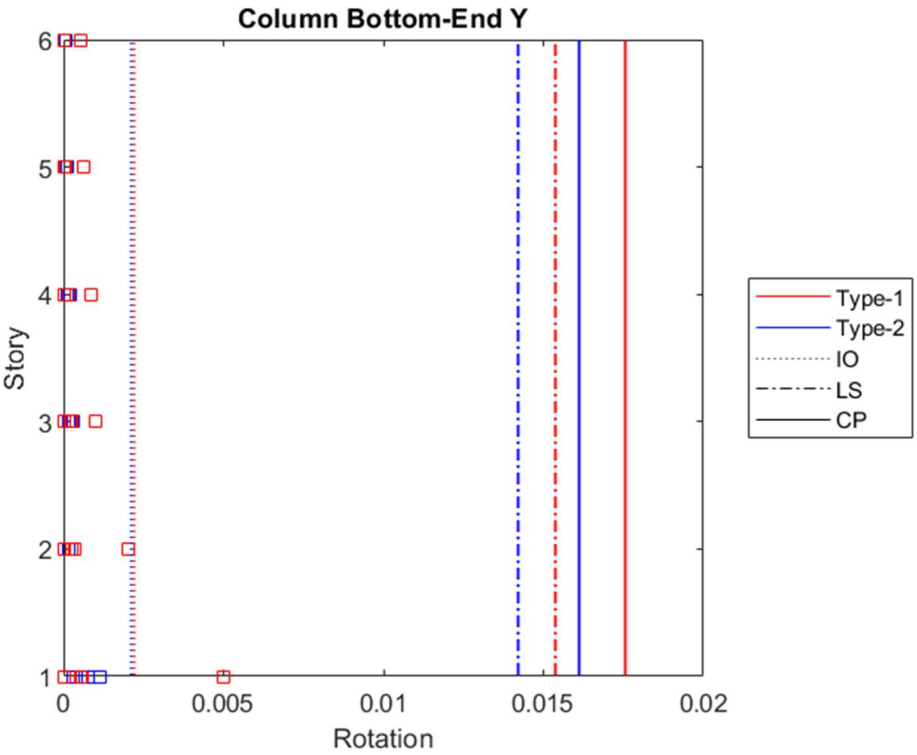

Figure 4.109. Rotations of bottom-end of column in y-direction at roof when its maximum in DD-1 level earthquake of frame with shear walls

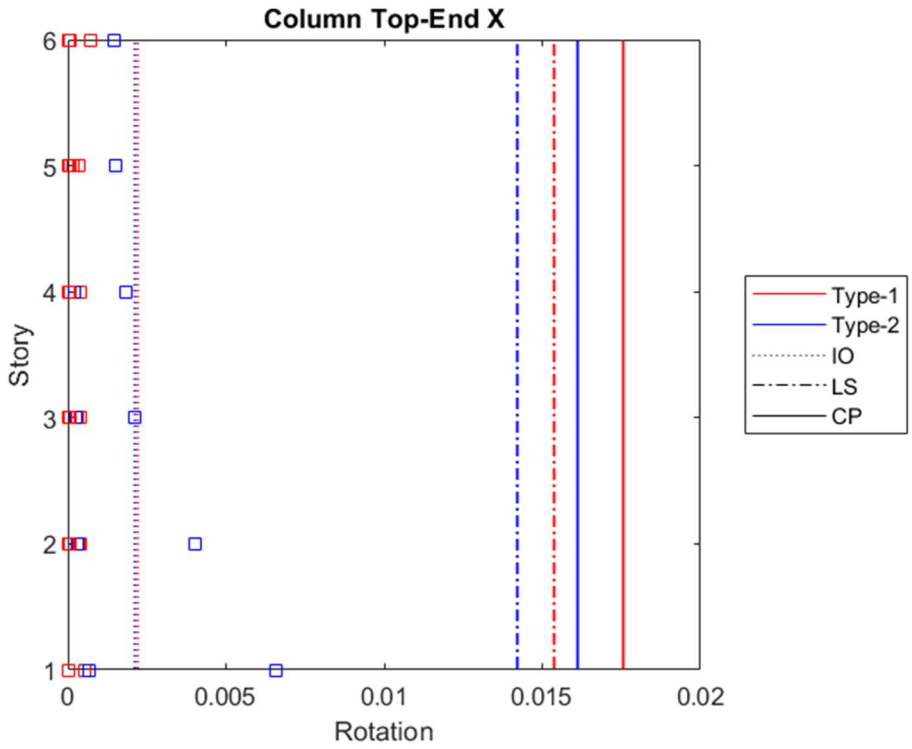

Figure 4.110. Rotations of top-end of column in x-direction at roof when its maximum in DD-1 level earthquake of frame with shear walls

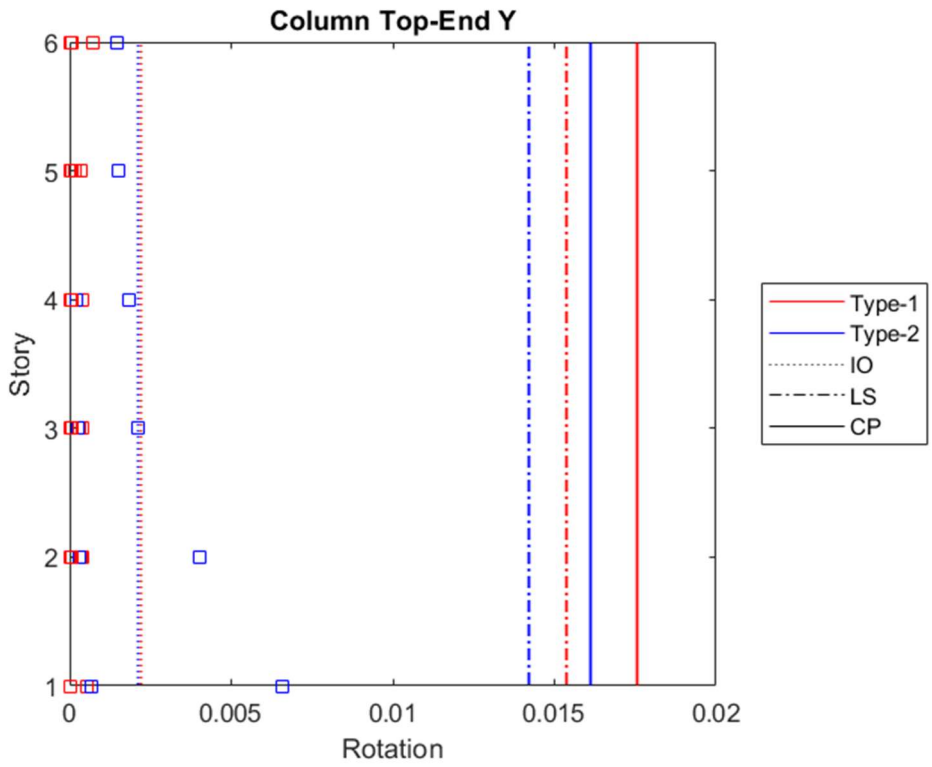

Figure 4.111. Rotations of top-end of column in y-direction at roof when its maximum in DD-1 level earthquake of frame with shear walls

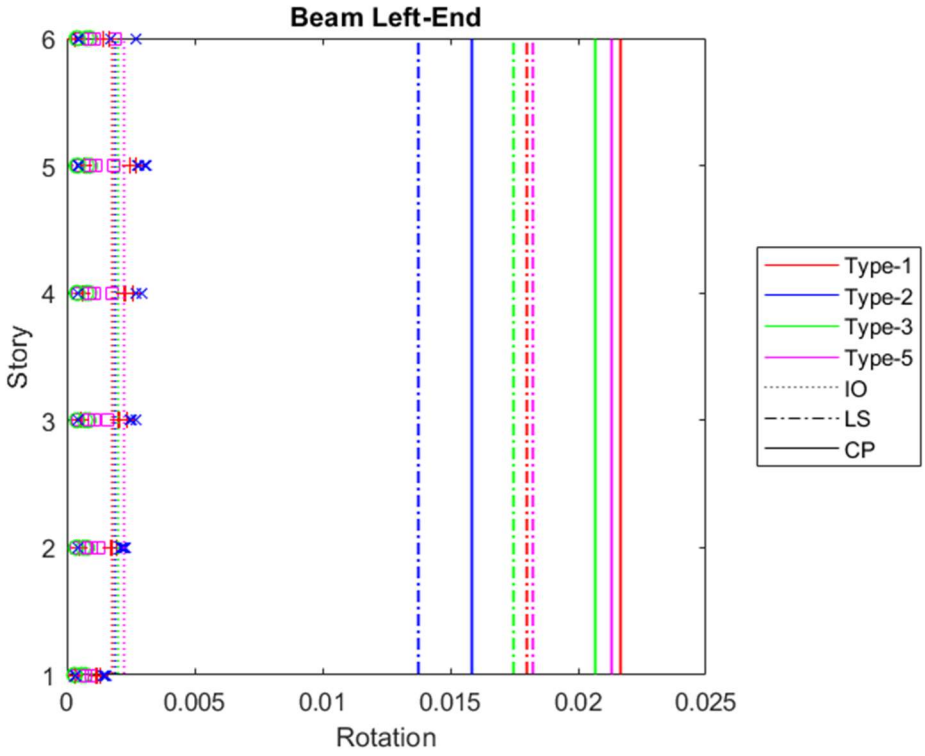

Figure 4.112. Rotations of left-end of beam in x-direction at roof when its maximum in DD-1 level earthquake of frame with shear walls

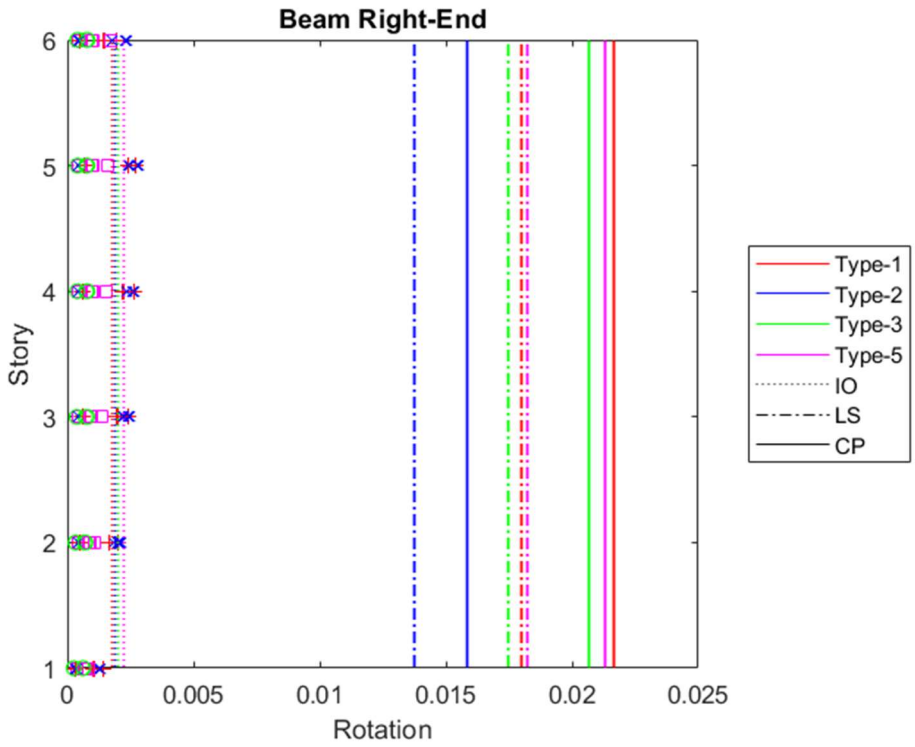

Figure 4.113. Rotations of right-end of beam in x-direction at roof when its maximum in DD-1 level earthquake of frame with shear walls

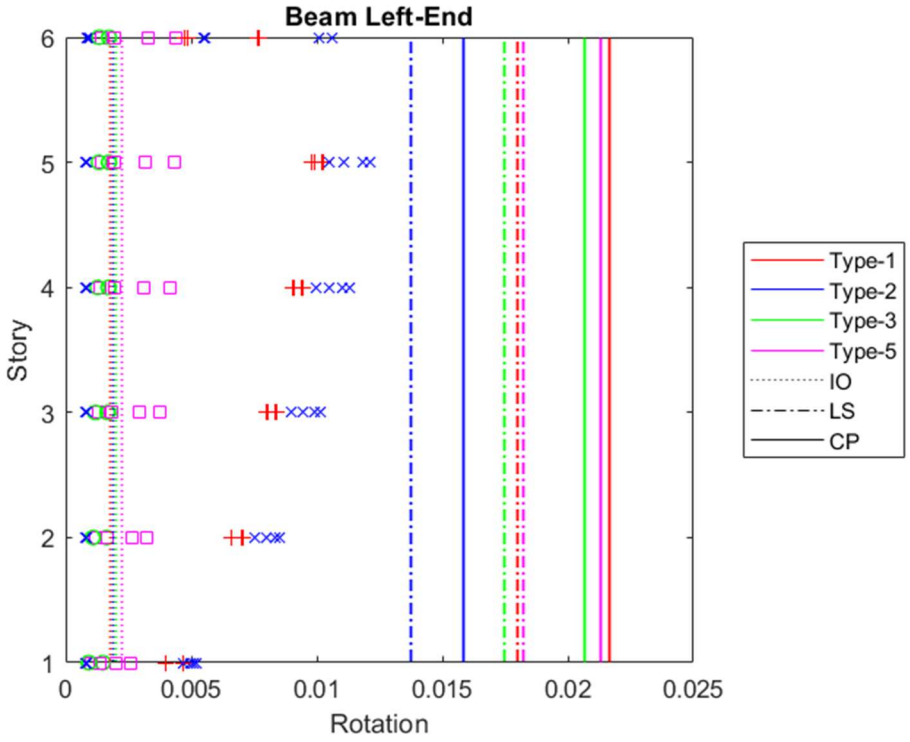

Figure 4.114. Rotations of left-end of beam in x-direction for the maximum envelope drifts in DD-1 level earthquake of frame with shear walls

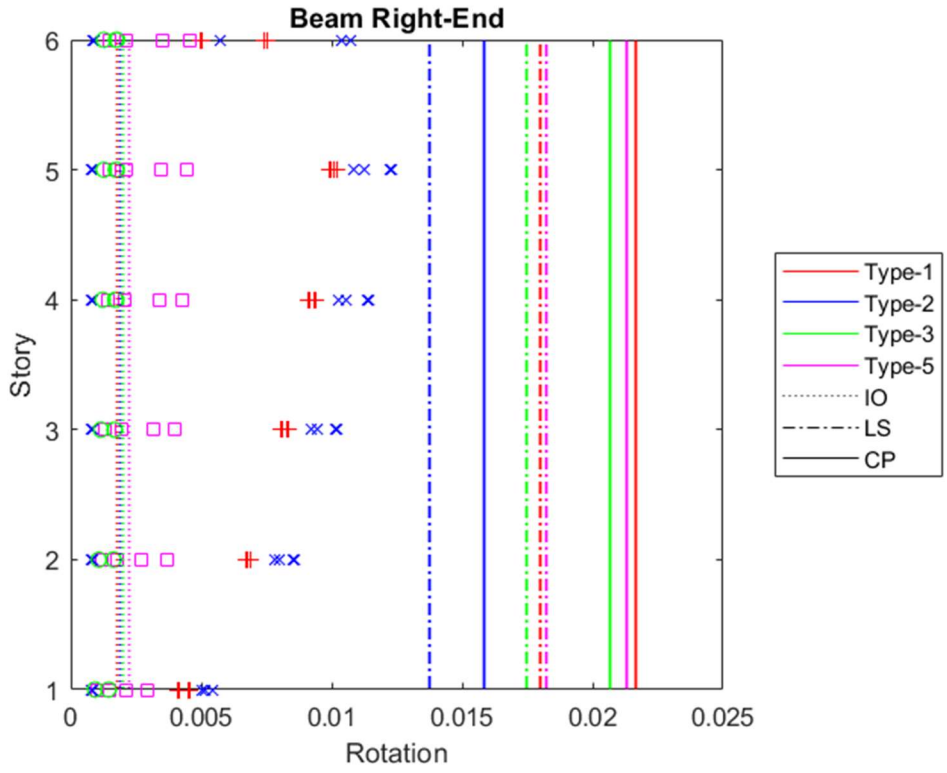

Figure 4.115. Rotations of left-end of beam in x-direction for the maximum envelope drifts in DD-1 level earthquake of frame with shear walls

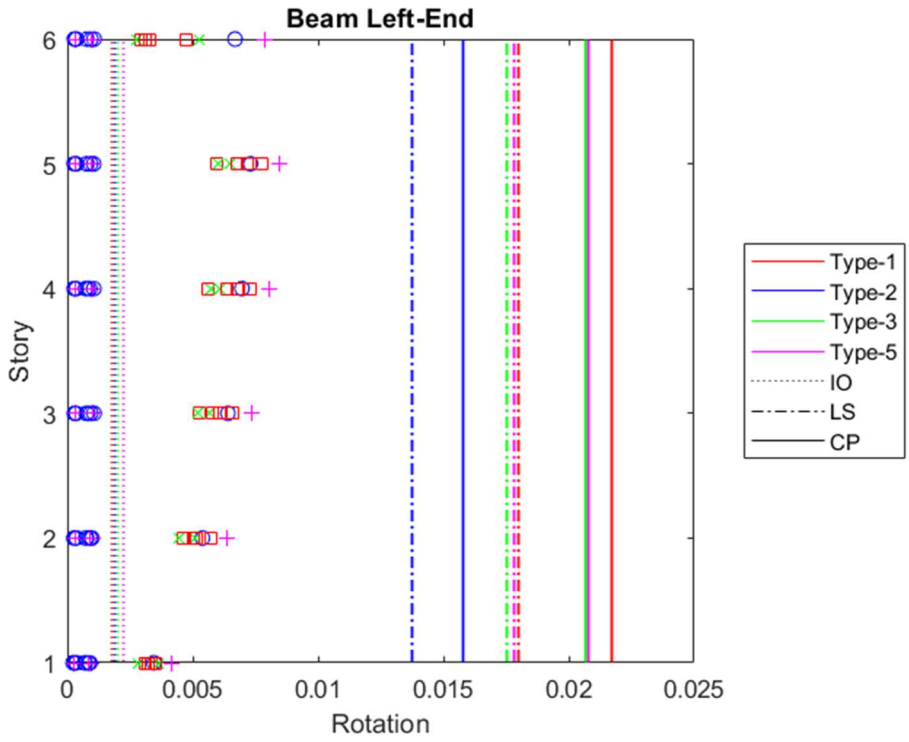

Figure 4.116. Rotations of left-end of beam in y-direction at roof when its maximum in DD-1 level earthquake of frame with shear walls

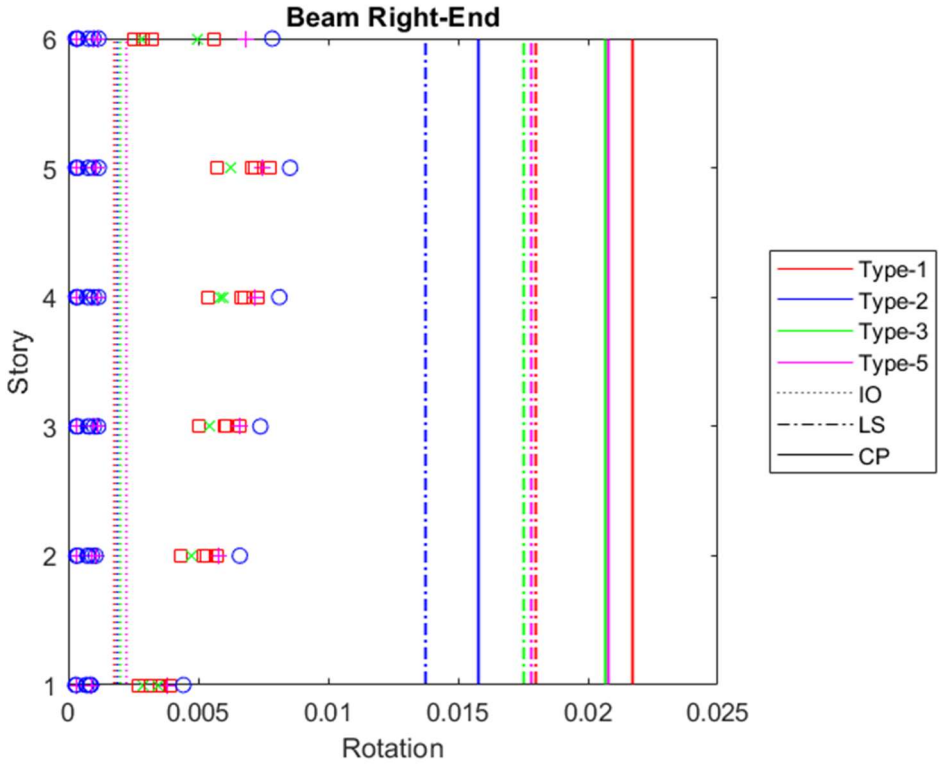

Figure 4.117. Rotations of left-end of beam in y-direction at roof when its maximum in DD-1 level earthquake of frame with shear walls

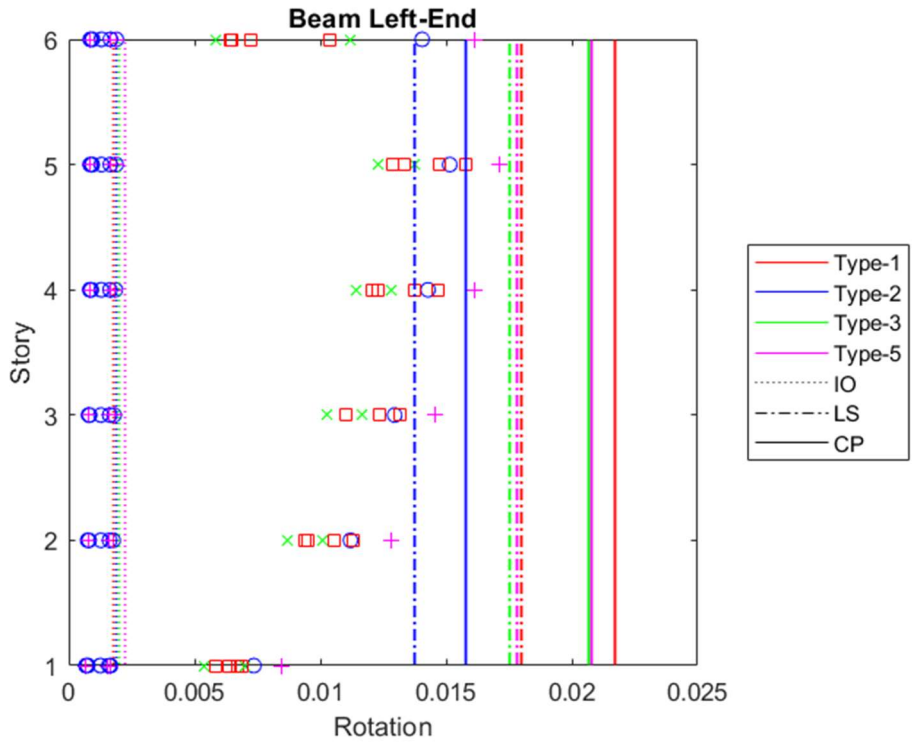

Figure 4.118. Rotations of left-end of beam in y-direction for the maximum envelope drifts in DD-1 level earthquake of frame with shear walls

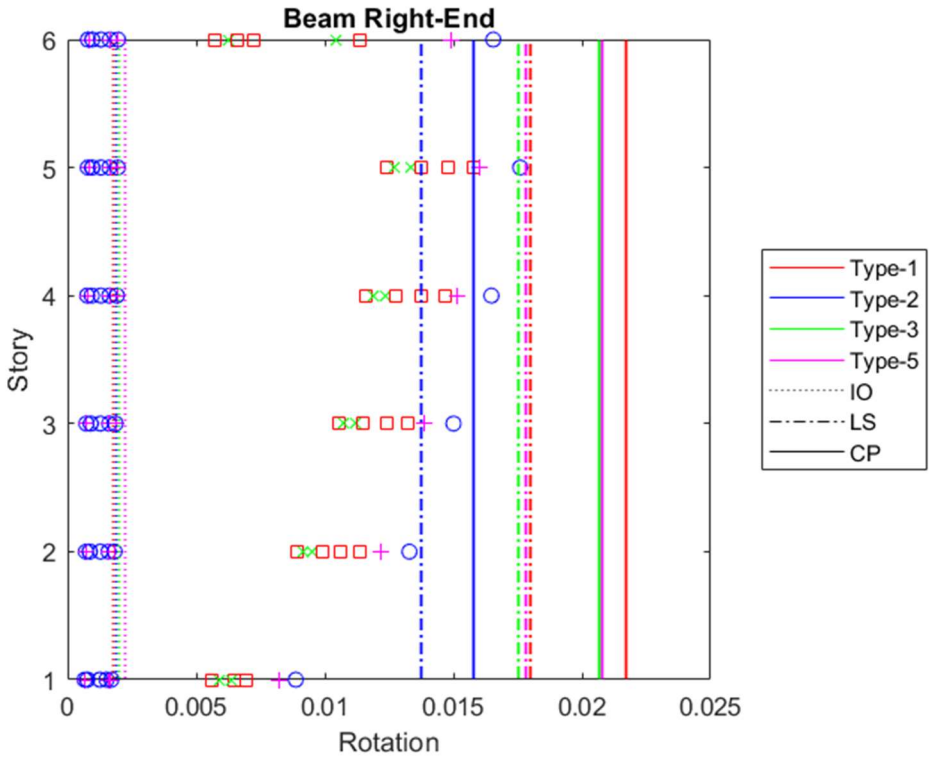

Figure 4.119. Rotations of left-end of beam in y-direction for the maximum envelope drifts in DD-1 level earthquake of frame with shear walls

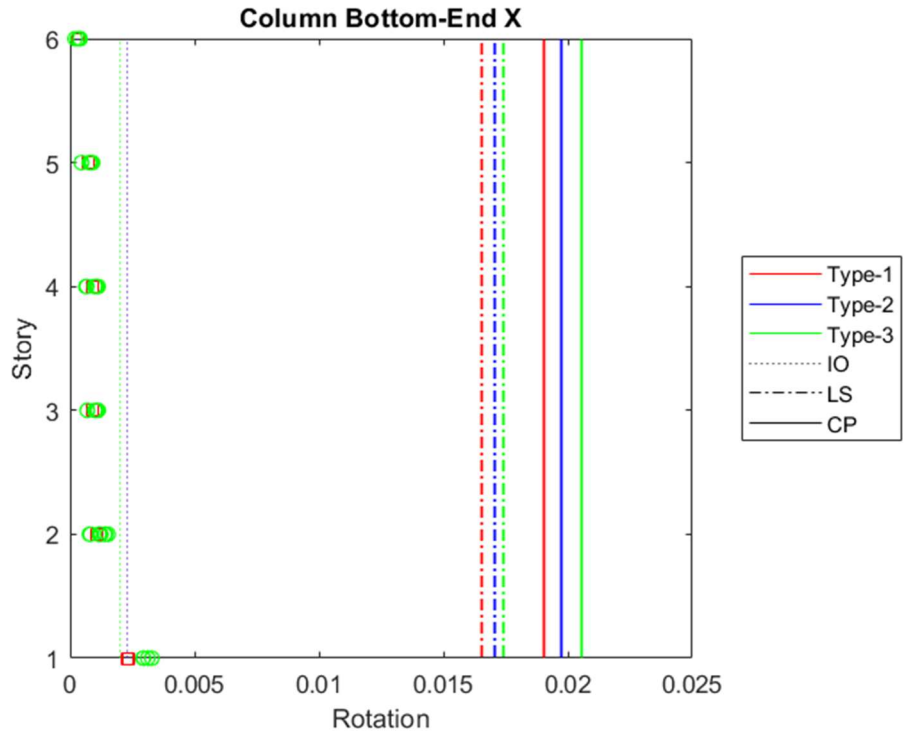

Figure 4.120. Rotations of bottom-end of column in x-direction for the maximum envelope drifts in DD-3 level earthquake of moment-resisting frame

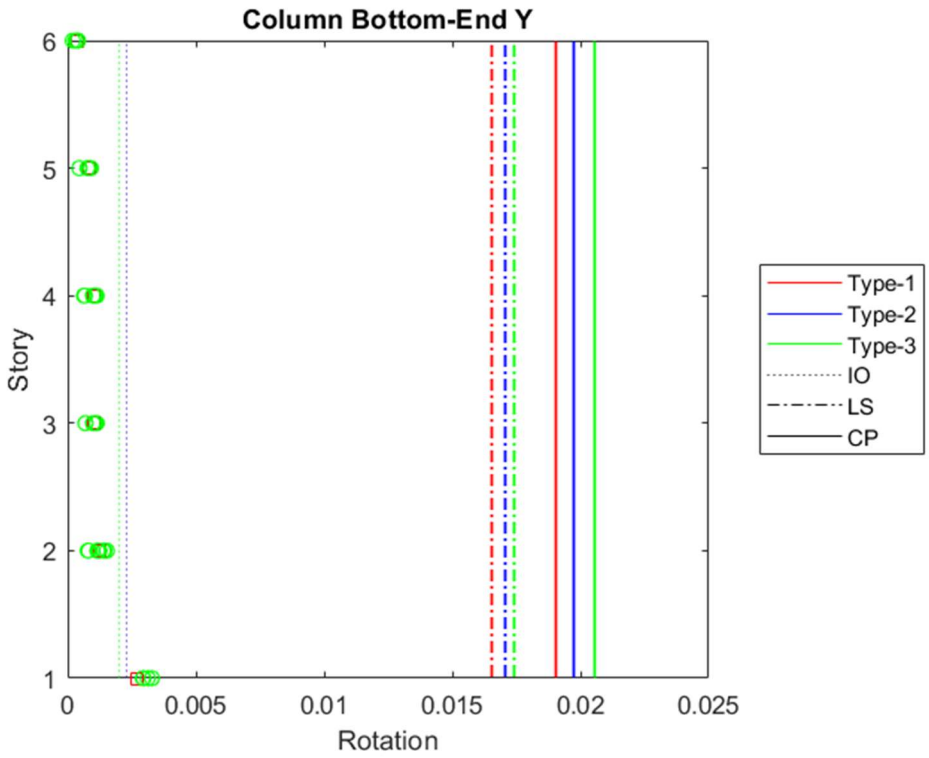

Figure 4.121. Rotations of bottom-end of column in y-direction for the maximum envelope drifts in DD-3 level earthquake of moment-resisting frame

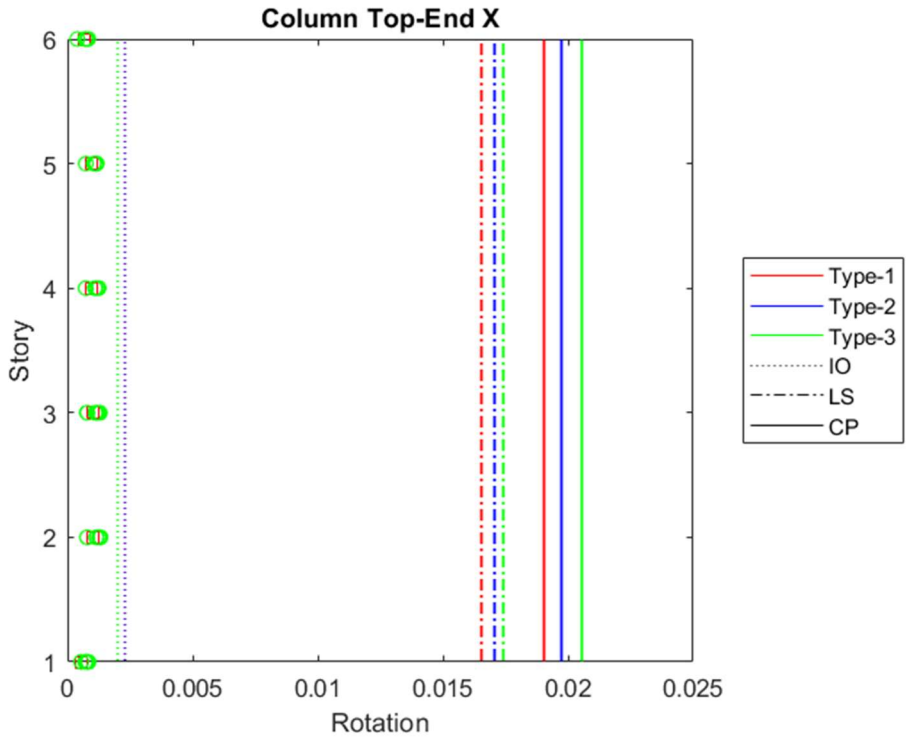

Figure 4.122. Rotations of top-end of column in x-direction for the maximum envelope drifts in DD-3 level earthquake of moment-resisting frame

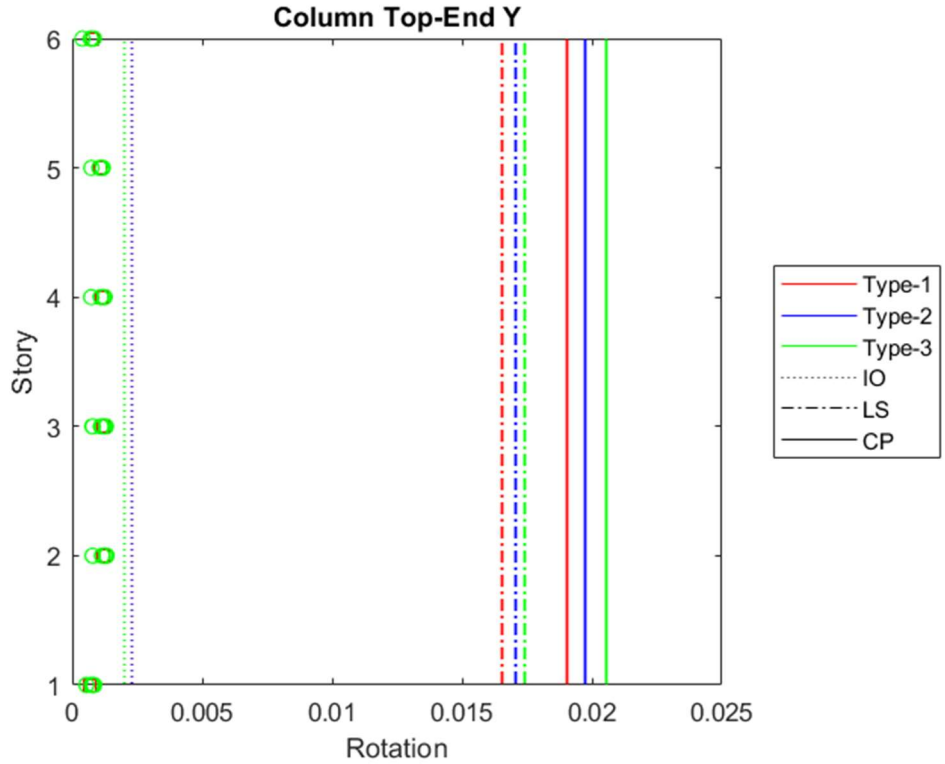

Figure 4.123. Rotations of top-end of column in y-direction for the maximum envelope drifts in DD-3 level earthquake of moment-resisting frame

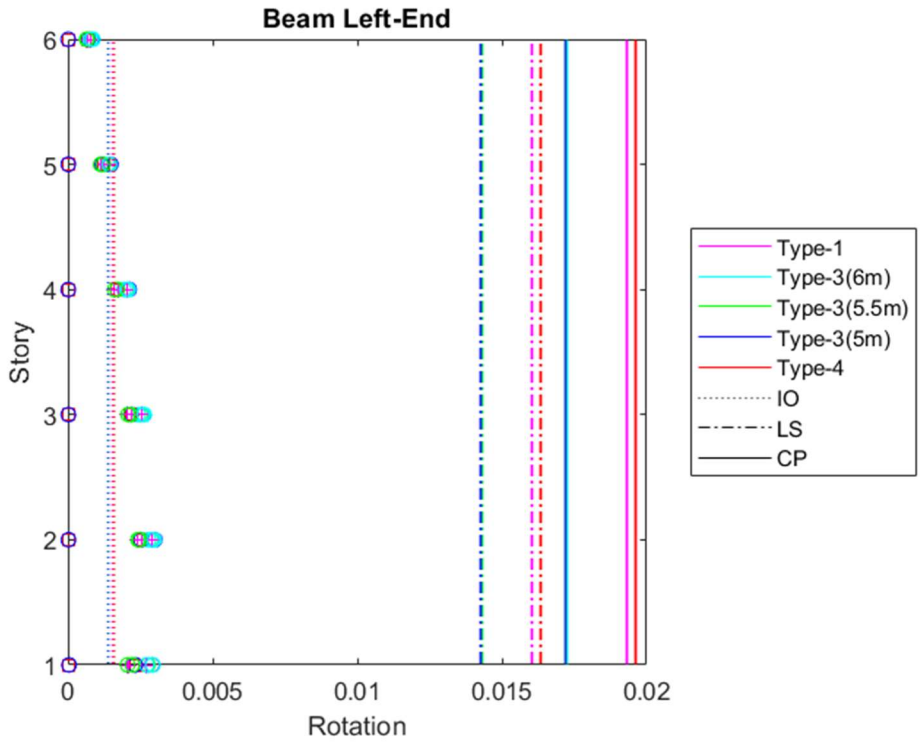

Figure 4.124. Rotations of left-end of beam in x-direction for the maximum envelope drifts in DD-3 level earthquake of moment-resisting frame

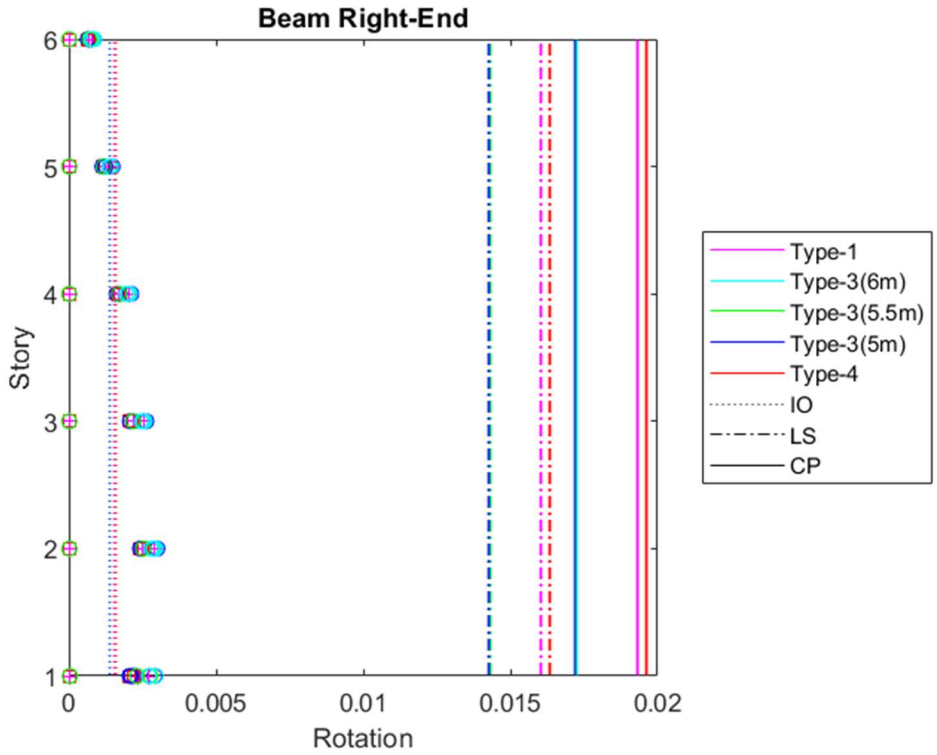

Figure 4.125. Rotations of right-end of beam in x-direction for the maximum envelope drifts in DD-3 level earthquake of moment-resisting frame

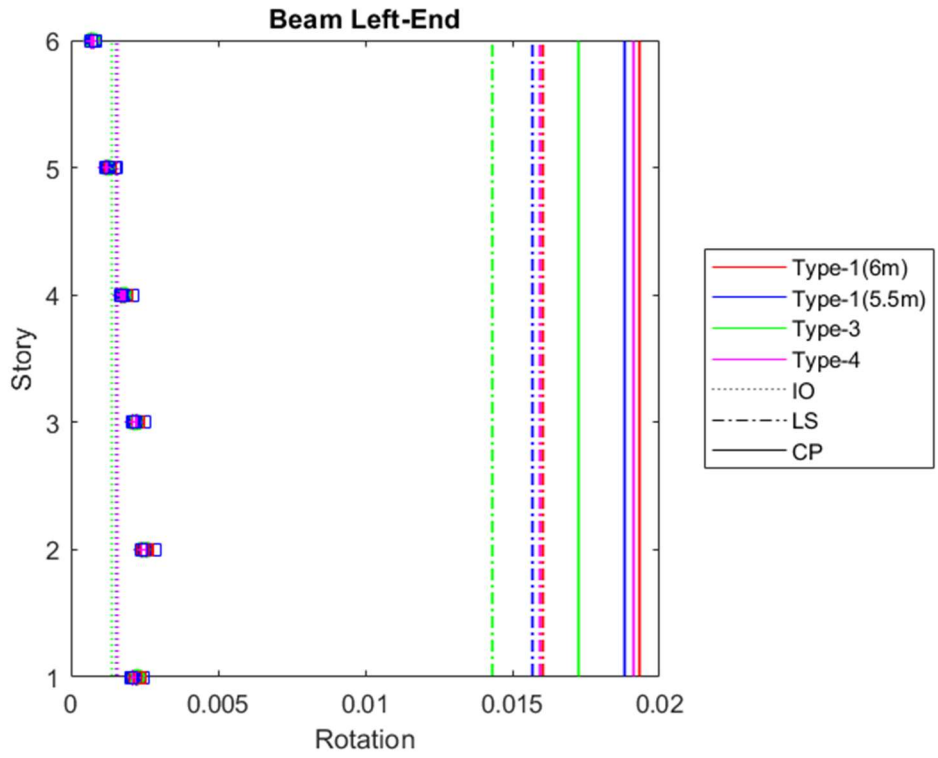

Figure 4.126. Rotations of left-end of beam in y-direction for the maximum envelope drifts in DD-3 level earthquake of moment-resisting frame

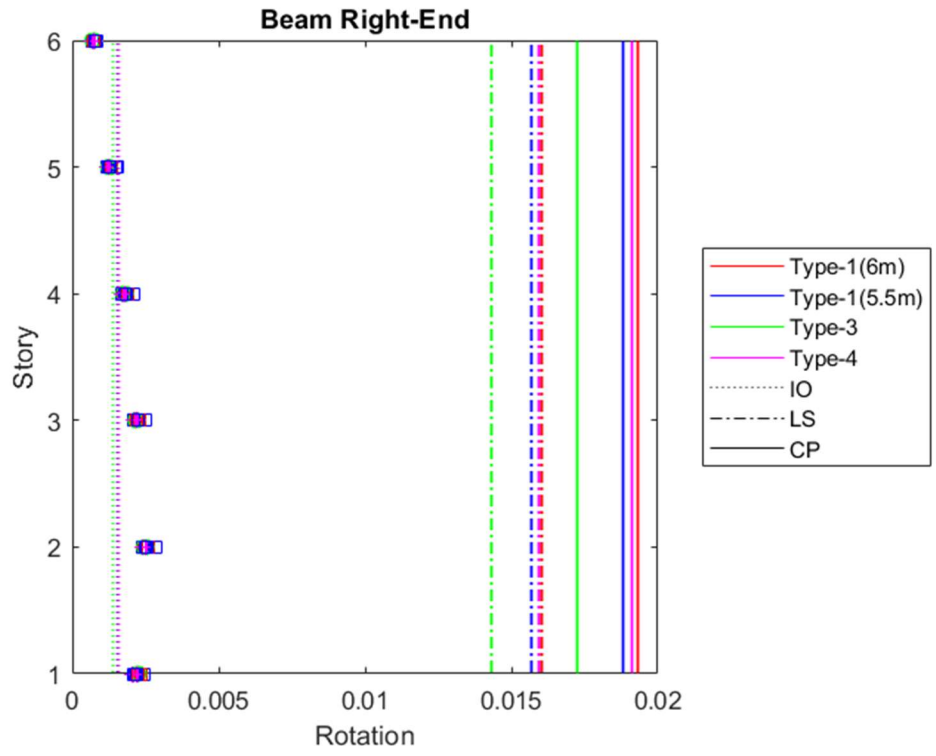

Figure 4.127. Rotations of right-end of beam in y-direction for the maximum envelope drifts in DD-3 level earthquake of moment-resisting frame

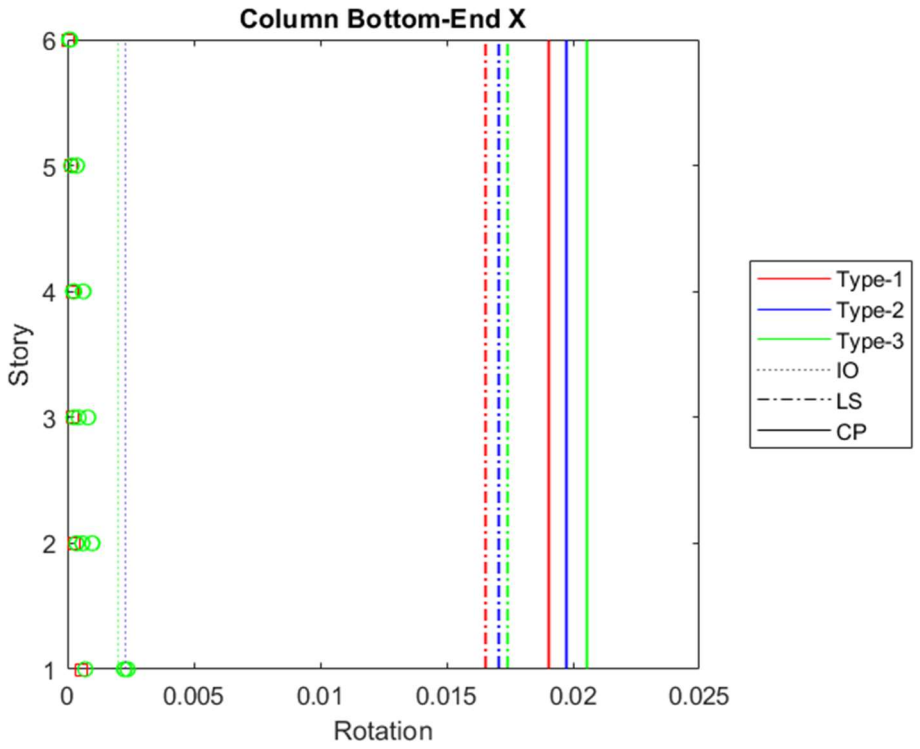

Figure 4.128. Rotations of bottom-end of column in x-direction at roof when its maximum in DD-3 level earthquake of moment-resisting frame

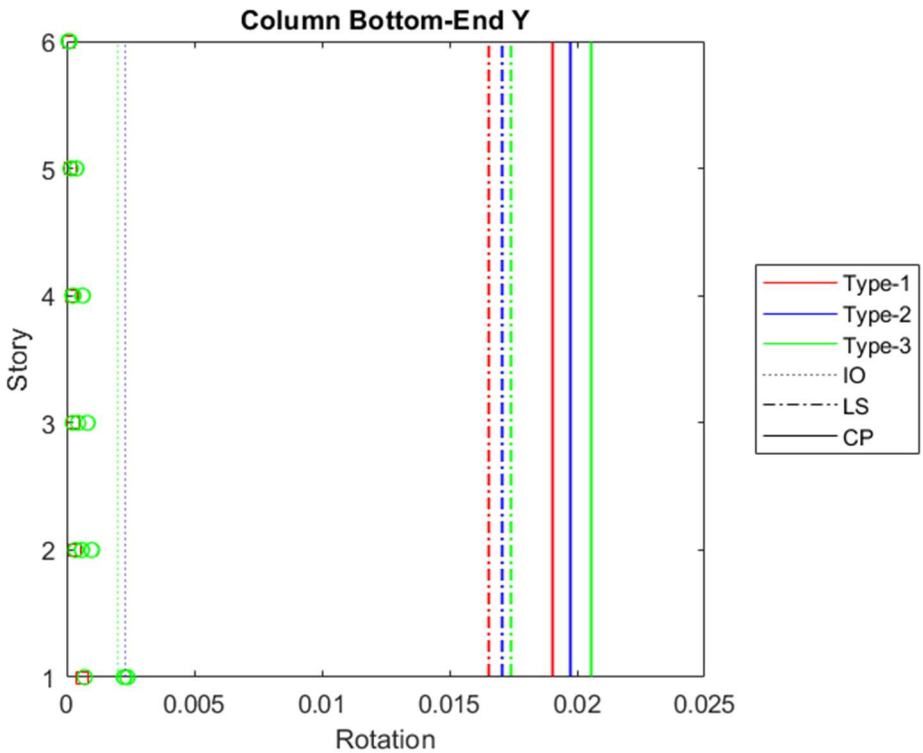

Figure 4.129. Rotations of bottom-end of column in y-direction at roof when its maximum in DD-3 level earthquake of moment-resisting frame

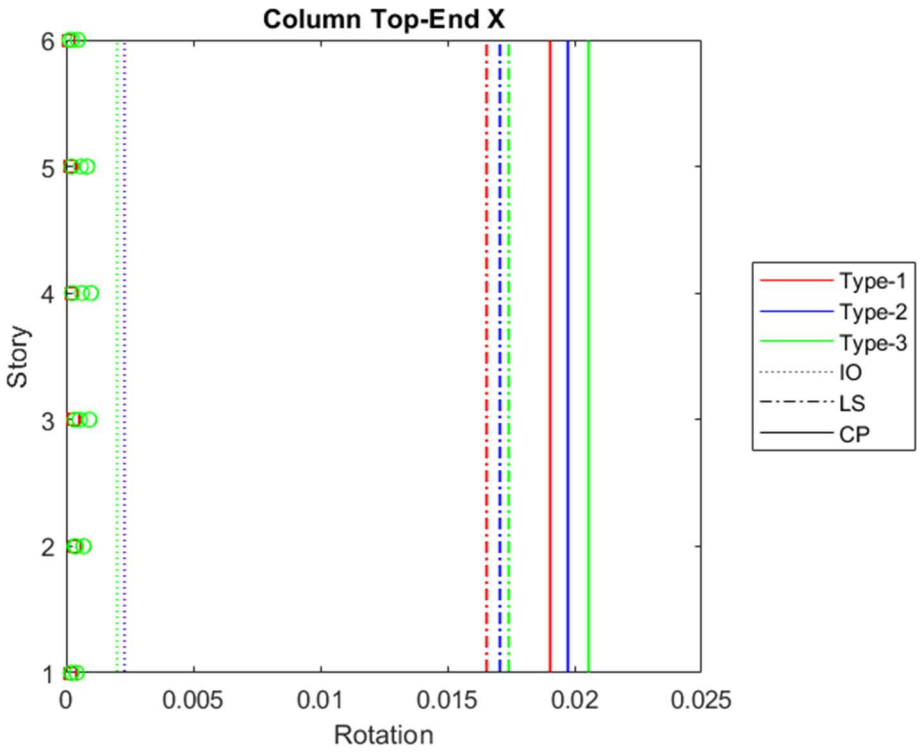

Figure 4.130. Rotations of top-end of column in x-direction at roof when its maximum in DD-3 level earthquake of moment-resisting frame

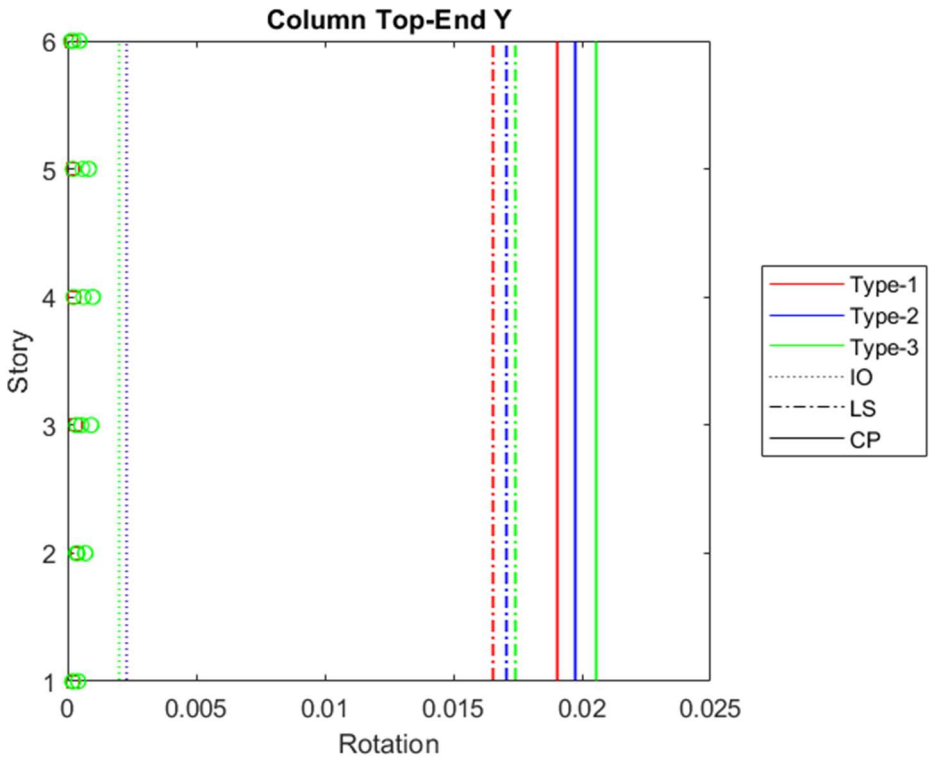

Figure 4.131. Rotations of top-end of column in y-direction at roof when its maximum in DD-3 level earthquake of moment-resisting frame

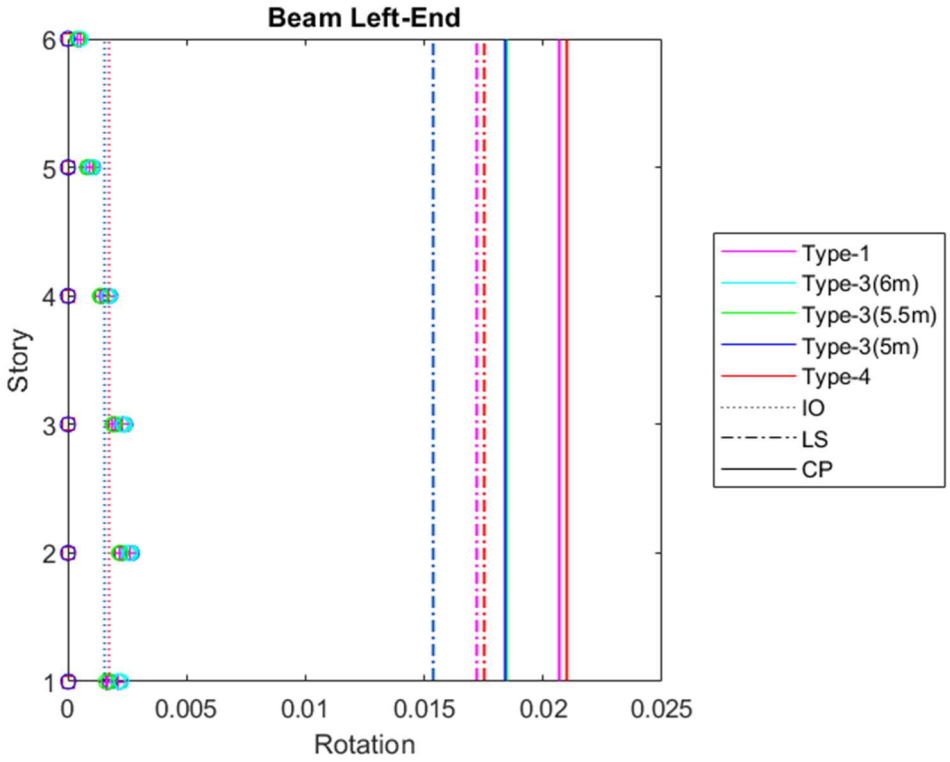

Figure 4.132. Rotations of left-end of beam in x-direction at roof when its maximum in DD-3 level earthquake of moment-resisting frame

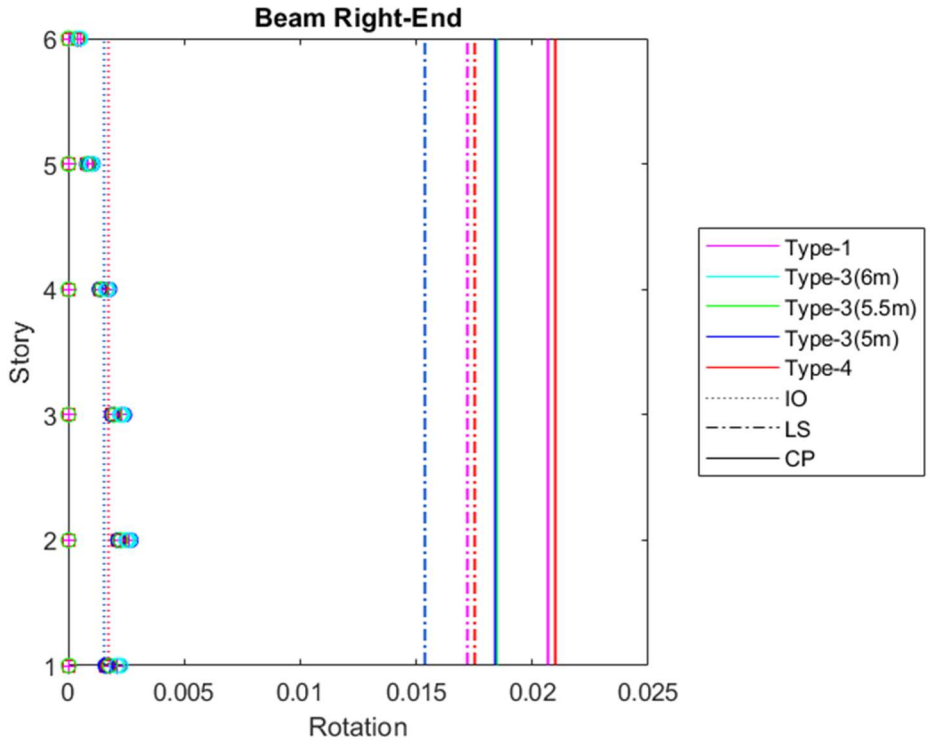

Figure 4.133. Rotations of right-end of beam in x-direction at roof when its maximum in DD-3 level earthquake of moment-resisting frame

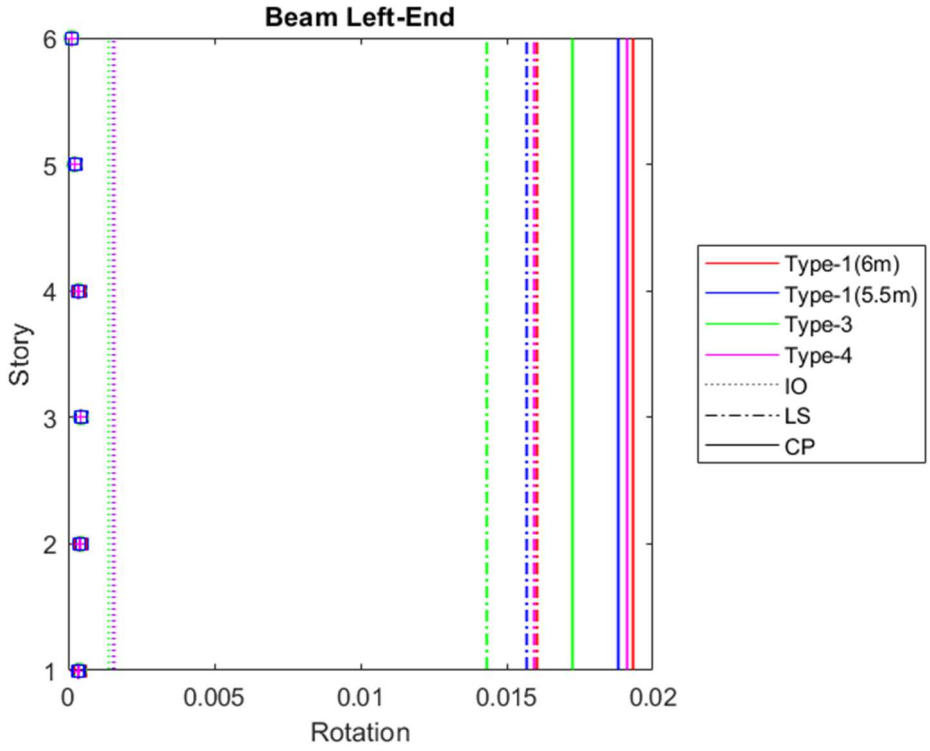

Figure 4.134. Rotations of left-end of beam in y-direction at roof when its maximum in DD-3 level earthquake of moment-resisting frame

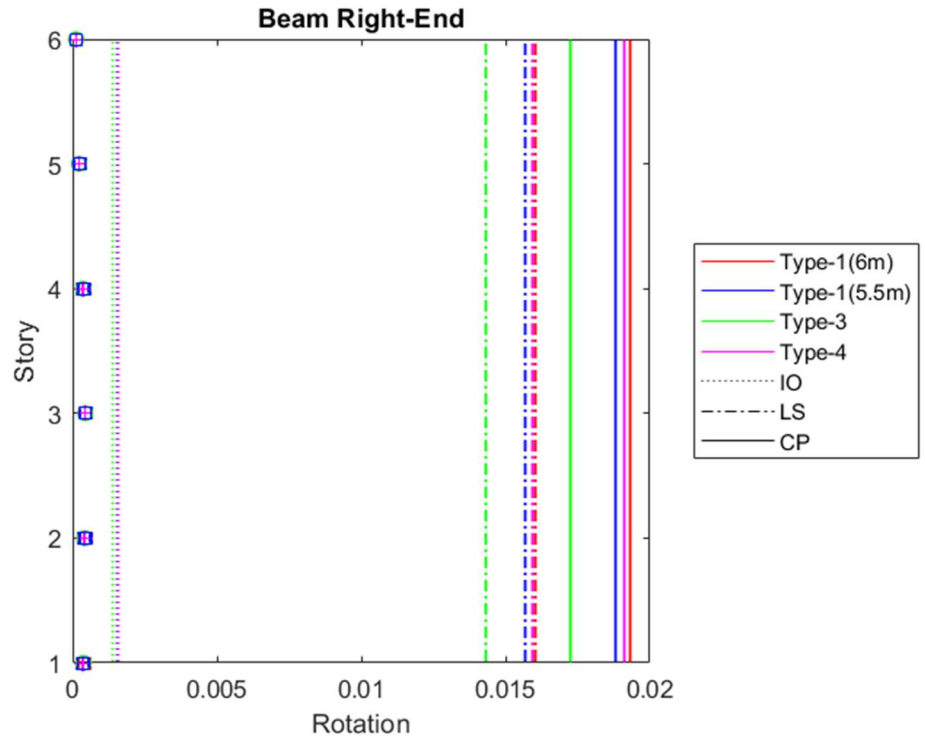

Figure 4.135. Rotations of right-end of beam in y-direction at roof when its maximum in DD-3 level earthquake of moment-resisting frame

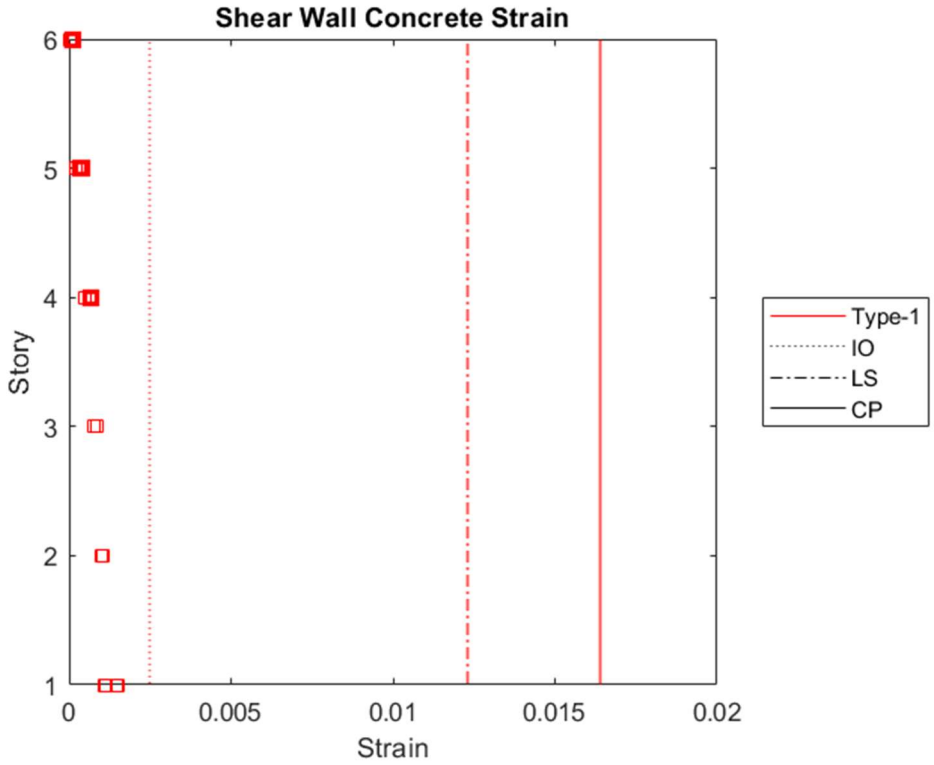

Figure 4.136. Concrete strain of bottom-end of shear wall Type-1 at roof when its maximum in DD-3 level earthquake of frame with shear walls

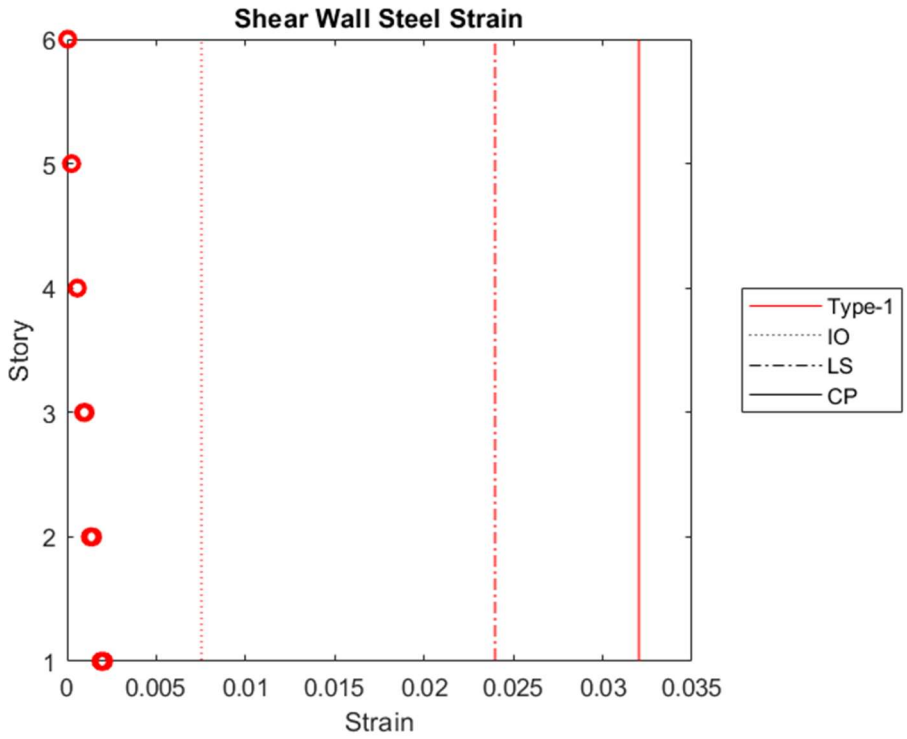

Figure 4.137. Steel strain of bottom-end of shear wall Type-1 at roof when its maximum in DD-3 level earthquake of frame with shear walls

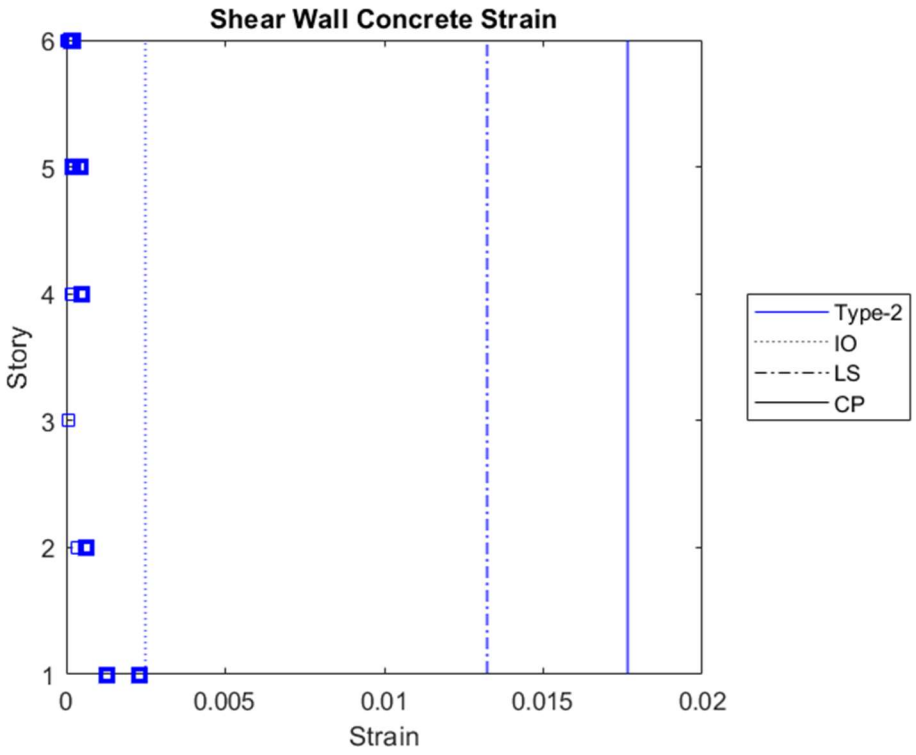

Figure 4.138. Concrete strain of bottom-end of shear wall Type-2 at roof when its maximum in DD-3 level earthquake of frame with shear walls

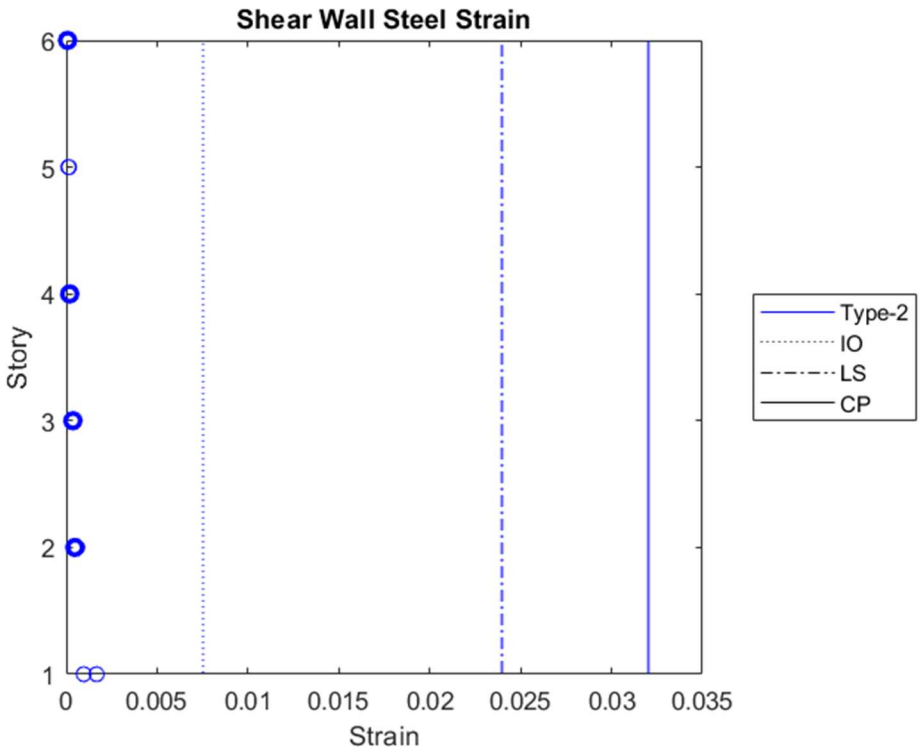

Figure 4.139. Steel strain of bottom-end of shear wall Type-2 at roof when its maximum in DD-3 level earthquake of frame with shear walls

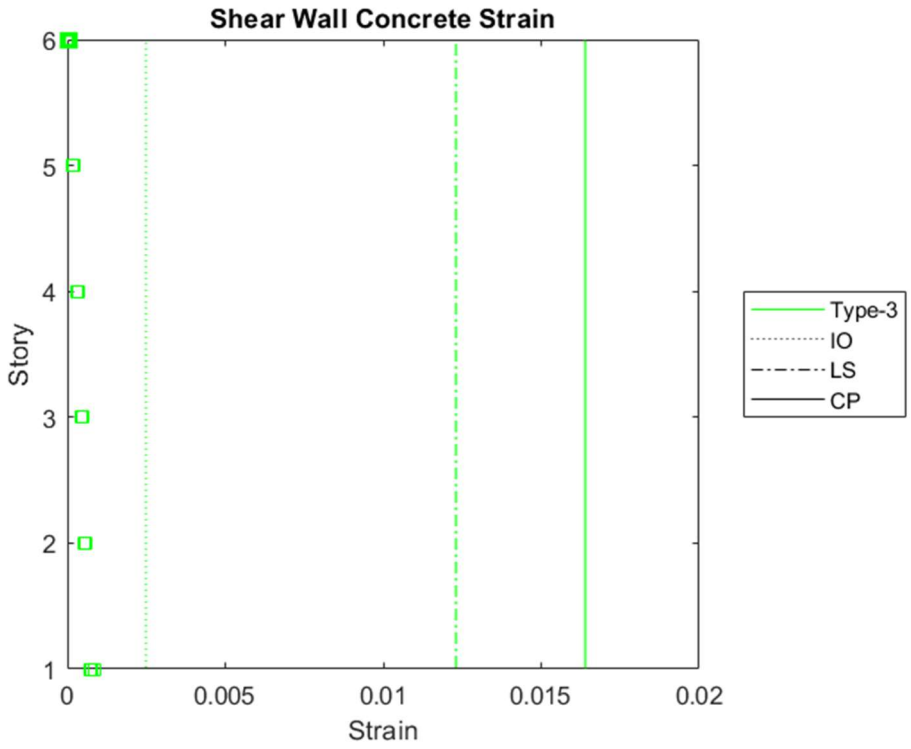

Figure 4.140. Concrete strain of bottom-end of shear wall Type-3 at roof when its maximum in DD-3 level earthquake of frame with shear walls

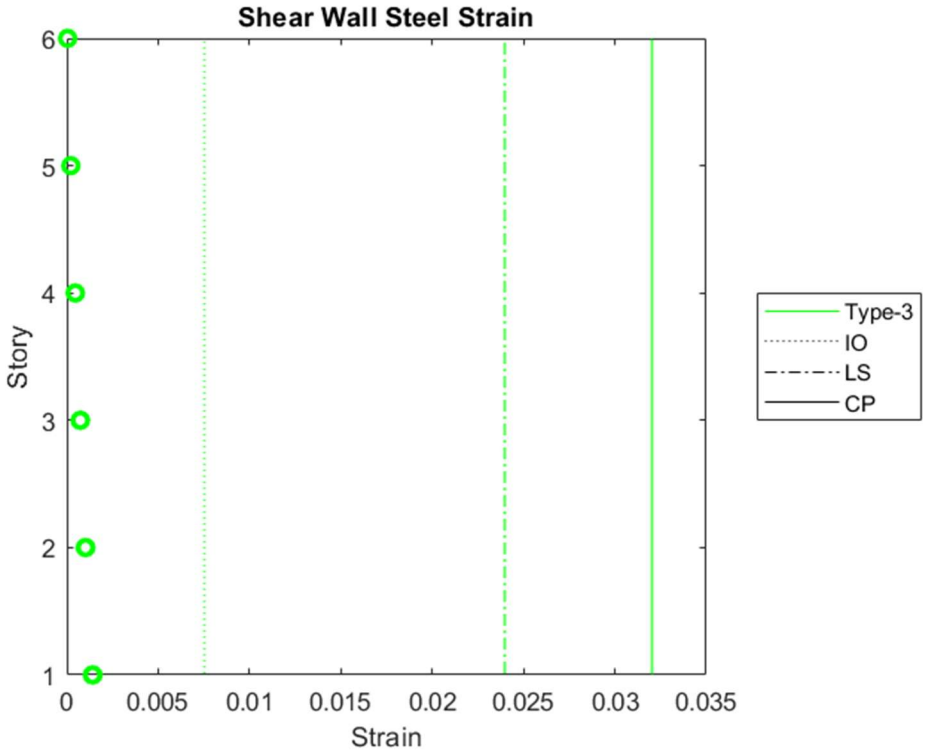

Figure 4.141. Steel strain of bottom-end of shear wall Type-3 at roof when its maximum in DD-3 level earthquake of frame with shear walls

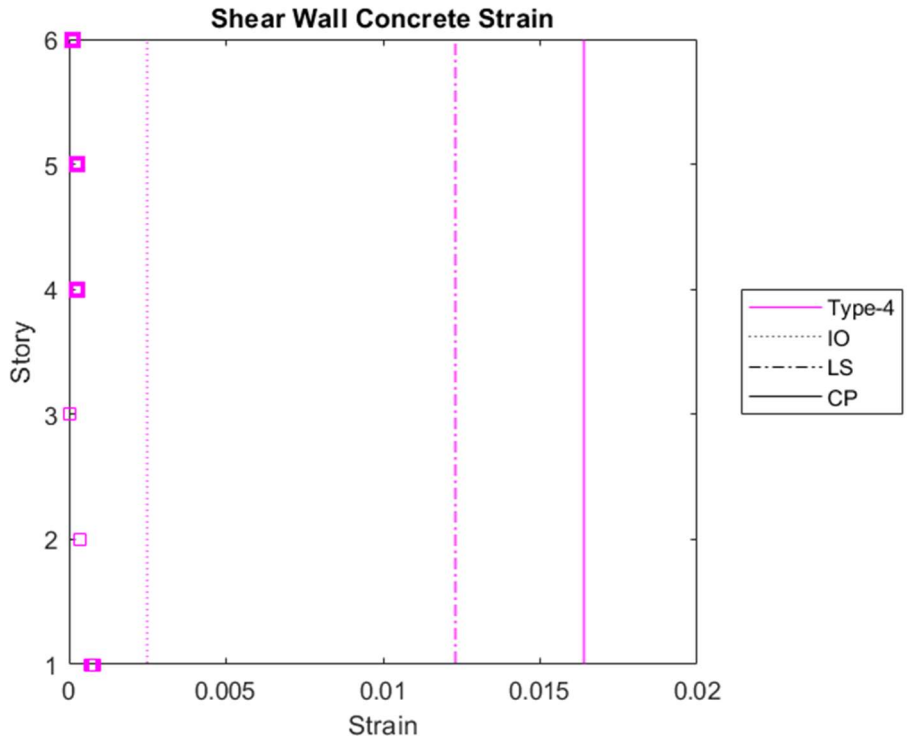

Figure 4.142. Concrete strain of bottom-end of shear wall Type-4 at roof when its maximum in DD-3 level earthquake of frame with shear walls

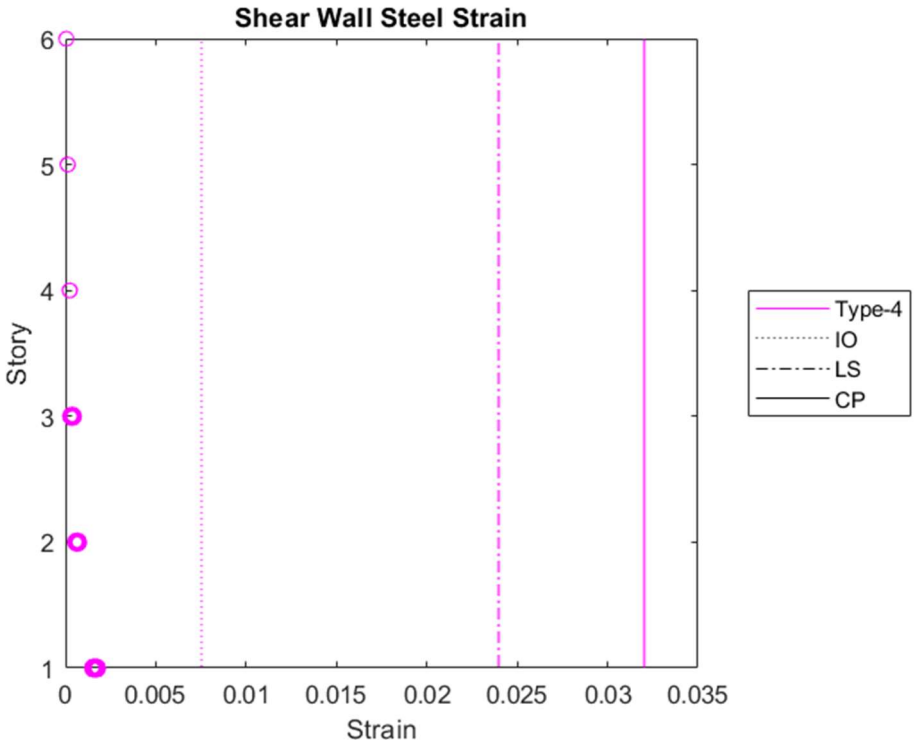

Figure 4.143. Steel strain of bottom-end of shear wall Type-4 at roof when its maximum in DD-3 level earthquake of frame with shear walls

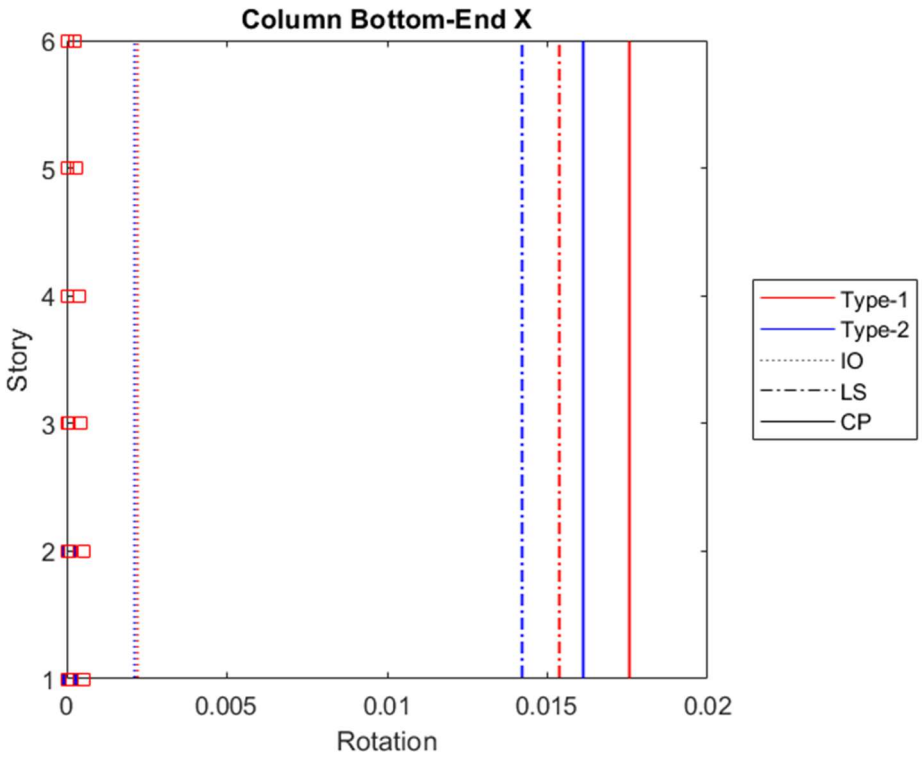

Figure 4.144. Rotations of bottom-end of column in x-direction at roof when its maximum in DD-3 level earthquake of frame with shear walls

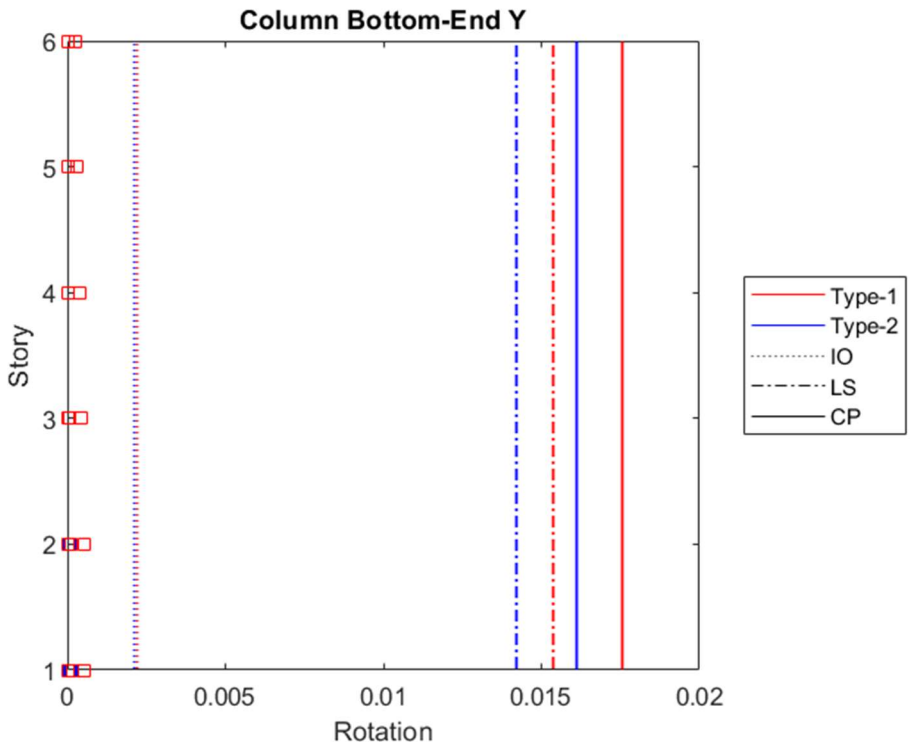

Figure 4.145. Rotations of bottom-end of column in y-direction at roof when its maximum in DD-3 level earthquake of frame with shear walls

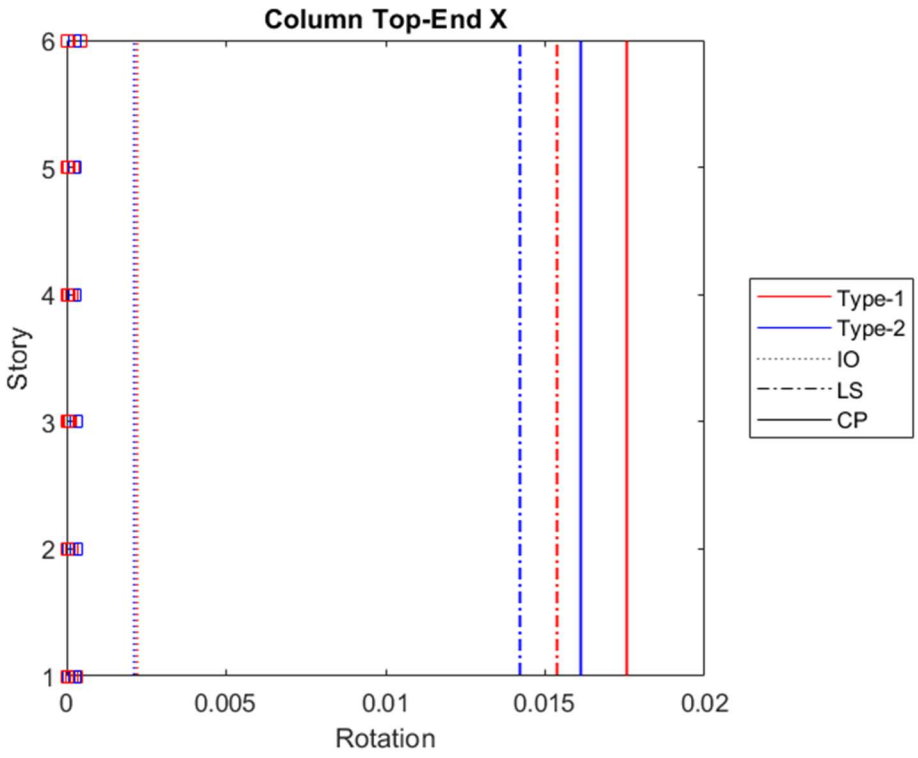

Figure 4.146. Rotations of top-end of column in x-direction at roof when its maximum in DD-3 level earthquake of frame with shear walls

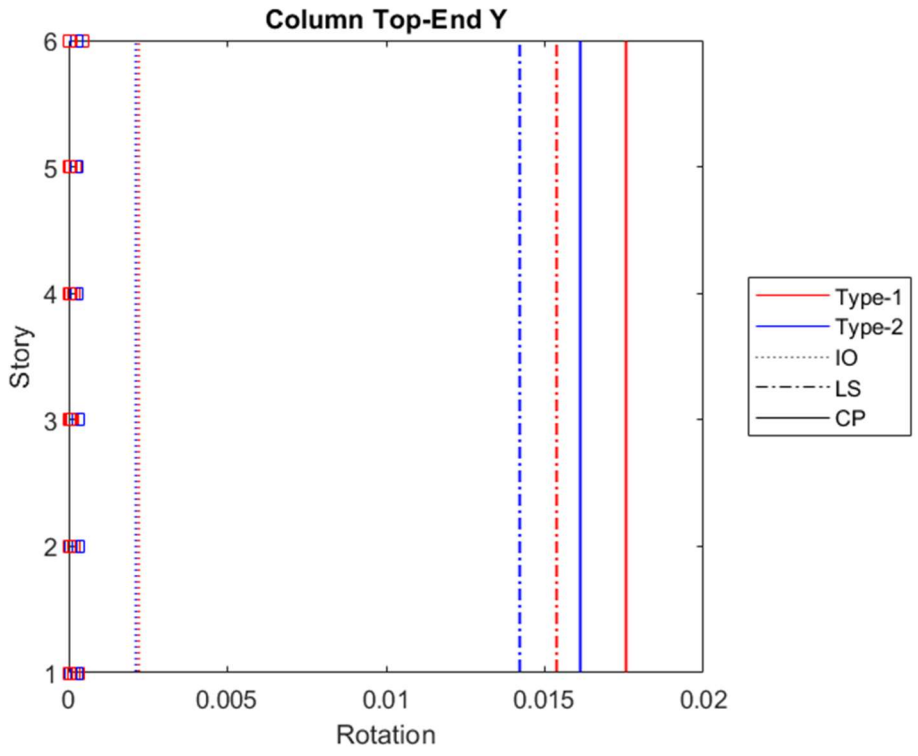

Figure 4.147. Rotations of top-end of column in y-direction at roof when its maximum in DD-3 level earthquake of frame with shear walls

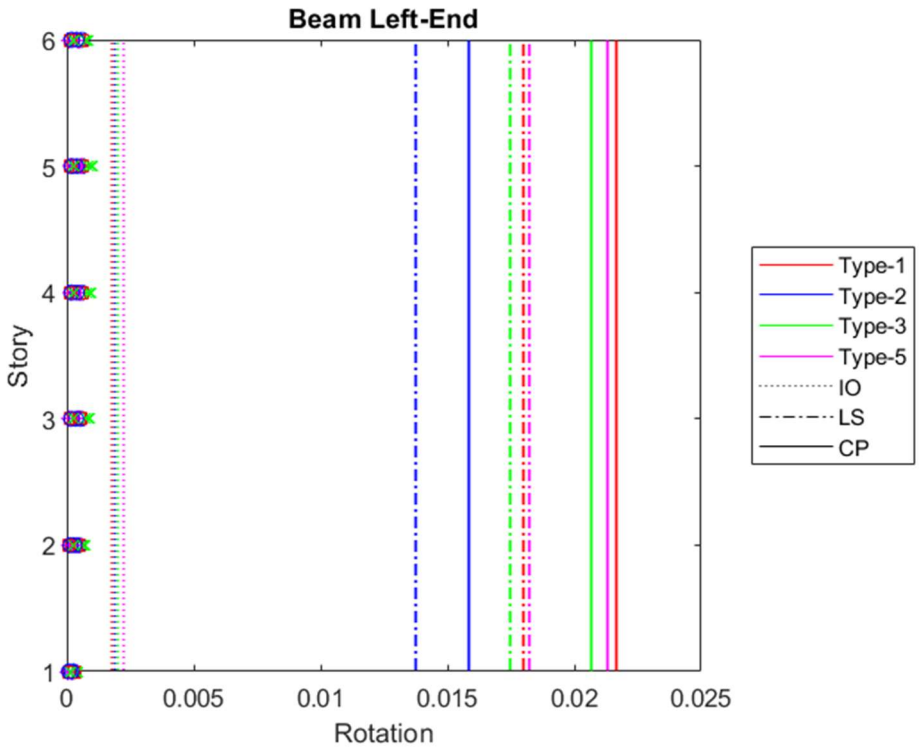

Figure 4.148. Rotations of left-end of beam in x-direction at roof when its maximum in DD-3 level earthquake of frame with shear walls

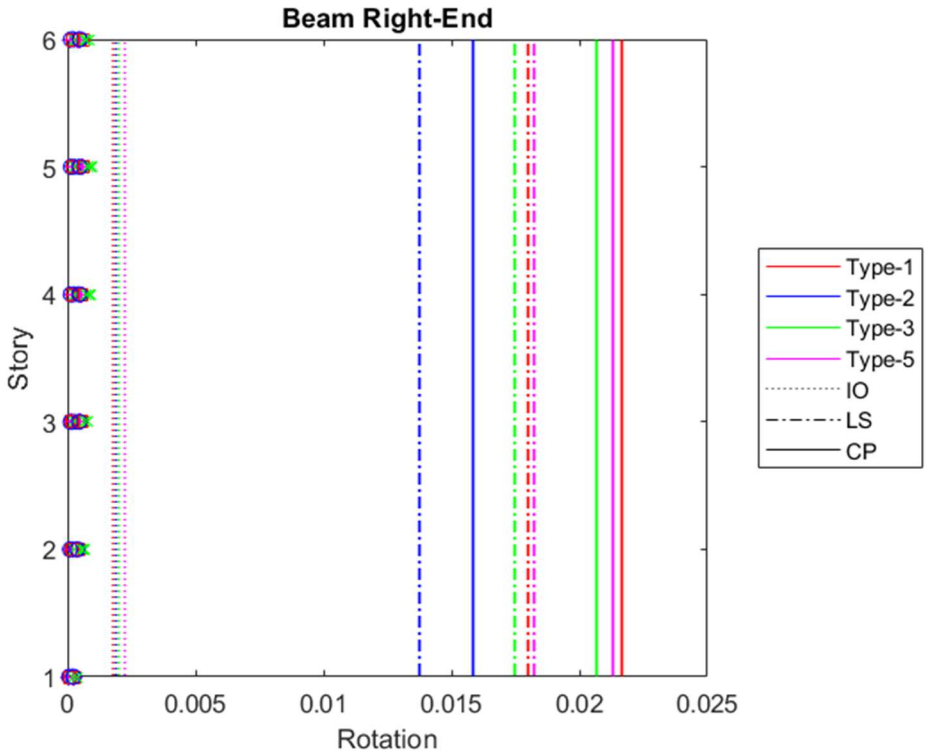

Figure 4.149. Rotations of right-end of beam in x-direction at roof when its maximum in DD-3 level earthquake of frame with shear walls

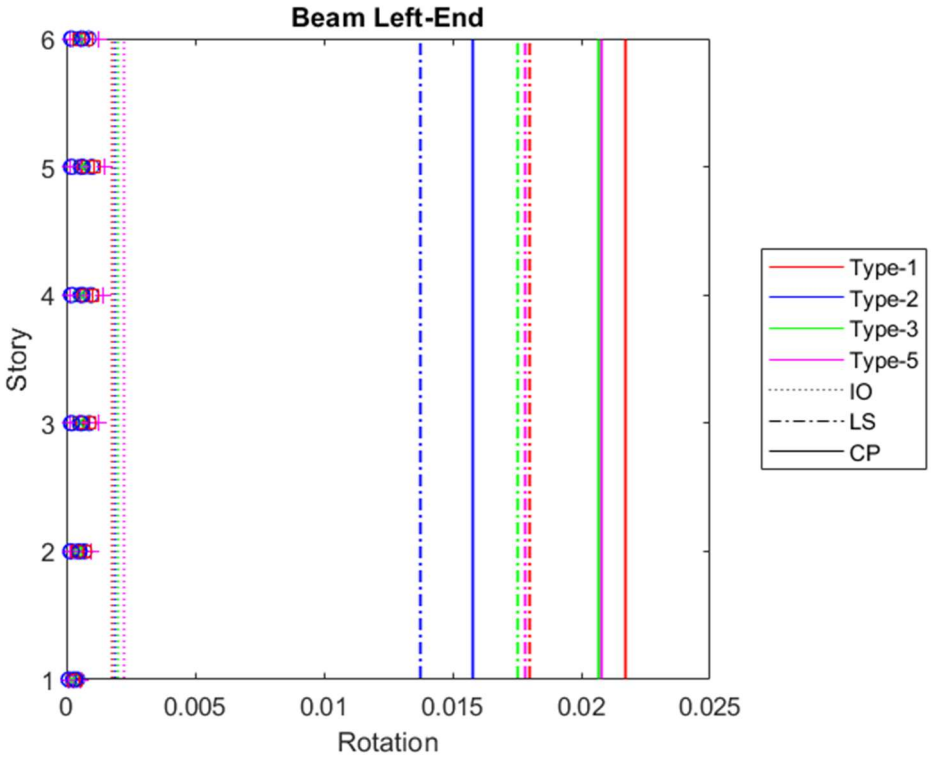

Figure 4.150. Rotations of left-end of beam in y-direction at roof when its maximum in DD-3 level earthquake of frame with shear walls

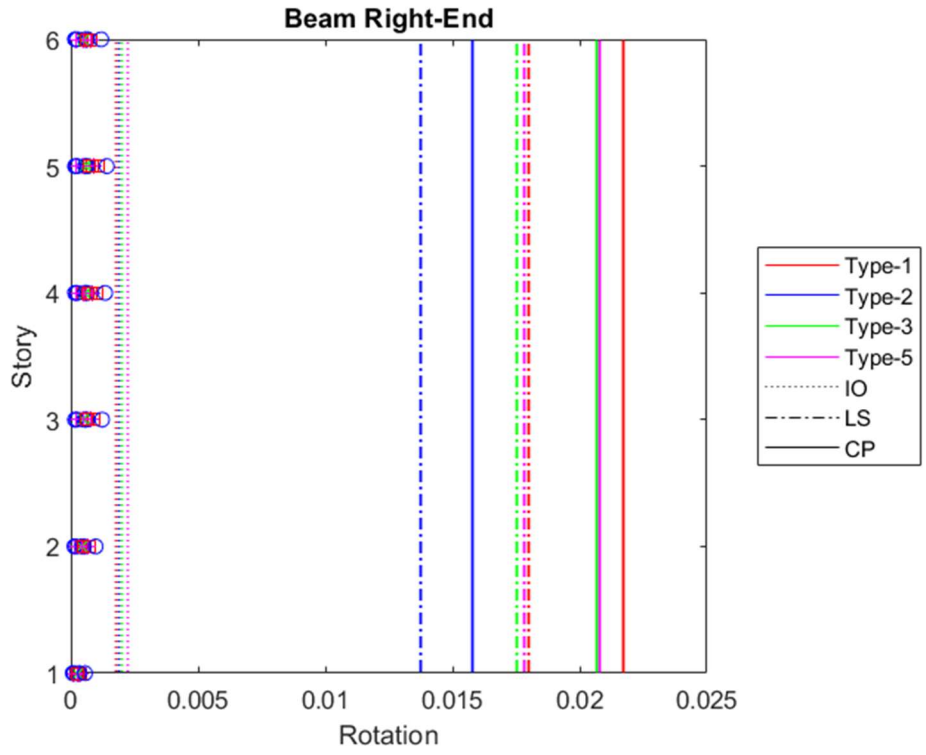

Figure 4.151. Rotations of right-end of beam in y-direction at roof when its maximum in DD-3 level earthquake of frame with shear walls

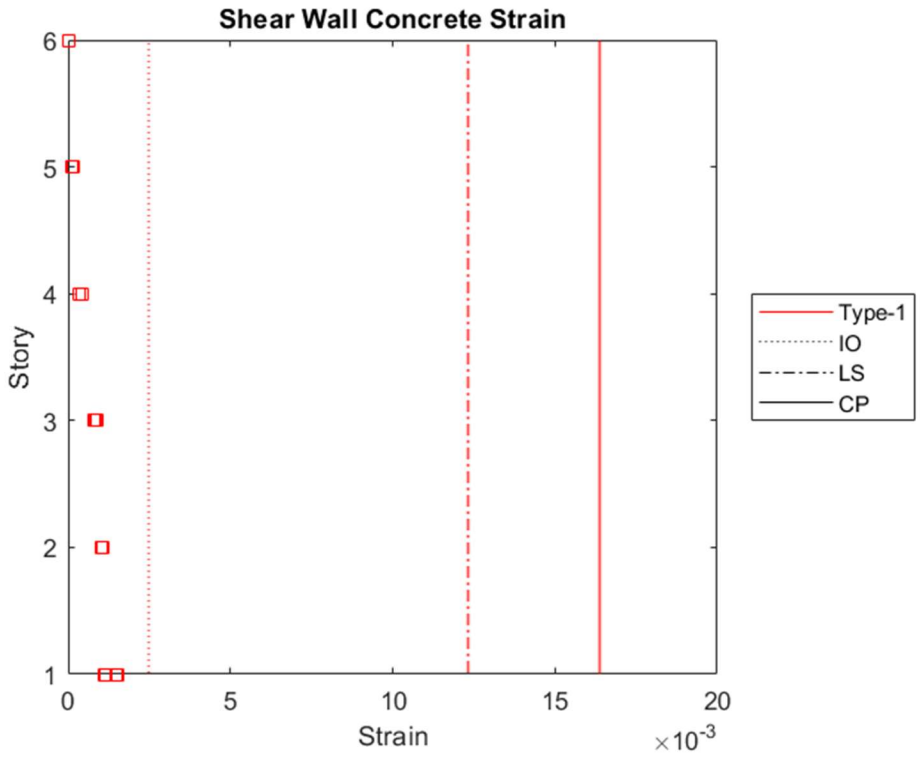

Figure 4.152. Concrete strain of bottom-end of shear wall Type-1 for the maximum envelope drifts in DD-3 level earthquake of frame with shear walls

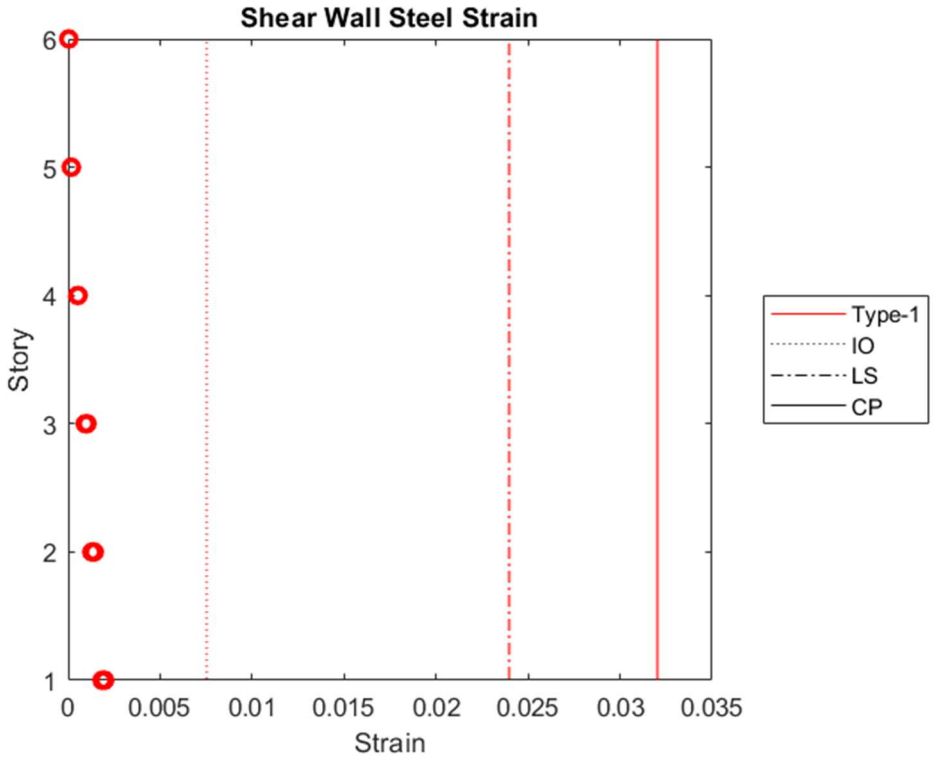

Figure 4.153. Steel strain of bottom-end of shear wall Type-1 for the maximum envelope drifts in DD-3 level earthquake of frame with shear walls

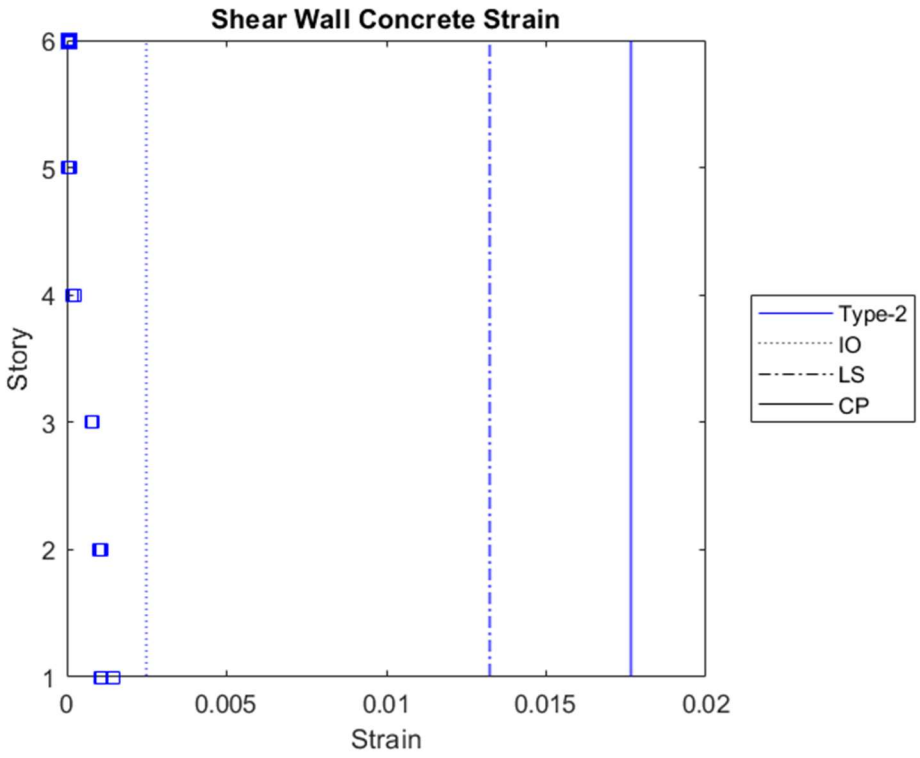

Figure 4.154. Concrete strain of bottom-end of shear wall Type-2 for the maximum envelope drifts in DD-3 level earthquake of frame with shear walls

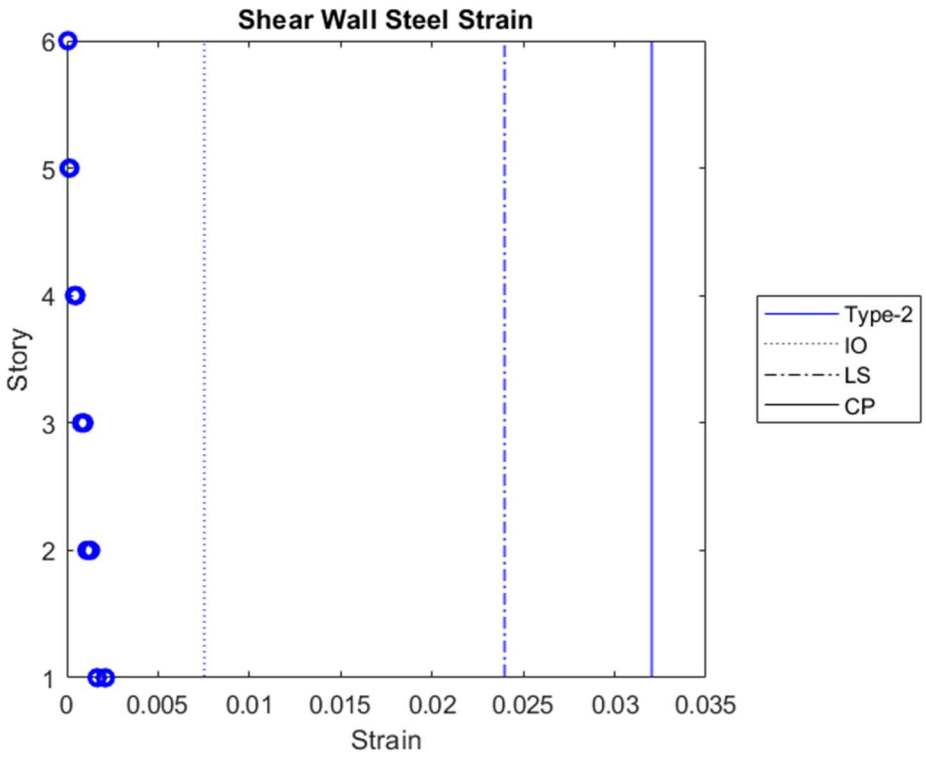

Figure 4.155. Steel strain of bottom-end of shear wall Type-2 for the maximum envelope drifts in DD-3 level earthquake of frame with shear walls

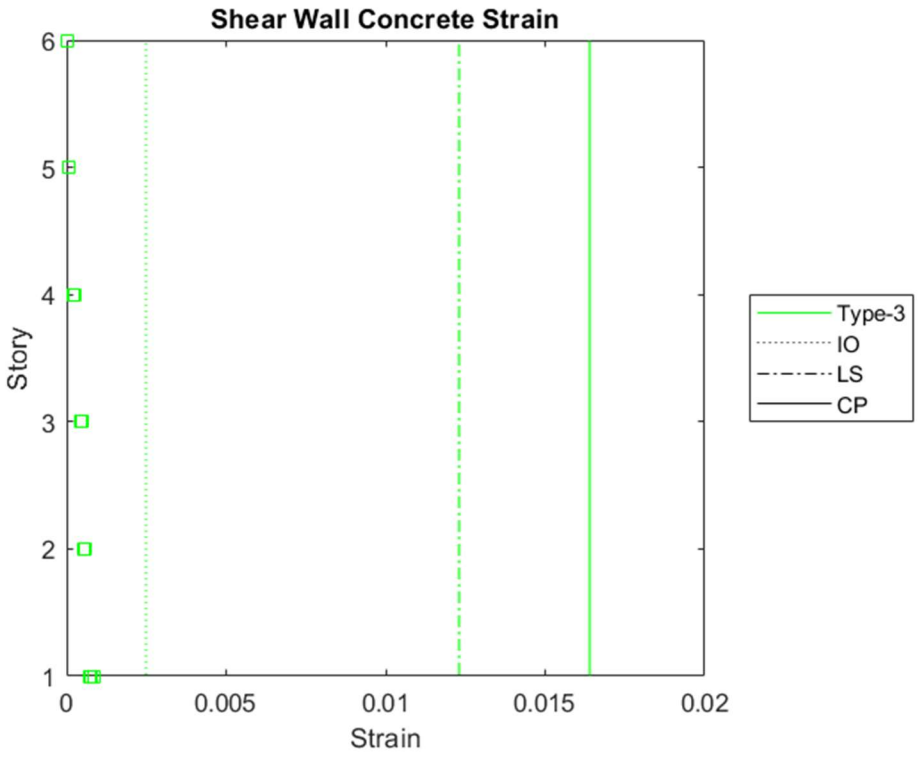

Figure 4.156. Concrete strain of bottom-end of shear wall Type-3 for the maximum envelope drifts in DD-3 level earthquake of frame with shear walls

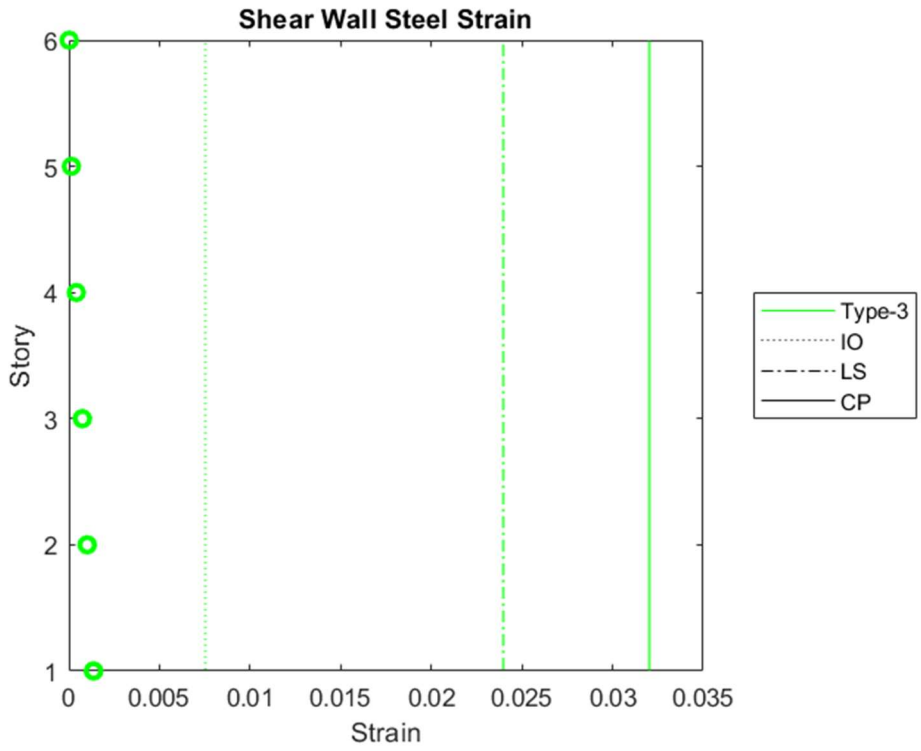

Figure 4.157. Steel strain of bottom-end of shear wall Type-3 for the maximum envelope drifts in DD-3 level earthquake of frame with shear walls

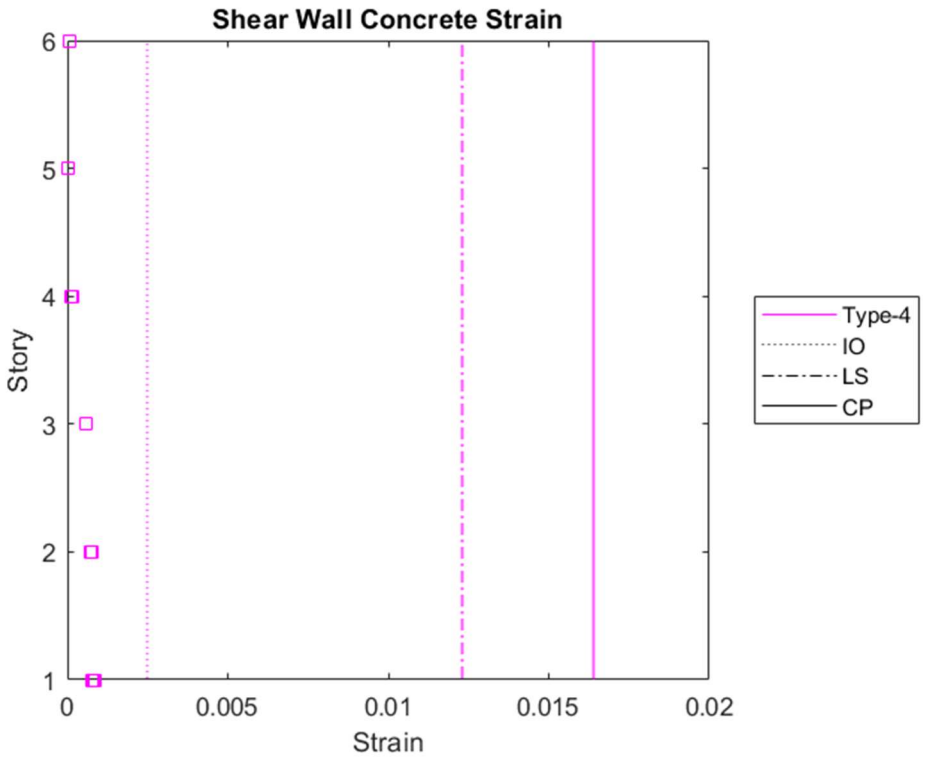

Figure 4.158. Concrete strain of bottom-end of shear wall Type-4 for the maximum envelope drifts in DD-3 level earthquake of frame with shear walls

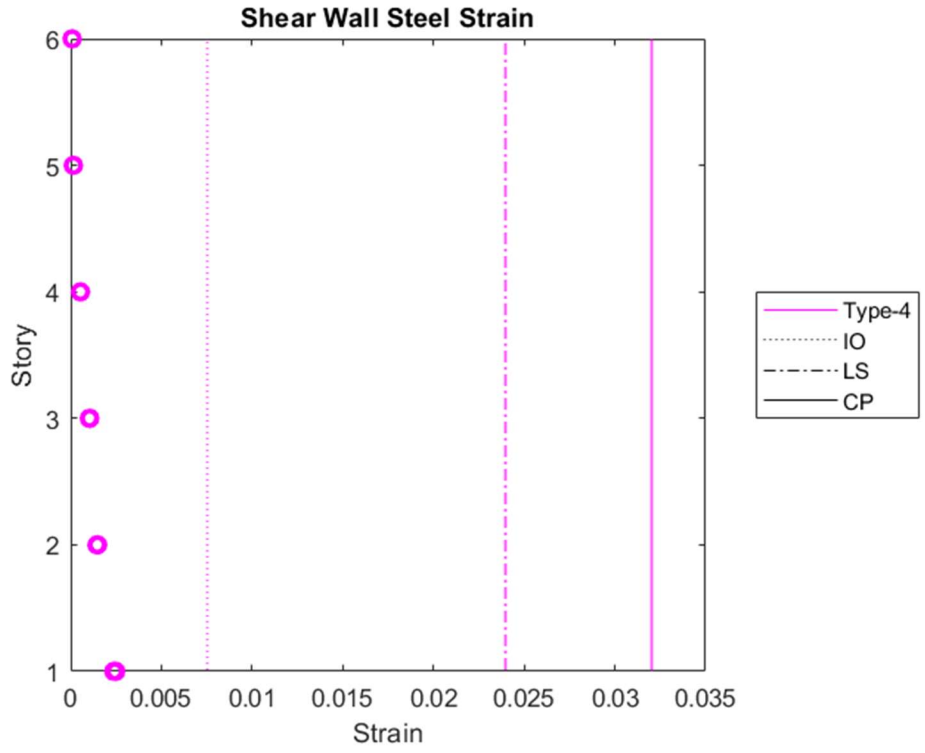

Figure 4.159. Steel strain of bottom-end of shear wall Type-4 for the maximum envelope drifts in DD-3 level earthquake of frame with shear walls

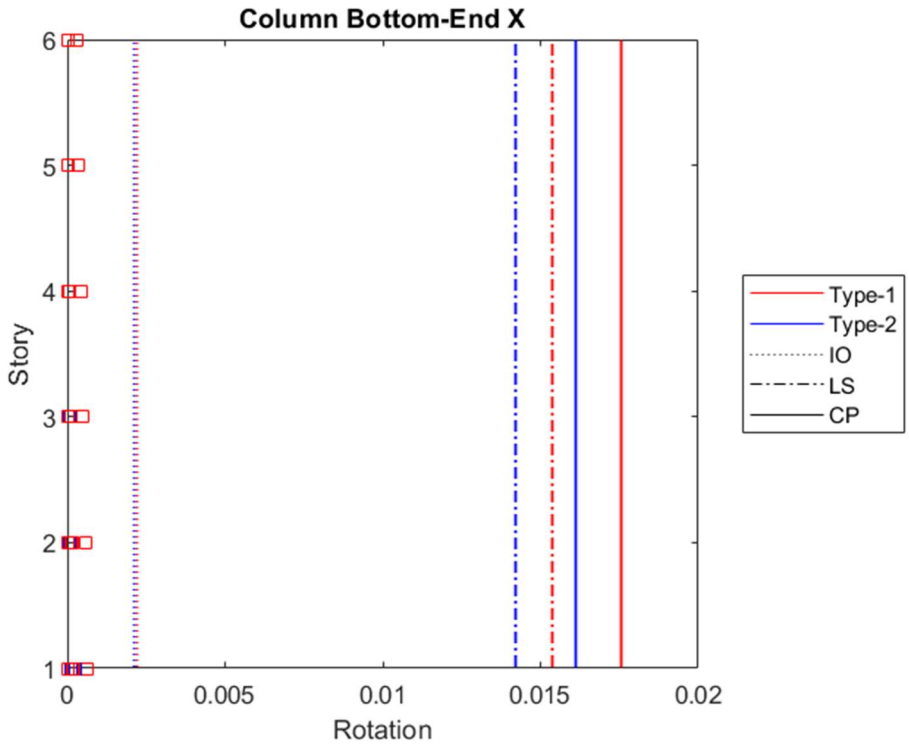

Figure 4.160. Rotations of bottom-end of column in x-direction for the maximum envelope drifts in DD-3 level earthquake of frame with shear walls

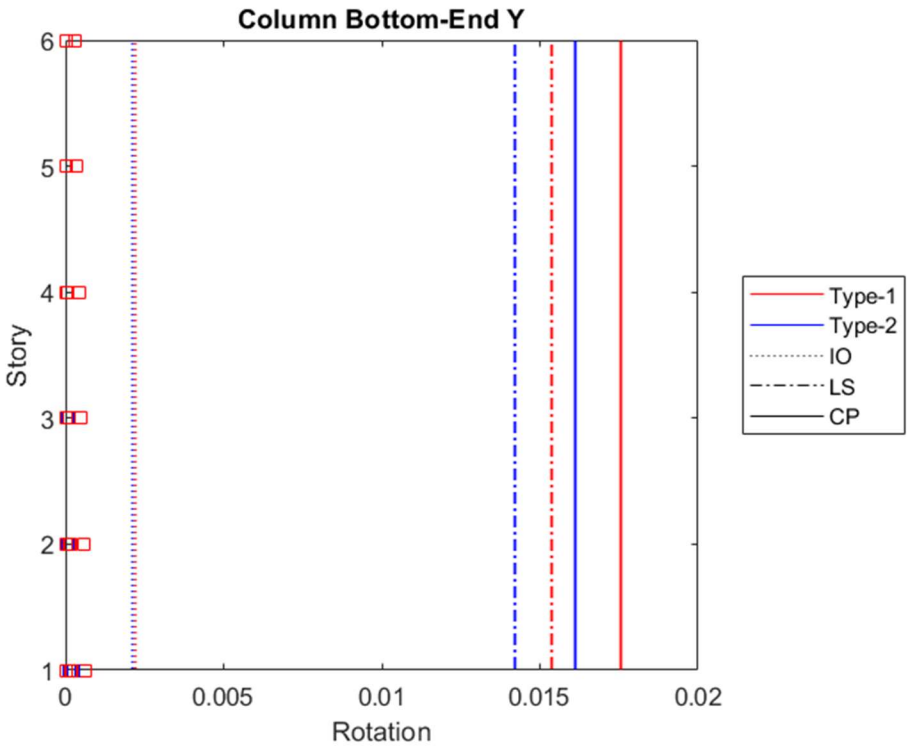

Figure 4.161. Rotations of bottom-end of column in y-direction for the maximum envelope drifts in DD-3 level earthquake of frame with shear walls

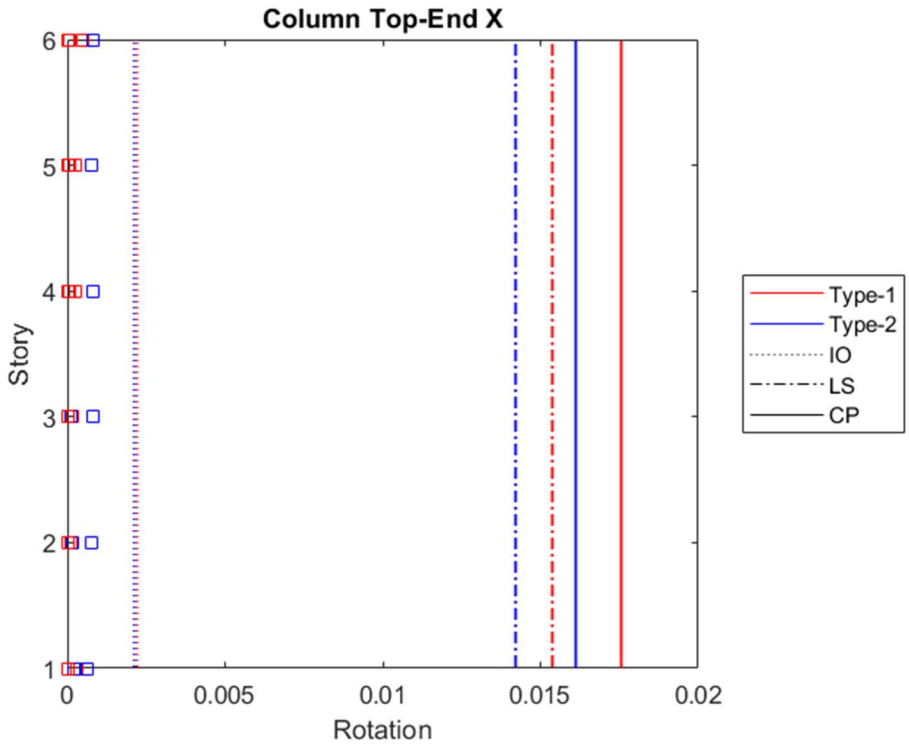

Figure 4.162. Rotations of top-end of column in x-direction for the maximum envelope drifts in DD-3 level earthquake of frame with shear walls

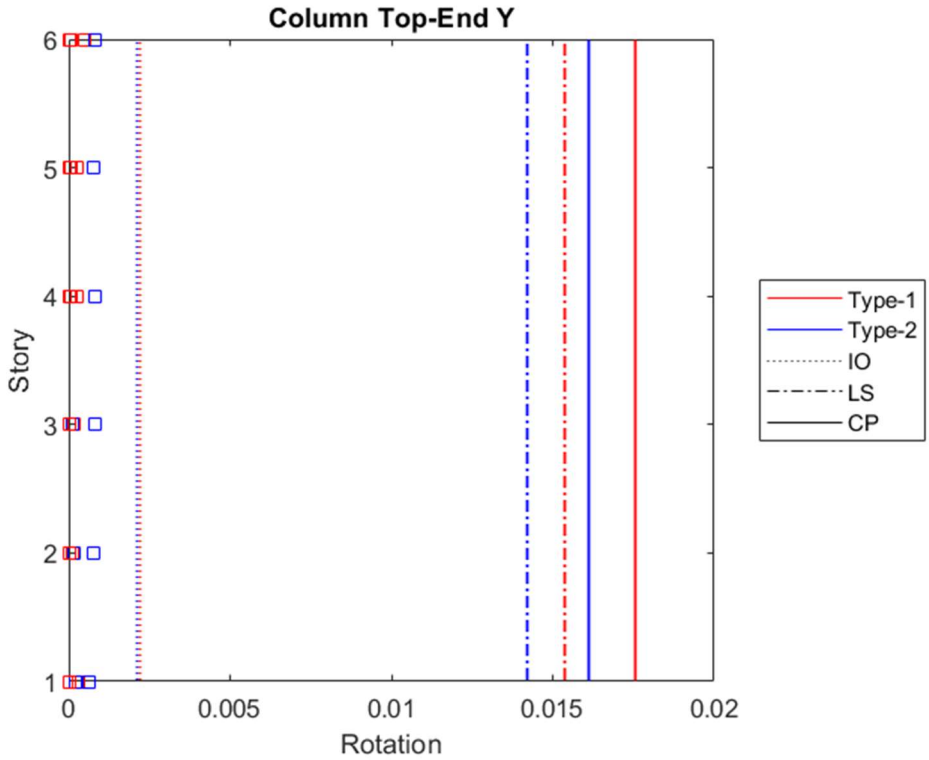

Figure 4.163. Rotations of top-end of column in y-direction for the maximum envelope drifts in DD-3 level earthquake of frame with shear walls

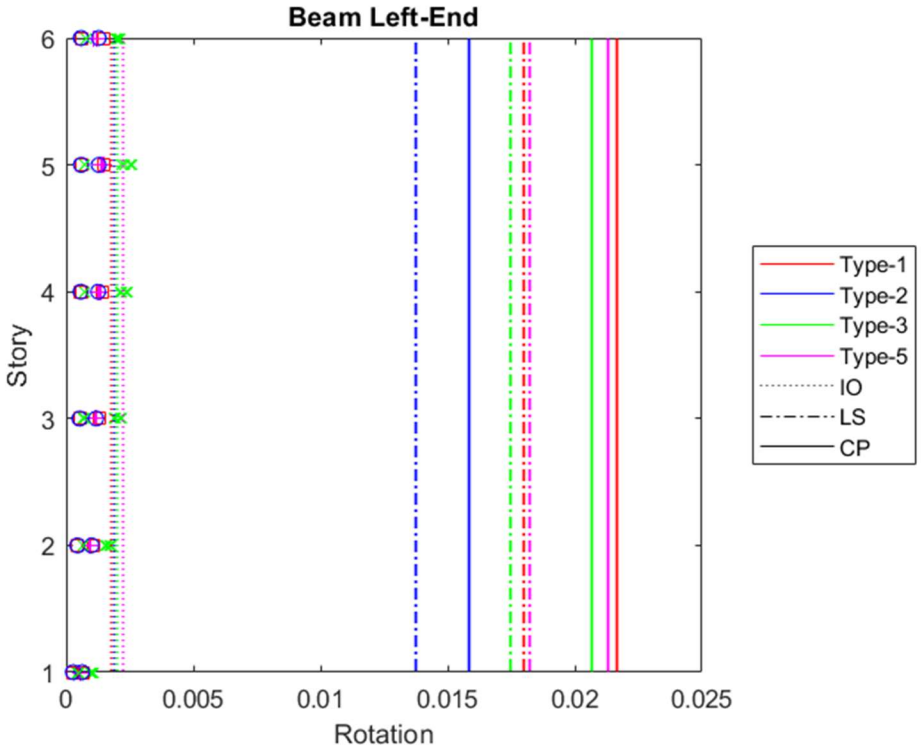

Figure 4.164. Rotations of left-end of beam in x-direction for the maximum envelope drifts in DD-3 level earthquake of frame with shear walls

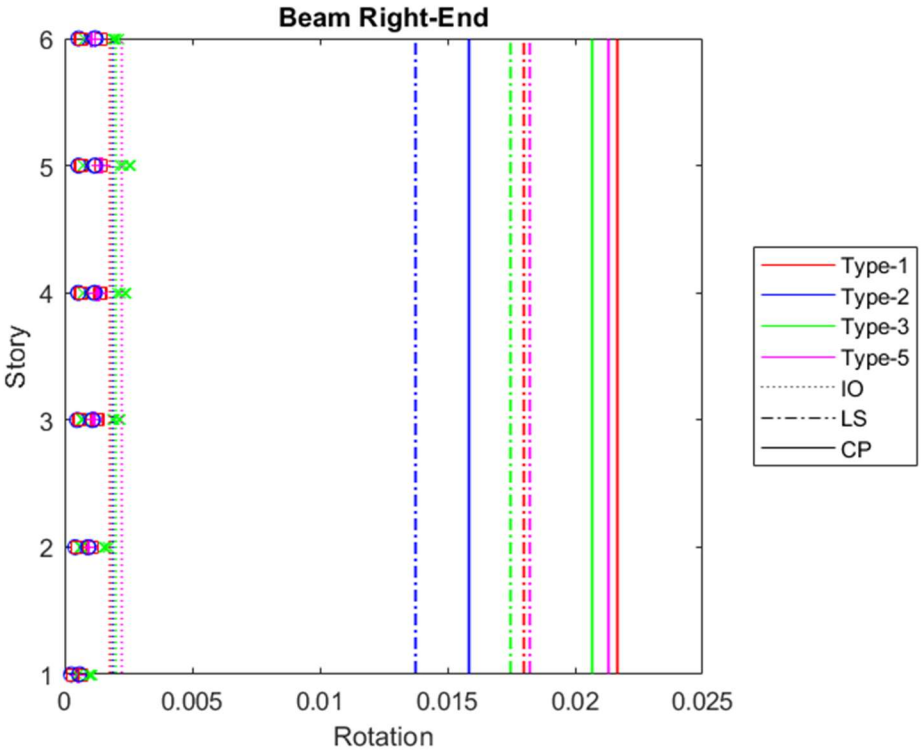

Figure 4.165. Rotations of right-end of beam in x-direction for the maximum envelope drifts in DD-3 level earthquake of frame with shear walls

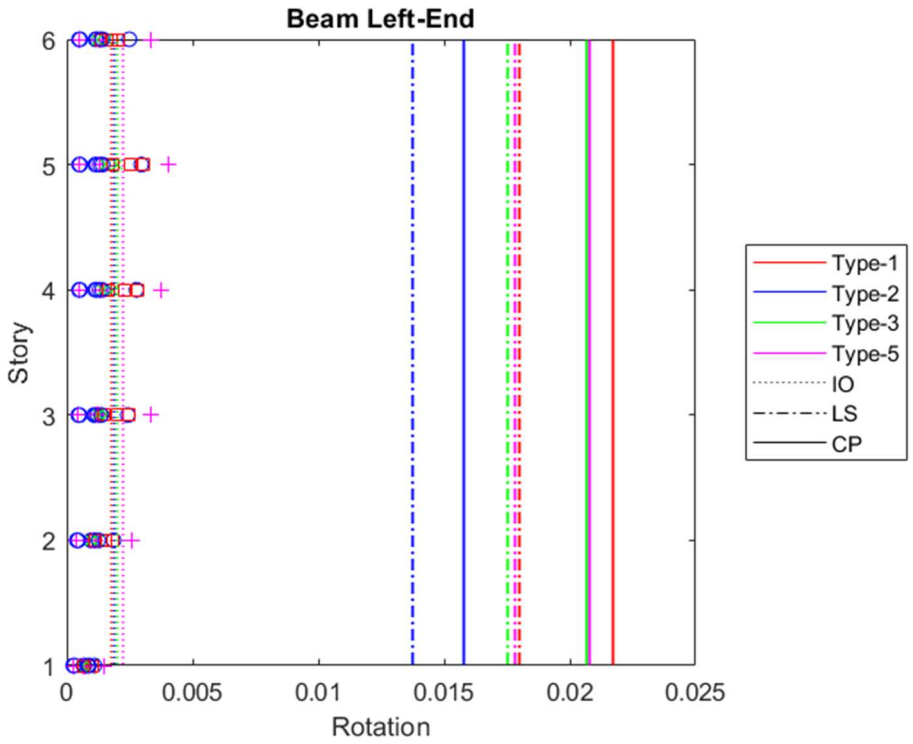

Figure 4.166. Rotations of left-end of beam in y-direction for the maximum envelope drifts in DD-3 level earthquake of frame with shear walls

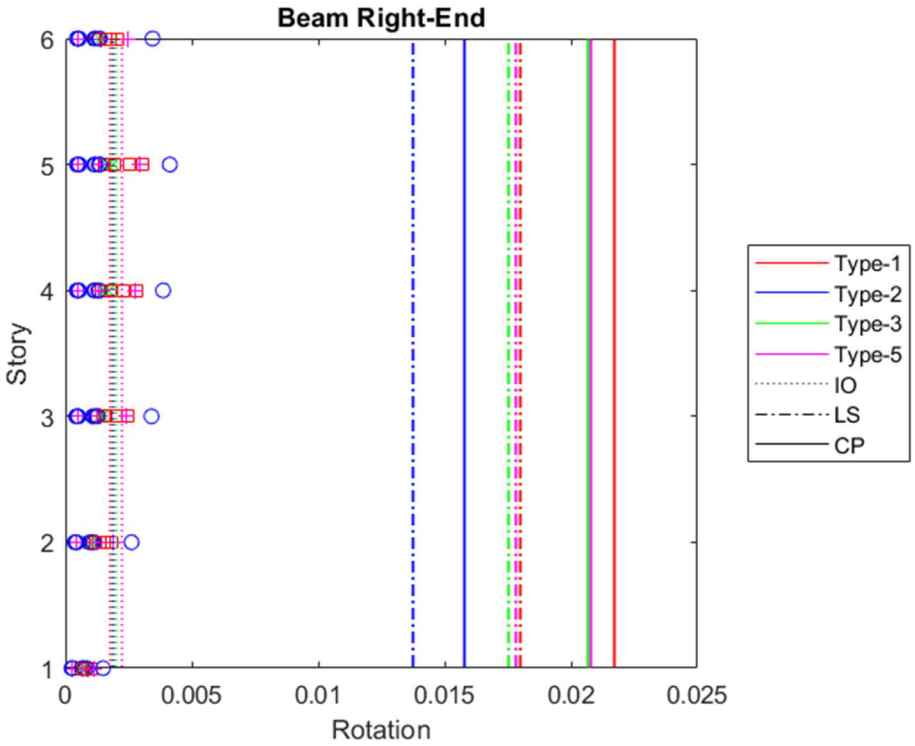

Figure 4.167. Rotations of right-end of beam in y-direction for the maximum envelope drifts in DD-3 level earthquake of frame with shear walls

CHAPTER 5

ENERGY ANALYSIS AND LIFE CYCLE ASSESSMENT

5.1. Energy Analysis

The evolving needs of human civilization results in the increase in energy production and consumption. The increase in production and consumption of energy reached a large portion of the economy and the CO_2 emission. The construction sectors consume a major portion of the total production.

The energy and environmental performance of the buildings are largely dependent on the decisions made in the early stages. According to the World Green Building Council (2019), buildings are currently responsible for 39% of global energy-related carbon emissions: 28% from operational emissions, from the energy needed to heat, cool, and power them, and the remaining 11% from materials and construction. In Türkiye, residential buildings consume 35% of the energy consumed (Gerçek, 2019). The embodied and operational energy are the major components of the energy budget considering the sustainability of the structure. Embodied energy involves the extraction of raw resources, processing materials, transportation, assembling product components, construction, maintenance, repair, deconstruction, and disposal. The operational energy involves the energy usage during the occupancy of buildings for heating, cooling, and ventilation purposes. The embodied energy typically dominated at the design and construction phase and the operational energy mainly governs the energy consumption throughout the whole operational life of a building.

If the structural framing of the buildings is considered, compared to moment frames shear wall buildings could be seen to have higher cost and environmental impact. The initial cost and environmental impact due to the use of additional material are the causes of the difference. However, if the total life cycle is considered, this initial estimate does not need to be true. The advantages that could be obtained through the use of shear walls could close the gap. One such example is the smart use of the thermal mass effect of the shear walls. If designed accordingly this advantage could have a positive impact

on the operational energy consumption of the building. The thermal mass of the concrete in shear walls can store and release heat, which affects the heating and cooling cycles and the energy consumption of the building in its operational phase.

In this study, the energy analysis of the frames discussed in the preceding chapters are done by using SketchUp (SketchUp, 2023), Open Studio (NREL, 2014) and EnergyPlus (EnergyPlus, 2023). The building model was imported from Revit to SketchUp. The imported model in Revit is presented in Figure 5.1. The material properties are attained to the elements in SketchUp. Default materials properties that are available in SketchUp are used for both frames. Then, Open Studio plug-in used to export the SketchUp model to Open Studio for the energy analysis. Open Studio includes default EnergyPlus in the program. EnergyPlus is a whole energy simulation program that can be used to model energy and water consumption in buildings (EnergyPlus, 2023). Heating and cooling of indoor, water use, ventilation, lighting, plug and process loads can be calculated in EnergyPlus. The weather data is obtained from EnergyPlus website for Istanbul. The energy analysis is performed after creating the spaces, attaining HVAC system and internal mass to the building in Open Studio as shown in Figure 5.2. There is no detailed information about the HVAC system of the buildings studied. Hence, the default HVAC systems are used during the energy analysis in Open Studio.

The results are given in Table 5.1-5.2. According to the results, the heating and cooling energy are almost the same for both frames with differences of less than 1%. Also, the water usage is very similar for both frames. These results are the operational energy consumption of the frames and will be used in life-cycle analysis in the coming sections.

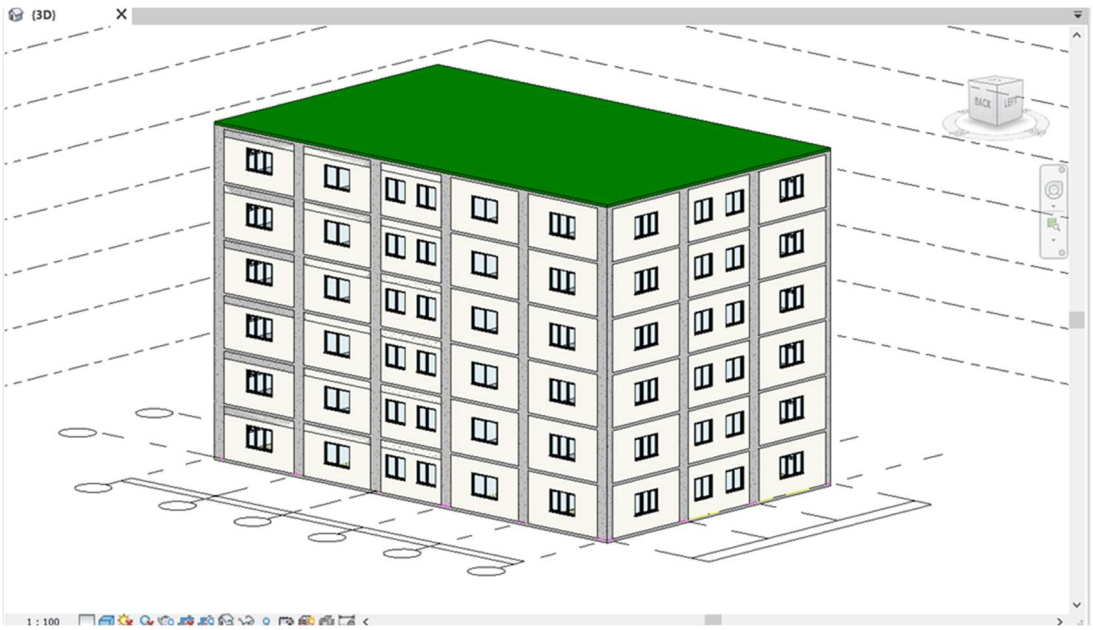

Figure 5.1.The 3D Revit model of the MRF

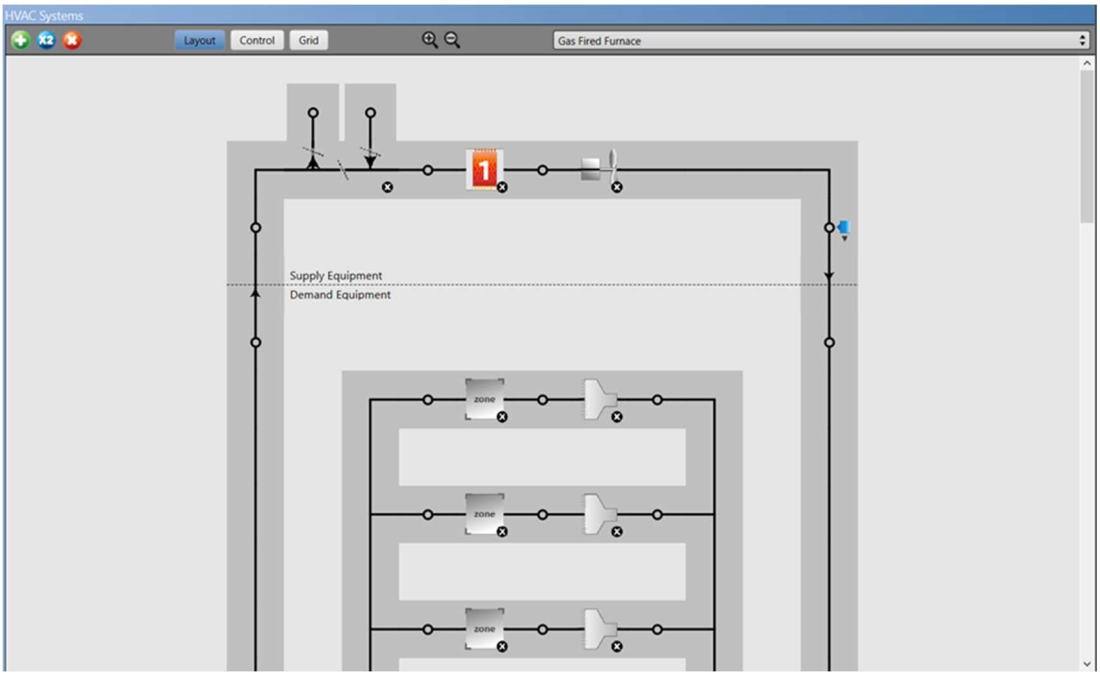

Figure 5.2.HVAC system attainment part of Open Studio

Table 5.1. Energy analysis result of MRF from Open Studio

	Electricity [GJ]	**Natural Gas [GJ]**	**Water [m3]**
Heating	0	241.39	0
Cooling	20.01	0	0
Interior Lighting	52.2	0	0
Exterior Lighting	25.92	0	0
Interior Equipment	406.87	0	0
Exterior Equipment	0	0	0
Fans	21.24	0	0
Pumps	7.09	0	0
Heat Rejection	5.1	0	9827.7
Humidification	0	0	0
Heat Recovery	0	0	0
Water Systems	0	0	0
Refrigeration	0	0	0
Generators	0	0	0
Total End Uses	538.42	241.39	9827.7

Table 5.2. Energy analysis result of RC system with shear walls from Open Studio

	Electricity [GJ]	**Natural Gas [GJ]**	**Water [m3]**
Heating	0	244.87	0
Cooling	19.76	0	0
Interior Lighting	52.2	0	0
Exterior Lighting	25.92	0	0
Interior Equipment	406.87	0	0
Exterior Equipment	0	0	0
Fans	21.24	0	0
Pumps	6.92	0	0
Heat Rejection	4.99	0	9766.89
Humidification	0	0	0
Heat Recovery	0	0	0
Water Systems	0	0	0
Refrigeration	0	0	0
Generators	0	0	0
Total End Uses	537.89	244.87	9766.89

5.2. Life Cycle Assessment

Life cycle assessment (LCA) evaluates the environmental impact from extracting raw material to recycle stage of a product or system. Structures have an environmental impact throughout their entire life cycle, consisting of the production, construction, use, and end-of-life stages. There are also externalized impacts beyond the system boundary, as shown in Figure 5.3. The production stage consists of the required energy and resources for raw materials extraction, transportation to facilities, and final production. In the construction stage, the transportation of materials to the construction site, energy consumed by construction equipment, procurement supporting construction materials, and disposal of any waste generated during the construction. The use stage concentrates on the environmental impacts of occupying a building over its lifetime due to lighting, heating, water use, and any materials used for maintenance, repairs, or replacement. The end-of-life stage involves the demolition, disposal of the building, and waste processing. The last stage considers the effects of reusing, recycling, and recovering materials, energy, or water from the project to minimize the environmental impact.

Emissions are typically translated to environmental impacts. There are five common standardized emissions. Global warming potential (GWP), acidification potential (AP), eutrophication potential (EP), ozone depletion potential (ODP), and smog formation potential (SFP) are the well-established impacts. In this study, the GWP is used in the LCA.

There are various assessment types in life cycle assessment (LCA) which are cradle-to-gate, cradle to grave and cradle-to-cradle. In cradle to gate from production to transportation from facilities is considered. In cradle to grave, from production to demolition is considered. In the cradle to cradle from production to recycling and reusing the disposal is considered. Cradle to cradle was used in this study.

The goal of this study in this chapter is to obtain the environmental impact of the designed buildings. The components of the building or the operations which have a higher impact can also be observed from this assessment.

Figure 5.3. Life cycle analysis phases (Skanska, 2019)

A series of software is used for life cycle analysis. Revit is used for modeling buildings. The output of Revit is used as an input to eTool for getting the required quantity takeoff values of the elements in the buildings. Then, with the eTool plug-in, the models are transferred to the eTool program that works online, as shown in Figure 5.4. Life cycle inventory (LCI) source, land area, location, assessment scope, structure type, service life limit, design quality, suburb redevelopment potential, number of stories, and building function properties etc. are entered into the eTool system. The default material types are attained to the imported components. In both buildings, the same materials are attained for the same kind of components to have compatibility. Architectural details are not developed in detail, due to the great variety there and the structural focus of the study.

The life cycle analysis is done in eTool by plug-in from Revit. The operational energy inputs are obtained from Open Studio. The results are categorized by the program and given in Figure 5.5 and 5.6. It could be observed that, if the operational costs are excluded the superstructure has an important impact on the life cycle assessment of both buildings. The total impact values are 1.239.690 GWP for the MRF and 1.467.574 GWP for the frame with shear walls. The introduction of shear walls and the related modification in the building causes an 18% increase in embodied consumption of the building. The size of the difference decreases if the operational part is considered. The consumption values are 5.190.583 GWP for MRF and 5.417.521 GWP for the frame with shear walls. The increase due to shear wall introduction drops to 4%. These results are presented in Figure 5.7 in graphical form.

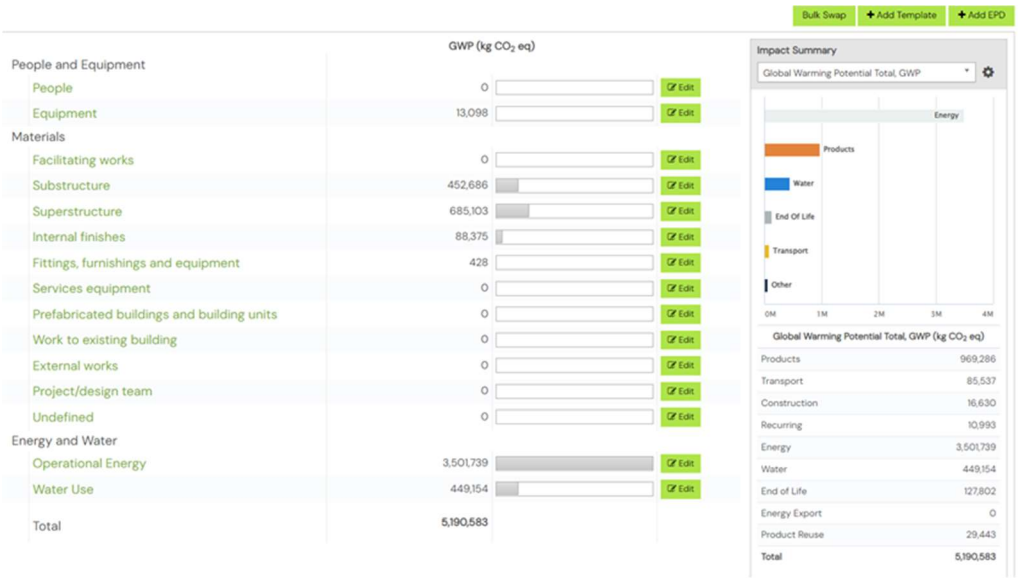

Figure 5.4.The eTool LCA program interface that shows the results

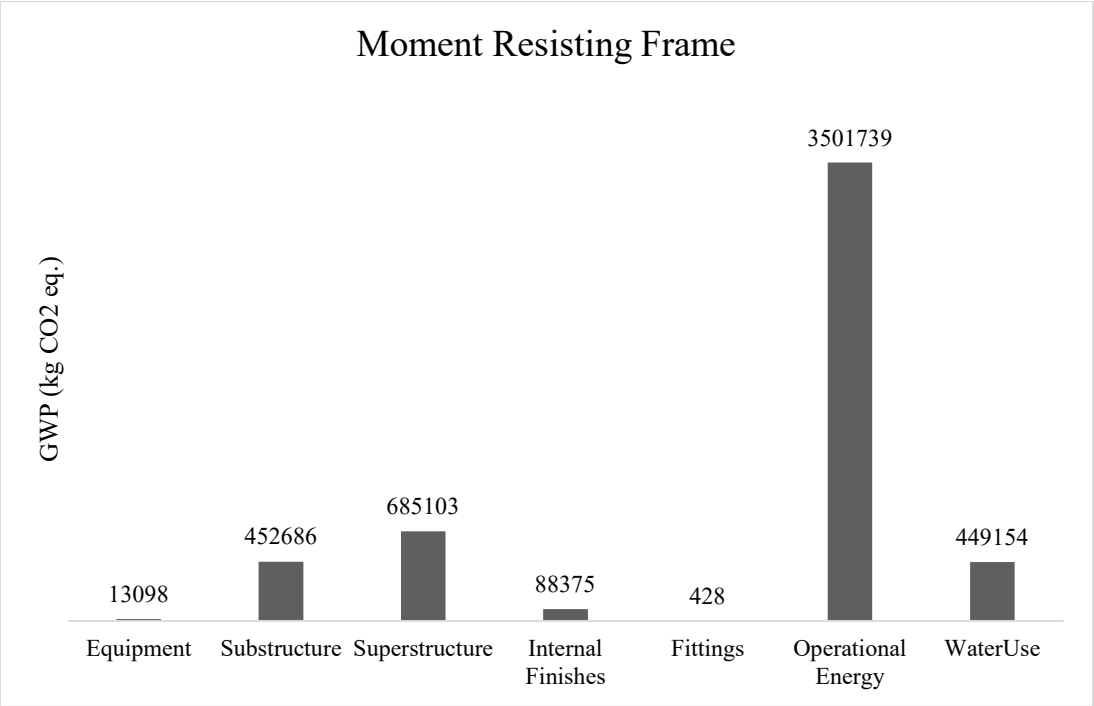

Figure 5.5. The life cycle analysis results of moment frame in GWP (kg CO_2 eq.)

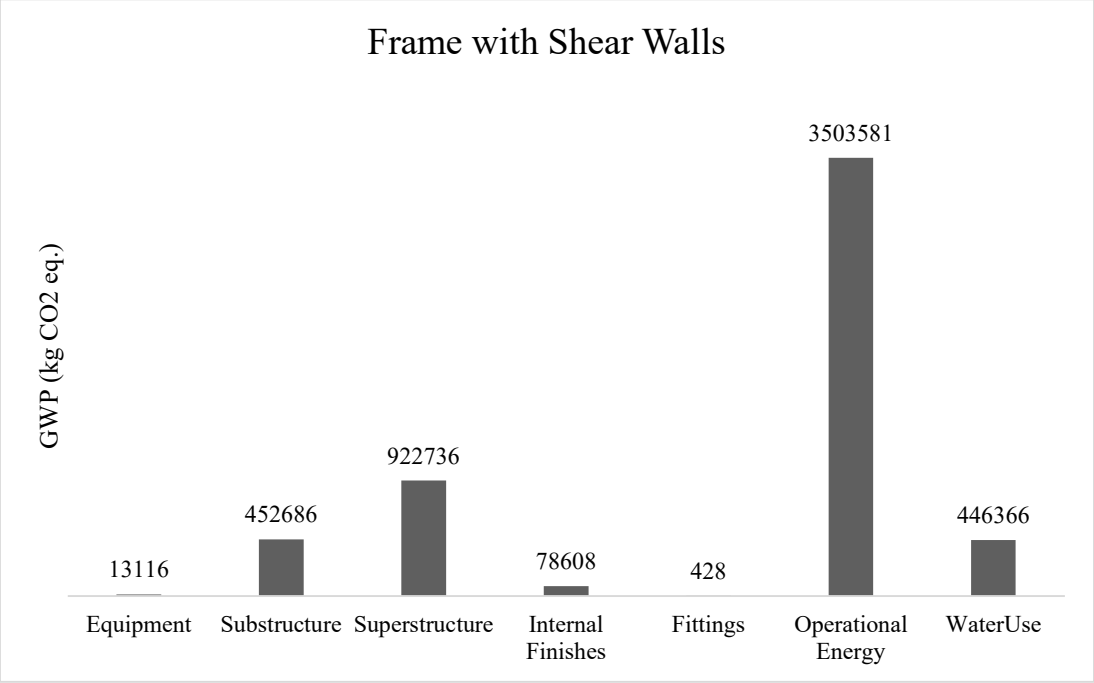

Figure 5.6. The life cycle analysis results of the RC frame with shear walls in GWP (kg CO_2 eq.)

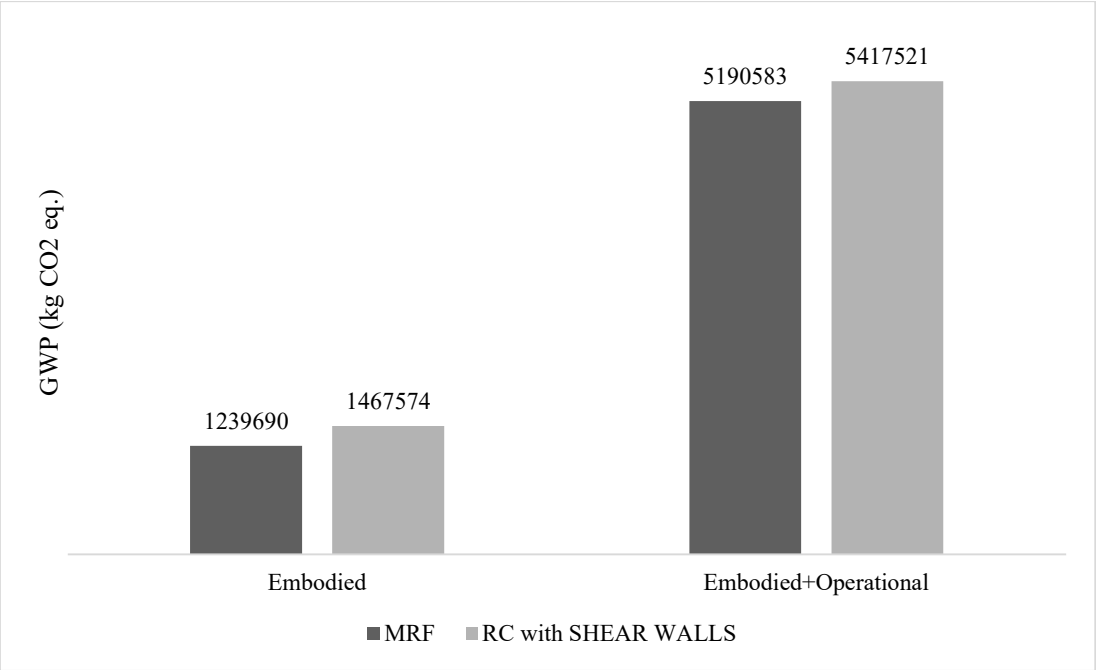

Figure 5.7. The life cycle analysis total results of the structures only embodied and embodied and operational considered in GWP (kg CO_2 eq)

LCA study indicates that the contribution of shear walls reduces the environmental impact on the whole life cycle rather than only considering initial environmental impact. Optimal design choices lead to a great balance between the embodied and operating stages, changing the misconception that the use of shear walls in RC systems leads to have higher impact. In essence, shear walls contribute significantly to the total environmental impact over the structure's life cycle.

The order of magnitude of the LCA results could be verified with the numbers provided by the guide of Skanska (Skanska, 2019). It is reported that the typical embodied carbon (total GWP/total area) of a building structure, foundation, and enclosure are typically less than 1000 kg CO_2 e/m^2. If the analysis results are converted into the same units, the moment-resisting frame has 421 kg CO_2 e/m^2, and the frame with the shear walls has 499 kg CO_2 e/m^2 carbon equivalent consumption. It should be noted that foundations are not considered in this study. Still, results seem in the right range.

CHAPTER 6

DISCUSSION OF RESULTS AND THE CONCLUSION

The presented study aimed to demonstrate that it is possible being resilient and sustainable could be achieved at the same time. Such results could be obtained through design and adaptations that serve resilience and sustainability together. The scope of the presented study was to improve the seismic performance without significantly creating an impact on the corresponding life cycle consumptions of an RC moment frame structure. Specifically, the capability of the shear walls to control the drift in a frame through proper design decisions is demonstrated. Also, the thermal mass effect of the shear walls to minimize the operational energy cost to control the total consumption budget is considered. A typical size RC moment frame in Türkiye is selected and modified to gain the expected resilience through using Hassan and Sozen's (1997) priority index (PI). As proposed by the Hassan Index studies, the PI was set to be more than 0.25%. Primarily, shear walls are provided to reach the targeted index level. The geometry and the layout of the structure resulted in a PI value of 0.37% in the modified frame. The walls are also attempted to be arranged to maximize the thermal mass effect of the shear walls on heating and cooling performance during the operational phase. Maximization is done by trial and error.

The summary of the text is as follows:

In Chapter 2, a literature survey is presented. It appeared that the construction industry could have a significant impact on sustainability efforts. The realization of the necessity of resilient buildings was observed. The importance of future studies in this subject is emphasized.

In Chapter 3, the layout of frames is selected. Two types of frames were studied for this purpose. The first frame was a moment-resisting frame that was selected to represent a typical moment frame in Türkiye. The second frame was designed to provide sufficient robustness and optimized energy efficiency. Shear walls were used to provide the needed robustness and energy efficiency of the building through its thermal mass. The

structural design of both frames was done according to the TS-500 and TER-2018. Ground motion sets are selected for non-linear time history analysis based on TER-2018 definitions. A pulse-like indicator was used to eliminate such motions during the selection process.

In Chapter 4, a 3D nonlinear model and the analysis of both structures are performed. Analysis is executed by OpenSees software. Beam and column elements in the frames are simulated by beamWithHinges. Beam nonlinearity is introduced by concentrated plastic hinges. In columns, fiber sections are preferred to simulate the axial load moment interaction. Both beams and columns have flexural nonlinearity at their ends. Shear walls are simulated by forcebeamcolumn element with six integration points. The Mander model was used for the simulation of the stress-strain relationship of confined concrete. The P-Δ effect is also considered in the analysis.

In Chapter 5, the energy analysis and life cycle assessment were conducted. The analyses provide information to evaluate the environmental impact of the structures. Life cycle assessment was conducted by Revit and eTool software, which provides the embodied part of the energy consumption. The operational energy analysis is performed by eTool, and the results computed from Open Studio and EnergyPlus are manually added to eTool.

6.1. Discussion of the Results

The analysis of the frames showed that the addition of a sufficient amount of shear walls improves the seismic behavior effectively. The moment frame response in the global sense indicates that for DD-2 earthquake the IDRs are within the regulation proposed values. The IDR values are in the vicinity of the 2% limit. If the DD-1 response is considered, IDR not only goes beyond 2% but also many members also pass the collapse prevention limits of the code. All the beams in the Y-direction in the first story, 18 of the 20 beams in the X-direction in the first story, and 17 of the 20 beams in the second story of the moment frame exceed the collapse prevention limit in a DD-1 level earthquake. Overall, the moment frame is not satisfactory from the Turkish Seismic Regulation perspective. It should be noted that even though it is intended to have a typical

frame in practice, the regularity of the selected frame is not that common in the Turkish common practice. Hence, it could be stated that the typical Turkish moment frames are more vulnerable than the frame considered. The drift levels attained in DD-2 earthquake show that the structure will have heavy non-structural and structural damages after the earthquake. The damage level for DD-1 earthquake means collapse for the structure.

The level of IDR for frame with shear walls for DD-2 earthquake is in the vicinity of 1.4%. The values are also below 2% for DD-1 earthquake. Based on the drift levels and member performance observations, it could be stated that this frame will sustain light structural damage for DD-2 earthquake. Non-structural partition damage will still develop for this frame. The structure will sustain heavy damage for some of its limited members and could be structurally repaired for reuse after the maximum expected earthquake.

The energy analysis of the frames reveals the contribution of each component of the structure itself and services to the total budget. The embodied energy of structure and the operational costs came out to be the dominant components. If the embodied part (initial costs) is considered moment frame has an 18% advantage over to frame with shear walls. But, if the total life cycle is considered, the offset in the operational consumption balances the budget and the difference drops to 4%. Considering the level of sophistication in the analysis and the uncertainties, it could be stated that structures have similar energy budgets for the full life cycle.

6.2. Conclusion

It is demonstrated that the proper and sufficient use of shear walls could increase resilience with a minor increase in the total life-cycle energy cost of an RC structure.

The decisions based on the initial costs (embodied part) could miss the advantages that could be obtained through the total life cycle of the structures. Strategies that cause an increase in the initial investment could be verified with the advantages and savings they create throughout the life cycle. The thermal-mass effect of the shear walls is demonstrated to be one of such a strategy.

The priority index (Hassan and Sozen, 1997) is shown to be a good and simple reference to provide the sought resilience in RC frames. The difference in the drift response of the X and Y-directions shows that further optimization is possible to improve resilience by controlling the drift levels.

Overall, the amount of shear walls proposed by Hassan and Sozen (1997) improves the robustness of the frame. Increased robustness is reflected in the drift levels, which control the damage to the structures. Hence, the maintenance and reconstruction costs will be less in the RC frame with shear walls. It could be stated that robustness leads to resilient structures under earthquake demands. The drawback of using shear walls due to their environmental impact can be compensated by their thermal impact. The LCA shows that the operational phase compensates for the initial impact of the shear walls when considering the whole life cycle.

The nature of an MSc thesis did not permit further detailed energy analysis and assessments considering the damages sustained after the scenario earthquakes. Such an approach could have provided a clear picture of the out-of-service and repair costs.

The optimization of the layout and energy analysis could have been performed more effectively through the collaboration of the design project team.

It is observed that the popularity of sustainability studies is not matched by the level of sophistication of the available analysis tools. The available base data and the analysis tools are observed to be in the developing stages. This lack of data and discrete analysis tools impair the success of applying complete LCA for decision-making.

In future studies, the repair and energy consequences of the earthquakes are proposed to be included in similar studies. FEMA P-58 approach was considered but not adopted in this study.

This study was constrained by the scope of an MSc thesis. However, it could be accepted as a step for future research by its perspective that the resilient structures with shear walls can be sustainable despite the impact on initial costs. Sustainable structural engineering is possible without losing the robustness and resilience of the structures.

REFERENCES

Abouhamad, M., and M. Abu-Hamd. 2021. “Life Cycle Assessment Framework for Embodied Environmental Impacts of Building Construction Systems.” *Sustainability (Switzerland)* 13 (2): 1–21. https://doi.org/10.3390/su13020461.

Algan, B. B. 1982. “Drift and Damage Considerations in Earthquake Resistant Design of Reinforced Concrete Buildings.” Ph.D. Dissertation, Urbana, IL: University of Illinois at Urbana-Champaign.

Anwar, G. A., Y. Dong, and C. Zhai. 2020. “Performance-Based Probabilistic Framework for Seismic Risk, Resilience, and Sustainability Assessment of Reinforced Concrete Structures.” *Advances in Structural Engineering* 23 (7): 1454–72. https://doi.org/10.1177/1369433219895363.

Asadi, E., Z. Shen, H. Zhou, A. Salman, and Y. Li. 2020. “Risk-Informed Multi-Criteria Decision Framework for Resilience, Sustainability and Energy Analysis of Reinforced Concrete Buildings.” *Journal of Building Performance Simulation* 13 (6): 804–23. https://doi.org/10.1080/19401493.2020.1824016.

Bragança, L., S. M. Vieira, and J. B. Andrade. 2014. “Early Stage Design Decisions: The Way to Achieve Sustainable Buildings at Lower Costs.” *The Scientific World Journal* 2014. https://doi.org/10.1155/2014/365364.

Caverzan, A., M. Lamperti Tornaghi, and P. Negro. 2018. “Matching Safety and Sustainability: The SAFESUST Approach.” In *IOP Conference Series: Materials Science and Engineering*. Vol. 442. Institute of Physics Publishing. https://doi.org/10.1088/1757-899X/442/1/012019.

“ETool.” 2023. Cerclos. https://etoollcd.com/Account/Login?ReturnUrl=%2f.

Ferreira, A., M. D. Pinheiro, J. de Brito, and R. Mateus. 2023. “Embodied vs. Operational Energy and Carbon in Retail Building Shells: A Case Study in Portugal.” *Energies* 16 (1). https://doi.org/10.3390/en16010378.

Gencturk, B., K. Hossain, and S. Lahourpour. 2016. “Life Cycle Sustainability Assessment of RC Buildings in Seismic Regions.” *Engineering Structures* 110 (March): 347–62. https://doi.org/10.1016/j.engstruct.2015.11.037 .

Gercek, M., and Z. Durmuş Arsan. 2019. “Energy and Environmental Performance Based Decision Support Process for Early Design Stages of Residential Buildings under Climate Change.” *Sustainable Cities and Society* 48 (July). https://doi.org/10.1016/j.scs.2019.101580.

Griffin, C. T., E. Douville, B. Thompson, and M. Hoffman. 2013. “A Multi-Performance Comparison of Long-Span Structural Systems.” In *Structures and Architecture*, edited by Paulo J. Cruz, 1st Edition. London: CRC Press. https://doi.org/10.1201/b15267.

Huang, M. 2019. “Life Cycle Assessment of Buildings: A Practice Guide.” http://hdl.handle.net/1773/41885.

“2019 Global Status Report for Buildings and Construction Towards a Zero-Emissions, Efficient and Resilient Buildings and Construction Sector.” 2019. www.iea.org.

Kardoutsou, V., I. Taflampas, and I. N. Psycharis. 2017. “A New Pulse Indicator for the Classification of Ground Motions.” *Bulletin of the Seismological Society of America* 107 (3): 1356–64. https://doi.org/10.1785/0120160301.

Keskin, F. S., P. Martinez-Vazquez, and C. Baniotopoulos. 2021. “An Integrated Method to Evaluate Sustainability for Vulnerable Buildings Addressing Life Cycle Embodied Impacts and Resource Use.” *Sustainability (Switzerland)* 13 (18). https://doi.org/10.3390/su131810204.

Manfredi, V., G. Santarsiero, A. Masi, and G. Ventura. 2021. “The High-Performance Dissipating Frame (HPDF) System for the Seismic Strengthening of RC Existing Buildings.” *Sustainability (Switzerland)* 13 (4): 1–16. https://doi.org/10.3390/su13041864.

“MATLAB (R2021b).” 2021. The Mathworks Inc.

Mavi, R. K., D. Gengatharen, N. K. Mavi, R. Hughes, A. Campbell, and R. Yates. 2021. “Sustainability in Construction Projects: A Systematic Literature Review.” *Sustainability (Switzerland)*. MDPI. https://doi.org/10.3390/su13041932.

Mazzoni, S., F. McKenna, M. H. Scott, and G. L. Fenves. 2006. “OpenSees Command Language Manual.”

McKenna, F., M. H. Scott, and G. L. Fenves. 2010. “Nonlinear Finite-Element Analysis Software Architecture Using Object Composition.” *J. Comput. Civ. Eng.* 24 (1): 95–107. https://doi.org/10.1061/(ASCE)CP.1943-5487.0000002 .

Menna, C., D. Asprone, F. Jalayer, A. Prota, and G. Manfredi. 2013. “Assessment of Ecological Sustainability of a Building Subjected to Potential Seismic Events during Its Lifetime.” *International Journal of Life Cycle Assessment* 18 (2): 504–15. https://doi.org/10.1007/s11367-012-0477-9.

Mergos, P. 2019. “Sustainable Seismic Design of RC Frames with Structural Optimization Techniques.” https://openaccess.city.ac.uk/id/eprint/23067/.

Merrill, E. M., and S. Giamarelos. 2020. “From the Pantheon to the Anthropocene: Introducing Resilience in Architectural History.” *Architectural Histories* 7 (1): 1–11. https://doi.org/10.5334/AH.406.

Mohammadgholibeyki, N., F. Nazari, V. Venkatraj, M. Koliou, W. Yan, M. Dixit, and P. Sideris. 2023. “A Decision-Making Framework for Life-Cycle Energy and Seismic Loss Assessment of Buildings.” *Structure and Infrastructure Engineering* 19 (7): 875–89. https://doi.org/10.1080/15732479.2021.1983613.

Nouri, A., P. Asadi, and M. Taheriyoun. 2021. “Life-Cycle Cost Analysis of Seismic Designed RC Frames Including Environmental and Social Costs.” *Journal of Earthquake Engineering*. https://doi.org/10.1080/13632469.2021.1911877.

“NREL’s OpenStudio Helps Design More Efficient Buildings (Fact Sheet).” 2014. Golden, CO (United States). https://doi.org/10.2172/1140096.

“OpenStudio.” 2023. Dan Macumber. https://github.com/openstudiocoalition/openstudio-sketchup-plugin/releases.

Pomè, A. P., C. Tagliaro, and G. Ciaramella. 2021. “A Proposal for Measuring In-Use Buildings’ Impact through the Ecological Footprint Approach.” *Sustainability (Switzerland)* 13 (1): 1–21. https://doi.org/10.3390/su13010355 .

Pongiglione, M., and C. Calderini. 2016. “Sustainable Structural Design: Comprehensive Literature Review.” *Journal of Structural Engineering* 142 (12): 04016139. https://doi.org/10.1061/(asce)st.1943-541x.0001621 .

Purchase, C. K., D. M. Al Zulayq, B. T. O'brien, M. J. Kowalewski, A. Berenjian, A. H. Tarighaleslami, and M. Seifan. 2022. "Circular Economy of Construction and Demolition Waste: A Literature Review on Lessons, Challenges, and Benefits." *Materials*. MDPI. https://doi.org/10.3390/ma15010076.

"Report on 2023 Kahramanmaraş and Hatay Earthquakes." 2023. https://www.sbb.gov.tr/2023-kahramanmaras-ve-hatay-depremleri-raporu/.

"Revit 2021." 2021. Autodesk.

Riddell, R., S. L. Wood, and J. C. de la Llera. 1987. "The 1985 Chile Earthquake: Structural Characteristics and Damage Statistics for the Building Inventory in Viña Del Mar." *Tech. Rep. Civil Engineering Studies SRS-534, University of Illinois at Urbana-Champaign.* http://hdl.handle.net/2142/14160.

Salgado, R. A., D. Apul, and S. Guner. 2020. "Life Cycle Assessment of Seismic Retrofit Alternatives for Reinforced Concrete Frame Buildings." *Journal of Building Engineering* 28 (March). https://doi.org/10.1016/j.jobe.2019.101064.

Sattar, S. 2021. "Recommended Options for Improving the Built Environment for Post-Earthquake Reoccupancy and Functional Recovery Time." Gaithersburg, MD. https://doi.org/10.6028/NIST.SP.1254.

Sattar, S., C. L. Segura, K. J. Johnson, T. P. Mcallister, and S. L. Mccabe. 2018. "Key Implementation Challenges and Crosscutting Research Themes for Developing Immediate Occupancy Performance Objectives." https://www.nist.gov/publications/key-challenges-and-crosscutting-research-themes-developing-immediate-occupancy.

Shiga, T., A. Shibata, and T. Takahashi. 1968. "Earthquake Damage and Wall Index of Reinforced Concrete Buildings." *12th Tohoku District Symposium, Japan. (in Japanese)*, 29–32.

Simonen, K., M. Huang, C. Aicher, and P. Morris. 2018. "Embodied Carbon as a Proxy for the Environmental Impact of Earthquake Damage Repair." *Energy and Buildings* 164 (April): 131–39. https://doi.org/10.1016/j.enbuild.2017.12.065.

"SketchUp." 2023. Trimble. https://www.sketchup.com/.

Son, S., K. Park, H. Fitriani, and S. Kim. 2021. “Embodied CO2 Reduction Effects of Composite Precast Concrete Frame for Heavily Loaded Long-Span Logistics Buildings.” *Sustainability (Switzerland)* 13 (3). https://doi.org/10.3390/SU13031060.

Sönmez, E. 2020. “Manipulation of Structural Design Parameters to Mitigate the Concentration of Interstory Drift Ratios.” Ph.D. Thesis, İzmir: İzmir Institute of Technology. https://tez.yok.gov.tr/UlusalTezMerkezi/tezDetay.jsp?id=x9gUfTIKzXu6p7bZH-atBA&no=sRNowCDMnsrozVoHINOhiw.

Sozen, M. A. 2003. “The Velocity of Displacement In Seismic Assessment and Rehabilitation of Existing Buildings.” *Kluwer Academic Publishers: Dordrecht, The Netherlands* 29: 11–28. https://doi.org/10.1007/978-94-010-0021-5_2.

Sozen, M.A., and A. Hassan. 1997. “Seismic Vulnerability Assessment of Low-Rise Buildings in Regions with Infrequent Earthqaukes.” *ACI Structural Journal*. https://doi.org/10.14359/458.

Stochino, F., C. Bedon, J. Sagaseta, and D. Honfi. 2019. “Robustness and Resilience of Structures under Extreme Loads.” *Advances in Civil Engineering*. Hindawi Limited. https://doi.org/10.1155/2019/4291703.

Turkish Earthquake Regulation for Building Structures: Specifications for Design of Buildings under Earthquake Forces. 2018. Presidency of Disaster and Emergency Management. https://www.resmigazete.gov.tr/eskiler/2018/03/20180318M1-2.htm.

United Nations. n.d.-a. “Sustainability.” Accessed January 12, 2024. https://www.un.org/en/academic-impact/sustainability.

———. n.d.-b. “The 17 Goals.” Accessed November 17, 2023. https://sdgs.un.org/goals.

“EnergyPlus.” 2023. U.S. Department of Energy’s (DOE). https://energyplus.net/.

Wei, H., M. J. Skibniewski, I. M. Shohet, and X. Yao. 2016. “Lifecycle Environmental Performance of Natural-Hazard Mitigation for Buildings.” *Journal of Performance of Constructed Facilities* 30 (3): 04015042. https://doi.org/10.1061/(asce)cf.1943-5509.0000803.

World Green Building Council. n.d. “Bringing Embodied Carbon Upfront.” Accessed November 17, 2023. https://worldgbc.org/advancing-net-zero/embodied-carbon/.

Yildirim, M. E., C. Yesilyurt, U. Gozun, B. Ozturk, and C. Donmez. 2023. “Structural Performance of R/C Buildings in 2023 Kahramanmaras Earthquakes under the Lens of Hassan Index.” In *7.ICEES*.

Zhong, Y., F. Yean Yng Ling, and P. Wu. 2016. “Using Multiple Attribute Value Technique for the Selection of Structural Frame Material to Achieve Sustainability and Constructability.” https://doi.org/10.1061/(ASCE)CO.1943-7862.0001210.